JULIUS-MAXIMILIANS-UNIVERSITÄT WÜRZBURG

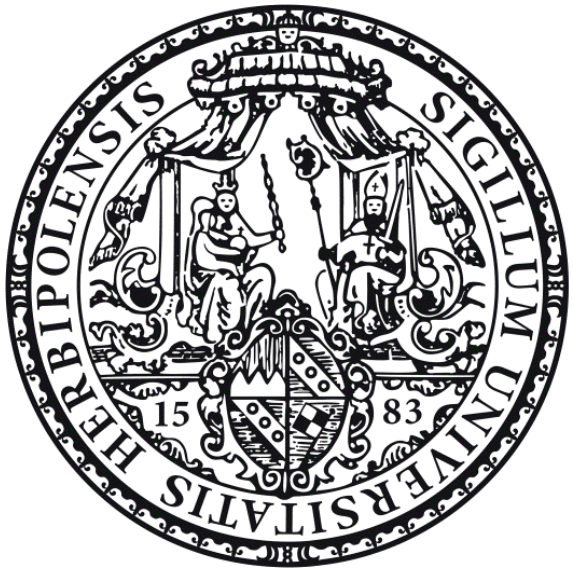

Novel Borane- and Phosphorane-Functionalized Anionic Carbene Ligands

Dissertation zur Erlangung des naturwissenschaftlichen Doktorgrades

der

Julius-Maximilians-Universität Würzburg

vorgelegt von

Ludwig Zapf

aus Schwaig b. Nürnberg

Würzburg 2023

Eingereicht bei der Fakultät für Chemie und Pharmazie der Julius-Maximilians-Universität Würzburg am

24. April 2023

Gutachter der schriftlichen Arbeit:

1. Gutachter: Prof. Dr. Maik Finze

2. Gutachter: Prof. Holger Braunschweig

Prüfer des öffentlichen Promotionskolloquiums:

1. Prüfer: Prof. Dr. Maik Finze

2. Prüfer: Prof. Dr. Holger Braunschweig

3. Prüfer: Prof. Dr. Ingo Fischer

4. Prüfer: Prof. Dr. Lorenz Meinel

5. Prüfer: Prof. Dr. Udo Radius

Datum des öffentlichen Promotionskolloquiums

30. Juni 2023

Doktorurkunde ausgehändigt am

Meiner Familie

Bei Gott allein ist Weisheit und Kraft, Rat und Verstand.

Hiob 12,13

Die vorliegende Arbeit wurde im Zeitraum von August 2020 bis April 2023 am Institut für Anorganische Chemie der Julius-Maximilians-Universität Würzburg unter der Leitung von Prof. Dr. Maik Finze angefertigt.

TABLE OF CONTENTS

LIST OF ABBREVIATIONS

aq	aqueous
c	concentration
cAAC	cyclic (alkyl)(amino)carbene
cat	catecholato
d	distance
d	days
DAC	*N*,*N*'-diamidocarbene
DFT	density functional theory
Dipp	2,6-di-*iso*-propylphenyl
DMAP	4-(dimethylamino)pyridine
DMSO	dimethyl sulfoxide
DSCC	dye-sensitized solar cell
eg	ethylene glycolato
FIA	fluoride ion affinity
FLP	frustrated Lewis pair
h	hours
HOMO	highest occupied molecular orbital
HDA	di-*iso*-propylamine
IL	ionic liquid
IAd	1,3-bis(1-adamantyl)imidazolin-2-ylidene
IDipp	1,3-bis(2,6-di-*iso*-propylphenyl)imidazolin-2-yliden
I*i*Pr	1,3-di-*iso*-propylimidazolin-2-yliden
IMe	1,3-dimethylimidazolin-2-yliden
IMes	1,3-dimesitylimidazolin-2-yliden
I*t*Bu	1,3-di-*tert*-butylimidazolin-2-yliden
IR	infrared
KHMDS	potassium hexamethyldisilazide
LA	Lewis acid
LB	Lewis base
LDA	lithium di-*iso*-propylamide
LiHMDS	lithium hexamethyldisilazide
LUMO	lowest unoccupied molecular orbital
Me	methyl
MeCN	acetonitrile
Mes	mesityl
min	minutes
*n*BuLi	1-lithiobutane
neop	neopentyl glycolato
NHC	*N*-heterocyclic carbene

Ph	phenyl
Pin	pinacolato
*p*Tol	*para*-tolyl
py	pyridine
r.t.	room temperature
SIMes	1,3-dimesitylimidazolidin-2-ylidene
THF	tetrahydrofuran
WCA	weakly coordinating anion
ZIF	zeolitic imidazolate framework

Analytics

δ	chemical shift
DSC	differential scanning calorimetry
DTA	differential thermal analysis
HRMS	high-resolution mass spectrometry
MAS	magic angle spinning
MS	mass spectrometry
NMR	nuclear magnetic resonance
ppm	parts per million
SC-XRD	single-crystal X-ray diffraction
STA	simultaneous thermal analysis
TG	thermogravimetric analysis

1. INTRODUCTION

1.1 Lewis Acid/Base Pairs with Boranes and Phosphoranes

About a century ago, Gilbert N. Lewis reported Lewis acids (*LA*s) and characterized these compounds as electron pair acceptors. Since they contain an appropriate vacant orbital, Lewis acids are able to react with Lewis bases (*LB*s). Lewis bases were distinguished as electron pair donors with an occupied orbital filled with two electrons, which are hardly or not at all involved in bonding.[1,2] The class of compounds formed by the reaction of an electron deficient Lewis acid and an electron rich Lewis base is called Lewis adducts. Examples of well-known Lewis acids are boranes of the general chemical formula BR_3 and phosphoranes of the formula PR_5, with R being one of various substituents. In general, these compounds readily react with Lewis bases like amines, phosphines, or carbenes to form the corresponding Lewis pair (Figure 1.1.1).

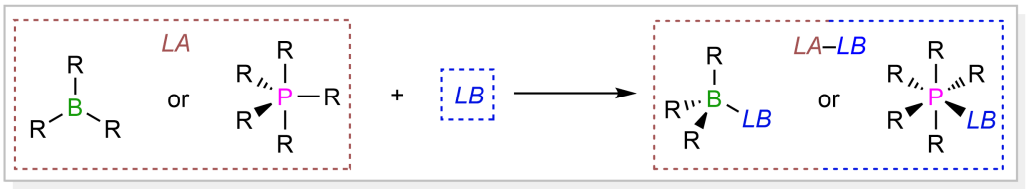

Figure 1.1.1 *Formation of Lewis pairs by Lewis acidic boranes or phosphoranes and Lewis bases.*

In contrast to the trigonal planar boranes BR_3 and the pentavalent phosphoranes PR_5 the Lewis acid/base adducts are less reactive and therefore easier to handle and store. Furthermore, the choice of Lewis base has a decisive influence on the reaction selectivity of the parent Lewis acid.[3-6] Lewis base stabilized boranes with the chemical formula $R_3B{\cdot}LB$ are not only relevant for inorganic main group element chemistry, but also play an important role in different fields of organic synthesis.[7,8] For instance, $BF_3{\cdot}OEt_2$ or $BH_3{\cdot}SMe_2$ are commercially available and are produced on a large scale in industry, since they are used in Friedel-Crafts reactions, cleavage of ethers, rearrangement reactions, hydroboration reactions or reductions.[9-11] In addition to comparatively easily dissociating adducts such as those mentioned before, it is also possible to synthesize more stable Lewis pairs, by increasing the Lewis basicity of the donor compounds. These include, for example, phosphine,[12] pyridine,[13] amine,[14] or carbene adducts[15] (Figure 1.1.2).

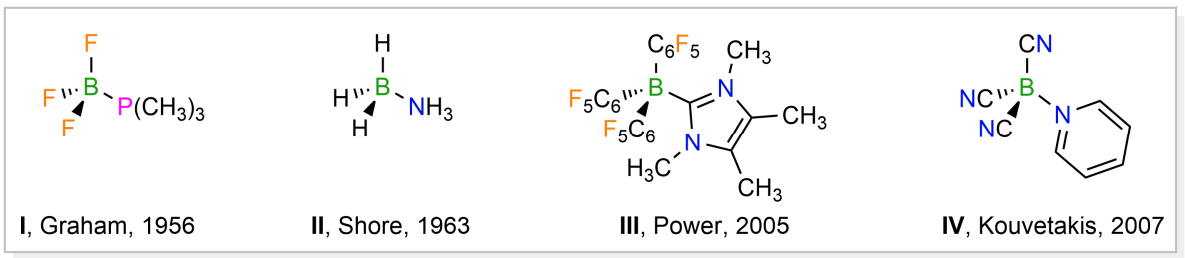

Figure 1.1.2 *Selected Lewis base stabilized boranes.*

In the field of Lewis base stabilized phosphoranes, significantly fewer compounds are known; some exemplary representatives are mentioned in the following. 1971 Brokke and co-workers synthesized several nitrile adducts of phosphorus pentafluoride by addition reactions (Figure 1.1.3).[16]

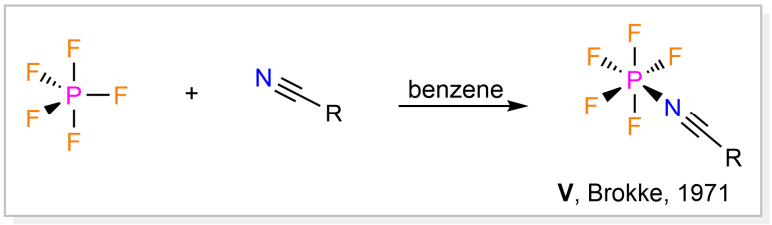

Figure 1.1.3 *Synthesis of nitrile stabilized phosphorus pentafluorides* ***V****.*

Phosphorane/carbene adducts can be synthesized in a similar approach, as first demonstrated by Arduengo *et al.* using phenyltetrafluorophosphorane[17] and recently in a work by Finze and Radius *et al.*, discussing the reaction of the sterically more demanding tris(pentafluoroethyl)difluoro-phosphorane $(C_2F_5)_3PF_2$ with different *N*-heterocyclic carbenes (NHCs).[18] For the latter it was found, that bulky NHCs like IDipp (1,3-bis(2,6-di-*iso*-propylphenyl)imidazolin-2-yliden) and I*t*Bu (1,3-di-*tert*-butylimidazolin-2-yliden) show a different reactivity and the corresponding phosphorane/NHC adducts do not form instantaneously. However, "abnormal" adducts with the NHC ligand coordinating *via* the backbone to the phosphorane were found (Figure 1.1.4).[18]

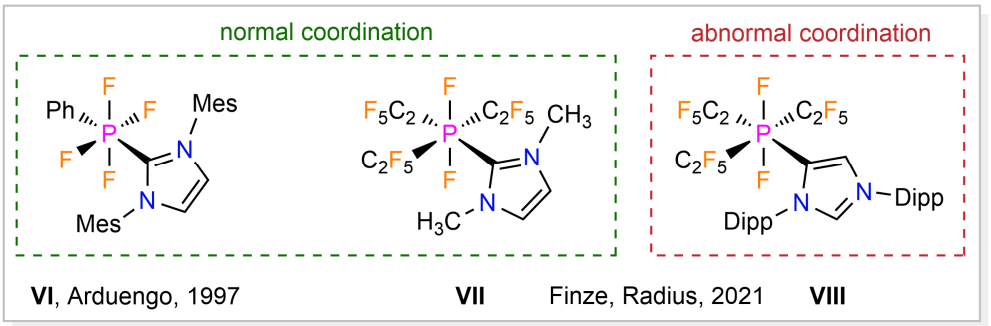

Figure 1.1.4 *Phosphorane/NHC adducts with the NHC in normal and abnormal coordination mode.*

A few years earlier, Hoge and co-workers reported about the first neutral Lewis pair of $(C_2F_5)_3PF_2$, which was stabilized by the strong Lewis base DMAP (4-(dimethylamino)pyridne). Furthermore, it was demonstrated that the adduct $(C_2F_5)_3PF_2$·DMAP is a valuable starting material for the synthesis of different phosphates (Figure 1.1.5).[6]

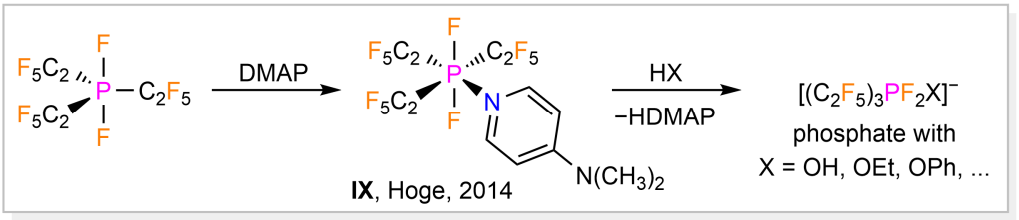

Figure 1.1.5 *Synthesis and follow-up reactions of 4-(dimethylamino)pyridine stabilized* $(C_2F_5)_3PF_2$ ***IX****.*

1.2 Borane- and Phosphorane-Substituted Imidazole Compounds

Another excellent Lewis base for the formation of Lewis pairs is imidazole and its derivatives. On one hand, the comparatively high Lewis basicity of the nitrogen atom(s) leads to the formation of stable adducts with various Lewis acids, and on the other hand, imidazole compounds are a very interesting class of compounds in general. These heteroaromatics attract the interest of science and industry not only because of their diverse occurrence in nature.[19-21] In particular, their electronic structure, the manifold substitution possibilities at all positions of the five-membered ring or the ampholytic character of this substance class render the imidazoles one of the most important structural motifs in the study and development of new materials and substances.[22] Neutral imidazole derivatives play an important role in pharmaceutical chemistry as drugs or as eluents of proteins, for instance.[23] In organic chemistry, for example, the π-aromaticity of imidazole is exploited to synthesize conductive polymers, and in coordination chemistry imidazole compounds are widely used as ligands or starting compounds for *N*-heterocyclic carbenes.[24,25] Imidazolium salts accessible from imidazoles are also an integral part of chemical research and industry.[26] Many derivatives of imidazolium cations form ionic liquids (ILs) with suitable anions, which are of particular interest for electrochemical applications, for example as liquid electrolytes with high conductivities, but also as solvent alternatives or in heterocatalysis, when combined with appropriate catalysts.[27-29] Imidazoles substituted on one of the nitrogen atoms with a hydrogen, alkyl, or aryl substituent form neutral compounds. 1*H*-imidaozle and 1-alkyl- or 1-arylimidazoles readily stabilize diverse boranes (Figure 1.2.1). Therefore, numerous imidazole/borane pairs of this type have been described in the literature.[30-32]

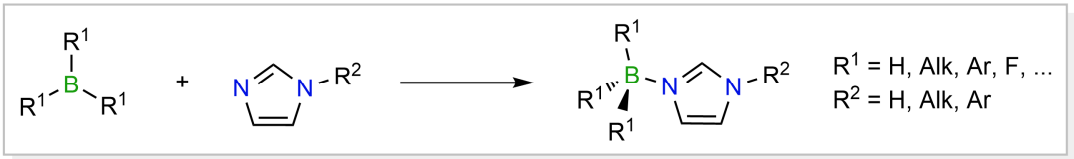

Figure 1.2.1 *Synthesis of 3-boraneimidazole compounds.*

However, anionic imidazole compounds with borane groups attached to both nitrogen atoms have been studied comparatively little and only a few bis(borane)imidazolates were described in the literature. The first compound of this substance class was synthesized by Kuhn *et al*. in 1997 by the reaction of sodium imidazolate with trimethylborane (Figure 1.2.2).[33]

Figure 1.2.2 *Synthesis of the first bis(borane)imidazolate Na**X**.*

However, the stability of compound Na**X** is limited due to the low Lewis acidity of BMe_3 and therefore decomposes even under inert conditions under trimethylborane liberation. Furthermore, the anion is unstable against comproportionation with sodium imidazolate to form the mono borane-substituted imidazolate. In 2000, LaPointe *et al*. succeeded in synthesizing another representative of this novel class of compounds by reacting tris(pentafluorophenyl)borane with imidazole and potassium imidazolate, respectively, to give compound [$HNEt_3$]**XI** (Figure 1.2.3).[34]

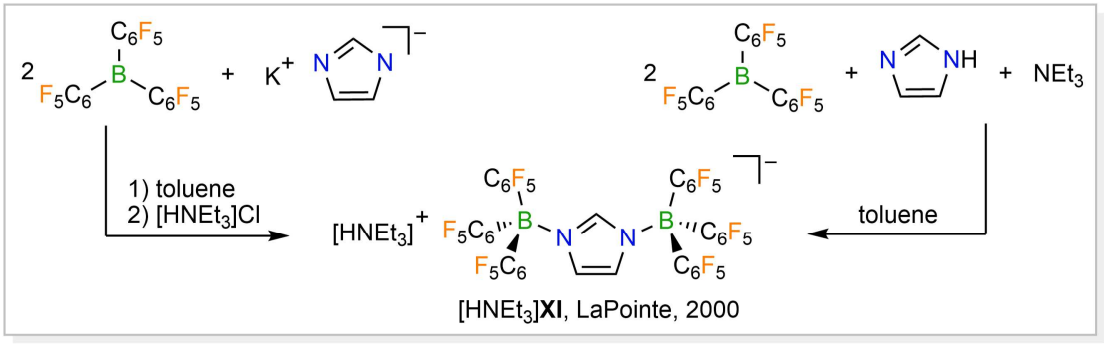

Figure 1.2.3 *Syntheses of a bis[tris(pentafluorophenyl)borane]imidazolate.*

The bis[tris(pentafluorophenyl)borane]imidazolate anion **XI** is discussed as a weakly coordinating anion (WCA) due to the high degree of delocalization of the negative charge. Its thermal stability and resistance towards hydrolysis are also significantly increased compared to the bis(trimethylborane)-substituted imidazolate anion **X**. In 2002, Erker *et al.* published a synthesis of the lithium salt of the already known bis[tris(pentafluorophenyl)borane]imidazolate anion **XI** and were able to show its weakly coordinating properties by metathesis reaction to [$H(OEt_2)_2$]**XI**. Furthermore, the metallocene cation [$Cp_2ZrMe(OEt_2)$]$^+$ was stabilized by this anion (Figure 1.2.4).[35]

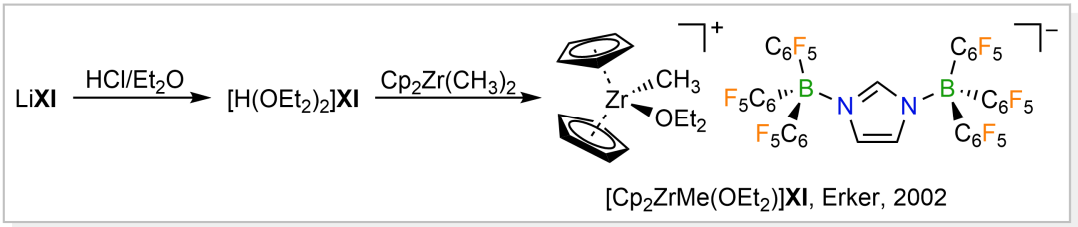

Figure 1.2.4 *Stabilization of reactive cations by the weakly coordinating bis[tris(pentafluorophenyl)-borane]imidazolate anion.*

Nevertheless, the pentafluorophenyl substituents of the boranes provide a target for CF activation processes or potential elimination of C_6F_5H. Due to the size, the relatively high mass of the anion, and the comparably rigid C_6F_5 groups, which limit ion mobility and conductivity at high concentrations, salts of anion **XI** are also rather unsuitable as conducting salts, which is another area of application for imidazolates.[36] A family of borane-substituted imidazolates, which can be produced inexpensively from $BF_3{\cdot}Et_2O$ and lithium imidazolates, that is more suitable as conducting salts for lithium ion batteries, was presented by Barbarich and co-workers in 2003 and 2004 (Figure 1.2.5).[36,37]

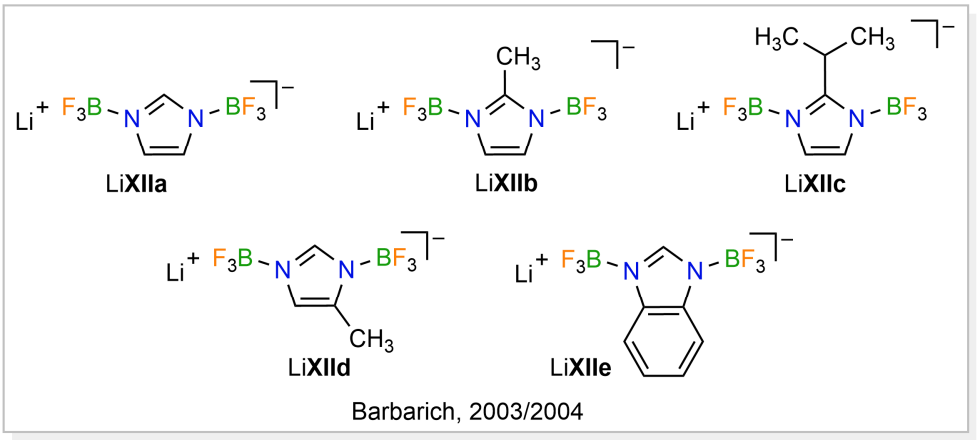

Figure 1.2.5 *Lithium bis(trifluoroborane)imidazolates suitable as conducting salts.*

Compound Li**XIIa** in particular is characterized by its high solubility, conductivity, and electrochemical stability. However, due to its sensitivity to hydrolysis, the substance must be synthesized and handled under strict exclusion of air and oxygen. However, even under inert handling, $Li[BF_4]$ occurs as a by-product or decomposition product, as described in the literature.[37]

Beside the bis(borane)-substituted imidazolate anions **X**, **XI**, and **XIIa-e** only two more compounds of this class were known in the literature; the bis(triethylborane)imidazolate Na**XIII**,[38] which can be synthesized in analogy to Na**X** (Figure 1.2.2) and the bis(triphenylborane)imidazolate anion **IX**, published by Stephan *et al*. in 2019.[39] Thus, one goal of this work was to extend the series of borane-functionalized imidazole compounds by preparing new stable imidazolates with other boranes, such as the tricyanoborane.

Concerning phosphorane/imidazole adducts there were only four examples described in the literature, before this work, and these are limited to compounds of pentafluoro- and pentachlorophosphorane, respectively. Compounds **XIIIa**, **XIIIb**, **XIVa**, and **XIVb** can be synthesized by the reaction of PF_5 and PCl_5 with the corresponding imidazole compound (Figure 1.2.6).[40-43]

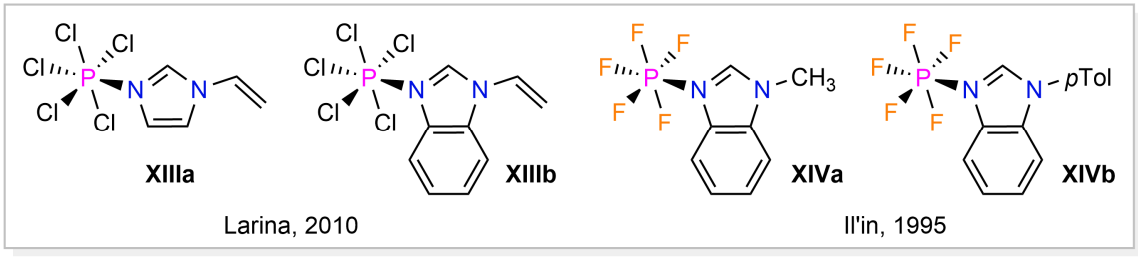

Figure 1.2.6 *Imidazole adducts of PCl_5 and PF_5.*

Bis(phosphorane)-substituted imidazole compounds have not been described previously in the literature. Within this work, bis(phosphorane)imidazolates will be synthesized and investigated for the first time.

1.3 *N*-Heterocyclic Carbenes

Carbenes, which are defined as compounds of a divalent carbon with six valence electrons, are considered as highly reactive compounds due to their incomplete electron octet and lack of coordinative saturation.[25] After the first synthesis attempts almost 200 years ago[44] and the report on the first isolable representatives by Bertrand *et al*. in 1988,[45] the year 1991 can be seen as the beginning of a new era in carbene chemistry.[46] In that year, Arduengo *et al*. published a work about the first isolable crystalline carbene incorporated into a nitrogen heterocycle (**XXa**). These so-called *N*-heterocyclic carbenes (NHCs) are characterized by their remarkable stability and comparative ease of preparation, namely by the deprotonation of imidazolium salts (Figure 1.3.1).[46,47] Nowadays NHCs are one of the most important class of compounds with widespread applications in chemical industry and academia, for example in organo- and transition metal catalysis or in medical applications.[48-62]

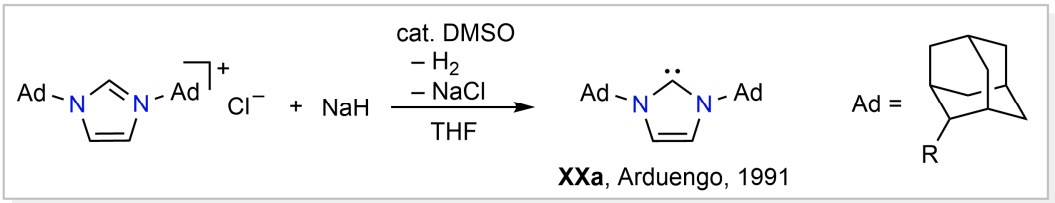

Figure 1.3.1 *Synthesis of 1,3-bis(1-adamantyl)imidazolin-2-ylidene (IAd).*

The high stability of NHCs is based on the electronic and steric environment of the carbene carbon atom. While the substituents on the adjacent nitrogen atoms provide kinetic stabilization of the carbene, the combination of mesomeric π-electron donation and inductive σ-electron acceptance of the nitrogen atoms leads to an electronic stabilization (Figure 1.3.2).[25] Thus, a singlet results as the electronic ground state for NHCs, where the highest occupied molecular orbital (HOMO) can be described as a carbon-centered sp^2-hybridized lone pair and the lowest unoccupied molecular orbital (LUMO) as an unoccupied carbon-centered p-orbital.

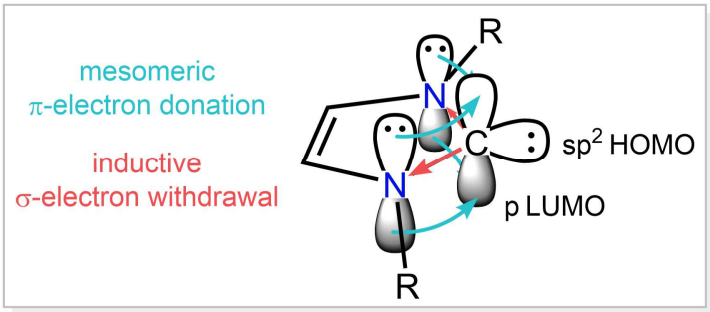

Figure 1.3.2 *Electronic structure and stabilizing effects of imidazolin-2-ylidenes.*

By modifying the electronic and steric environment of the carbene center, the properties of NHCs, e.g. its strong σ-donor and π-acceptor ability and its steric demand, can be tuned over a wide range.[63] Four basic parameters can be identified, which can be used to tailor their properties (Figure 1.3.3).

I.) The Nitrogen Substituents

Starting from the first isolated NHC, 1,3-bis(1-adamantyl)imidazolin-2-ylidene (IAd, **XXa**), which carries sterically very demanding adamantyl substituents (R = Ad),[46] a large number of other NHCs with alkyl and aryl substituents can be derived. Among the most widely used NHCs are those with methyl (IMe),[64] *tert*-butyl (I*t*Bu),[65] mesityl (IMes),[64] and 2,6-di-*iso*-propylphenyl (IDipp)[66] groups. Of course, the size of the substituents directly influences the properties of the carbene. NHC IAd, for example, is thermally very robust and decomposes only at temperatures higher than 240 °C,[46] while formal replacement of the sterically demanding adamantyl groups with methyl groups causes the NHC IMe to decompose already at room temperature.[64] Besides the steric influence, the groups also affect the electronic situation of the carbene. Thus, NHCs with aryl substituents are generally better π-acceptors than those with alkyl groups.[48] In order to influence the donor and acceptor properties of NHCs even more significantly, the introduction of charged substituents is particularly effective, as described below (Chapter 1.4).

II.) The Backbone

The first NHCs were prepared starting from heteroaromatics such as imidazolium salts. The partial aromaticity causes an additional stabilization of the resulting imidazolinylidens. Nevertheless, it is also possible to use the saturated imidazolidine motive for NHCs. The first example of such NHCs with an unsaturated backbone, the 1,3-dimesitylimidazolidin-2-ylidene (SIMes), was presented by Arduengo and co-workers in 1995.[67] Saturation of the imidazoline backbone results in increased σ-donor and π-acceptor abilities and has therefore direct influence on the electronic properties of the NHC.[68] Furthermore, it is possible to introduce more substituents *via* the functionalization of the backbone. Depending on the group introduced, the electronic properties of the carbene can be influenced significantly, but a small effect on the steric properties of the carbene can also be observed by substituting hydrogen with, for example, methyl groups.[64] A formal substitution of one of the carbon atoms of the backbone against nitrogen is also possible, resulting in triazolylidenes.[69]

III) The Ring Size

In addition to the degree of saturation and substitution of the backbone, its size and thus the overall ring size of the heterocycle also provides adjustability of the properties of an *N*-heterocyclic carbene. Beside the most commonly used five membered NHCs, six membered NHCs are also useful for several applications.[70-74] By increasing the ring size, the steric properties of the carbene change, as the N–C–N internal angle increases, and the increased carbene bond angle is reflected in an increase in the p-character of the HOMO and the LUMO of the carbene, which leads to a reduced HOMO-LUMO gap and thus to improved donor and acceptor properties.[73]

IV) The Change of Heteroatoms

Changing one of the nitrogen atoms of the imidazole motive probably has the greatest influence on the properties of the NHC. When an oxygen or sulfur atom is introduced oxazolylidenes or thiazolylidenes result, respectively.[25,75,76] However, probably the most striking change occurs when a carbon is chosen as the neighbor of the carbene center, instead of the two electronegative amino groups of the imidazole.[77] For a quaternary carbon with two strongly donating alkyl groups, the corresponding NHCs are called cyclic (alkyl)(amino)carbenes (cAAC).[73,78-82] This substance class was first reported by Bertrand *et al*. in 2005.[79] If the nitrogen is exchanged for a tertiary carbon and a second amino moiety is found in the backbone, it is called an abnormal NHC.[49,83]

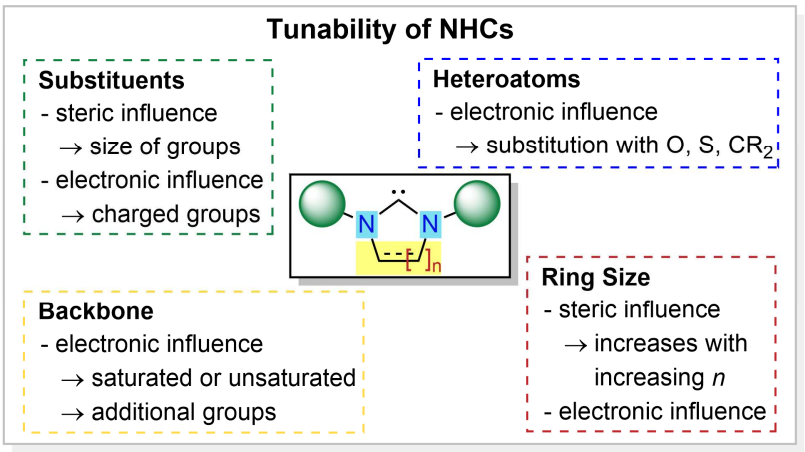

Figure 1.3.3 *Four ways to tune the properties of an NHC.*

The combination of these four tuning options for NHCs results in a variety of different subclasses of carbenes. A selection of the most common representatives is shown in Figure 1.3.4. Starting from differently substituted Arduengo type NHCs with unsaturated (**XX**)[46,64,65] and saturated backbones (**XXI**)[67] and abnormal NHCs (**XXII**),[49,83] which are deprotonated at the C5-position of the imidazole ring, the heterocycle can also be changed to a triazole (**XXIII**)[69] or thiazole (**XXIV**).[75] More recently, *N*,*N*'-diamidocarbenes (DACs, **XXV**)[74] and cyclic (alkyl)(amino)carbenes (cAACs, **XXVI**)[79] have been added to the family of *N*-heterocyclic carbenes. DACs and cAACs are examples for NHCs with modified ring size and additional functional groups.

In the context of this thesis, especially the substitution of groups at the nitrogen atoms of imidazoles will be investigated, with Lewis acids being introduced as functional groups (Chapter 2.1−2.2), in order to synthesize novel anionic carbenes and to characterize their properties. However, the exchange of a nitrogen atom of the imidazole ring for a quaternary carbon atom and the influence of ring sizes will also play a role in this work in Chapter 2.3, which reports on the preparation of novel anionic cAACs.

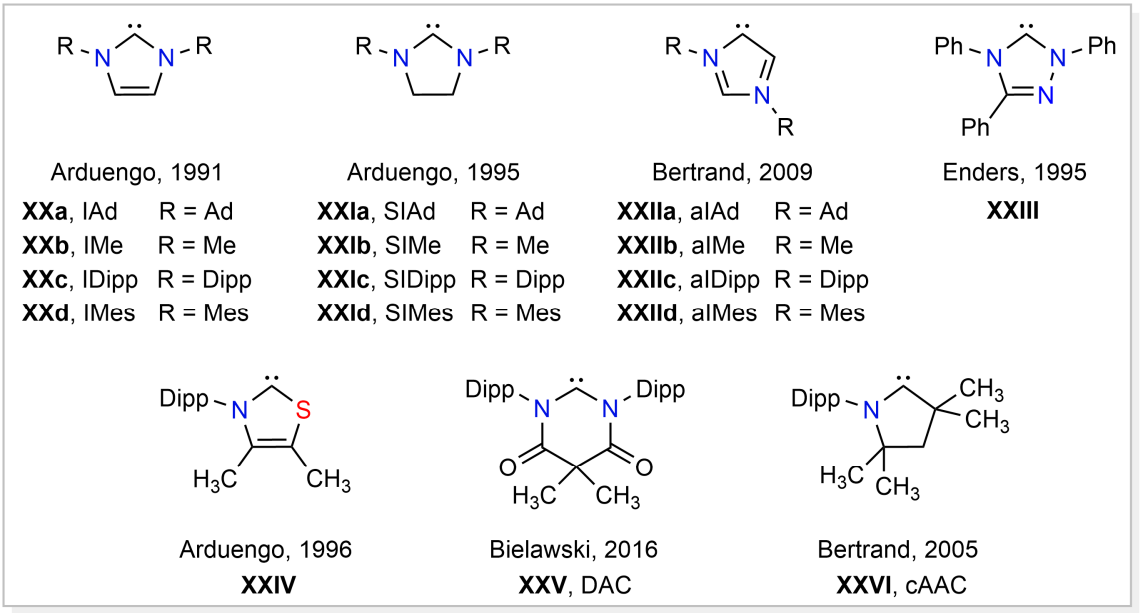

Figure 1.3.4 *Selected NHCs with different substituents, backbones, ring sizes, and heteroatoms.*

1.4 Anionic *N*-Heterocyclic Carbenes

In contrast to the abundance of various neutral *N*-heterocyclic carbenes (Chapter 1.3), the number of anionic or even dianionic NHCs is limited, so far.[84] One approach for the synthesis of anionic NHCs is the deprotonation of neutral or anionic imidazole derivatives, which bear Lewis acids, e.g. boranes, instead of alkyl or aryl substituents at nitrogen. Following this strategy, the anionic triscarbene **XXVII** (Figure 1.4.1) was obtained in 1996 by Fehlhammer *et al*.[85] and a number of related monoanionic tris- and biscarbenes have been investigated and used as chelating ligands in coordination chemistry.[86-90] In 1998, the first anionic NHC was published with a BH_3 moiety bonded to nitrogen (**XXVIII**, Figure 1.4.1).[30] A further, rare example for a related anionic borane-substituted NHC (**XXIX**, Figure 1.4.1) was presented in 2012 by Tamm and co-workers, but the weakly coordinating tris(pentafluorophenyl)borane group was attached to the backbone of the heterocyclic ring.[91] In recent years it was demonstrated that this type of anionic borane-substituted NHC is a versatile tool for the synthesis of unusual group 13, 16, and 17 derivatives,[92-95] for the activation of organic compounds, and for the preparation of catalytically active transition metal complexes.[91,94,96-98] In 2014, anionic carboranyl units were introduced as substituents at the imidazole nitrogen atoms,[99-101] for example in the dianion **XXX** (Figure 1.4.1).[99] The concept of using anionic boron clusters as substituents at NHCs *via* $C_{cluster}$–N bonds was extended to other boron cages such as {*nido*-7,8-C_2B},[102] halogenated {*closo*-1-CB_{11}} cages,[103] and recently {*closo*-1-CB_9} clusters have been attached as well.[104]

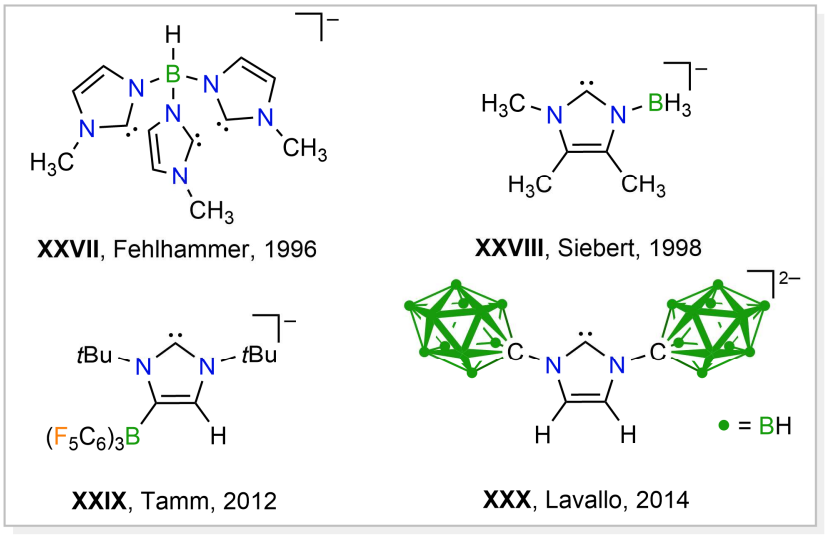

Figure 1.4.1 *Selected anionic borane-substituted NHCs.*

In contrast, to the few examples of anionic or dianionic NHCs, many carbenes with one or two tethered anionic groups have been studied in the past.[95] Beside the formation of **XXVIII** and **XXIX**, attempts on the synthesis of other borane-imidazole derivatives did not lead to the respective anionic carbene. In the first place it is surprising that no dianionic NHCs in which both nitrogen atoms are substituted with a borane have been described so far, although potential 1,3-bis(borane)imidazolate precursors are

known, as described before (Chapter 1.2). Most likely, these 1,3-bis(borane)imidazolate ions would undergo immediate follow-up reactions upon initial formation of the related carbene by deprotonation. This hypothesis is supported by reports on the reactivity of 3-triethylborane-1,4,5-trimethylimidazole **XXXIa**[30] and 3-tris(pentafluorophenyl)borane-1-methylimidazole **XXXIIa** (Figure 1.4.2).[105] Deprotonation of **XXXIa** is followed by migration of the Et_3B moiety even at −78 °C to give the NHC−BEt_3 adduct **XXXIc**.[30] This behavior reflects the low Lewis acidity of the alkylborane and the corresponding weakness of the B−N bond. In contrast, the stronger B−N bond in **XXXIIa** remains intact after deprotonation, but an intramolecular nucleophilic attack of the carbene C atom at one of the C_6F_5 rings occurs to result in **XXXIIc**.[105]

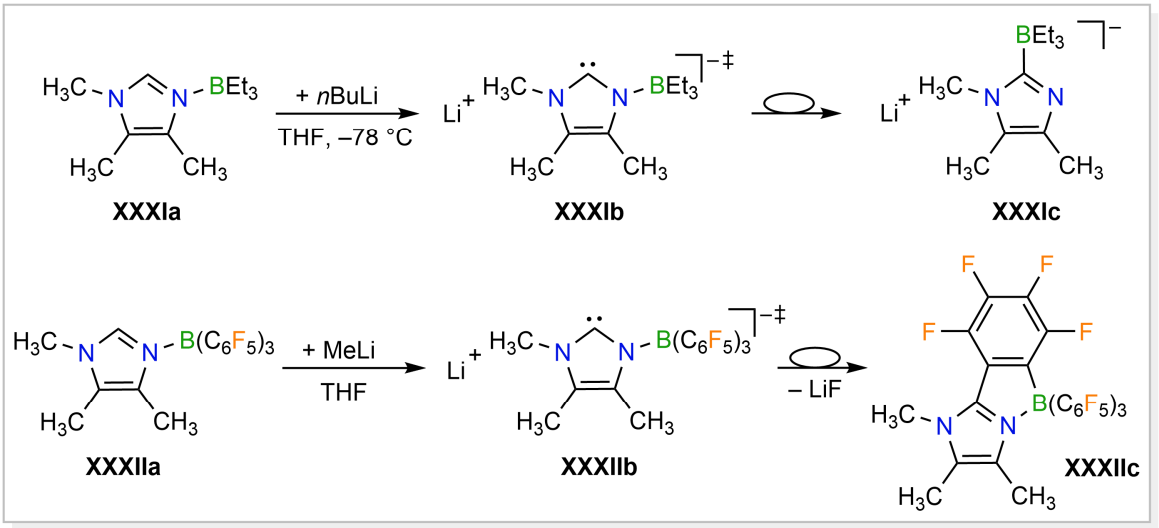

Figure 1.4.2 *Intramolecular follow-up reactions of in situ generated borane-substituted anionic NHCs.*

Anionic NHCs with other Lewis acidic substituents are also known in a small number. However, these NHCs are always functionalized in the backbone with the corresponding Lewis acids, but never at the Lewis basic nitrogen atoms. Examples of such anionic NHCs carry alane (**XXXIII**),[106] gallane (**XXXIV**),[107] phosphinidene (**XXXV**),[108] amide (**XXXVI**),[109] or siliconate (**XXXVII**) groups (Figure 1.4.3).[110]

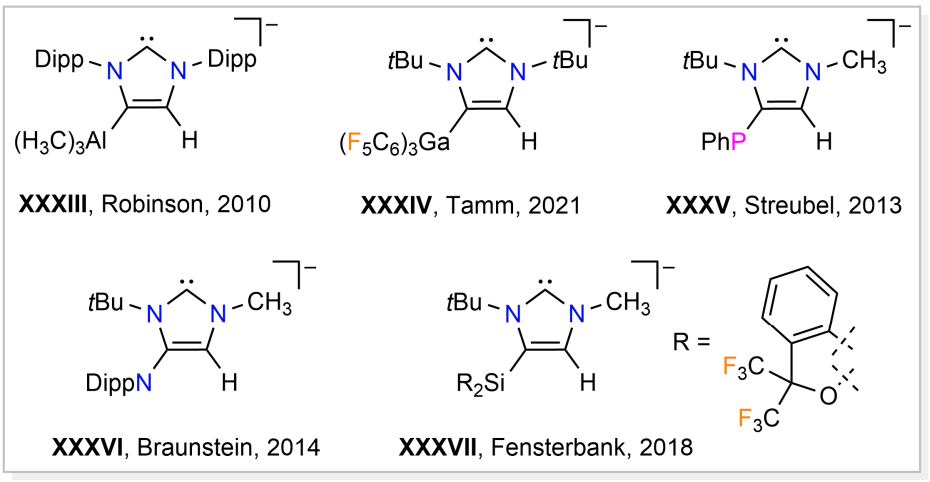

Figure 1.4.3 *Selected anionic alane-, gallane-, phosphinidene-, amide-, and siliconate-NHCs.*

The aim of this work is the preparation of literature unknown 1,3-bis(borane)imidazolates, which are suitable precursors for novel dianionic NHCs (Chapter 2.1). In addition, Lewis acids other than boranes will be used as substituents at the nitrogen atoms for the first time to prepare new classes of anionic NHCs (Chapter 2.2). A focus will be on the investigation of the properties of the obtained carbenes, in particular to what extent their abilities like σ-donor and π-acceptor strength or steric shielding can be adjusted by the choice of Lewis acid or substitution pattern. Furthermore, it should be noted that the anionic NHCs known so far in the literature are based on modified imidazole rings. In this work heterocycles with only one nitrogen atom will be investigated, as well, in order to prepare first examples of anionic cAACs (Chapter 2.3).

CHAPTER I

TRICYANOBORANE IMIDAZOLE COMPOUNDS

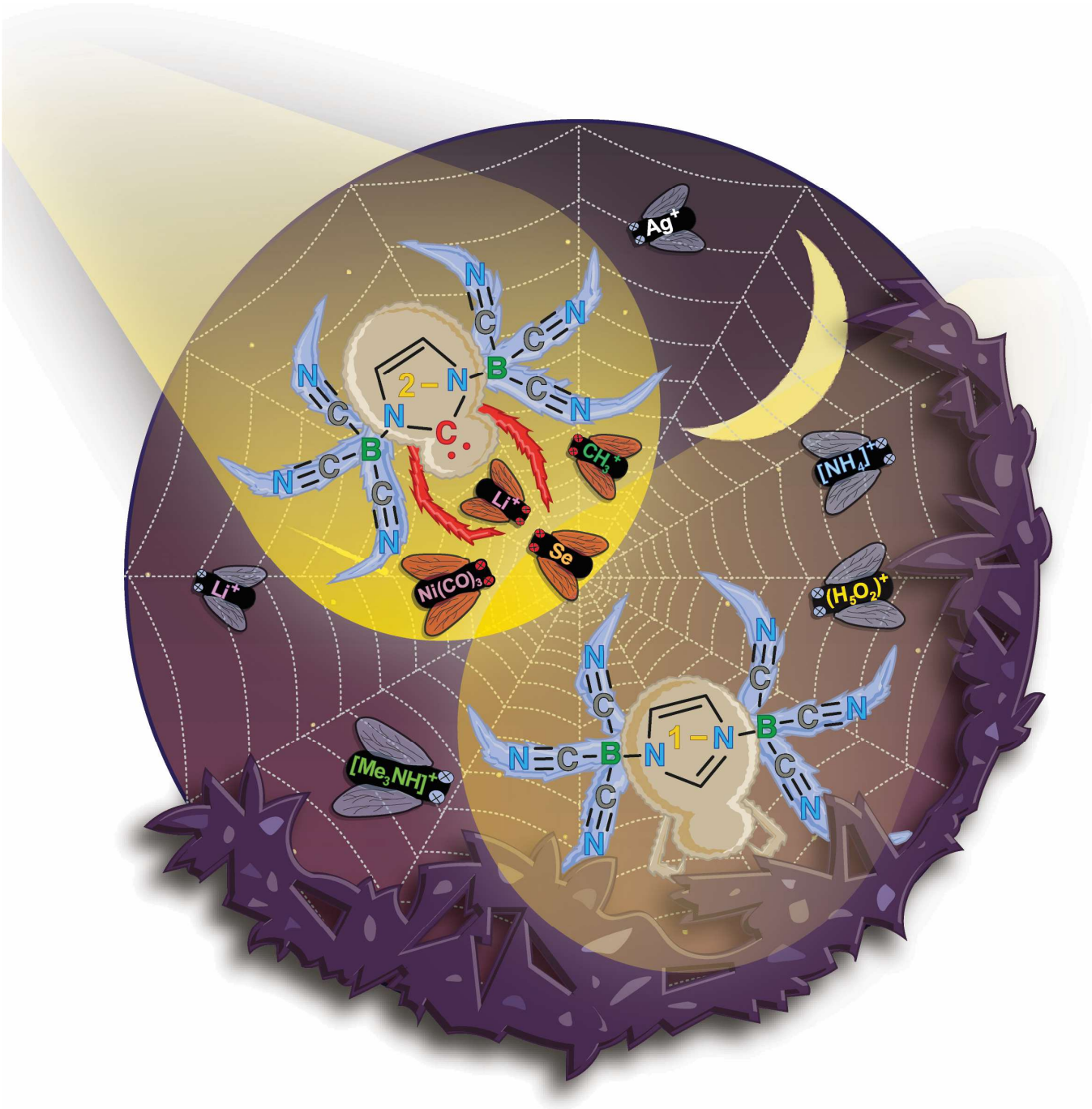

2. RESULTS AND DISCUSSION

2.1 Tricyanoborane Imidazole Compounds

2.1.1 Introduction

As described at the beginning of Chapter 1.2, borane imidazole compounds can be prepared by reacting Lewis acidic boranes with Lewis basic imidazole derivatives (Figure 1.2.1). In order for adducts with stable B−N bonds to be formed, it is crucial to use boranes with high Lewis acidity, otherwise the borane imidazole adducts will prove unstable to attack by nucleophiles and will hydrolyze readily in air.[30] If borane imidazole compounds shall be used as precursors for anionic *N*-heterocyclic carbenes, a high bond strength of the B−N bond is also a basic requirement to prevent an immediate follow-up reaction, namely a 1,2-rearrangement of the borane to the carbene carbon atom (Figure 1.4.2).[30] A second demand is necessary to qualify borane imidazoles as precursors for anionic NHCs, which is that no inter- or intramolecular nucleophilic attack of the carbene carbon on any of the substituents of the borane must occur after deprotonation. Otherwise, anellated bicyclic compounds may form, as shown in the example of **XXXIIc** (Figure 1.4.2).[105] Thus, the two criteria that can be derived for borane imidazoles to be suitable as precursors for stable anionic NHCs are:

- The borane must be highly Lewis acidic
- The substituents of the borane must be sufficiently chemically inert against nucleophilic attack

Cyano groups are well known to stabilize both boranes and borate ions due to their strong electron-withdrawing nature and their chemical and electrochemical stability.[111] Tricyanoborane $B(CN)_3$, which is a coordination polymer due to B−C≡N−B units,[112] is a strong Lewis acid as is obvious from its high fluoride ion affinity (FIA, 540 kJ·mol^{-1}).[113] The Brønsted acidity of its hydride adduct $[BH(CN)_3]^-$[114] was demonstrated by deprotonation to give the $B(CN)_3^{2-}$ dianion.[115,116] Furthermore, the large number of chemically stable tricyanoborate ions $[RB(CN)_3]^-$ with different substituents (R = CN,[112,117] F,[118,119] perfluoroalkyl,[120] CO_2H,[115] OH,[121] OMe,[122] …) shows the large stabilization effect of the $B(CN)_3$ group. The cyano groups attached to the boron are the reason for the unprecedented stability of the $[B_2(CN)_6]^{2-}$ dianion as well.[123] Keeping this high thermodynamic and kinetic stability of heteroatom−$B(CN)_3$ bonds accompanied by the high Lewis acidity of $B(CN)_3$ in mind, tricyanoborane was assumed to be an ideal building block for robust borane imidazole compounds and corresponding anionic NHCs.

The results of the chapter *Tricyanoborane Imidazole Compounds* were published in:
"*Tricyanoborane-Functionalized Anionic N-Heterocyclic Carbenes: Adjustment of Charge and Stereo-Electronic Properties*" L. Zapf, S. Peters, R. Bertermann, U. Radius, M. Finze, *Chem. Eur. J.* **2022**, *28*, e202200275; "*The crystal structure of poly[(μ_3-imidazolato-κ^3N:N:N')(tetrahydrofuran-κ^1O)lithium(I)], $C_7H_{11}LiN_2O$*" L. Zapf, M. Finze, *Z. Kristallogr. NCS* **2021**, *236*, 1007–1009; "*1,3-Bis(tricyanoborane)imidazoline-2-ylidenate Anion — A Ditopic Dianionic N-Heterocyclic Carbene Ligand*" L. Zapf, U. Radius, M. Finze, *Angew. Chem. Int. Ed.* **2021**, *60*, 17974–17980.
Experimental details can be found in the corresponding Supporting Information.

2.1.2 1-Methyl-3-(tricyanoborane)imidazole and 1,3-Bis(tricyanoborane)imidazolates

1-Methyl-3-(tricyanoborane)imidazole **1** was prepared from tricyanoborane-pyridine ($B(CN)_3$·py, py = pyridine)[13,124] and 1-methylimidazole in acetonitrile (Figure 2.1.2.1). Since the starting materials are easily accessible and because of the high yield of more than 95%, **1** can be synthesized on a multigram scale. Neutral **1** melts at 182 °C and decomposes at 360 °C (DSC, onset). It is stable towards air, moisture, and water. It was characterized by NMR and vibrational spectroscopy, single-crystal X-ray diffraction (SC-XRD), and high-resolution mass spectrometry (HRMS). Single crystals of **1** were obtained by slow evaporation of an acetone solution. The B1−N3 distance of 155.3(2) pm is in the range of related $B(CN)_3$ Lewis base adducts, for example 157.1 pm in $B(CN)_3$·py.[13]

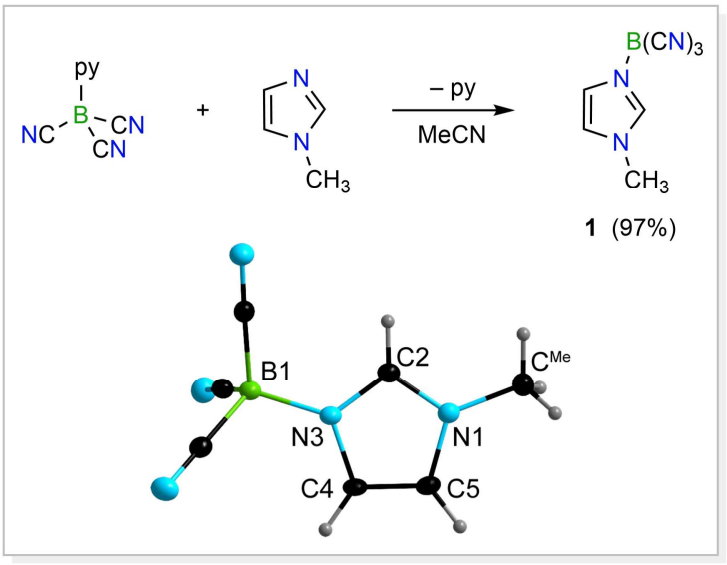

Figure 2.1.2.1 *Synthesis and crystal structure of **1** (ellipsoids are shown with 50% probability except for H atoms that are depicted with arbitrary radii). Selected bond lengths [pm] (mean value where applicable): B1–N3 155.3(2), C^{Me}–N1 146.6(2), N1–C2 132.9(2), C2–N3 133.3(2), N3–C4 138.9(2), C4–C5 134.9(2), C5–N1 138.1(2), B1–CN 159.9(2), C≡N 114.5(2).*

In order to increase the amount of $B(CN)_3$ groups attached to the imidazole ring and to introduce a negative charge, lithium imidazolate Li**2** can be used instead of 1-methylimidazole. Lithium imidazolate is a valuable starting compound for the synthesis of various imidazole-based derivatives and materials. Examples include biologically active compounds,[125] ligands for coordination chemistry,[126] and Li-ion conducting materials,[127] weakly coordinating anions (WCAs),[34,35] as well as components of electrolytes.[36,37] Molecular lithium imidazolate was studied by theoretical methods.[128-130] Furthermore, Li−N coordination in imidazolate species is an important motif in coordination chemistry, e.g. in covalent organic frameworks[131] and zeolitic imidazolate frameworks (ZIFs).[132,133] Surprisingly, no crystal structure analysis on lithium imidazolate has been published, before. Solvent free Li**2** was prepared in analogy to a literature known procedure, by deprotonating imidazole in toluene. Recrystallization of Li**2** in THF gave poly-[(μ_3-imidazolato-$\kappa^3N{:}N{:}N'$)(tetrahydrofuran-κ^1O)lithium(I)]

$^{2}_{\infty}$[Li**2**(THF)] as a two-dimensional coordination polymer (Figure 2.1.2.2). The lithium cation Li1 is tetrahedrally coordinated by the O atom of THF (*d*(Li1–O1) = 195.9(2) pm) and N atoms of three different imidazolate anions. The Li–N distances of the bridging N atom (*d*(Li1–N3'') = 208.8(2) pm and *d*(Li1–N3''') = 216.7(2) pm) are significantly shorter compared to *d*(Li1–N1) = 201.9(2) pm of the terminal coordinated N atom. The Li–N coordination results in a two-dimensional coordination polymer. In contrast, for lithium-bis(DMSO) benzimidazolate a chain structure was described, in which the Li ion is coordinated by two DMSO molecules and two N atoms of different benzimidazolate ions.[134]

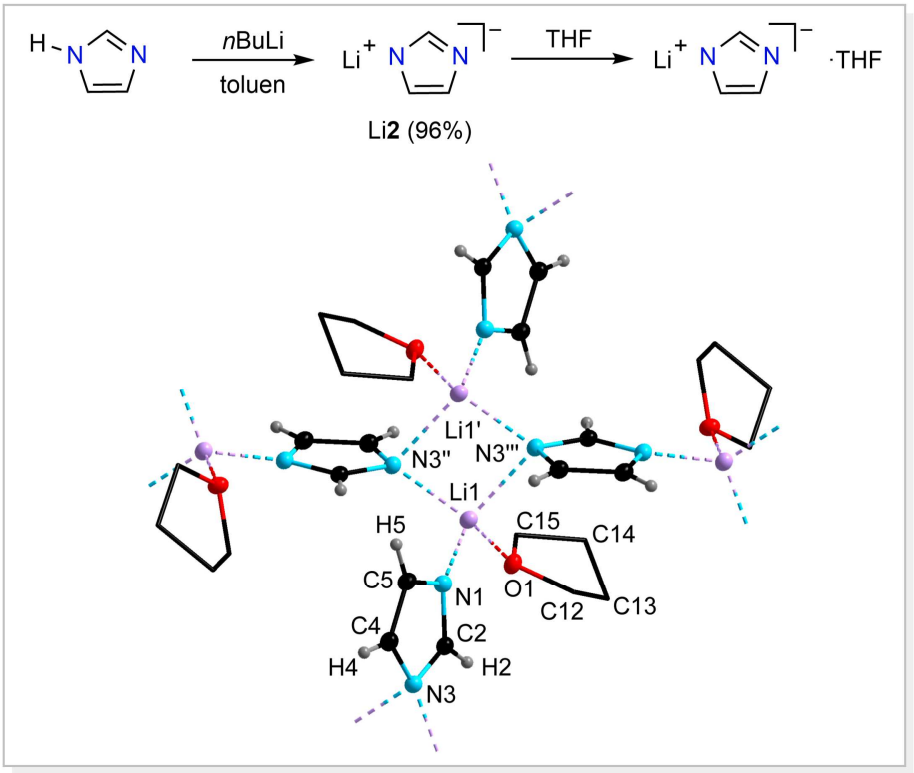

Figure 2.1.2.2 *Synthesis of Li**2** and crystal structure of* $^{2}_{\infty}$*[Li**2**(THF)] (ellipsoids are shown with 50% probability except for H atoms that are depicted with arbitrary radii, H atoms of the THF solvate molecules are omitted for clarity and the C atoms are shown as stick model). Selected bond lengths [pm] (mean value where applicable): Li1–O1 195.9(2), Li1–N1 201.9(2), Li1–N3'' 208.8(2), Li1–N3''' 216.7(2), N1–C2 133.8(1), C2–N3 134.9(1), N3–C4 138.1(1), C4–C5 136.7(1), C5–N1 137.5(1).*

Reacting Li**2** with two equivalents of $B(CN)_3$·py[13,124] afforded lithium 1,3-bis(tricyanoborane)imidazolate (Li**3**). The synthesis can be performed with a yield higher than 90% on a multigram scale. Li**3** is stable towards air, moisture, and even against aqueous acids and bases and it is thermally stable up to 336 °C (DSC, onset). It was characterized by NMR and vibrational spectroscopy and by SC-XRD. The intermediate of the formation of Li**3**, the mono-substituted lithium tricyanoborane-imidazolate (Li**4**) was isolated from a reaction mixture of $B(CN)_3$·py with Li**2** in dichloromethane and characterized by NMR spectroscopy and SC-XRD (Figure 2.1.2.3). Both salts Li**3** and Li**2** form three-dimensional coordination polymers in the crystals with tetrahedrally coordinated Li ions. The Li ion in

Li**4** is coordinated by the N atom of the imidazolate ion and three cyano N atoms. In Li**3** solely cyano N atoms are involved in the coordination to the metal ions. So, four of the six nitrogen atoms of the cyano groups are bonded to lithium, leaving one cyano group of each $B(CN)_3$ moiety without coordination. The bond length of the imidazolate rings in **3** and **4** reveal some differences that reflect the numbers of bonded $B(CN)_3$ groups.

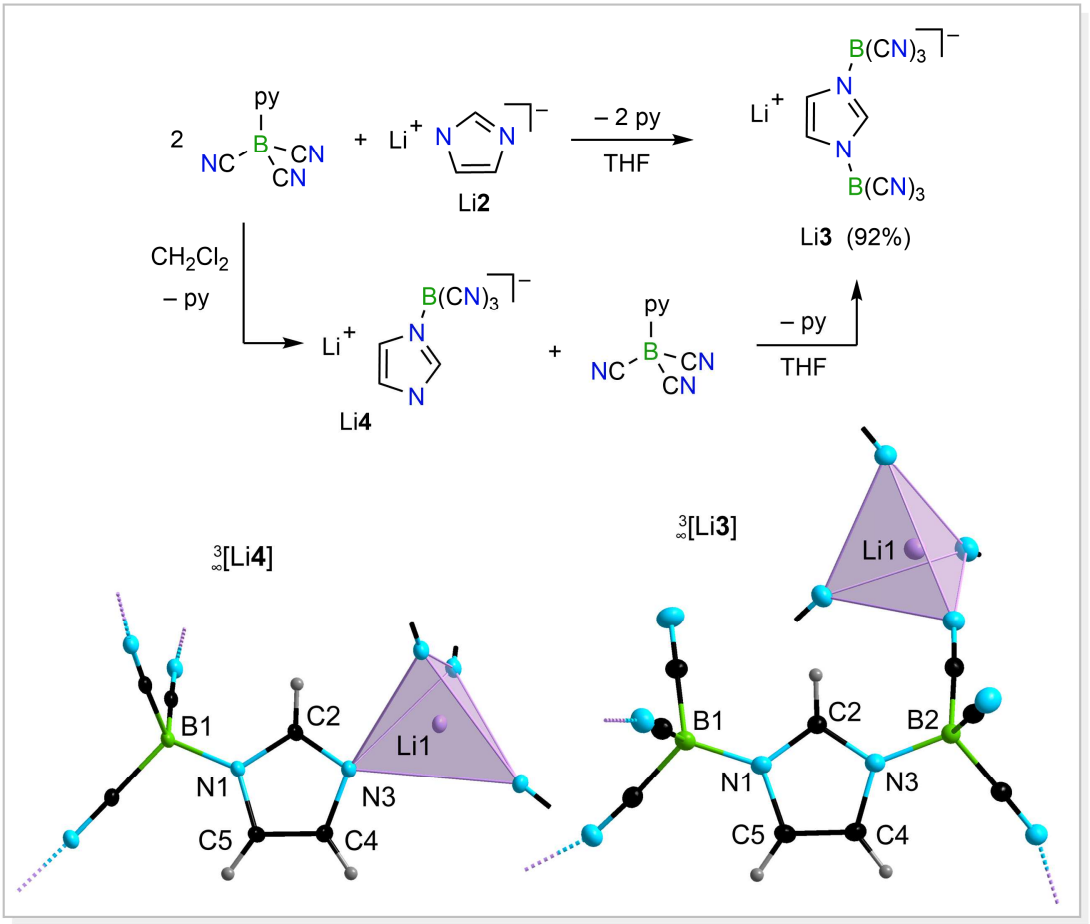

Figure 2.1.2.3 *Synthesis of Li**3** and crystal structures of* $^{3}_{\infty}$*[Li**3**] and* $^{3}_{\infty}$*[Li**4**] (ellipsoids are shown with 25% probability except for the H atoms that are depicted with arbitrary radii). Selected bond lengths [pm] (mean value where applicable):* $^{3}_{\infty}$*[Li**3**]: B1–N1 153.4(4), B2–N3 155.8(4), B–CN 159.2(4), C≡N 115.0(4), B–CN*^{Li} *159.9(5), C≡N*^{Li} *114.0(4), N1–C2 133.0(4), N3–C2 133.1(3), N1–C5 139.1(4), N3–C4 138.1(4), C4–C5 134.9(4), Li···N 202.6(5);* $^{3}_{\infty}$*[Li**4**]: B1–N1 153.2(2), B1–CN*^{Li} *160.2(2), C≡N*^{Li} *114.2(2), N1–C2 135.1(2), N3–C2 131.1(2), N1–C5 135.5(2), N3–C4 135.3(2), C4–C5 136.1(2), Li···N3 201.0(3), Li···NC 204.1(3).*

As exemplified by the coordination motif in crystalline Li**3**, anion **3** acts as bridging ligand that forms coordination polymers. The silver salt Ag**3**, which was obtained from the reaction of Li**3** and $AgNO_3$ in water in 86% yield, is an example for a transition metal salt of **3** (Figure 2.1.2.4). Ag**3** forms a complex three-dimensional coordination polymer with six independent formula units in the unit cell (monoclinic, *I*2/*a*, *Z* = 48). The silver ions are distorted tetrahedrally coordinated. Like Li**3**, two cyano groups per $B(CN)_3$ unit are bonded to Ag^{I} and the remaining third CN group is not coordinated.

The reaction of aqueous solutions of [Me_3NH]Cl and Li**3** gave the corresponding trimethylammonium salt of **3** (91% yield), which is an example for an organic salt of **3**. Discrete [Me_3NH]**1** units are present in the crystal. The ions, [Me_3NH]$^+$ and **3**, are connected by a single H bond from the ammonium hydrogen atom to one CN group (Figure 2.1.2.4). The salts Ag**3** and [Me_3NH]**3** are thermally very robust. Ag**3** melts under decomposition at 313 °C (DSC, onset). [Me_3NH]**3** melts at 161 °C and decomposition starts at 220 °C (DSC, onset).

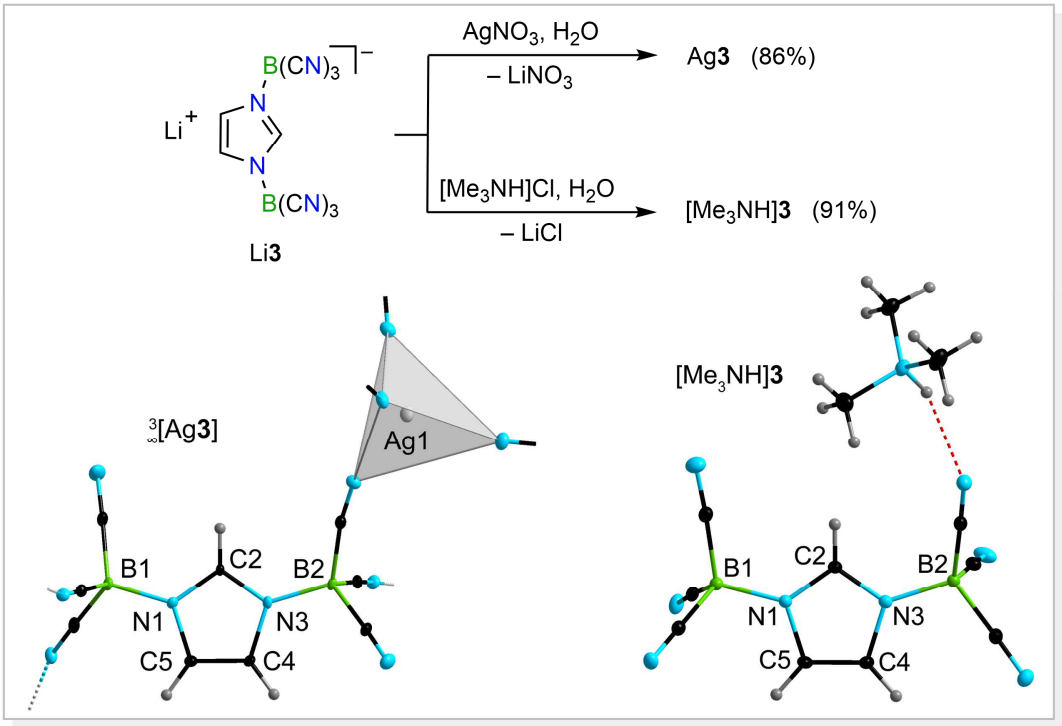

Figure 2.1.2.4 *Synthesis of Ag**3** and [Me_3NH]**3** and crystal structures of $^3_\infty$[Ag**3**] and [Me_3NH]**3** (ellipsoids are shown with 25% probability except for the H atoms that are depicted with arbitrary radii). Selected bond lengths [pm]: $^3_\infty$[Ag**3**] (distances ranges for all three independent formula units): B–N 153.4(8)–155.7(8), B–C 156.9(9)–161.4(8), C≡N 112.9(8)–115.5(8), N–C2 133.2(7)–134.2(7), N1–C5/N3–C4 137.2(8)–140.0(8), C4–C5 132.7(10)–135.4(8), Ag···N 221.6(8)–234.2(8); [Me_3NH]**3** (mean values where applicable): B1–N1 155.4(2), B2–N3 155.6(3), B–CN 159.7(3), C≡N 114.4(3), N1–C2 133.0(2), N3–C2 133.9(2), N1–C5 138.6(2), N3–C4 138.5(2), C4–C5 134.6(3), N^{cation}···H 96(2), N^{CN}···H 216(2), N^{cation}···N^{CN} 296.6(2).*

Treatment of Li**3** with hydrochloric acid followed by extraction with diethyl ether resulted in (H_5O_2)**3** in 77% yield (Figure 2.1.2.5). (H_5O_2)**3** is an example for a non-metal coordination polymer in which the Zundel ions and **3** form a three-dimensional network. The non-hygroscopic salt (H_5O_2)**3** melts at 141 °C, which is accomplished by loss of one equivalent of water. At 164 °C release of HCN, CO, and minor amounts of H_2O was observed *via* IR spectroscopy and mass spectrometry by STA measurements. The thermal analysis was repeated in a melting capillary, which gave crystals of [NH_4]**3**. Similar to (H_5O_2)**3**, cations and anions are connected by albeit weak H bonds (Figure 2.1.2.5). This latter thermal behavior is close to that of (H_3O)[$B(CN)_4$].[135]

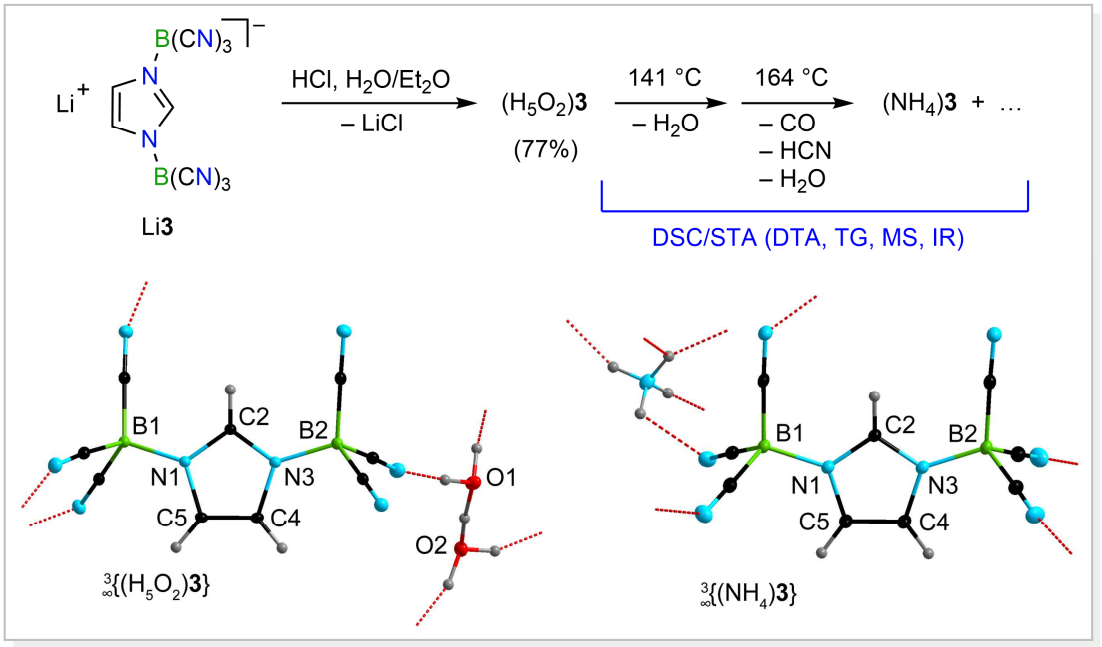

Figure 2.1.2.5 *Synthesis of (H_5O_2)**3** and its transformation into $[NH_4]$**3** and crystal structures of $^3_\infty\{(H_5O_2)$**3**$\}$ and $^3_\infty\{(NH_4)$**3**$\}$ (ellipsoids are shown with 30% probability except for the H atoms that are depicted with arbitrary radii). Selected bond lengths [pm] (mean values where applicable): $^3_\infty\{(H_5O_2)$**3**$\}$: B1–N1 154.38(14), B2–N3 155.26(15), B–CN 159.1(2), C≡N 114.5(2), N1–C2 133.53(14), N3–C2 133.38(13), N1–C5 138.42(14), N3–C4 138.57(14), C4–C5 134.73(15), O1–H 91(2) and 93(2), O2–H 89(2) and 90(2), O1–H^{bridge} 124(3), O2–H^{bridge} 119(3), O1···O2 242.9(1), N···H^{range} 178(2)–197(2), N···O^{range} 270.98(14)–283.54(14); $^3_\infty\{(NH_4)$**3**$\}$: B–N 155.1(5), B–CN 159.5(5), C≡N 114.5(4), N–C2 132.8(4), N1–C5/N3–C4 137.9(5), C4–C5 134.8(5).*

2.1.3 Ditopic Tricyanoboraneimidazolin-2-ylidenate Anions

With the neutral 1-methyl-3-(tricyanoborane)imidazole **1** as starting material for an anionic NHC in hand, its deprotonation was investigated. Lithium and potassium hexamethyldisilazide were found to be suitable bases for the formation of the 1-methyl-3-(tricyanoborane)imidazolin-2-ylidenate anion **5**. Treatment of **1** with a small excess of LiHMDS in THF resulted in Li**5**·$(THF)_{0.5}$ as a solid in a yield of 85% (Figure 2.1.3.1). K**5**·(Et_2O) precipitated upon addition of diethyl ether from the reaction mixture in THF and was isolated in 96% yield (Figure 2.1.3.1). The selective deprotonation of **1** at the C2 atom to result **5** was confirmed by NMR spectroscopy (Figure 2.1.3.1). The ^{11}B NMR signal is shifted from −22.5 (**1**) to −24.1 ppm (**5**). The signal of the backbone H atom at C5 (H5) of **5** reveals coupling to boron ($^4J(^{11}B,^1H)$) that is not observed for **1** (Figure 2.1.3.1). The most significant difference was observed in the $^{13}C\{^1H\}$ NMR spectrum for the C2 nucleus. Its signal was shifted from 139.7 (**1**) to 205.4 ppm (Li**5**) or 211.9 ppm (K**5**), which is in the typical range observed for $C_{carbene}$ nuclei, for example 215.2 ppm for IMe (1,3-dimethylimidazolin-2-ylidene),[64] or 211.2 ppm for **XXIX** (1,3-di-*tert*-butyl-5-(tris(pentafluorophenyl)-borane)imidazolin-2-ylidenate).[91] Furthermore, the signal is split into a quartet due to the coupling to ^{11}B with $^2J(^{13}C,^{11}B)$ of 11.8 Hz.

To evaluate if solvated anion **5** can be considered as NHC and not only as a lithio- or potassio-carbenoid, metathesis with $[Me_4N]F$ to yield $[Me_4N]$**5** in a yield of 79% was performed (Figure 2.1.3.1). $[Me_4N]$**5** was characterized by NMR and vibrational spectroscopy as well as by elemental analysis. The tetramethylammonium salt is stable and storable as a solid. In solution, anion **5** is methylated at the C2 atom by $[NMe_4]^+$ under formation of trimethylamine. Due to the relatively fast decomposition, it was not possible to obtain a meaningful $^{13}C\{^1H\}$ NMR spectrum in solution. However, solid state ^{13}C MAS NMR spectra of both salts, $[Me_4N]$**5** and Li**5**, respectively, were recorded (Figure 2.1.3.1). Surprisingly, a minor shift of the signal of the C2 nucleus from 200.7 (Li**5**) to 202.0 ppm ($[Me_4N]$**5**) was observed, supporting the assumption that the electronic influence of the Li^+ and K^+ cation on the anionic NHC **5** is small. This is in accordance with $\delta(^{13}C)$ of **XXIX** with Li^+ ($\delta(^{13}C)$ = 217.4 ppm) and $[PPh_4]^+$ ($\delta(^{13}C)$ = 218.8 ppm) as a counter cation. In contrast to $[Me_4N]$**5**, Li**5** and K**5** are stable in solution and in the solid state for month at room temperature. Decomposition starts at more than 70 °C in solution and in the solid state (DSC, onset). Hence, Li**5**·$(THF)_{0.5}$ and K**5**·$(Et_2O)_{0.5}$ are thermally more robust than IMe, which gradually decomposes already at room temperature.[64] This highlights the stabilizing effect of the tricyanoborane moieties as substituent at the N atom of NHCs.

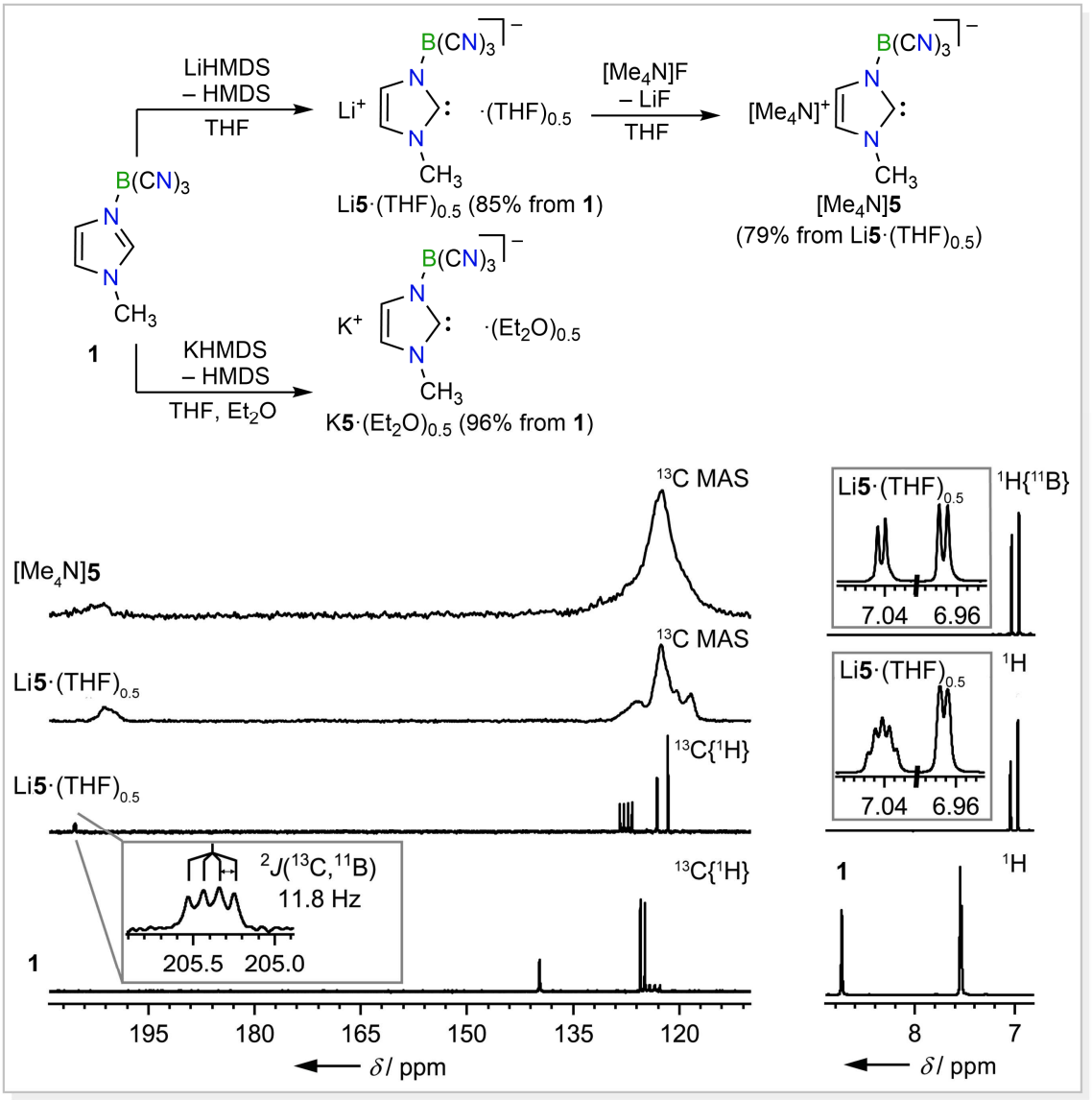

Figure 2.1.3.1 *Syntheses of Li**5**·(THF)$_{0.5}$, K**5**·(Et$_2$O)$_{0.5}$, and [Me$_4$N]**5** (top) and NMR spectra of **1**, Li**5**·(THF)$_{0.5}$, and [Me$_4$N]**5** (bottom).*

For 1,3-bis(tricyanoborane)imidazolate **3** the deprotonation of the lithium (Li**3**) and trimethylammonium salts ([Me$_3$NH]**3**) were investigated. LiHMDS and *n*BuLi proved to be suitable bases to yield the 1,3-bis(tricyanoborane)imidazolin-2-ylidenate dianion (**6**), which is the first example for a dianionic bis(borane)-substituted NHC. For example, Li**3** and one equivalent of *n*BuLi were used for the synthesis of Li$_2$**6** in a yield of 95% (Figure 2.1.3.2). The ^{11}B NMR signal is shifted from −25.4 (**3**) to −24.1 ppm (**6**). In the ^{1}H NMR spectrum of **6** only one resonance for the backbone H atoms was detected. The most significant difference was observed in the ^{13}C{^{1}H} NMR spectrum for the signal of the C2 nucleus. This signal was shifted from 140.9 (**3**) to 205.9 ppm (**6**), which is almost identical to the shift of 205.4 ppm for the lithium salt of monoanionic NHC **5**. However, for **6** the signal is split into a septet due to the coupling to two ^{11}B nuclei with $^{2}J(^{13}C,^{11}B)$ of 11.7 Hz (Figure 2.1.3.2). The lithium salt Li$_2$**6**·THF starts to lose THF at ca. 100 °C in the solid state and is stable to more than 150 °C. Hence, Li$_2$**6**·THF is thermally

more robust than Li**5**·(THF)$_{0.5}$ underlining the trend that formal substitution of methyl groups against $B(CN)_3^-$ improves the thermal stability of an NHC.

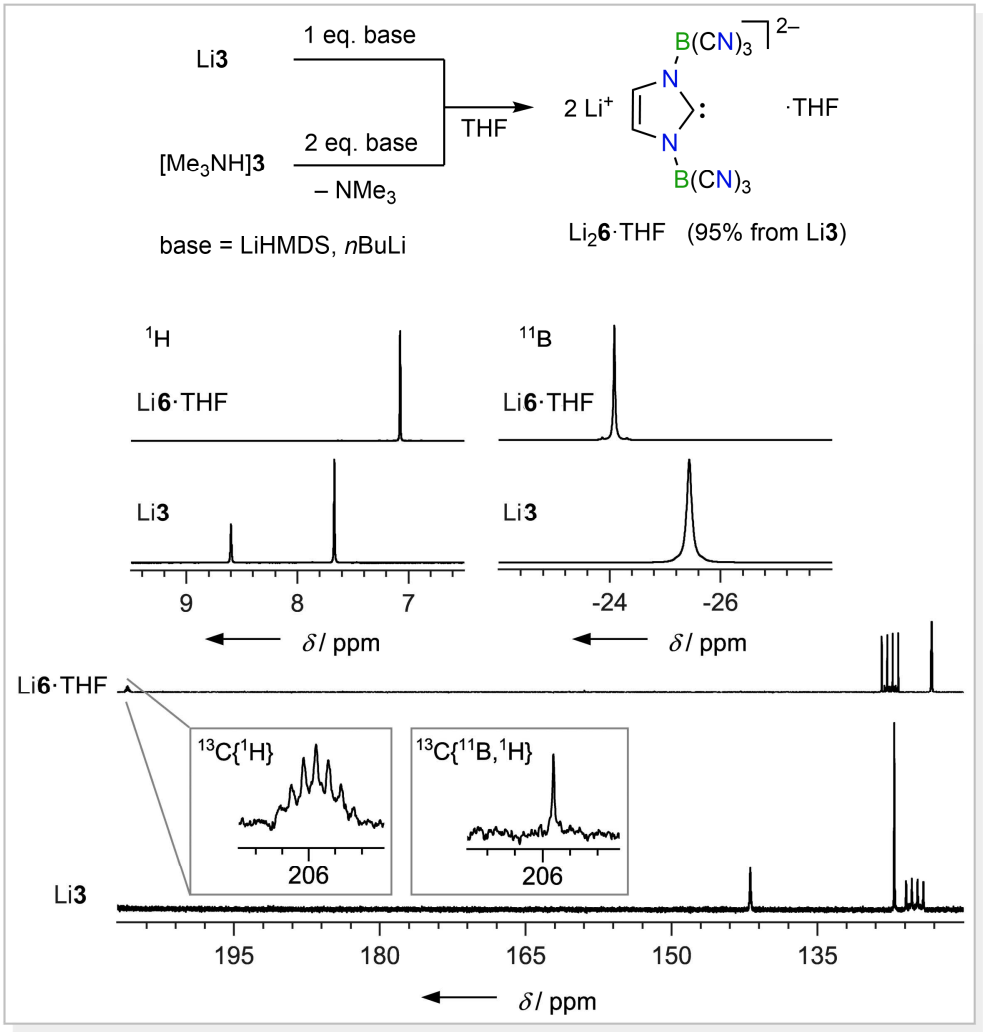

Figure 2.1.3.2 *Syntheses of Li$_2$**6**·THF (top) and NMR spectra of Li**3** and Li$_2$**6**·THF (bottom).*

Single crystals of $^2_\infty$[Li**5**(THF)] were obtained from THF. The carbene units form cyclic dimers *via* bridging Li1 atoms (Figure 2.1.3.3). These dimers are interconnected to strands. The lithium ion is coordinated to the C2 carbene atom and to two CN groups of different anions **5**, which highlights the ditopic nature of **5**. The distorted tetrahedral coordination at the lithium cation is completed by a THF ligand. The Li1···C2 distance of 217.0(6) pm is similar to related Li···C$_{carbene}$ separations, for example 215.5(4) pm in [I*t*Bu$_2$]Li(η^5-1,2,4-(Me$_3$Si)$_3$C$_5$H$_2$)][136] and 209.2(2)/209.4(3) in [Li**XXIX**(THF)$_2$].[91] Crystallization of Li**5** from THF in the presence of 12-crown-4 led to single crystals of [{Li(12-crown-4)}**5**]·(12-crown-4) (Figure 2.1.3.3). The Li ion in [{Li(12-crown-4)}**5**]·(12-crown-4) is coordinated to the C2 carbene atom and to all four oxygen atoms of 12-crown-4. In contrast to $^2_\infty$[Li**5**(THF)], the cyano N atoms do not participate in the coordination to lithium. Single crystals of $^3_\infty$[K**5**(THF)] were obtained by diffusion of hexane into THF. Two formula units of K**5**·THF form dimers, similar to $^2_\infty$[Li**5**(THF)]. The potassium cation

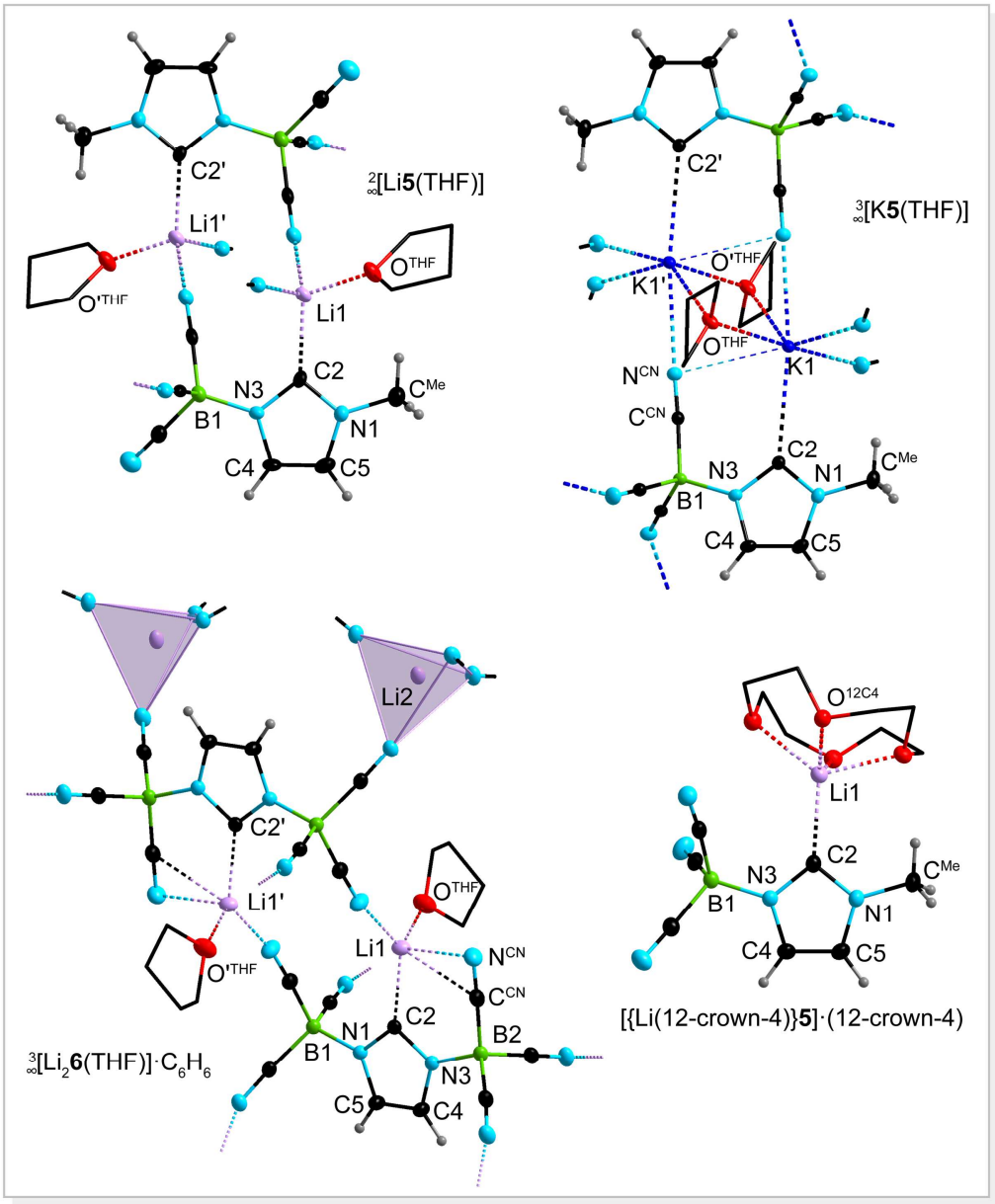

Figure 2.1.3.3 *Crystal structures of* $^{2}_{\infty}$*[Li**5**(THF)],* $^{3}_{\infty}$*[K**5**(THF)], [{Li(12-crwon-4)}**5**]·(12-crown-4), and* $^{3}_{\infty}$*[Li$_2$**6**(THF)]·C$_6$H$_6$ (ellipsoids are shown with 50% probability (*$^{2}_{\infty}$*[Li**5**(THF)],* $^{3}_{\infty}$*[K**5**(THF)], [{Li(12-crwon-4)}**5**]·(12-crown-4)) or 25% probability (*$^{3}_{\infty}$*[Li$_2$**6**(THF)]·C$_6$H$_6$) except for the H atoms that are depicted with arbitrary radii, disorder and H atoms of the THF solvate molecules and of the coordinated 12-crown-4 are not shown and their C atoms are depicted as wireframe model, the co-crystallized C$_6$H$_6$ and 12-crown-4 are omitted for clarity). Selected bond lengths [pm] (mean value where applicable):* $^{2}_{\infty}$*[Li**5**(THF)]: B1–N3 153.4(4), C^{Me}–N1 146.0(4), N1–C2 135.9(4), C2–N3 137.7(4), N3–C4 138.7(4), C4–C5 133.7(4), C5–N1 138.4(4), B1–CN 160.4(6), C≡N 114.9(4), Li1···C2 217.0(6), Li1···O^{thf} 196.7(6), Li1···NC 196.5(5);* $^{3}_{\infty}$*[K**5**(THF)]: B1–N3 152.1(2), C^{Me}–N1 146.0(2), N1–C2 136.5(2), C2–N3 137.3(2), N3–C4 139.4(2), C4–C5 134.3(2), C5–N1 138.2(2), B1–CN 160.7(2), C≡N 114.4(2), K1···C2 298.7(1), K1···O^{thf} 306.6(2), K1···NC 285.6(1), K1···N^{CN} 307.1(1); [{Li(12-crwon-4)}**5**]: B1–N3 153.3(2), C^{Me}–N1 145.9(2), N1–C2 136.4(2), C2–N3 137.3(2), N3–C4 138.8(2), C4–C5 134.4(2), C5–N1 138.2(2), B1–CN 160.4(2), C≡N 114.7(2), Li1···C2 221.8(3), Li1···O^{12C4} 215.2(2);* $^{3}_{\infty}$*[Li$_2$**6**(THF)]: B1–N1 152.7(3), B2–N3 153.0(4), B–CN 160.0(5), C≡N 114.5(5), N1–C2 136.2(3), N3–C2 136.9(3), N1–C5 139.3(4), N3–C4 138.6(4), C4–C5 133.9(5), Li1···C2 215.1(6), Li1···N 200.2(5), Li1···N^{CN} 243.4(7), Li1···C^{CN} 259.5(6), Li1···O1 190.1(12), Li2···N^{range} 200.9(5)–203.5(5).*

adopts a distorted pentagonal bipyramidal coordination sphere spanned by one $C_{carbene}$ atom, four CN groups, and two THF molecules (Figure 2.1.3.3). The K1···C2 distance of 298.7(1) pm is similar to related K···$C_{carbene}$ separations, for example 298.6(2) pm in $[\{H_2C(I\textit{i}Pr)_2\}KN(SiMe_3)_2]_2$.[137] Compared to **1**, the B−N distance in **5** is slightly shorter (153.4(3) pm), whereas *d*(C2−N) are a little longer. Both differences reflect the increased electron density at the C2 carbene atom in **5**, which results in a slight weakening of the C2−N bonds, an increased basicity of the N atoms in the ring, and in turn, a stronger B−N bond.

Single crystals of $^{3}_{\infty}[Li_2\mathbf{6}(THF)]\cdot C_6H_6$ were obtained from a saturated benzene solution of the dilithium salt. The benzene molecules are severely disordered and their contribution to the structure factors was taken into account using the SQUEEZE routine as implemented in the Platon program.[138,139] Two carbene units form cyclic dimers *via* bridging Li1 atoms (Figure 2.1.3.3). Li1 is coordinated to the C2 carbene carbon atom and to one CN group of the second NHC moiety. In addition, Li1 is oriented towards a $B(CN)_3$ unit of the parent dianionic NHC resulting in CN π-coordination. The coordination sphere of Li1 is completed by a THF ligand. The Li1···C2 distance of 215.1(6) pm is similar to that in $^{2}_{\infty}[Li\mathbf{5}(THF)]$. The lithium cation Li2 is tetrahedrally coordinated by CN groups of different anions **6**. In accordance to anionic NHC **5**, the B−N and C−N bond lengths of **6** differ from those of **3**, indicating the increased electron density at the C2 carbene atom and the increased basicity of the N atoms in the ring.

DFT calculations (def2-TZVPP/B3LYP/D3(BJ)/COSMO [ε = infinite]) were performed to evaluate the electronic features of anionic NHC **5** and dianionic NHC **6** in comparison to the neutral NHC IMe. For IMe, the electronic structure can be considered as a 6 π-electron aromatic system that is superimposed with the NHC carbene σ-type orbital, which is basically a sp^2-type hybrid orbital. The latter is the HOMO of the molecule and lies at −6.36 eV calculated at this level of theory (Figure 2.1.3.4). The carbene π-orbital of IMe is the LUMO+1 (the LUMO is another orbital of the NHC π-system), mainly centered at the carbene carbon atom, and is mostly composed of the carbene p orbital. This unoccupied orbital lies at +0.70 eV, which leads to a σ/π-separation of 7.06 eV. This separation decreases continuously upon successive formal replacement of the methyl against $B(CN)_3^-$ substituents to 6.82 eV for **5** and 6.61 eV for **6**. The HOMO is always the NHC σ-orbital, whereas the relevant NHC π-orbital varies. In case of IMe it is the LUMO+1, in case of **5** the LUMO+3, and for **6** the LUMO+6 (Figure 2.1.3.4). For the cyanoboron-substituted compounds, some C≡N antibonding combinations are located in between the NHC σ- and π-orbitals. However, as $B(CN)_3$ substitution proceeds, the NHC π-orbitals decrease in energy going from +0.70 eV (IMe) to +0.58 eV (**5**) to +0.48 eV (**6**), whereas the orbital energy of the σ-orbital increases going from −6.36 eV (IMe) to −6.24 eV (**5**) to −6.13 eV (**6**). Thus, the donor and the acceptor capabilities of the different NHCs increase in the row IMe < **5** < **6**, as verified experimentally (Chapter 2.1.4).

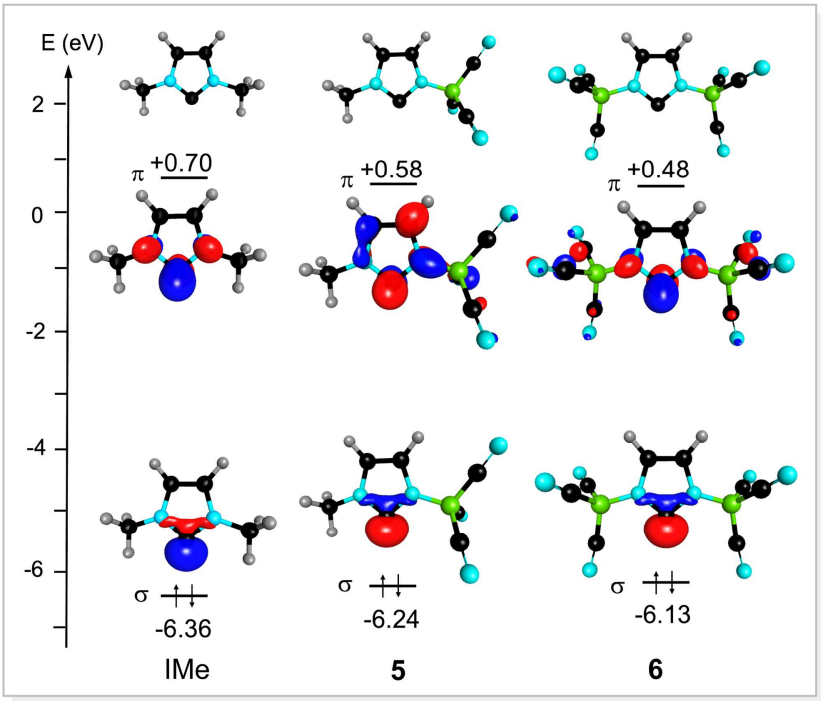

Figure 2.1.3.4 *NHC σ- and π-orbitals of IMe,* ***5****, and* ***6****. Energies were calculated at the def2-TZVPP/B3LYP/D3(BJ)/COSMO [ε = infinite] level of theory and orbital plots were drawn at the 0.1 isosurface.*

2.1.4 Alkylation, Main Group Element Adducts, and Transition Metal Complexes

To get an impression on the basic reactivity of the novel anionic NHCs **5** and **6** and to assess their σ-donating and π-accepting properties experimentally, Li**5** and Li_2**6** were reacted with methyl iodide, the chalcogens sulfur, selenium, and tellurium, as well as nickel tetracarbonyl as archetypical reactions for organic, main group element, and transition metal substrates.

Methylation of **6** with methyl iodide afforded anion **7** that was isolated as tetraethylammonium salt (Figure 2.1.4.1), which melts at 125 °C and decomposes at 326 °C (DSC, onset). The bond parameters of the imidazolate ring and the $B(CN)_3$ units in **7** are close to those of the parent protonated species **3**.

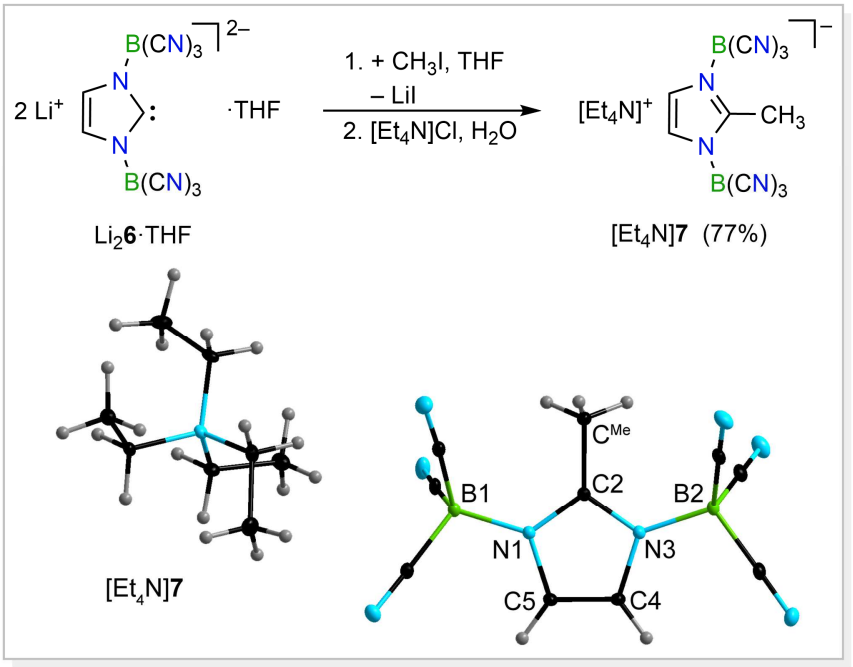

Figure 2.1.4.1 *Synthesis (top) and crystal structure (bottom) of [Et_4N]**7** (ellipsoids are shown with 25% probability except for H atoms that are depicted with arbitrary radii). Selected bond lengths [pm] (mean values where applicable): C2–C^{Me} 149.04(13), B1–N1 155.75(13), B2–N3 155.46(12), B–CN 159.9(2), C≡N 114.5(2), N1–C2 134.06(11), N3–C2 134.25(12), N1–C5 138.82(12), N3–C4 138.72(11), C4–C5 134.63(11).*

Treatment of **5** with methyl iodide resulted in the formation of 1,2-dimethyl-3-(tricyanoborane)-imidazole **8** in an internal yield of 52%. However, 1-Methyl-3-(tricyanoborane)imidazole (**1**) and the related ethylated imidazole **9** were obtained as side products in equimolar amounts (24%, Figure 2.1.4.2). Formation of **1** and **9** can be rationalized by a methylene intermediate, which is formed by the deprotonation of **8** with unreacted anionic NHC **5**. The methylene intermediate subsequently reacts with methyl iodide to form **9** (Figure 2.1.4.2). The ethyl derivative **9** was obtained as sole product by the reaction of Li**5** and ethyl iodide. The synthesis of the related methylene derivative 1,3-dimethyl-2-methyleneimidazole was also accomplished by deprotonation of 1,2,3-trimethylimidazole with strong bases such as KHMDS or KH as reported previously.[140,141] Anyway, considering all side products the reaction of Li**5** with methyl iodide proceeds quantitatively. The different behavior of Li**5** and Li_2**6**

towards methyl iodide may be explained by the higher steric hindrance of **6** or the different electronic properties of both NHCs and consequently of the related C2-ethylated derivatives. Single crystals of $^{3}_{\infty}$[**3**·LiI(H_2O)] were obtained from the reaction mixture under air (Figure 2.1.4.2). The Li cation is coordinated to three CN groups of different imidazole units and one aqua ligand. Thus, the structure exemplifies the coordination ability of the tricyanoborane moiety even in case of neutral imidazole derivatives such as **8**.

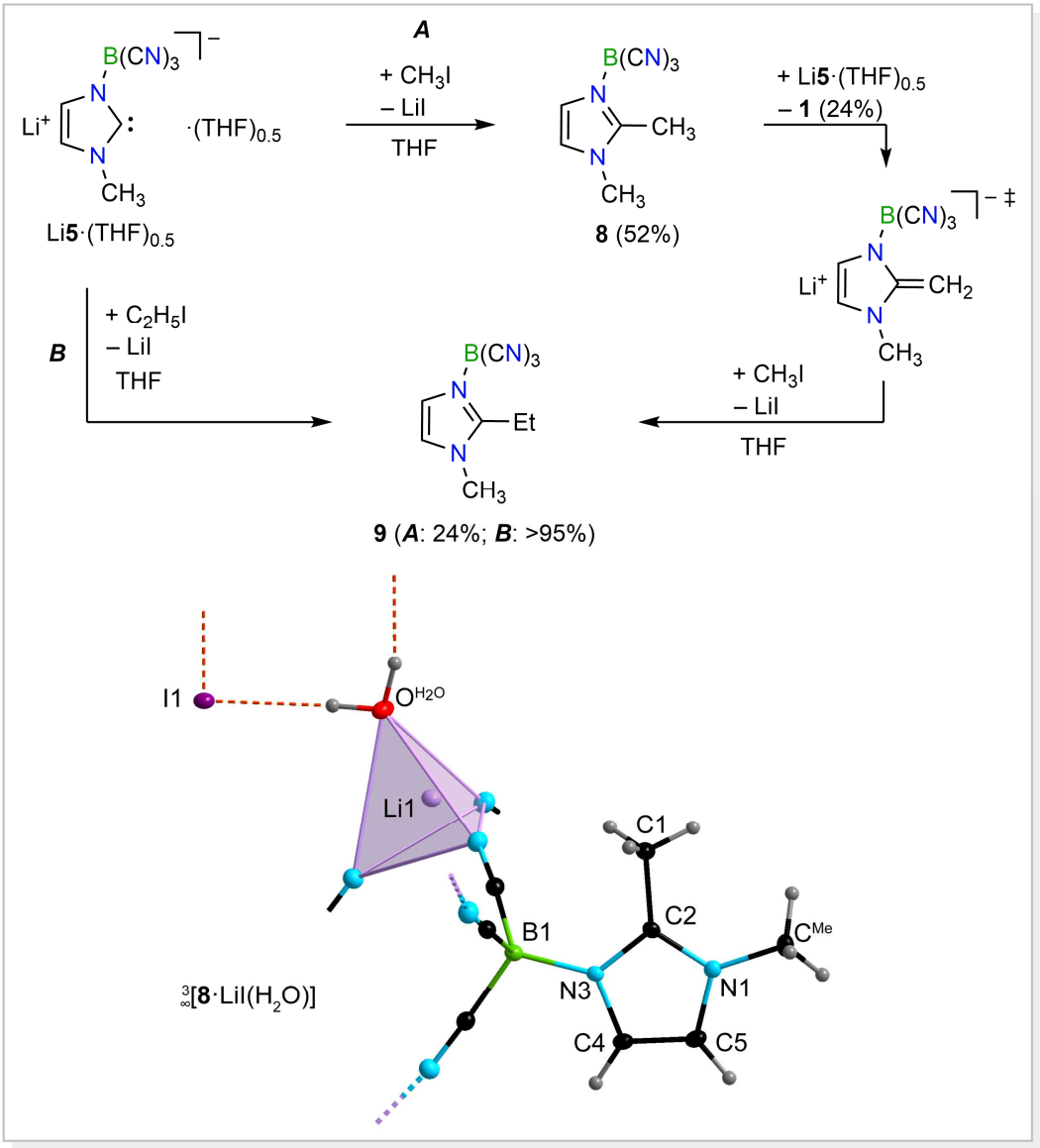

Figure 2.1.4.2 *Formation of a mixture of **8**, **9**, and **1** and selective synthesis of **9** by ethylation of Li**5** (top) and crystal structure $^{3}_{\infty}$[**8**·LiI(H_2O)] (ellipsoids are shown with 35% probability except for H atoms that are depicted with arbitrary radii). Selected bond lengths [pm] (mean value where applicable): C^{Me}–N1 146.7(2), N1–C2 133.6(2), C2–N3 134.9(2), N3–C4 138.8(2), C4–C5 135.0(2), C5–N1 138.2(2), B1–N3 154.3(2), B1–CN 160.6(2), C≡N 114.4(2), C1–C2 148.8(2), Li1···NC 207.1(3), Li1···O^{H2O} 187.5(3), I1···H^{H2O} 255.2(16).*

The reaction of elemental selenium with Li**5**·(THF)$_{0.5}$ and Li$_2$**6**·(THF) in tetrahydrofuran gave the selenourea Li**10**·(THF) and Li$_2$**11**·(H$_2$O)$_4$ (Figure 2.1.4.3). Crystallization of Li**10** from wet THF afforded single crystals of $^3_\infty$[Li**10**(H$_2$O)]. The tetrahedral coordination at lithium is composed of three cyano groups and an aqua ligand (Figure 2.1.4.4).

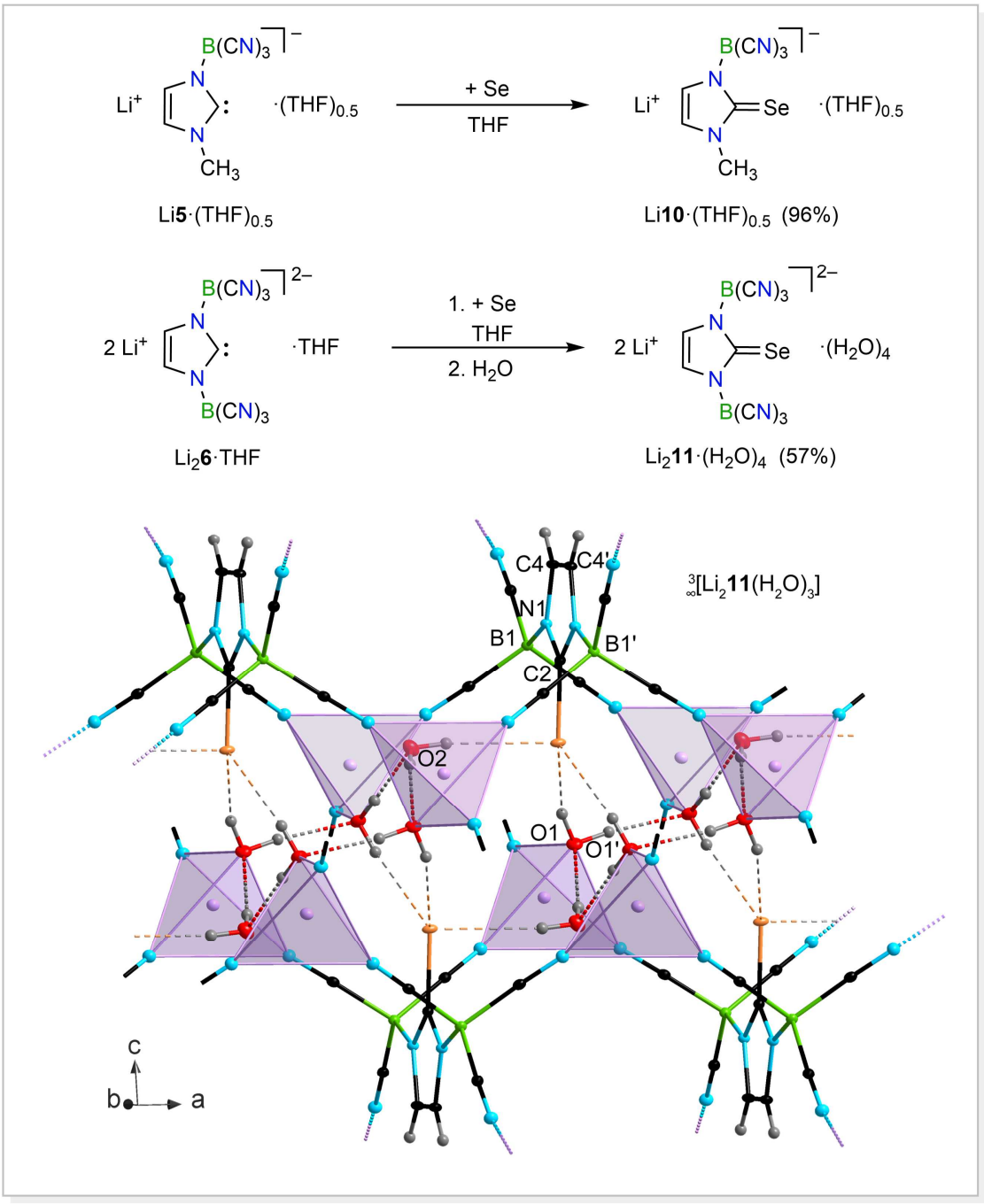

Figure 2.1.4.3 *Syntheses of Li**10**·(THF)$_{0.5}$ and Li$_2$**11**·(H$_2$O)$_4$ and crystal structure of $^3_\infty$[Li$_2$**11**(H$_2$O)$_3$] (ellipsoids are shown with 25% probability except for H atoms that are depicted with arbitrary radii, disorder of the H atoms of the water molecules are not shown). Selected bond lengths [pm] (mean values where applicable): $^3_\infty$[Li$_2$**11**(H$_2$O)$_3$]: C2=Se 185.2(2), B1–N1 153.5(3), B1–CN 160.5(3), C≡N 114.4(3), N1–C2 135.5(2), N1–C4 139.7(2), C4–C4' 134.4(3), Li···N 203.2(4), Li···O 192.5(4), O1···O1'' 274.6(2), O1···O2 277.6(2), Se···O1 331.48(17), Se···H^{O1} 263(3), Se···O2 343.1(2), Se···H^{O2} 262(6).*

The C=Se distance of 185.3(5) pm is in the typical range observed for selenoureas, for instance 184.2(4) pm in IMe=Se. $^{3}_{\infty}$[Li**10**(H_2O)] reveals weak Se···H_2O bonds[142] of 279.1(14) and 281.5(12) pm. Crystallization of Li_2**11** from water yielded crystals of $^{3}_{\infty}$[Li_2**11**$(H_2O)_3$] while a mixed solvent system of THF and dichloromethane gave single crystals of $^{2}_{\infty}$[Li_2**11**$(THF)_2$]. The Li atoms are tetrahedrally coordinated in both structures. All cyano groups are involved in coordination, which is complemented by the O atoms of THF or water, respectively. In $^{3}_{\infty}$[Li_2**11**$(H_2O)_3$] two crystallographically independent water molecules are arranged to cyclic hexamers with chair conformation[143] (Figure 2.1.4.3).

These water clusters are coordinated to four Li atoms (Li···O1). The C=Se distances in both related structures are significantly different (>3σ) with 183.34(14) and 185.2(2) pm for $^{3}_{\infty}$[Li_2**11**$(H_2O)_3$] and $^{2}_{\infty}$[Li_2**11**$(THF)_2$], respectively. A close inspection of the structure of $^{3}_{\infty}$[Li_2**11**$(H_2O)_3$] shows the presence of three weak Se···H bonds (263(3) (2×) and 262(6) pm (1×)) with H_2O as hydrogen bond donor. This intermolecular selenium hydrogen bonding might be the reason for a slight lengthening of the C=Se bond in $^{3}_{\infty}$[Li_2**11**$(H_2O)_3$]. The importance of intermolecular Se···H interactions was mentioned earlier.[144] Recently, intermolecular selenium-hydrogen interactions were used to rationalize deviations of $\delta(^{77}Se)$ from expected values.[145] The difference in *d*(C=Se) observed for dianion **11** in $^{3}_{\infty}$[Li_2**11**$(H_2O)_3$] and $^{2}_{\infty}$[Li_2**11**$(THF)_2$] thus provides further evidence for the sensitivity of the carbon selenium double bond against H bonding.

The ^{77}Se chemical shift of Li**10** was observed at 74.8 ppm in $(CD_3)_2CO$, which fits almost perfectly between the shifts of Li_2**11** (139.1 ppm) and IMe (8.5 ppm) (Figure 2.1.4.4). $\delta(^{77}Se)$ is a well-accepted measure for the π-acceptor ability, in general.[144-148] So, the increasing $\delta(^{77}Se)$ with increasing number of $B(CN)_3$ groups indicates an increasing π-acceptor ability in the row IMe < **5** < **6**, as predicted by theory (chapter 2.1.3). The $^{1}J(^{77}Se,^{13}C)$ coupling constant of **10** (228.0 Hz) is smaller than the one of IMe (234.4 Hz) but larger than the one of **11** (214.5 Hz) (Figure 2.1.4.4). An analogous trend is observed for $^{1}J(^{13}C,^{1}H)$ in [D_6]DMSO for the parent imidazole derivatives that decrease in the order 1,3-dimethylimidazolium cation (221.9 Hz, counterion I^-), **1** (220.3 Hz), and anion **3** (217.8 Hz). Both coupling constants $^{1}J(^{77}Se,^{13}C)$ and $^{1}J(^{13}C,^{1}H)$ are indicative for the σ-donor strength of the corresponding NHC,[147,148] which increases with decreasing coupling constants. Thus, the σ-donor strength increases in the same order as the π-acceptor ability (IMe < **5** < **6**). Both experimental trends are in line with those derived from quantum chemical calculations.

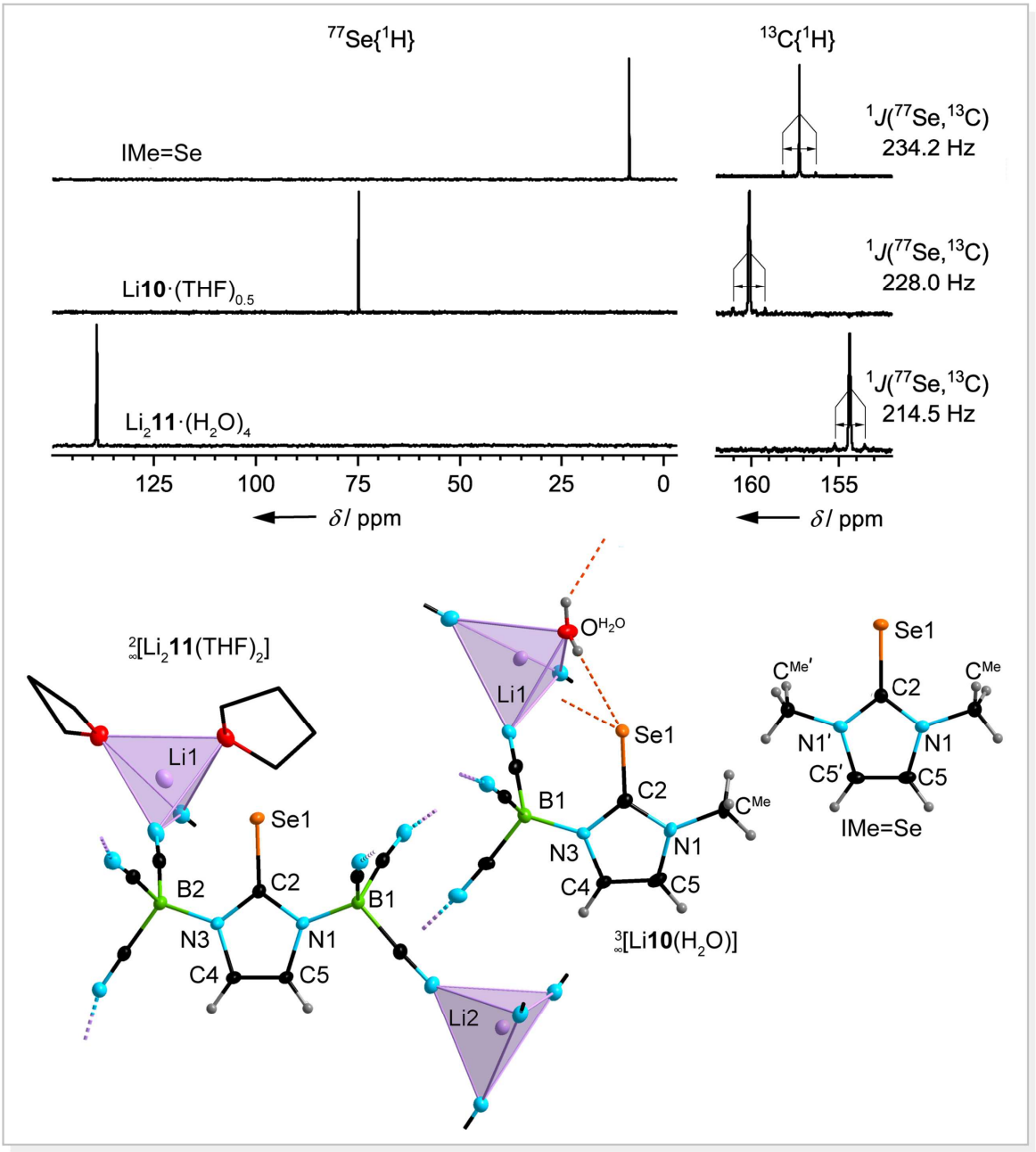

Figure 2.1.4.4 *NMR spectra of IMe=Se, Li**10**·(THF)$_{0.5}$, and Li$_2$**11**·(H$_2$O)$_4$ (top) and crystal structures of IMe=Se,[149] $^3_\infty$[Li**10**(H$_2$O)], and $^2_\infty$[Li$_2$**11**(THF)$_2$] (ellipsoids are shown with 50% ($^3_\infty$[Li**10**(H$_2$O)] and IMe=Se) or 30% ($^2_\infty$[Li$_2$**11**(THF)$_2$]) probability except for H atoms that are depicted with arbitrary radii, partial disorder of the imidazolin-2-ylidene ring in $^2_\infty$[Li$_2$**11**(THF)$_2$] and disorder and H atoms of the THF solvate molecules are omitted for clarity; the C atoms of THF are shown as stick model). Selected bond lengths [pm] (mean values where applicable): IMe=Se: C^{Me}–N1 146.0(4), N1–C2 135.3(3), C5–N1 138.8(3), C5–C5' 135.3(6), Se1=C2 184.2(4); $^3_\infty$[Li**10**(H$_2$O)]: C^{Me}–N1 146.2(6), N1–C2 135.6(6), C2–N3 135.7(6), N3–C4 139.2(6), C4–C5 133.9(7), C5–N1 138.5(6), B1–N3 153.9(6), B1–CN 159.8(7), C≡N 114.3(7), Se1=C2 185.3(5), Se1···H^{H2O} 279.1(14), Se1···H^{H2O} 281.5(12), Li1···NC 201.9(10), Li1···O^{H2O} 192.0(9); $^2_\infty$[Li$_2$**11**(THF)$_2$]: C2=Se 183.34(14), B1–N1 152.7(9), B2–N3 153.1(10), B–CN 160.3(3), C≡N 114.3(2), N1–C2 136.7(9), N3–C2 136.9(9), N1–C5 139.4(8), N3–C4 139.5(8), C4–C5 134.7(5), Li1···N 203.3(4), Li2···N 202.8(4), Li2···O 189.6(19).*

In analogy to the syntheses of anionic selenoureas **10** and **11**, the homologous NHC chalcogen derivatives of **5** and **6** with sulfur and tellurium were obtained. The reaction of Li**5** with S_8 gave Li**12**·$(THF)_{0.5}$, which was isolated in a yield of 96%. Similarly, Li_2**6** was reacted with elemental sulfur to yield 71% of Li_2**13**. Both sulfur compounds are stable against water and air. The crystal structures of $^3_\infty$[Li**12**(H_2O)] and $^3_\infty$[Li_2**13**$(THF)_2$] emphasize the ditopic nature of the $B(CN)_3$-imidazoline compounds (Figure 2.1.4.5).

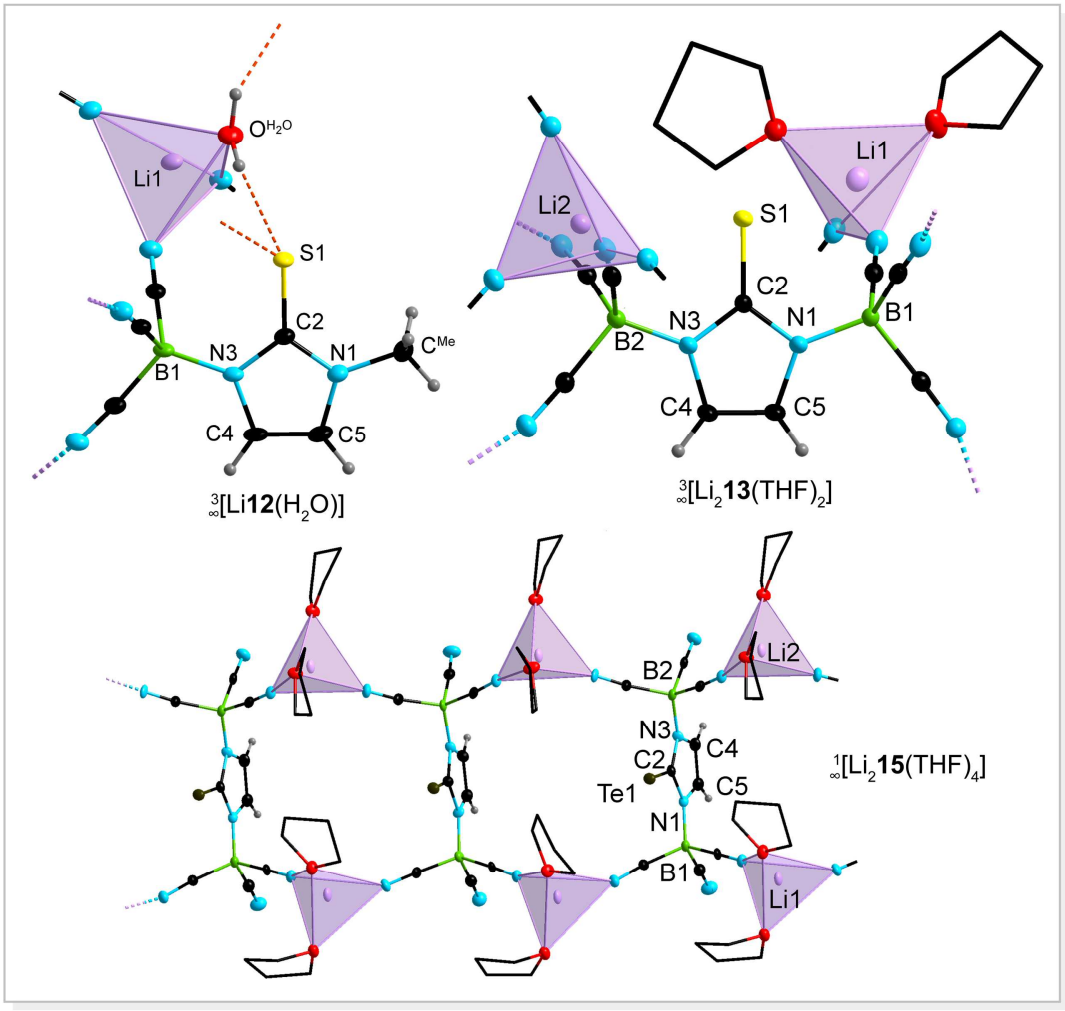

Figure 2.1.4.5 *Crystal structures of $^3_\infty$[Li**12**(H_2O)], $^3_\infty$[Li_2**13**$(THF)_2$], and $^1_\infty$[Li_2**15**$(THF)_4$] (ellipsoids are shown with 50% ($^3_\infty$[Li**12**(H_2O)]) or 35% ($^3_\infty$[Li_2**13**$(THF)_2$] and $^1_\infty$[Li_2**15**$(THF)_4$]) probability except for H atoms that are depicted with arbitrary radii, partial disorder of the imidazolin-2-ylidene ring in $^3_\infty$[Li_2**13**$(THF)_2$] and disorder and H atoms of the THF solvate molecules are omitted for clarity; the C atoms of THF are shown as stick model). Selected bond lengths [pm] (mean value where applicable): $^3_\infty$[Li**12**(H_2O)]: C^{Me}–N1 145.9(4), N1–C2 135.5(3), C2–N3 136.4(3), N3–C4 139.4(3), C4–C5 134.4(4), C5–N1 138.4(3), B1–N3 153.0(4), B1–CN 159.7(4), C≡N 114.5(4), S1=C2 169.7(3), S1···H^{H2O} 252.6(30), S1···H^{H2O} 261.3(30), Li1···NC 201.3(5), Li1···O^{H2O} 193.4(5); $^3_\infty$[Li_2**13**$(THF)_2$]: B1–N1 153.0(2), N1–C2 136.3(2), C2–N3 136.8(2), B2–N3 152.4(2), B–CN 160.5(2), C≡N 114.4(2), S=C2 167.5(2), Li1···NC 202.3(3), Li2···NC 203.2(3), Li2···O^{thf} 191.4(5); $^1_\infty$[Li_2**15**$(THF)_4$]: B1–N1 154.0(14), N1–C2 133.7(12), C2–N3 136.5(12), N3–C4 139.1(13), C4–C5 133.7(14), C5–N1 141.5(12), B2–N3 153.1(14), B–CN 160.5(16), C≡N 114.3(15), Te=C2 207.6(10), Li1···NC 204.4(19), Li1···O^{thf} 191.0(20) Li2···NC 204.1(19), Li2···O^{thf} 193.1(20).*

The C=S distances of 169.7(3) pm ($^3_\infty$[Li**12**(H_2O)] and 167.5(2) pm ($^3_\infty$[Li_2**13**$(THF)_2$]) are in the typical range observed for *d*(C=S) of thioureas, for instance 168.1(5) pm for the corresponding 1,3-dimethyl-substituted thiourea IMe=S.[150] The tellurium derivatives of Li**5** and Li_2**6** were synthesized, as well. Li**14**·THF and Li_2**15**·$(THF)_4$ are sensitive towards moisture, air, and light, which is in agreement to reports on related NHC-tellurium compounds.[94] The crystal structure of $^1_\infty$[Li_2**15**$(THF)_4$] exhibits a chain pattern with bridging lithium cations (Figure 2.1.4.5). The C=Te distance of 207.6(10) pm is similar to *d*(C=Te) in related compounds, for example 207.6(2) pm in Li[{$(C_6F_5)_3$B}IDipp=Te][94] and 205.5(3) pm in IDipp=Te.[151]

The reaction of nickel tetracarbonyl with anionic NHC Li**5** or dianionic NHC Li_2**6** gave the nickel tricarbonyl complexes Li**16**·THF in 86% yield and Li_2**17**·$(THF)_2$ in 83% yield, respectively (Figure 2.1.4.6). For a further assessment of the relative donor strengths of the dianionic NHC **6**, anionic **5**, and neutral IMe, the Tolman electronic parameter (TEP),[152] which is defined as the $\nu_{CO}(A_1)$ band position of [*L*Ni$(CO)_3$] with *L* being a two electron donor ligand, was determined. The IR spectra of [(IMe)Ni$(CO)_3$],[153] [(**5**)Ni$(CO)_3$]$^-$ (**16**), and [(**6**)Ni$(CO)_3$]$^{2-}$ (**17**) were measured in THF solution to minimize coordination effects of the lithium counter ions (Figure 2.1.4.6). In accordance with the quantum chemical calculations (Figure 2.1.3.4), $^1J(^{77}Se,^{13}C)$, and $^1J(^{13}C,^1H)$, the TEP of **16** (2048 cm^{-1}) is in-between those of [(IMe)Ni$(CO)_3$] (2050 cm^{-1}) and **17** (2045 cm^{-1}), which shows that the donor strength of IMe, **5**, and **6** depends on the number of $B(CN)_3$ groups attached.

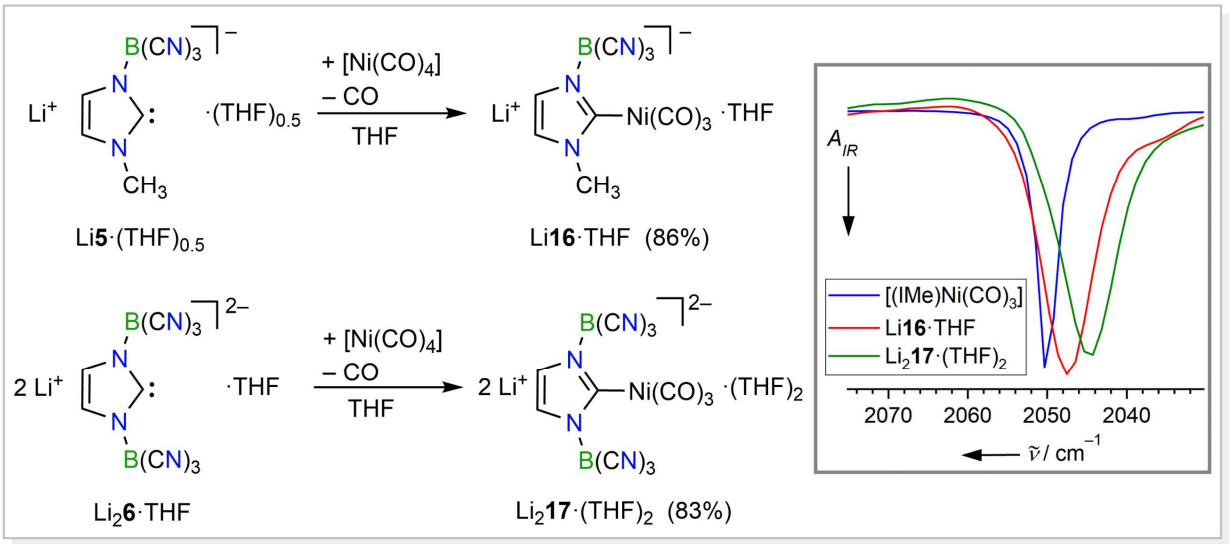

Figure 2.1.4.6 *Syntheses of Li**16**·THF and Li_2**17**·$(THF)_2$ (left) and a section of the IR spectra of [(IMe)Ni$(CO)_3$], Li**16**·THF, and Li_2**17**·$(THF)_2$ (right).*

The crystal structures of $^3_\infty$[Li**16**(THF)] and $^2_\infty$[Li_2**17**$(THF)_2$] reveal tetrahedral coordination at lithium composed of three CN groups and one THF molecule and the common tetrahedral coordination at Ni^0 (Figure 2.1.4.7). The Ni1−C2 bonds of 197.2(4) (**16**) and 198.4(5) pm (**17**) are in the range typically

observed for neutral [(NHC)Ni(CO)$_3$] complexes, for example, [(IMes)Ni(CO)$_3$] (197.1(3) pm), and [(IDipp)Ni(CO)$_3$] (197.9(3) pm).[68] From the structural data, the buried volume (%V_{bur})[154,155] of the free NHCs **5** and **6** was estimated to 32.8% (**5**) and 39.9% (**6**), which reflects the sterically less demanding methyl group compared to B(CN)$_3$. The buried volume of **5** is similar for example to the one of IDipp (%V_{bur} = 29%).[68] However, the steric shielding in **5** is highly unsymmetrical, as evident from the steric map (Figure 2.1.4.7). %V_{bur} of **6** exceeds the steric demand of bulky neutral NHCs, for example I^{t}Bu (37%),[68] and it is similar to %V_{bur} of sterically crowded cyclic (alkyl)(amino)carbenes (cAACs)[156] due to the bulky B(CN)$_3$ substituents.

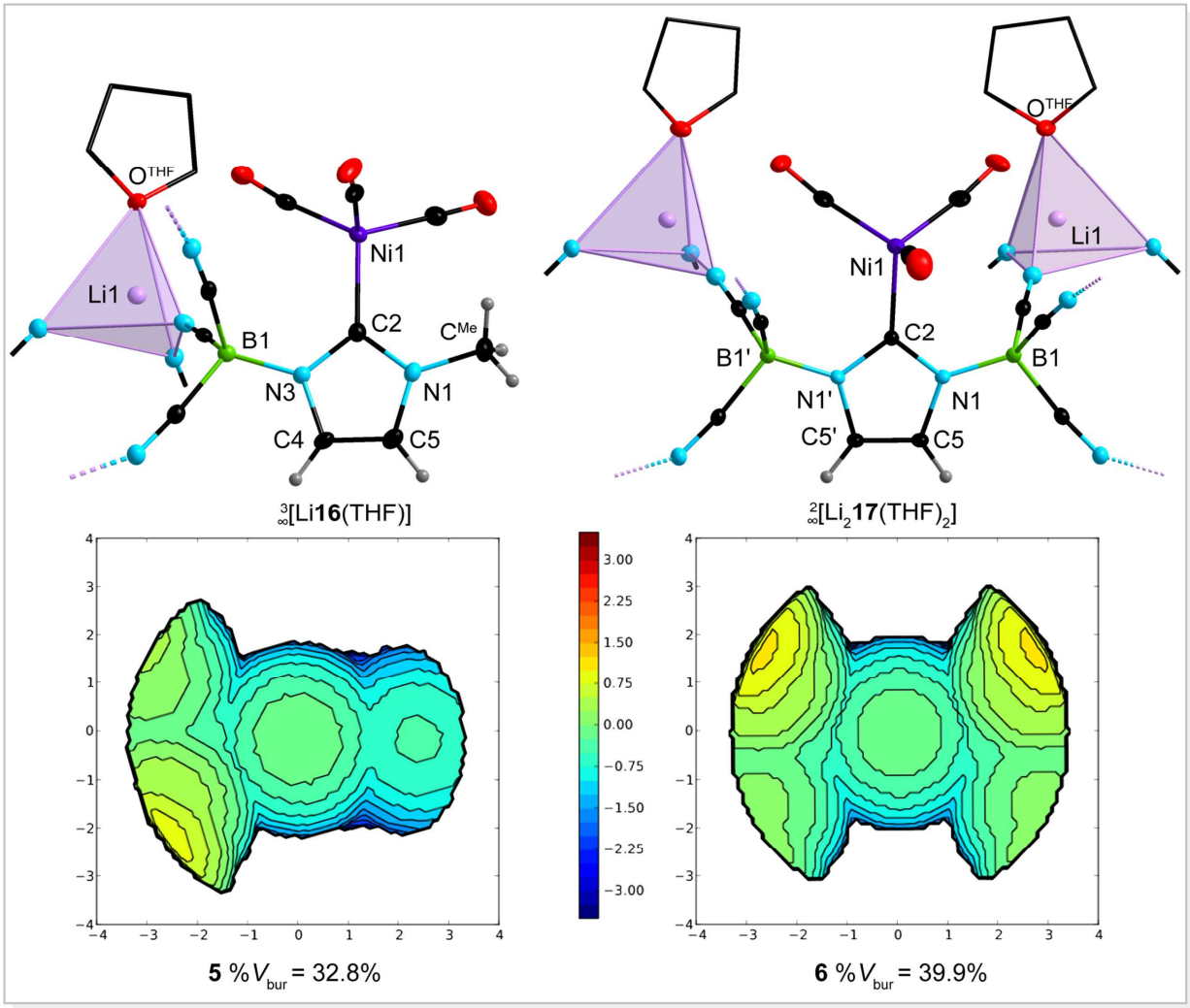

Figure 2.1.4.7 *Crystal structures of $^3_\infty$[Li**16**(THF)] and $^2_\infty$[Li$_2$**17**(THF)$_2$] (top) and steric maps of **5** and **6** (bottom); (ellipsoids are shown with 30% ($^3_\infty$[Li**16**(THF)]) or 35% ($^2_\infty$[Li$_2$**17**(THF)$_2$]) probability except for H atoms that are depicted with arbitrary radii, disorder and H atoms of the THF solvate molecules are omitted for clarity; the C atoms of THF are shown as stick model) and steric maps of **5** and **6**. Selected bond lengths [pm] (mean values where applicable): $^3_\infty$[Li**16**(THF)]: C^{Me}–N1 146.0(9), N1–C2 136.1(7), C2–N3 137.7(7), N3–C4 139.2(6), C4–C5 133.5(9), C5–N1 138.5(6), B1–N3 155.2(3), B1–CN 160.6(7), C≡N 114.7(7), Ni1–C2 197.2(4), Ni1–CO 179.5(7), C≡O 114.3(9), Li1···NC 203.7(9), Li1···O^{thf} 190.9(9); $^2_\infty$[Li$_2$**17**(THF)$_2$]: C2–Ni 198.4(5), C≡O 115.2(8), B–N1 152.3(5), B–CN 160.8(5), C≡N 114.1(5), N1–C2 136.5(4), N1–C4 139.6(4), C4–C4' 133.5(5), Li···N 203.4(7), Li···O 190(2).*

2.1.5 Conclusion

The tricyanoborane-substituted imidazole **1** as well as various salts of the imidazolate anion **3** and the related anionic or dianionic NHCs **5** and **6** have been obtained on gram scale in high yield. The NHC precursors **1** and **3** and the anionic NHCs **5** and **6** possess unprecedented stabilities compared to related species, which is due to a stabilization by the strong Lewis acid $B(CN)_3$ bonded the N atom(s) of the central heterocycle. The presented cyanoboraneimidazole compounds are promising ligands in coordination chemistry as exemplified by their salts and complexes described herein. While anion **5** is a novel unsymmetrical ditopic ligand with coordination being possible at the carbene center and the cyano groups alike, dianion **6** even exceeds the strength of its σ-donor and π-acceptor abilities. Furthermore, it can provide stabilization of a metal fragment coordinated to the carbene center *via* a cyano group as exemplified by the crystal structure of $^{3}_{\infty}[Li_2\mathbf{6}(THF)]\cdot C_6H_6$ (Figure 2.1.3.3). According to results of quantum chemical calculations (Figure 2.1.3.4), NMR spectroscopic data of the selenium adducts of IMe, **5**, and **6** (Figure 2.1.4.4) and the Tolman electronic parameter of the Ni^0 complexes $[(IMe)Ni(CO)_3]$, $[(\mathbf{5})Ni(CO)_3]^-$ (**16**), and $[(\mathbf{6})Ni(CO)_3]^{2-}$ (**17**) (Figure 2.1.4.7), the electronic properties of NHCs can be effectively tuned by the number of $B(CN)_3$ groups at the NHC core. The combination of electronic properties, the large buried volume ($\%V_{bur}$), the negative charge, the possibility to act as ditopic ligands, and the ease of accessibility render **5** and **6** unique novel NHCs.

Chapter II

Tris(pentafluoroethyl)difluorophosphorane Imidazole Compounds

2.2 Tris(pentafluoroethyl)difluorophosphorane Imidazole Compounds

2.2.1 Introduction

The introduction of Lewis acidic boranes as substituents at the nitrogen atoms or the carbon backbone of imidazole rings is a fruitful way towards novel mono- or even dianionic NHCs with a variation of electronic and steric properties, as described in Chapter 1.4 and 2.1. In 2012 Tamm and coworkers reported about the first example of an anionic NHC bearing a weakly coordinating tris(pentafluorophenyl)borane group attached to the carbon backbone (**XXIX**, Figure 2.2.1.1), which is an example for a so called weakly coordinating anionic NHC (WCA-NHC).[91] This type of WCA-NHC is a versatile tool for the synthesis of unusual main group element derivatives,[157-159] for the activation of organic compounds, and as ligand in catalytically active transition metal complexes.[159-161] Beside **XXIX** only few examples of WCA-NHCs are known.[95,103,110,162] However, dianionic WCA-NHCs with two very weakly coordinating, *i.e.* perfluorinated, groups are unknown.

In Chapter 2.1 the $B(CN)_3$-substituted anionic ditopic NHCs 1-methyl-3-tricyanoboraneimidazolin-2-ylidenate **5** and 1,3-bis(tricyanoborane)imidazolin-2-ylidenate **6** were presented. The reason for the unprecedented stability of **5** and **6** is the $B(CN)_3$ moiety, which is a Lewis superacid,[113] explaining the very robust B−N bonds and thus the stability of **5** and **6**. The dianionic ditopic 1,3-bis(tricyanoborane)-imidazoline-2-ylidenate (**6**, Figure 2.2.1.1) exemplifies the ditopic nature of this novel NHC class. Furthermore, the $B(CN)_3$ moiety influences the σ-donor and π-acceptor abilities and thus the stereoelectronics.

The introduction of anionic NHCs with very weakly coordinating units remains a challenge, in general, and especially the introduction of anionic perfluorinated and thus weakly coordinating groups at the N atoms of the imidazole ring has so far not been achieved. So, it is not possible to use tris(pentafluorophenyl)borane as Lewis acid substituent since deprotonation of 1,4,5-trimethyl-3-tris(pentafluorophenyl)boraneimidazole **XXXIIa** led via an intramolecular nucleophilic attack of the carbene C atom at a C_6F_5 ring to **XXXIIc** (Figure 2.2.1.1).[105] This example demonstrates the importance of the proper choice of the Lewis acid (LA), which has to be chemically stable with respect to the highly nucleophilic carbene center and has to be strong enough to result in stable LA–$N_{imidazole}$ bonds.

Tris(pentafluoroethyl)difluorophosphorane $(C_2F_5)_3PF_2$[163] is a strong Lewis acid[164] as evident from its fluoride ion affinity (FIA) of 388 kJ·mol^{-1}.[113] Its fluoride adduct $[(C_2F_5)_3PF_3]^-$ (**FAP**) is a weakly coordinating anion (WCA) that is used for the stabilization of reactive cations[165,166] and in electrolyte compositions.[167] The large number of chemically stable tris(pentafluoroethyl)difluorophosphorane

The results of the chapter *Tris(pentafluoroethyl)difluorophosphorane Imidazole Compounds* were published in: "*Anionic N-Heterocyclic Carbenes Featuring Weakly Coordinating Perfluoroalkylphosphorane Moieties*" L. Zapf, U. Radius, M. Finze, **2023**, *submitted*.
Experimental details can be found in the corresponding Supporting Information.

derivatives of the general formula $(C_2F_5)_3PF_2R$ (*R* = NHC,[18] amine,[168] DMAP[6] (DMAP = 4-(dimethylamino)pyridine), …) underlines the ability to form stable Lewis acid/base pairs.[169]

Herein, the synthesis of mono- and dianionic tris(pentafluoroethyl)difluorophosphorane-functionalized WCA-NHCs with the highly sterically demanding $(C_2F_5)_3PF_2$ Lewis acid[170] attached to the $N_{imidazole}$ atom(s) is described (Figure 2.2.1.1). These carbenes are the first representatives of phosphorane-modified NHCs with a negative charge and a weakly coordinating group, which is distinct from the few other NHCs with N–P bonds.[171-174] The stereo-electronic and chemical properties of the novel WCA-NHCs have been assessed and are compared to other neutral and anionic NHCs in a comparative experimental and theoretical study.

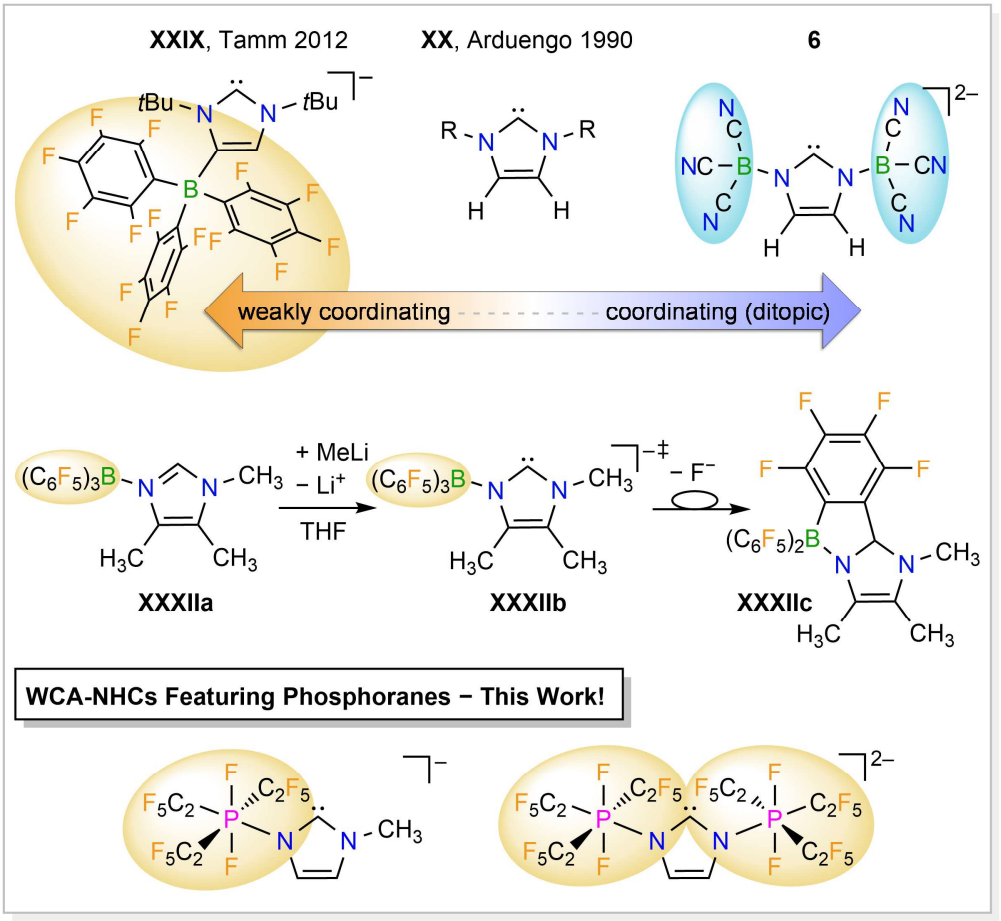

Figure 2.2.1.1 *First class of neutral NHCs (**XX**, top middle), selected anionic borane-substituted NHCs with a weakly (**XXIX**, top left) and coordinating (ditopic) groups (**6**, top right), intramolecular follow-up reaction of in situ generated anionic carbene **XXXIIb**, and novel WCA-NHCs (bottom) presented in this work.*

2.2.2 1-Methyl-3-(tris(pentafluoroethyl)difluorophosphorane)imidazole and 1,3-Bis(tris(pentafluoroethyl)difluorophosphorane)imidazolates

1-Methyl-3-(tris(pentafluoroethyl)difluorophosphorane)imidazole (**18**) was prepared from tris(pentafluoroethyl)difluorophosphorane ($(C_2F_5)_3PF_2$)[163] and 1-methylimidazole in diethyl ether (Figure 2.2.2.1). Since the starting materials are readily available and because of the high yield of more than 95%, **18** can be synthesized on a multigram scale. Neutral **1** is stable up to a temperature of 125 °C (DSC, onset), hydrolyzes slowly in the presence of moisture, but is indefinitely stable under inert conditions. **18** was characterized by NMR and vibrational spectroscopy and single-crystal X-ray diffraction (SC-XRD). Single crystals of **1** were obtained by slow evaporation of a diethyl ether solution (Figure 2.2.2.1). The P1−N3 distance of 186.4(3) pm is in the range of related $(C_2F_5)_3PF_2$ Lewis base adducts, for example 190.9(1) pm in $(C_2F_5)_3PF_2$·DMAP.[6]

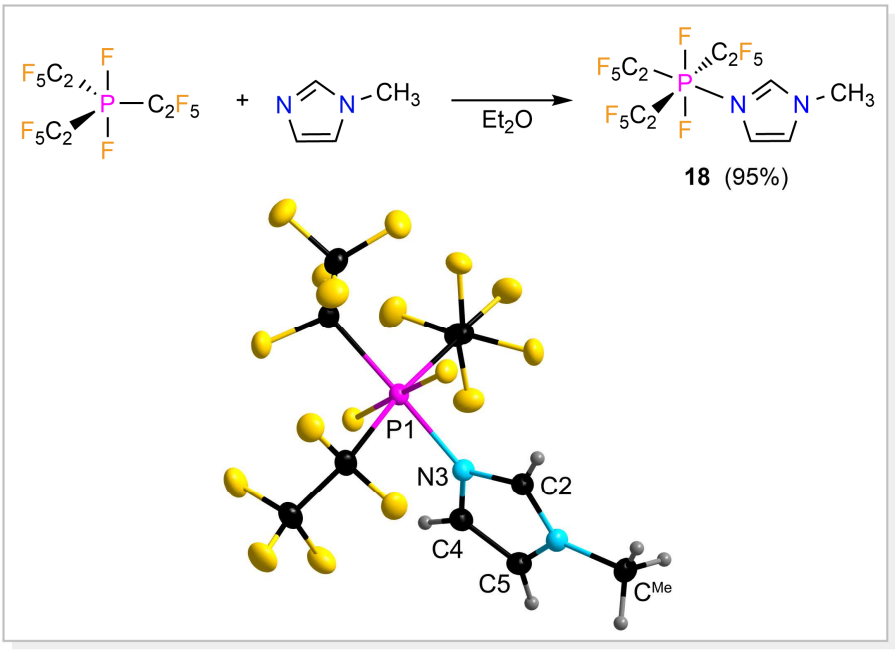

Figure 2.2.2.1 *Synthesis and crystal structure of **18** (ellipsoids are drawn at the 50% probability level except for the H atoms that are depicted with arbitrary radii). Selected bond lengths [pm] and angles [°] (mean value where applicable): P1–N3 186.4(2), C^{Me}–N1 146.8(3), N1–C2 132.4(2), C2–N3 133.6(3), N3–C4 138.8(3), C4–C5 134.6(3), C5–N1 138.4(3), P1–F 162.3(1), P1–C 197.2(2), C^{F2}–F 136.2(3), C^{F2}–C^{F3} 155.0(3), C^{F3}–F 133.2(3), P1–N3–C2 125.1(1), H2–C2–N3 125.1(2), H2–C2–N1 125.1(2), C^{Me}–N1–C2 125.2(2).*

Potassium 1,3-bis(tris(pentafluoroethyl)difluorophsphorane)imidazolate (K**19**) was formed by nucleophilic substitution starting from two equivalents of $(C_2F_5)_3PF_2$[163] and potassium imidazolate in diethyl ether (Figure 2.2.2.2). As evident from NMR spectra and elemental analysis, K**19** contains 0.5 equivalents of diethyl ether. K**19**·$(Et_2O)_{0.5}$ is accessible on a multigram scale in almost quantitative yield. The solvent free organic phosphonium salt [Ph_4P]**19** was prepared by metathesis of *in situ* synthesized Li**19** with [PPh_4]Cl. The salts K**19**·$(Et_2O)_{0.5}$ and [PPh_4]**19** are stable up to 110 and 125 °C,

respectively (DSC, onset). Like **18**, both salts of **19** hydrolyze slowly in the presence of moisture but can be stored indefinitely under inert conditions. Single crystals of [PPh$_4$]**19** were obtained by slow evaporation of a diethyl ether solution (Figure 2.2.2.2). The P1−N1 distance of 185.6(1) pm is only slightly smaller than *d*(P−N) in **18**.

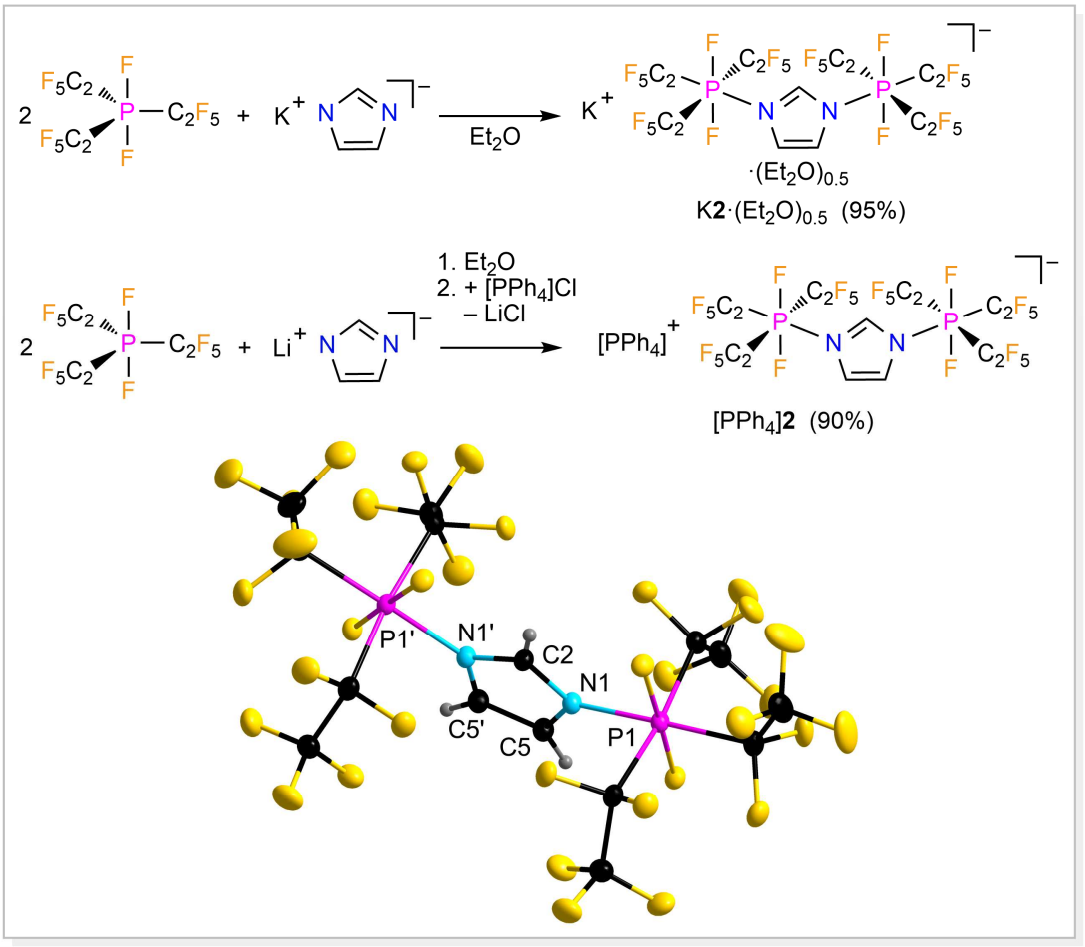

Figure 2.2.2.2 *Syntheses of K**19**·(Et$_2$O)$_{0.5}$ and [PPh$_4$]**19** and crystal structure of **19** in [PPh$_4$]**19**; (ellipsoids are drawn at the 50% probability level except for the H atoms that are depicted with arbitrary radii). Selected bond lengths [pm] and angles [°] (mean value where applicable): P1–N1 185.6(1), N1–C2 133.0(2), C5'–C5 134.8(2), C5–N1 139.1(2), P1–F 162.2(1), P1–C 197.2(2), C^{F2}–F 136.3(2), C^{F2}–C^{F3} 154.8(2), C^{F3}–F 133.1(2), P1–N1–C2 125.0(1), H2–C2–N1 124.5(1).*

2.2.3 Weakly Coordinating Tris(pentafluoroethyl)difluorophosphoraneimidazolin-2-ylidenate Anions

With the phosphoranyle-substituted imidazole **18** and imidazolate K**19**·$(Et_2O)_{0.5}$ as starting materials in hand, their deprotonation to the respective imidazolin-2-ylidenate anions was investigated. For **18** potassium hydride in tetrahydrofuran proved to be a suitable base to result in the selective deprotonation at C2, furnishing K**20**·$(THF)_{0.5}$ in a yield of 97% (Figure 2.2.3.1). The potassium salt K**20** contains 0.5 equivalents of THF per formula unit according to NMR spectroscopy and elemental analysis. Deprotonation of **18** under formation of anion **20** is confirmed by NMR spectroscopy (Figure 2.2.3.1). The ^{31}P NMR signal is shifted from −146.9 (**18**) to −151.4 ppm (**20**) and in the ^{1}H NMR spectrum of **20** only two resonances for the backbone H atoms were detected. However, the most significant difference was observed in the $^{13}C\{^{1}H\}$ NMR spectrum for the signal of the C2 nucleus. This signal was shifted from 141.2 (**18**) to 218.1 ppm (**20**), the latter being in the typical range observed for carbene carbon nuclei, e.g. 213.2 ppm for 1,3-di-*tert*-butyl-imidazolin-2-ylidene (I*t*Bu)[175] or 211.2 ppm for **XXIX**.[91] The signal is split into a doublet due to the coupling to ^{31}P with $^{2}J(^{31}P,^{13}C)$ of 38.2 Hz (Figure 2.2.3.1). In contrast, the signal of C2 of **18** reveals no coupling to ^{31}P.

The potassium salt K**20**·$(THF)_{0.5}$ is stable to temperatures higher than 110 °C in the solid state and starts to slowly decompose in THF solution at temperatures higher than 70 °C. Therefore, K**20**·$(THF)_{0.5}$ provides a similar thermal stability like the $B(CN)_3$-substituted anionic NHC 1-methyl-3-tricyanoboraneidazolin-2-ylidenate (**5**) and an even higher stability compared to the neutral Arduengo NHC 1,3-dimethylimidazolin-2-yilidene (IMe), which gradually decomposes already at room temperature.[176]

Selective deprotonation of K**19**·$(Et_2O)_{0.5}$ at the C2 atom revealed to be more difficult as standard potassium bases for the deprotonation of NHCs like KO*t*Bu, KHMDS, or KH did not result in deprotonation of **19**. Presumably, this is due to the high sterically shielding of the C2−H unit by the phosphorane moieties, which to some extend embrace the H at C2 (*vide infra*). Therefore, benzyl potassium, which is molecular in solution and therefore less sterically hindered,[177] was employed, resulting in the formation of K_2**21**·$(Et_2O)_{0.5}$,·$(C_7H_8)_{0.5}$ in 95% yield (Figure 2.2.3.1). The potassium salt contains 0.5 equivalents of diethyl ether and 0.5 equivalents of toluene per formula unit according to NMR spectroscopy and elemental analysis. Selective deprotonation of **19** at C2 under formation of anion **21** was confirmed by NMR spectroscopy (Figure 2.2.3.1). The ^{31}P NMR signal is shifted from −147.1 (**19**) to −150.0 ppm (**21**) and in the ^{1}H NMR spectrum of **21** only one resonance for the backbone H atoms was observed. In the $^{13}C\{^{1}H\}$ NMR spectrum the signal of the C2 nucleus of **22** was detected at 230.0 ppm. The signal is split into a triplet due to the coupling to both ^{31}P nuclei with $^{2}J(^{31}P,^{13}C)$ of 44.0 Hz (Figure 2.2.3.1).

The dipotassium salt K_2**21**·$(Et_2O)_{0.5}$,·$(C_7H_8)_{0.5}$ is stable to temperatures higher than 110 °C in the solid state and starts to slowly decompose in solution at temperatures higher than 100 °C. Therefore, K_2**21**·$(Et_2O)_{0.5}$,·$(C_7H_8)_{0.5}$ provides a similar thermal stability like K**20**·$(THF)_{0.5}$.

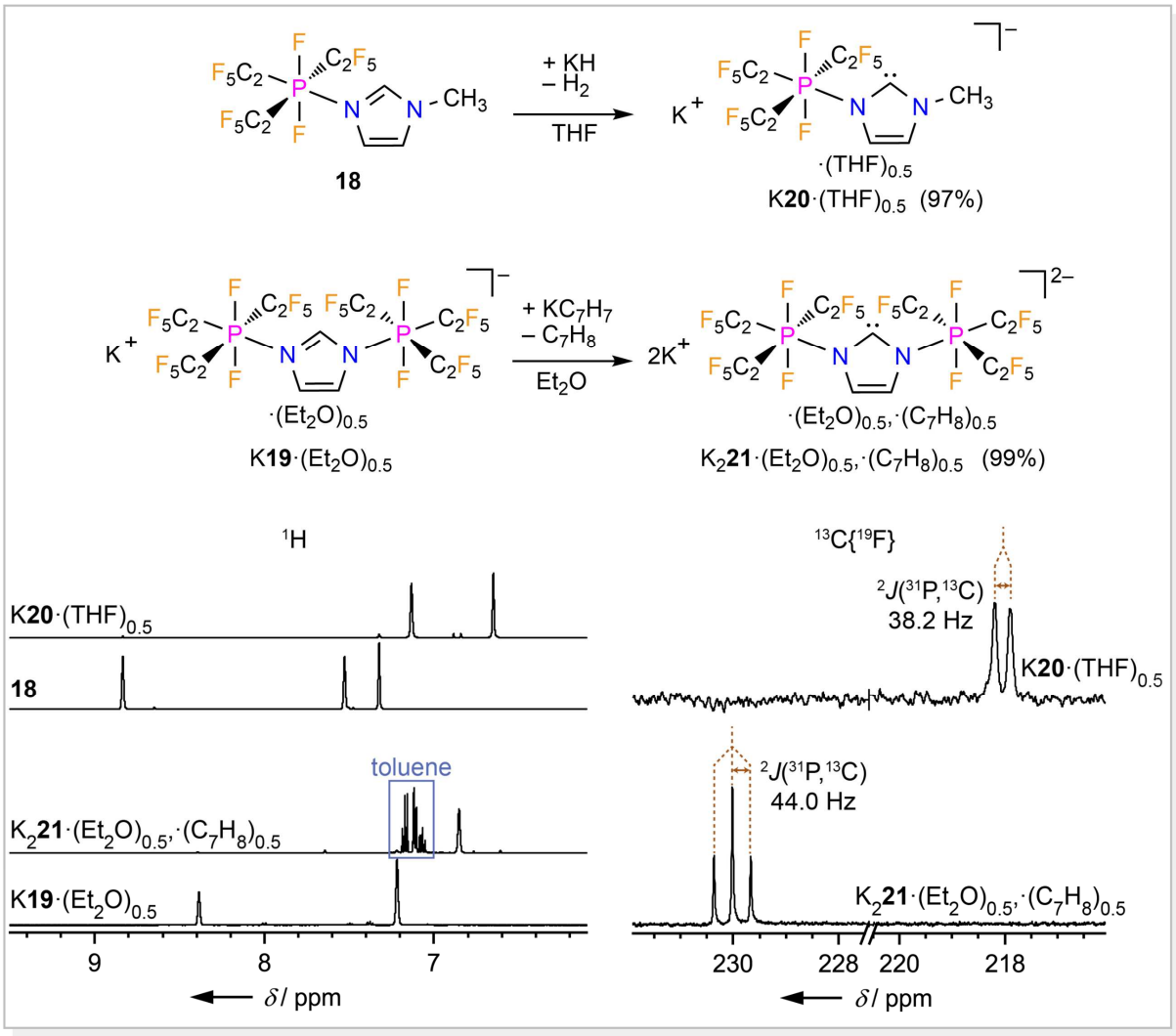

Figure 2.2.3.1 *Syntheses of K**20**·(THF)$_{0.5}$ and K_2**21**·$(Et_2O)_{0.5}$,·$(C_7H_8)_{0.5}$ (top) and NMR spectra of **18**, K**19**·$(Et_2O)_{0.5}$, K**20**·$(THF)_{0.5}$, and K_2**21**·$(Et_2O)_{0.5}$ (bottom).*

Single crystals of [K**20**$(THF)_2]_2$ were obtained by diffusion of hexane into a THF solution of the potassium salt. Two carbene units form cyclic dimers *via* bridging K1 atoms (Figure 2.2.3.2). K1 is coordinated to the C2 carbene atom and the oxygen atoms of two THF ligands. In addition, K1 is oriented towards fluorine substituents of the parent anionic NHC resulting in weak K1···F interactions. The K1–C2 distances of 300.8(4) and 291.9(4) ppm are similar to related K···$C_{carbene}$ separations, for example 298.6(2) pm in [{H_2C(I*i*Pr)$_2$}KN(SiMe_3)$_2$]$_2$.[178] The bond lengths of **20** differ from those of **18**. Noteworthy, the P–N distance is slightly shorter whereas *d*(C2–N) are a little longer. Both differences reflect the increased electron density at the C2 carbene atom in **20**, which results in a slight weakening of the C2–N bonds, an increased basicity of the N atoms in the ring, and in turn a stronger P–N bond.

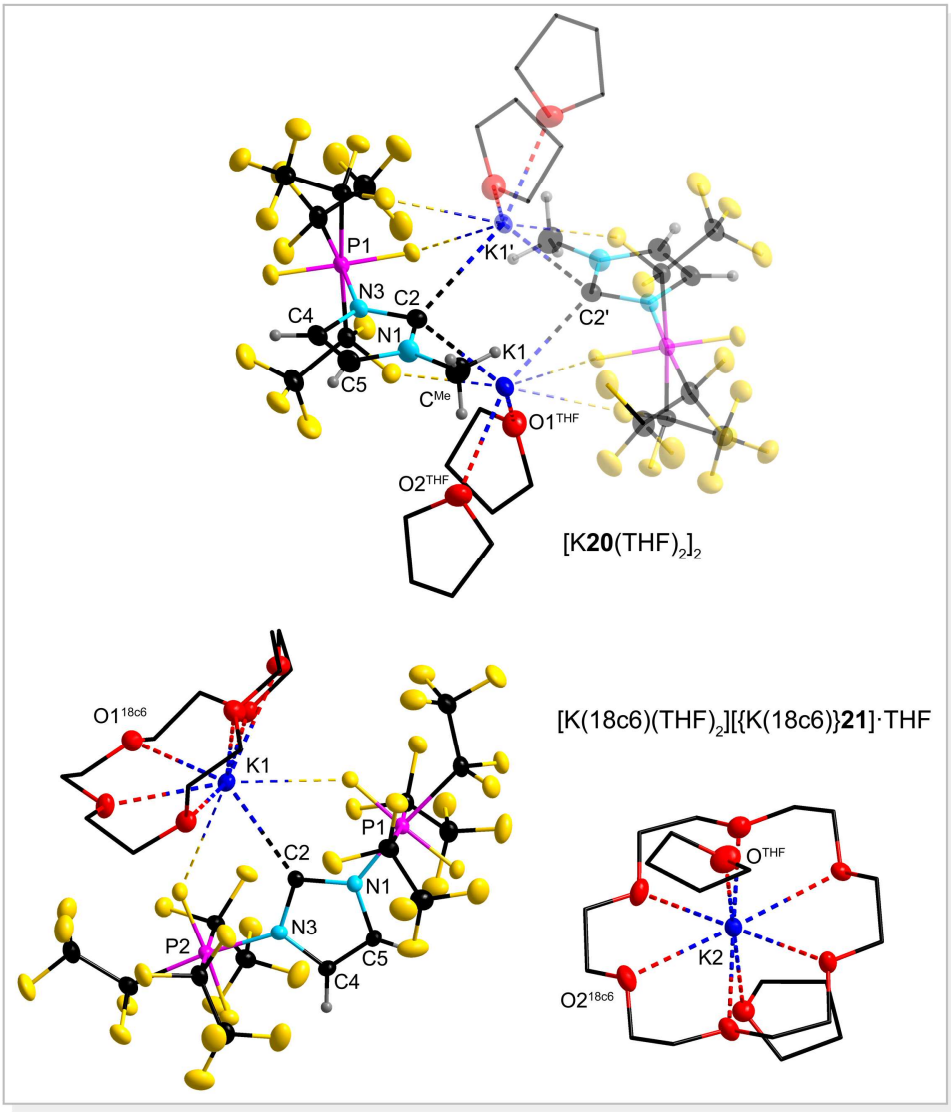

Figure 2.2.3.2 *A dimer of [K**20**(THF)$_2$]$_2$ (top) and a unit of [K(18c4)(THF)$_2$][{K(18c6)}**21**]·THF in the crystal structures (bottom; ellipsoids are drawn with 30% ([K**20**(THF)$_2$]$_2$) or 50% ([K(18c4)(THF)$_2$][{K(18c6)}**21**]·THF) probability except for H atoms that are depicted with arbitrary radii, disorder and H atoms of the THF solvate molecules are not shown and their C atoms are depicted as wireframe model, the co-crystallized THF is omitted for clarity). Selected bond lengths [pm] and angles [°] (mean value where applicable): [K**20**(THF)$_2$]$_2$: P1–N3 180.2(3), C^{Me}–N1 146.1(6), N1–C2 135.2(5), C2–N3 139.5(5), N3–C4 140.1(5), C4–C5 134.5(7), C5–N1 138.3(6), P1–F 162.6(2), P1–C 197.6(4), C^{F2}–F 136.6(5), C^{F2}–C^{F3} 154.5(6), C^{F3}–F 133.1(6), K1···C2 300.8(4), K1'···C2 291.9(4), K1···O1^{thf} 269.7(11), K1···O2^{thf} 268.3(14), K1···F^{PF} 277.9(2), K1···F^{CF2} 268.5(3), K1'···F^{CF2} 280.3(3), P1–N3–C2 123.8(3), K1–C2–N3 121.0(2), K1–C2–N1 106.4(3), C^{Me}–N1–C2 122.5(4); [K(18c4)(THF)$_2$][{K(18c6)}**21**]·THF: P1–N1 179.4(3), P2–N3 179.4(3), N1–C2 137.5(4), C2–N3 137.8(4), N3–C4 140.8(4), C4–C5 133.2(5), C5–N1 140.5(4), P–F 162.8(2), P–C 199.0(3), C^{F2}–F 136.4(4), C^{F2}–C^{F3} 154.7(5), C^{F3}–F 133.3(4), K1···C2 294.4(3), K1···O1^{18c6} 296.6(4), K1···F1^{PF} 288.5(2), K1···F2^{PF} 310.0(2), P1–N1–C2 124.7(2), K1–C2–N1 125.3(2), K1–C2–N3 130.4(2), P2–N3–C2 125.1(2), O1^{18c6}···K1···O1^{18c6} 111.4(1), 123.4(1), 162.1(1), K2···O2^{18c6} 279.8(3), K2···O^{thf} 274.3(3), O1^{18c6}···K1···O1^{18c6} 177.9(1), 178.4(1), 178.4(1).*

Single crystals of [K(18c4)(THF)$_2$][{K(18c6)}**21**]·THF (18c6 = 18-crown-6) were obtained in the presence of 18c6 from a THF solution of the dipotassium salt (Figure 2.2.3.2). K1 is coordinated to the C2 carbene atom and to all six oxygen atoms of 18c6. In addition, K1 is oriented towards the P–F fluoride

substituents of the parent anionic NHC resulting in weak K1···F interactions. The K1–C2 distance of 294.4(3) pm is similar to the ones in [K**20**(THF)$_2$]$_2$ (300.8(4) pm, 291.9(4) pm). The second potassium cation K2 is coordinated by all six oxygen atoms of an equivalent of 18c6 and the oxygen atoms of two THF ligands but not to **20**. In contrast to K1, K2 lies almost perfectly in the plane of 18c6, whereas the 18c6 ring around K1 is heavily distorted due to the bulky phosphorane substituents of NHC **21**. Similar to [K**20**(THF)$_2$]$_2$ the bond lengths of **21** differ from those of the NHC precursor (**19**), with regard to the shortened P–N distances and longer *d*(C2–N).

DFT calculations (def2-TZVPP/B3LYP/D3(BJ)/COSMO [ε = infinite]) have been performed to evaluate the electronic features of mono- and dianionic NHCs **20** and **21** and to compare them to other neutral and charged NHCs. The relevant NHC orbitals, *i.e.* the occupied σ-orbital and the unoccupied π-orbital, of **20**, **21**, IMe, and the B(CN)$_3$-substituted anionic NHCs IMeB(CN)$_3^-$ (**5**) and IB(CN)$_3^{2-}$ (**6**), are depicted in Figure 2.2.3.3. The NHC σ-orbital is in any case the HOMO, whereas the relevant NHC π-orbital is the LUMO for **20** and **21** but LUMO+*n* for IMe (*n* = 1), IB(CN)$_3^{2-}$ (*n* = 6), and IMeB(CN)$_3^-$ (*n* = 3). The HOMO energy increases with decreasing Lewis acidity of the substituents (CH_3^+ > B(CN)$_3$ > $(C_2F_5)_3PF_2$) at the N atoms of the imidazole ring. Thus, the σ-donor ability increases from –6.36 to –5.44 eV along the series IMe < IMeB(CN)$_3^-$ < IB(CN)$_3^{2-}$ < **20** < **21**.

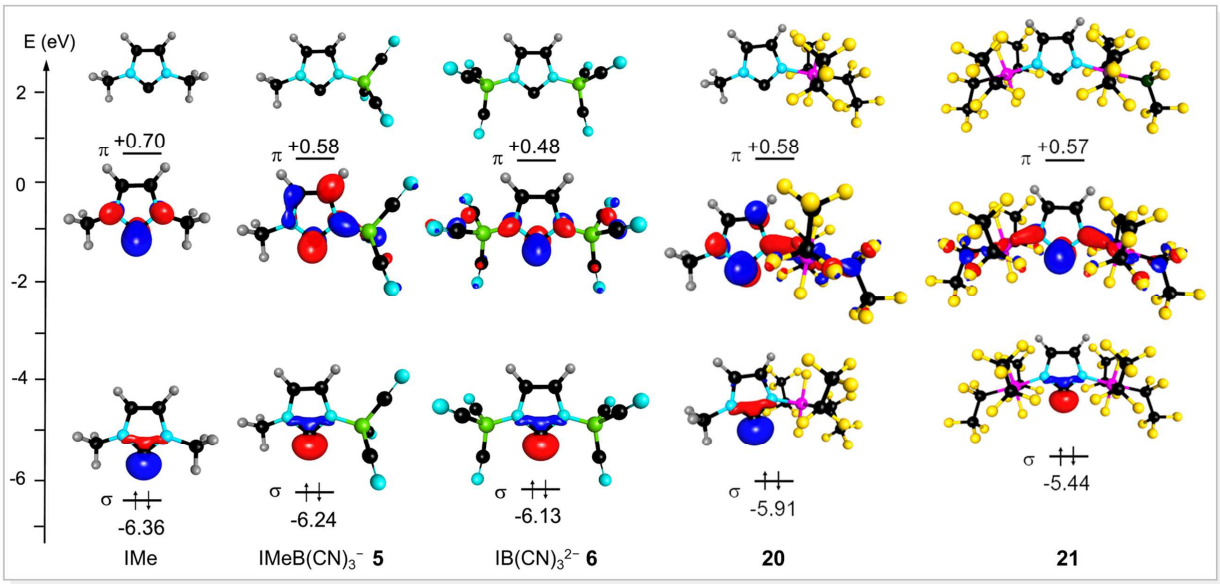

Figure 2.2.3.3 *NHC σ- and π-orbitals of IMe, IMeB(CN)$_3^-$ (**5**), IB(CN)$_3^{2-}$ (**6**), **20**, and **21**. Energies were calculated at the DFT/def2-TZVPP/B3LYP/D3(BJ)/COSMO [ε = infinite] level of theory and orbital plots are drawn at the 0.1 isosurface.*

The influence of the Lewis acids at the N atoms of the imidazole core on the π-orbital is more complex as the delocalization of this orbital throughout these substituents has a decisive influence. So, especially the B(CN)$_3$ and to a lesser extend the $(C_2F_5)_3PF_2$ units enable an efficient delocalization of the electron density (Figure 2.2.3.3). However, for all four anionic NHCs **20**, **21**, IB(CN)$_3^{2-}$, and IMeB(CN)$_3^-$

a drop of the NHC π-orbital energy is predicted by DFT calculations. So, they are stronger π-acceptors than IMe with smaller σ/π-separations. The separation decreases continuously upon successive formal replacement of CH_3^+ against $(C_2F_5)_3PF_2$ from 7.06 eV for IMe to 6.49 eV for **20** and 6.01 eV for **21**. Furthermore, the σ/π-separation of **20** and **21** are smaller than those of the related anionic $B(CN)_3$ derivatives of 6.82 eV for $IB(CN)_3^{2-}$ and 6.61 eV for $IMeB(CN)_3^-$ (Chapter 2.1.3).[179]

2.2.4 Main Group Element Adducts and Transition Metal Complexes

The reaction of elemental selenium with K**20**·$(THF)_{0.5}$ in tetrahydrofuran gave the selenourea **22**. Its potassium salt was isolated with one equivalent of THF (Figure 2.2.4.1). The ^{77}Se chemical shift of 142.1 ppm in [D_8]THF is indicative for a stronger π-acceptor ability of **20** compared to related backbone unsaturated NHCs. For example, ^{77}Se NMR shifts of 35, 87 ($(CD_3)_2CO$),[146,180] and 114 ppm ([D_8]THF)[159] have been reported for the corresponding Se adducts of 1,3-dimesitylimidazolin-2-ylidene (IMes), 1,3-bis(2,6-di-*iso*-propylphenyl)imidazolin-2-ylidene (IDipp), and the 1,3-bis(2,6-di*iso*propylphenyl) derivative of anionic carbene **XXIX**, previously. According to the ^{77}Se chemical shift, $B(CN)_3$ derivative **5** (δ(^{77}Se) = 77.2 ppm in [D_8]THF) should be a significantly weaker π-acceptor than **20**, but quantum chemical calculations predict them to have similar π-acceptor properties (Figure 2.2.3.3). An explanation for the limited significance of the ^{77}Se shift of **22** with respect to π-acceptor ability of **20** may be provided by the crystal structure of **22** (*vide infra*).

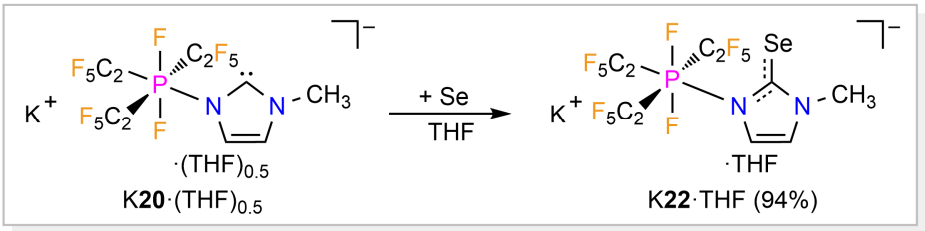

Figure 2.2.4.1 *Synthesis of K**22**·THF.*

The ^{77}Se signal of **22** reveals coupling to ^{31}P and ^{19}F with ^3J(^{77}Se,^{31}P) = 70.8 Hz and ^4J(^{77}Se,^{19}F) = 9.7 Hz, respectively (Figure 2.2.4.2). The ^1J(^{77}Se,^{13}C) coupling constant of 236 Hz, which was derived from the ^{13}C{^{1}H} NMR spectrum (Figure 2.2.4.2), suggests that **20** is a moderate σ-donor, since ^1J(^{77}Se,^{13}C) is larger than in the selenourea of IMeB$(CN)_3^-$ (**5**, 228 Hz) and comparable to the selenourea of IMe (234 Hz).[179] Therefore, the prediction of the σ-donor strength based on the ^{77}Se-^{13}C coupling constant seems to be inconsistent with the DFT results. The ^{13}C signal of C2 reveals coupling to ^{31}P and ^{19}F with ^2J(^{31}P,^{13}C) = 6.1 Hz and ^3J(^{19}F,^{13}C) = 6.0 Hz (Figure 2.2.4.2).

Crystallization of K**22**·THF from 1,2-difluorobenzene afforded crystals of $^2_\infty$[K**22**]·$C_6F_2H_4$ (Figure 2.2.4.2). The C–Se distance of 187.9(9) pm is comparatively long for *d*(C=Se) in other selenoureas. It tends to be in the range of a C–Se single bond as shown by a comparison with the bond lengths of selenourea WCA-NHC **XXIX** (*d*(C=Se) = 184.5(2) pm) and its protonated derivate (*d*(C–SeH) = 188.5(1) pm).[159] Furthermore, the Se atom in **22** is bent towards the methyl substituent as evident from the uneven angles Se1–C2–N3 131.0(7)° and Se1–C2–N1 120.9(7)°. These experimental values are well reproduced by DFT calculations (133.1° and 120.8°). The P1–N3–C2 132.6(6)° angle in **22** is also significantly larger than in **20** (123.8(3)°) or **18** (125.0(1)°). These observations show the strong influence of the sterically demanding $(C_2F_5)_3PF_2$ moiety, leading to an unusual C–Se bonding situation in **22**. Presumably, this is

the reason for the discrepancy between the NMR spectroscopic data of **20** and the DFT predictions on the π-acceptor and σ-donor abilities (*vide supra*). The sensitivity of $d(^{77}Se)$ on bulky substituents causing a wrong assessment of the π-acceptor ability has been discussed by Bertrand and coworkers, earlier.[181]

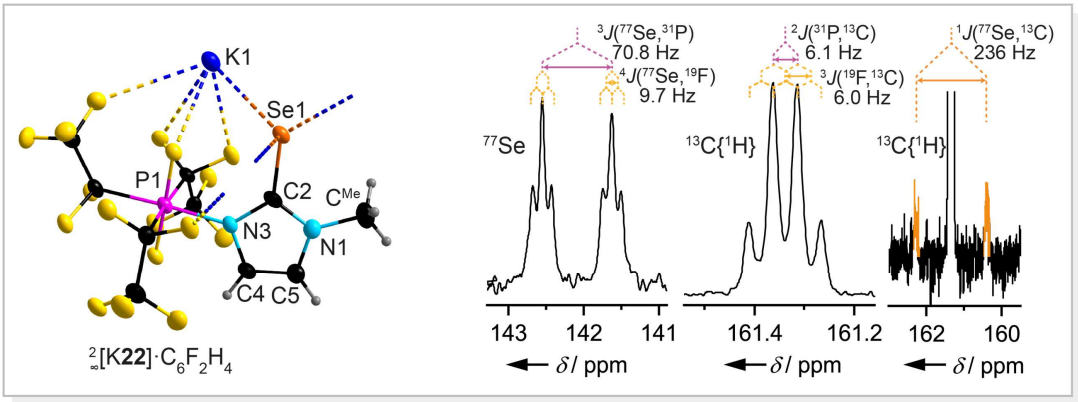

Figure 2.2.4.2 *NMR spectra (right) of K**22**·THF and a unit in the crystal structure of $^2_\infty$[K**22**]·C$_6$F$_2$H$_4$ (left, ellipsoids are drawn at the 30% probability level except for the H atoms that are depicted with arbitrary radii, severely disordered C$_6$F$_2$H$_4$ and its contribution to the structure factors was taken into account using the SQUEEZE routine as implemented in the Platon program.[138,139] Selected bond lengths [pm] and angles [°] (mean value where applicable): P1–N3 185.0(8), C^{Me}–N1 145.9(12), N1–C2 131.9(15), C2–N3 141.3(9), N3–C4 141.1(13), C4–C5 133.1(14), C5–N1 139.2(12), P1–F 161.5(5), P1–C 197.5(9), C^{F2}–F 136.5(11), C^{F2}–C^{F3} 154.8(14), C^{F3}–F 132.6(12), Se1–C2 187.9(9), K1···Se1 327.9(3), 331.1(2), 341.0(2), K1···F^{PF} 285.4(5), K1···F^{CF2} 261.5(5), 287.0(6), 304.5(5), K1···F^{CF3} 329.7(5), P1–N3–C2 132.6(6), Se1–C2–N3 131.0(7), Se1–C2–N1 120.9(7), C^{Me}–N1–C2 125.5(8).*

The synthesis of the analogous selenium adduct of dianionic NHC **21** was unsuccessful despite several attempts even with the more reactive red selenium allotrope and at higher reaction temperatures (Figure 2.2.4.3). Obviously, the two sterically demanding $(C_2F_5)_3PF_2$ groups surrounding the carbene center provide so much steric bulk to prevent the reaction (Figure 2.2.4.3). The optimized (DFT, *vide supra*) structure of the Se adduct of **21** shows that both P–N–C2 units would be strongly bent (∡(P–N–C2) = 133.4°) compared to **21** (∡(P–N–C2) = 124.7(2) and 125.1(2)°). The LAB-Rep model[170] (Chapter 2.4) for the analysis of Lewis acid/base adduct formation also shows that the Se adduct of **21** is sterically very encumbered (%V_{bur_all} of 101.0%) and hence its formation is unfavored.

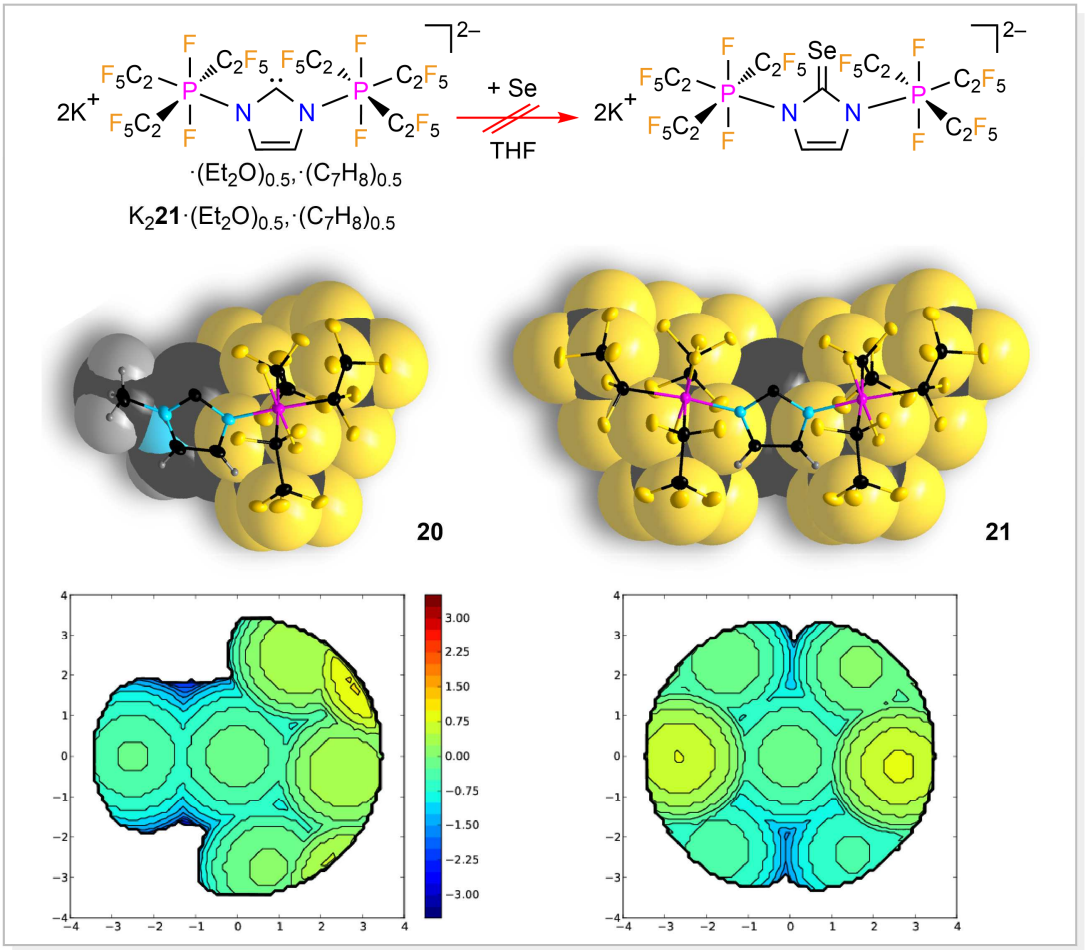

Figure 2.2.4.3 *Attempt to synthesize the selenourea of* ***21*** *(top), space filling models (middle), and steric maps of WCA-NHCs* ***20*** *and* ***21****.*

Despite the high steric shielding of the carbene centers in the WCA-NHCs **20** and **21**, they can coordinate to metal centers as exemplified by the synthesis of linear gold(I) complexes. K**20**·$(THF)_{0.5}$ and K_2**21**·$(Et_2O)_{0.5}$,·$(C_7H_8)_{0.5}$ were reacted with chlorophosphinegold(I) precursors (Figure 2.2.4.4). The reaction of K**20**·$(THF)_{0.5}$ and $(H_3C)_3PAuCl$ selectively yielded with ligand dismutation the complex salt [{$(H_3C)_3P$}$_2$Au]**23** containing the linear bis(WCA-NHC)gold(I) anion **23** and the linear bis(trimethylphosphine)gold(I) cation, as proven by SC-XRD (Figure 2.2.4.5).

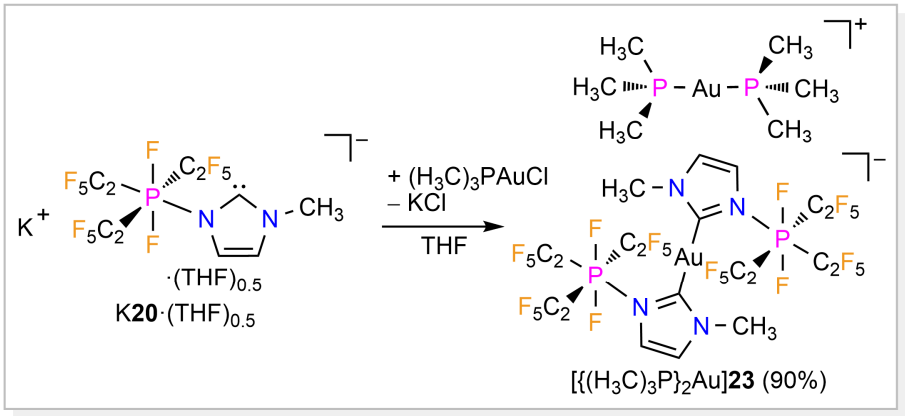

Figure 2.2.4.4 *Synthesis of [{$(H_3C)_3P$}$_2$Au]****23****.*

Crystals of [{(H$_3$C)$_3$P}$_2$Au]**23** were obtained by slow diffusion of hexane into a THF solution. The two WCA-NHCs in the anion are twisted with a torsion angle of 124.4(4)° to each other. The C2−Au1 distance of 204.1(3)/203.4(3) pm is in the range of linear NHC-gold(I) complexes, for instance 207.1(2) pm in **XXIX**−AuPPh$_3$.[159] The C_2F_5 groups of the $(C_2F_5)_3PF_2$ substituent of both (cryst-allographically independent) anionic NHC ligands of anion **23** reveal different orientations, which are furthermore distinct from those in the crystal structures of all other $(C_2F_5)_3PF_2$-functionalized imidazole derivatives described in this study.

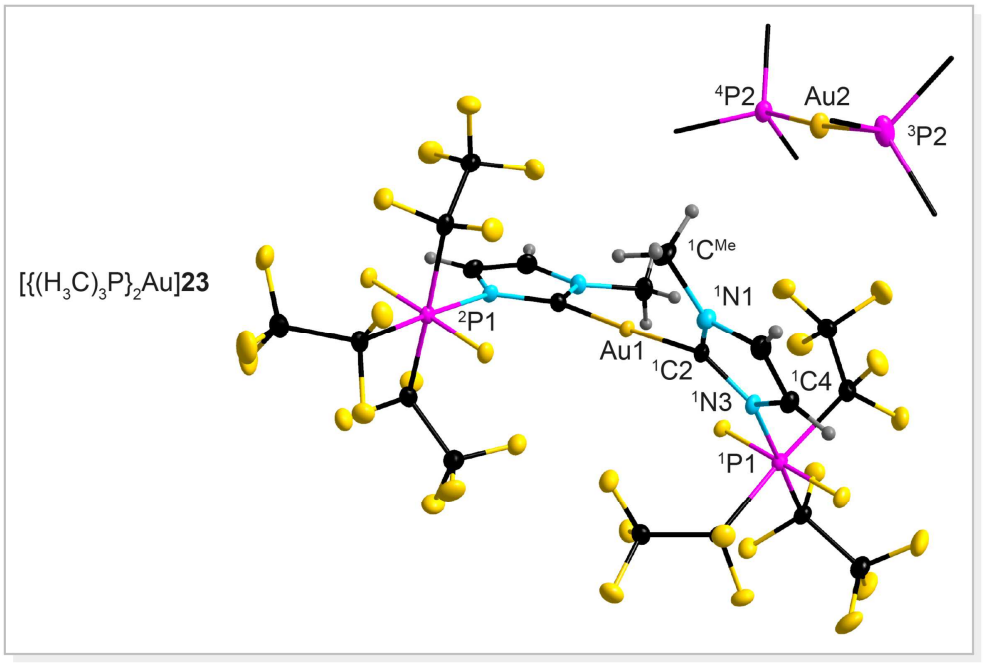

Figure 2.2.4.5 *A unit of [{(H$_3$C)$_3$P}$_2$Au]**23** in the crystal structure (ellipsoids are drawn with 50% probability except for H atoms that are depicted with arbitrary radii, H atoms of the Me$_3$P moieties are not shown and their C atoms are depicted as wireframe model). Selected bond lengths [pm] and angles [°] (mean value where applicable): ^{1}P1–^{1}N3 184.9(3), ^{2}P1–^{2}N3 183.5(3), ^{1}C^{Me}–^{1}N1 146.5(5), ^{1}C^{Me}–^{1}N1 146.(4), ^{1}N1–^{1}C2 134.5(4), ^{2}N1–^{2}C2 135.1(5), ^{1}C2–^{1}N3 138.1(4), ^{2}C2–^{2}N3 138.0(4), ^{1}N3–^{1}C4 139.9(3), ^{2}N3–^{2}C4 140.6(4), ^{1}C4–^{1}C5 134.1(5), ^{2}C4–^{2}C5 133.5(5), ^{1}C5–^{1}N1 138.3(3), ^{2}C5–^{2}N1 138.3(3), ^{1}P1–^{1}F 162.1(2), ^{2}P1–^{2}F 161.9(2), ^{1}P1–^{1}C 197.7(3), ^{2}P1–^{2}C 198.0(3), ^{1}C^{F2}–^{1}F 136.7(4), ^{2}C^{F2}–^{2}F 136.8(4), ^{1}C^{F2}–^{1}C^{F3} 155.1(5), ^{2}C^{F2}–^{2}C^{F3} 154.9(5), ^{1}C^{F3}–^{1}F 133.2(4), ^{2}C^{F3}–^{2}F 133.3(4), Au1–^{1}C2 204.1(3), Au1–^{2}C2 203.4(3), Au2–^{3}P2 229.9(1), Au2–^{4}P2 230.3(1), ^{1}P1–^{1}N3–^{1}C2 128.7(2), ^{2}P1–^{2}N3–^{2}C2 128.2(2), Au1–^{1}C2–^{1}N3 133.5(2), Au1–^{2}C2–^{2}N3 133.5(2), Au1–^{1}C2–^{1}N1 121.1(2), Au1–^{2}C2–^{2}N1 120.8(2), ^{1}C^{Me}–^{1}N1–^{1}C2 124.9(3), ^{2}C^{Me}–^{2}N1–^{2}C2 125.0(3), ^{1}C2–Au1–^{2}C2 177.8(1), ^{3}P2–Au1–^{4}P2 175.2(1).*

While in all other crystal structures the two *trans* located pentafluoroethyl groups reveal a torsion angle τ^1(F$_3$C−CF$_2$−CF$_2$−CF$_3$) of ca. 0° and are oriented towards the imidazole backbone [τ^2(F$_3$C−CF$_2$−N3−C2) ≈ 118°] and the third C_2F_5 moiety is oriented towards the C2 atom [τ^3(F$_3$C−CF$_2$−N3−C2) ≈ 0°], the C_2F_5 groups around ^{1}P1 switch orientation [τ^1 = 0.1(4)°, τ^2 = 1.2(3)° / 1.4(3)°, τ^3 = 176.7(3)°]. However, for the second NHC moiety the C_2F_5 groups around ^{2}P1 show another orientation pattern with one of the *trans* groups pointing to C2 and the other to the center of the imidazole ring, while the third group is oriented to the carbon backbone [τ^1 = 109.4(3)°, τ^2 = 1.6(3)° /

80.6(3)°, τ^3 = 174.2(3)°]. So, the buried volume (%V_{bur})[155,182] calculated for the sterically flexible ligand **20** differs from 38.9 [^{2}P1; τ^1 = 0.1(4)°, τ^2 = 1.2(3)° / 1.4(3)°, τ^3 = 176.7(3)°] to 41.5% [^{1}P1; τ^1 = 109.4(3)°, τ^2 = 1.6(3)° / 80.6(3)°, τ^3 = 174.2(3)°] in **23**. Ligand **20** is sterically demanding as obvious from a comparison to the neutral Arduengo NHC IDipp (%V_{bur} = 29%)[183] and the anionic NHC IMeB(CN)$_3^-$ **5** (%V_{bur} = 32.8%). However, despite its large %V_{bur}, ligand **20** is highly unsymmetrical due to the huge steric difference between methyl and $(C_2F_5)_3PF_2$ (Figure 2.2.4.3).

The reaction of K$_2$**21**·$(Et_2O)_{0.5}$,·$(C_7H_8)_{0.5}$ with one equivalent of Ph_3PAuCl resulted in the formation of the linear triphenylphosphine-(WCA-NHC)-gold(I) complex, which was isolated as potassium salt K**24**·$(THF)_2$ (Figure 2.2.4.6).

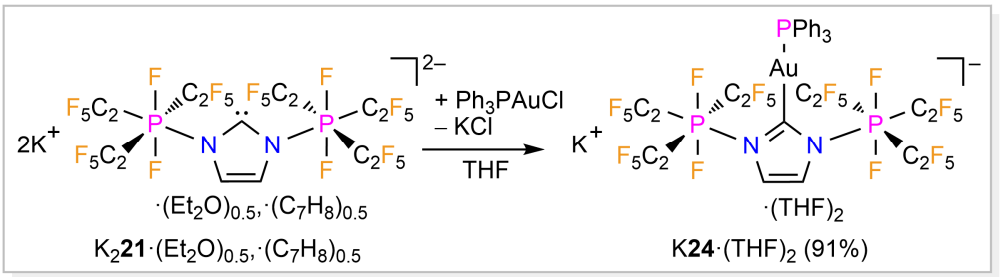

Figure 2.2.4.6 *Synthesis of K**24**·(THF)$_2$.*

Crystals of $^1_\infty$[K**24**$(NCCH_3)_2$] were obtained by slow diffusion of hexane into an acetonitrile solution (Figure 2.2.4.7). The potassium cations K1, which are coordinated by two acetonitrile molecules, connect the anions **24** *via* weak K1···F interactions. The C2−Au1 distance of 207.2(3) is close to the distance observed in [{$(H_3C)_3P$}$_2$Au]**23**. The buried volume of WCA-NHC **21** was determined to be 47.0% [τ^1 = 4.0(4)°, τ^2 = 117.5(3)°, τ^3 = 1.7(4)°; (mean values)] reflecting the two sterically demanding $(C_2F_5)_3PF_2$ substituents. Thus, **21** is sterically bulkier than **20** and the dianionic B(CN)$_3$ derivate **6** (%V_{bur} = 39.9%)[184] and it covers almost the full hemisphere around a metal atom as evident from the steric map (Figure 2.2.4.3).

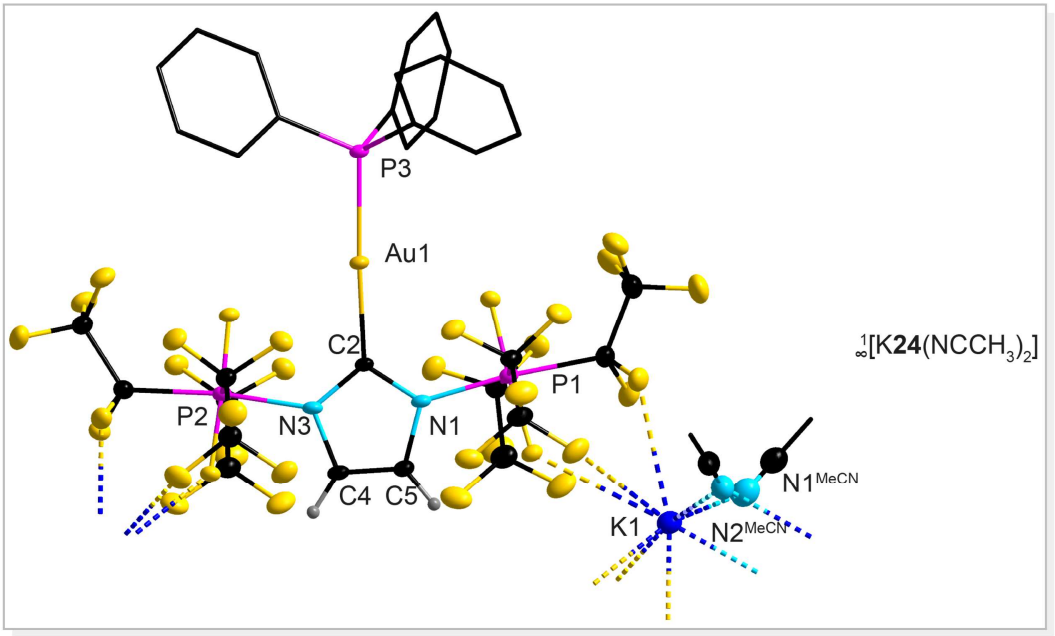

Figure 2.2.4.7 *A unit of $^{1}_{\infty}$[K**24**(NCCH$_3$)$_2$] in the crystal structure (ellipsoids are drawn with 35% probability except for H atoms that are depicted with arbitrary radii, H atoms of the acetonitrile solvate molecules are not shown and their C atoms are depicted as wireframe model; H atoms of the Ph$_3$P moieties are not shown and their C atoms are depicted as wireframe model). Selected bond lengths [pm] and angles [°] (mean value where applicable): P1–N1 185.4(3), P2–N3 185.2(3), N1–C2 136.4(4), C2–N3 135.8(4), N3–C4 140.1(3), C4–C5 132.5(4), C5–N1 139.2(4), P–F 162.3(2), P1–C 197.7(4), C^{F2}–F 136.2(4), C^{F2}–C^{F3} 154.9(5), C^{F3}–F 133.0(5), Au1–C2 207.2(3), Au1–P3 226.4(1), K1···$N1^{MeCN}$ 275.2(4), K1···$N2^{MeCN}$ 276.4(4), K1···F^{PF} 313.8(2), K1···F^{CF2} 300.3(2), P1–N1–C2 130.3(2), Au1–C2–N1 125.5(2), Au1–C2–N3 127.1(2), P2–N3–C2 130.9(2).*

2.2.5 Conclusion

First anionic phosphorane-substituted NHCs **20** and **21** have been obtained on gram scale in high yield (Figure 2.2.3.1). These NHCs featuring weakly coordinating groups distinguish them self by unprecedented stabilities compared to related species, which is a consequence of the stabilization by the strong Lewis acid $(C_2F_5)_3PF_2$ bonded to one or both N atoms of the central heterocycle. Monoanion **20** and dianion **21** are promising ligands in coordination chemistry due to their large buried volume and their enhanced σ-donor and π-acceptor abilities compared to neutral NHCs as exemplified by the gold(I) complexes **23** and **24** (Figure 2.2.4.5 and Figure 2.2.4.7) as well as quantum chemical calculations (Figure 2.2.3.3). Furthermore, the crystal structure of **23** underlines the flexibility of the steric environment of the phosphoranes achieved by the orientation of the C_2F_5 groups. The combination of electronic properties, the large buried volume (%V_{bur}), the single or double negative charge, the possibility to act as sterically flexible ligand, the weakly coordinating substituents, and the ease of accessibility render **20** and **21** unique novel NHCs.

CHAPTER III

BORANE-FUNCTIONALIZED ANIONIC CYCLIC (ALKYL)(AMINO)CARBENE COMPOUNDS

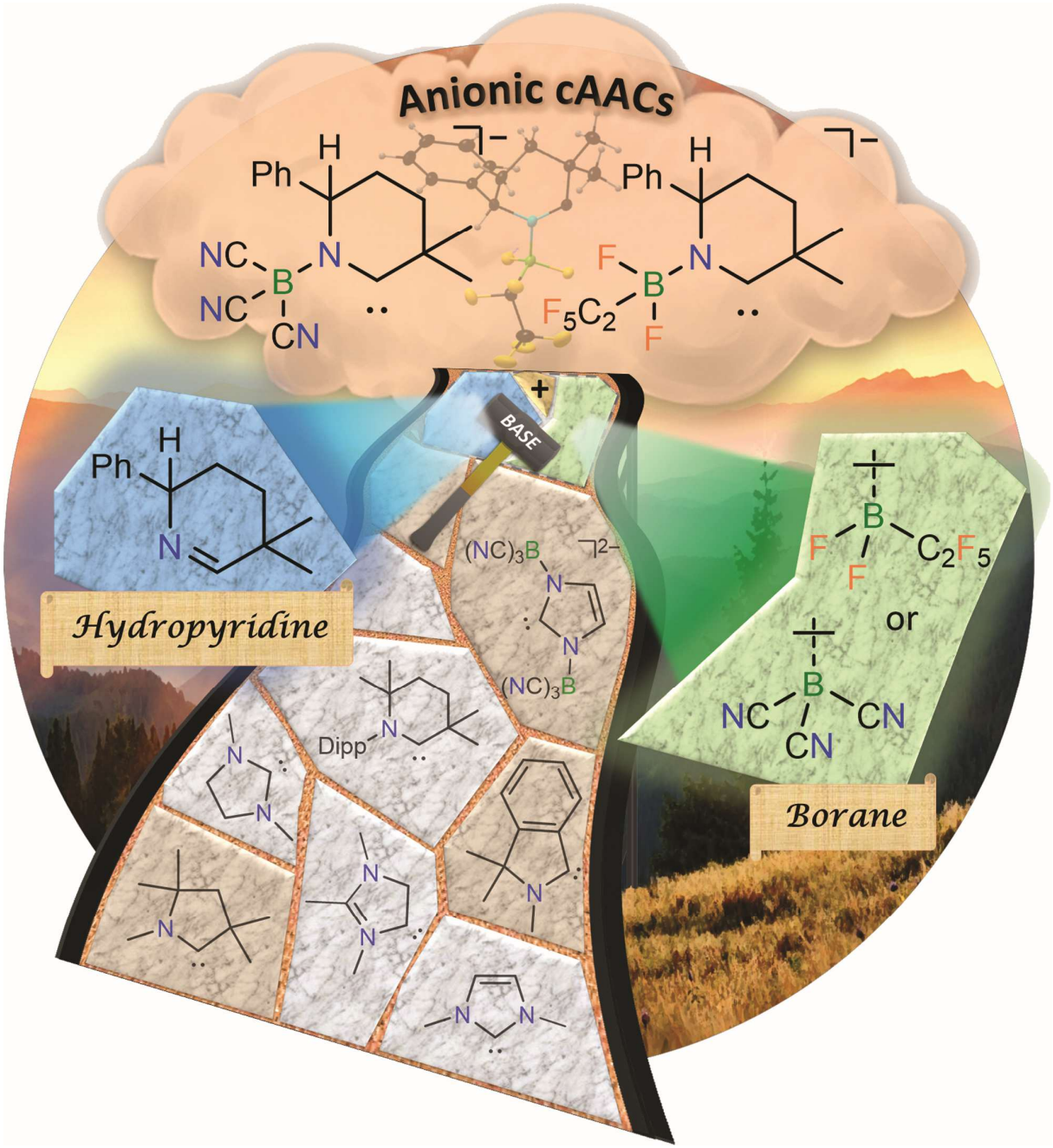

2.3 Borane-Functionalized Anionic Cyclic (Alkyl)(amino)carbene Compounds

2.3.1 Introduction

The steric and electronic properties of NHCs can be modified by different approaches, as illustrated in Chapter 1.3. The introduction of substituents at the imidazole ring is the most important strategy for the variation of properties, *i.e.* charge, number and type of coordination sites, steric demand, and σ-donor and π-acceptor abilities.[30,84,85,91] The utilization of Lewis acids such as boranes or phosphoranes as substituents at the nitrogen atoms is a valuable method that provides access to mono- and even dianionic NHCs accompanied by the variation of electronic and steric properties, as demonstrated in the previous chapters (Chapter 2.1 and 2.2).

However, there are more options, which allow tunability of carbenes. Beside the variation of substituents at the central ring, the heterocycle itself can be modified to improve the stereo-electronic properties of an NHC. In 2005 Bertrand and coworkers published the synthesis of the first cyclic (alkyl)(amino)carbenes (cAAC) (cAAC^{Me}-5, Figure 2.3.1.1). One of the nitrogen units of the imidazoline core is formally replaced by a quaternary carbon atom with σ-donating alkyl substituents.[79] Since then, five-membered cAACs and related cyclic (amino)(aryl)carbenes (cAArCs)[185,186] have been successfully applied in catalysis,[187-200] for the activation of small molecules and strong bonds,[201-210] in low-valent main-group chemistry,[50,206,211-216] and for the stabilization of radical species.[217] These studies highlighted the increased σ-donor and π-acceptor ability compared to imidazoline NHCs. A further increase in nucleo- and electrophilicity was achieved recently by enlarging the cAAC ring size from five to six (cAAC^{Me}-6, Figure 2.3.1.1).[73]

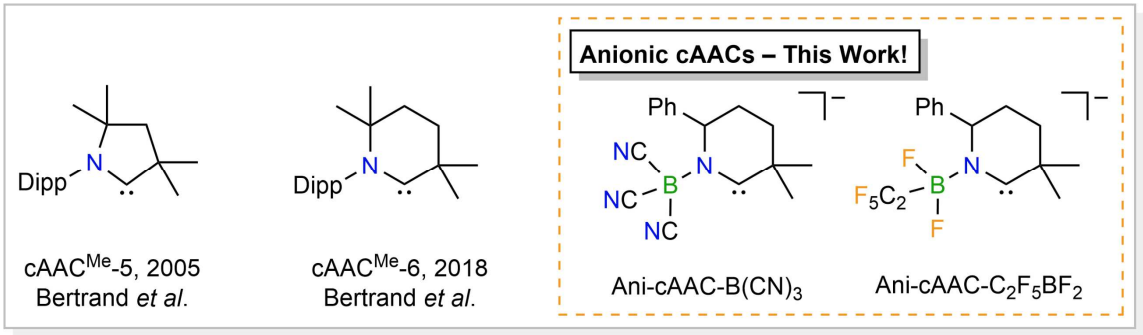

Figure 2.3.1.1 *Neutral cAACs (left) and novel anionic borane-substituted cAACs (right).*

Keeping the improved stereo-electronic properties of borane-substituted anionic NHCs in mind (Chapter 2.1), the synthesis of first examples of anionic cAACs (Ani-cAACs, Figure 2.3.1.1) was aimed

The results of the chapter *Borane-functionalized Anionic Cyclic (Alkyl)(amino)carbene Compounds* were published in:
"*Boranes Paving the Way to Anionic Cyclic (Alkyl)(amino)carbenes (Ani-cAACs)*" L. Zapf, S. Peters, U. Radius, M. Finze, *Angew. Chem. Int. Ed.* **2023**, *63*, e202300056.
Experimental details can be found in the corresponding Supporting Information.

to push boundaries of previously known carbenes forward. In the search for suitable precursors, borane-hydropyridine adducts were chosen, following the borane-imidazole adducts used earlier (Chapter 2.1).[179,218] According to a modular principle, these can be prepared from literature-known Lewis basic hydropyridines[219-221] and various boranes. Thus, a tedious multi-step ring closure synthesis, as currently used for the preparation of neutral cAACs, can be elegantly circumvented. In addition, the direct influence of two different boranes and the introduced negative charge on the stereo-electronic properties of this carbenes and how Ani-cAACs can outperform the σ-donor and π-acceptor abilities of their neutral analogous, is exemplified. The following chapter covers syntheses, structural and spectroscopic properties as well as first metal- and non-metal derivatives of a promising novel class of carbenes in a comparative experimental and theoretical study.

2.3.2 1-Borane-3,3-dimethyl-6-phenyltetrahydropyrdines

Adducts of 5,5-dimethlyl-2-phenyl-2,3,4,5-tetrahydropyridine[220] (**25**) with tricyanoborane $B(CN)_3$ (**26**) and pentafluoroethyldifluoroborane ($C_2F_5BF_2$) (**27**) were prepared from $B(CN)_3$·py-4-CN[124] (py-4-CN = 4-cyanopyridine) or $C_2F_5BF_2$·THF, respectively (Figure 2.3.2.1). Both adducts **26** and **27** have been synthesized on multi-gram scale from readily available starting materials in yields of 90 and 99%, respectively. Hydropyridine **25** was used as racemate and thus, **26** and **27** have been obtained as racemates, as well. Adduct **26** is stable against air and moisture, melts at 196 °C (DSC, onset), and decomposes at 258 °C (DSC, onset). In contrast, **27** slowly hydrolyzes in the presence of moisture but is indefinitely stable under inert conditions. It melts at 100 °C (DSC, onset) and is stable up to 268 °C (DSC, onset). The related adducts **26** and **27** were characterized by multinuclear NMR and vibrational spectroscopy and by single-crystal X-ray diffraction (SC-XRD). Single crystals of **26**·CH_2Cl_2 and **27** were obtained from solutions in CH_2Cl_2 and THF by slow diffusion of pentane and hexane, respectively (Figure 2.3.2.1). The B1–N1 distances of 159.3(4) (**26**) and 159.7(2) pm (**27**) are in the range of related strong borane Lewis base adducts, for example 155.3(2) pm in 1-methyl-3-$B(CN)_3$-imidazole.[179] The C–C and C–N distances in the hydropyridine rings reveal only slight differences to those observed for the parent compound **25**.

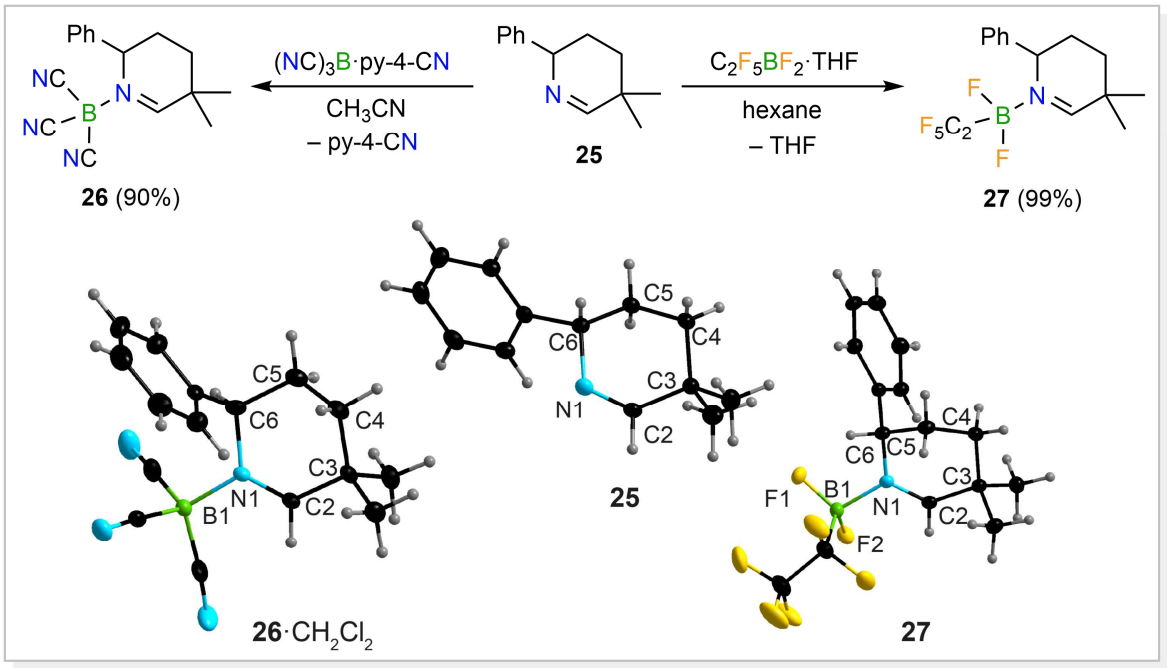

Figure 2.3.2.1 *Syntheses and crystal structures of **25**, **26**, and **27** (ellipsoids are drawn at the 50% (**25**) or 40% (**26**·CH_2Cl_2 and **27**) probability level except for the H atoms that are depicted with arbitrary radii, disordered co-crystallized dichloromethane in **26**·CH_2Cl_2 is omitted for clarity). Selected bond lengths [pm] and angles [°] (mean value where applicable): **25**: N1=C2 126.8(1), C2–C3 151.8(1), C3–C4 153.2(1), C4–C5 152.5(1), C5–C6 153.1(1), C6–N1 148.1(1), N1–C2–C3 129.6(1); **26**·CH_2Cl_2: N1=C2 127.3(3), C2–C3 149.4(3), C3–C4 154.7(3), C4–C5 152.0(4), C5–C6 152.1(3), C6–N1 150.6(3), B1–N 157.9(3), B1–CN 159.3(4), C≡N 114.6(4), N1–C2–C3 127.8(2); **27**: N1=C2 128.6(2), C2–C3 149.4(2), C3–C4 153.0(2), C4–C5 152.3(2), C5–C6 152.8(2), C6–N1 148.7(2), B1–N 159.7(2), B1–F1 137.3(2), B1–F2 137.7(2), B1–C^{F2} 163.9(3), C^{F2}–F 138.0(2), C^{F2}–C^{F3} 152.3(3), C^{F3}–F 132.2(3), N1–C2–C3 127.4(1).*

2.3.3 Borane-Functionalized Anionic Cyclic (Alkyl)(amino)carbenes

With the neutral borane-substituted cAAC-precursors **26** and **27** as starting materials in hand, their deprotonation to give the respective anionic cyclic (alkyl)(amino)carbenes was investigated. Treatment of **26** with LiHMDS did not lead to the formation of a stable anionic cAAC, but a complex mixture of boron-containing species was observed by NMR spectroscopy. Lithium (2-cyano-3,3-dimethyl-6-phenylpiperidine-1-yl)tricyanoborate Li**28** had formed as major product and was isolated in a yield of 51% (Figure 2.3.3.1). Crystals of Li**28**·CH_2Cl_2 were obtained by slow diffusion of CH_2Cl_2 into the reaction mixture. It was characterized by NMR and vibrational spectroscopy, mass spectrometry, and SC-XRD (Figure 2.3.3.1). $^2_\infty$[Li**28**·CH_2Cl_2] forms a two-dimensional coordination polymer with tetrahedrally coordinated Li ions. Li1 is coordinated by three cyano N atoms of different $B(CN)_3$ units and one N atom of the cyanopiperidine moiety. Formation of Li**28** is rationalized by initial deprotonation of **26** to give the respective anionic cAAC. This anionic cAAC undergoes subsequent intermolecular nucleophilic addition to a cyano group of a $B(CN)_3$ unit to result in an imine analogue. Related addition reactions of lithium organyls with cyanoborates have been described, earlier.[115] The B–C bond of the imine moiety is cleaved and the formal transfer of the cyano group to the carbene center is completed. It is not clear at which stage of the reaction the H atom is added to the C2 atom. However, THF is not the hydrogen source as the reaction in [D_8]THF did not result in monodeuterated **28**.

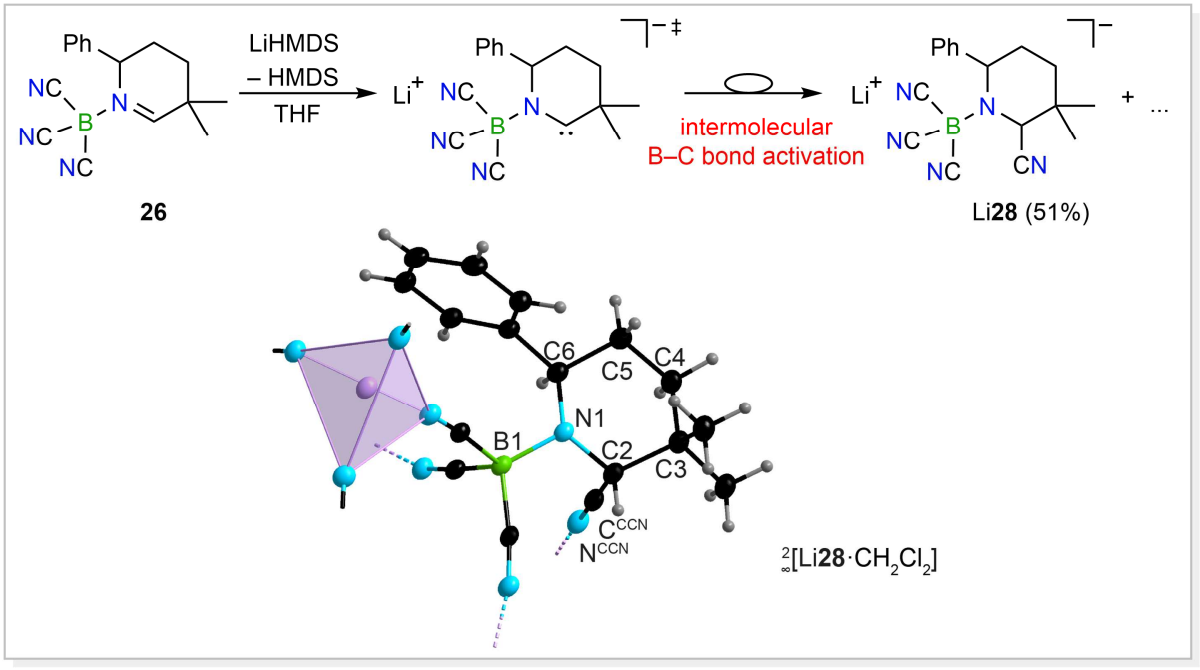

Figure 2.3.3.1 *Intermolecular follow-up reaction after deprotonation of **26** and a unit of $^2_\infty$[Li**28**·CH_2Cl_2] in the crystal structure (ellipsoids are drawn with 30% probability except for H atoms that are depicted with arbitrary radii, disordered co-crystallized dichloromethane of $^2_\infty$[Li**28**·CH_2Cl_2] is omitted for clarity). Selected bond lengths [pm] and angles [°] (mean value where applicable): N1–C2 147.5(3), C2–C3 154.3(4), C3–C4 153.5(5), C4–C5 152.6(4), C5–C6 152.4(4), C6–N1 149.6(4), B1–N 152.2(4), B1–CN 161.6(5), C≡N 114.7(4), C2–CN 150.5(3), C^{CCN}≡N^{CCN} 114.6(3), N1–C2–C3 114.5(2).*

In contrast to the deprotonation of **26**, treatment of **27** with lithium di-*iso*-propylamide (LDA) led to quantitative and selective deprotonation and formation of the lithium derivative of Ani-cAAC **29** (Figure 2.3.3.2). Surprisingly, the reaction of **27** with the weaker base LiHMDS in THF did not result in any reaction although bis(trimethylsilyl)amides are often employed for the synthesis of cAACs.[73,80,222] The high selectivity of the formation of **29** is in part attributed to the chemically inert substituents of the borane moiety in **27**. Lithium salt Li**29**·THF was isolated in 85% yield on a multi-gram scale, and it contains one equivalent of THF per formula unit as evident from NMR spectroscopy, elemental analysis, and SC-XRD. Deprotonation of **27** at the C2 atom under formation of anion **29** was confirmed by NMR spectroscopy (Figure 2.3.3.2). The ^{11}B NMR signal is shifted from 0.5 (**27**) to 1.0 ppm (**29**) and in the ^{1}H NMR spectrum of **29** the signal of the acidic proton (8.53 ppm for **27**) is absent. The most significant difference was observed in the ^{13}C{^{1}H} NMR spectrum for the signal of the C2 nucleus. This signal was shifted from 186.1 for **27** to 289.4 ppm for **29**, which is in the typical range observed for cAAC carbon nuclei, e.g. 304.2 ppm for cAAC^{Me}-5[79] or 330.3 ppm for cAAC^{Et}-6.[73] In the ^{13}C{^{19}F} NMR spectrum the signal is split into a quartet [^{2}J(^{13}C,^{11}B) ≈ 32 Hz] due to the coupling with ^{11}B (Figure 2.3.3.2). Related anionic NHC **5** reveals a ^{2}J(^{13}C,^{11}B) coupling of 11.8 Hz.[179]

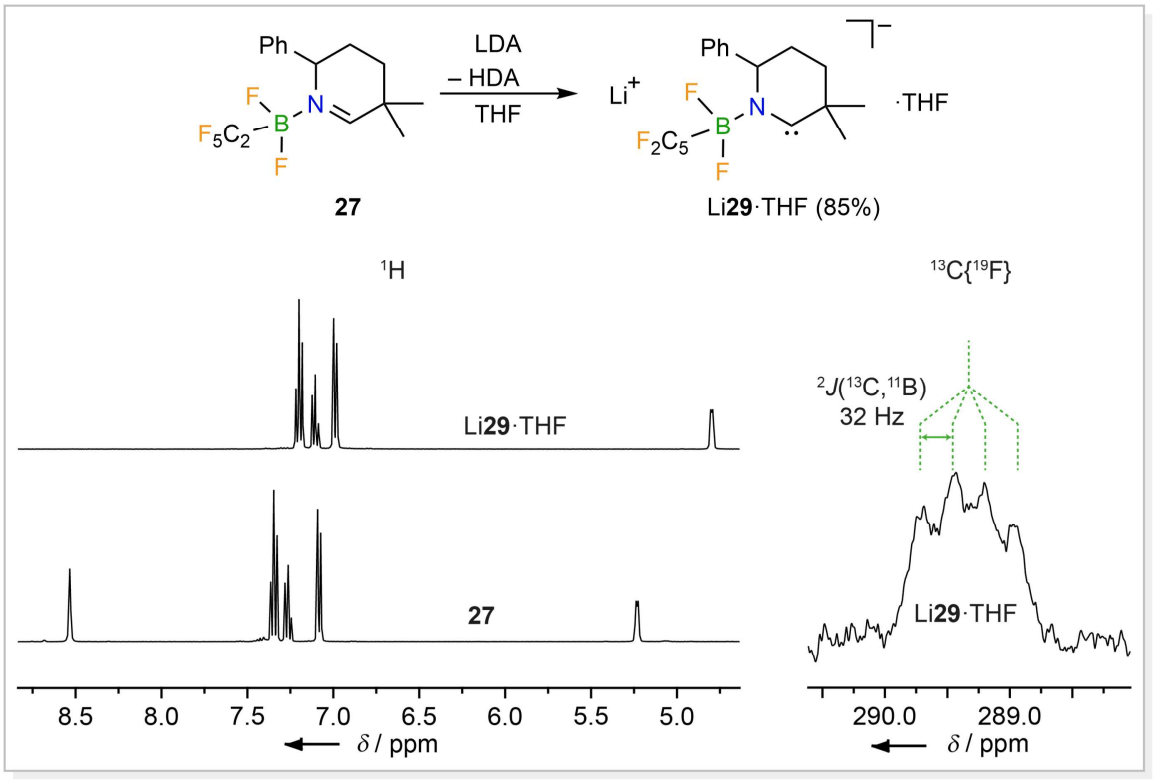

Figure 2.3.3.2 *Synthesis Li**29**·THF (top) and NMR spectra of **27** and Li**29**·THF (bottom).*

Single crystals of [Li**29**·THF]$_2$ were obtained by diffusion of hexane into a THF solution. Two carbene units form cyclic dimers *via* bridging Li1 atoms (Figure 2.3.3.3). Li1 is coordinated to the carbene atom C2 and the oxygen atom of a THF ligand. In addition, Li1 is oriented towards fluoride substituents of

the parent anionic cAAC, which is indicative for weak Li1···F interactions. The Li1–C2 distance of 212.7(9) pm is similar to related Li···$C_{carbene}$ separations, for example 217.0(6) pm in $^{2}_{\infty}$[Li**5**·THF].[179] The bond lengths and angles of **29** differ from those of **27**. The B–N distance is slightly shorter in **29** whereas *d*(C2–N1) and *d*(C2–C3) are slightly longer. Furthermore, the N1−C2−C3 angle is smaller in **29** (119.0(3)°) than in **27** (127.4(1)°) and is therefore even larger than in neutral cAAC-6.[73] All differences reflect the increased electron density at the carbene atom C2 in **29**, which results in a slight weakening of the C2–N1 and C2−C3 bonds, an increased basicity of the N atom in the ring and in turn a stronger B–N bond.

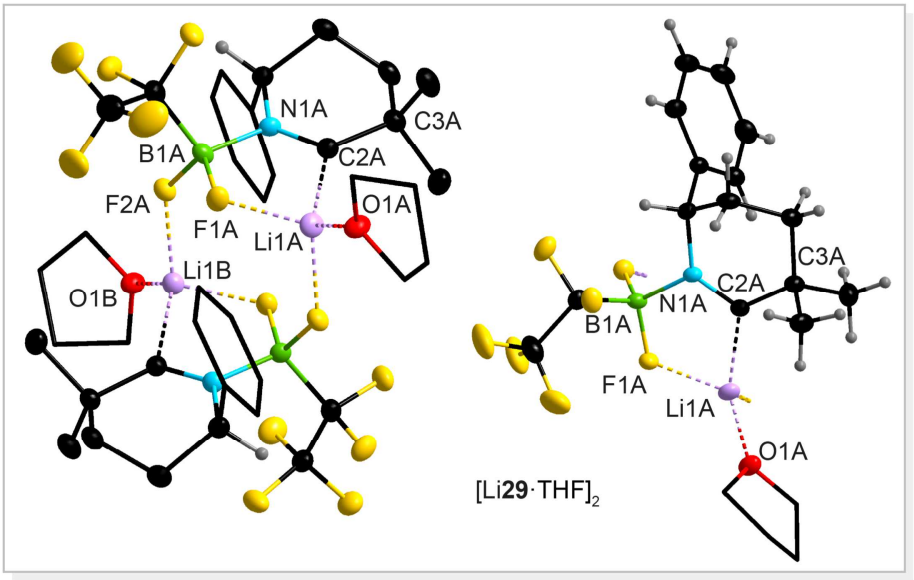

Figure 2.3.3.3 *A dimer and its monomer of [Li**29**·THF]$_2$ in the crystal structure (ellipsoids are drawn with 30% probability except for H atoms that are depicted with arbitrary radii, H atoms of the THF solvate molecules are not shown and their C atoms are depicted as wireframe model). Selected bond lengths [pm] and angles [°] (mean value where applicable): N1−C2 131.5(5), C2−C3 152.4(5), C3–C4 152.8(6), C4–C5 151.7(6), C5–C6 152.9(6), C6–N1 150.0(6), B1−N 154.8(6), B1−F1 141.2(6), B1−F2 141.3(6), B1−C^{F2} 163.6(6), C^{F2}−F 138.2(6), C^{F2}−C^{F3} 151.1(6), C^{F3}−F 133.6(6), Li1···C2 212.7(9), Li1···O1 190.3(8), Li1···F1 193.0(7), Li1···F2 192.0(8), N1−C2−C3 119.0(3).*

Lithium salt Li**29**·THF is stable up to 100 °C (DSC, onset) in the solid state and in solution decomposition is slow and takes weeks at room temperature. In the solid state, Li**29**·THF was stored without decomposition for month under an inert atmosphere.

DFT calculations (def2-TZVPP/B3LYP/D3(BJ)/COSMO [ε = infinite]) have been performed to evaluate the electronic features of Ani-cAAC-B(CN)$_3$, and Ani-cAAC-$C_2F_5BF_2$ (**29**) and of the related neutral cAAC^{Me}-5[79] and cAAC^{Me}-6.[73] The electronic structure of cAAC^{Me}-5 and cAAC^{Me}-6 can be considered as a 2 π-electron system superimposed by a carbene σ-type orbital, which is basically a sp^2-type hybrid orbital. The latter is the HOMO of the molecule and lies at –5.53 eV (cAAC^{Me}-5) or −4.99 eV (cAAC^{Me}-6, respectively (Figure 2.3.3.4). The carbene π-orbital of cAAC^{Me}-5 and cAAC^{Me}-6 is the LUMO and the

LUMO+2 orbital of cAAC^{Me}-6 is an additional π-orbital. These orbitals are mainly centered at the carbene C atom and are mostly composed of the carbene p-orbital. They lie at −0.42 eV (cAAC^{Me}-5), and −0.34 eV and 0.04 eV (cAAC^{Me}-6) resulting in σ/π-separations of 5.11 eV (cAAC^{Me}-5) and 4.65 eV (cAAC^{Me}-6). The separation decreases upon replacement of the Dipp group (Dipp = 2,6-di-*iso*-propylphenyl) against the anionic $B(CN)_3^-$ unit to 4.41 eV for Ani-cAAC-$B(CN)_3$. Related Ani-cAAC-$C_2F_5BF_2$ (**29**) with the anionic $C_2F_5BF_2^-$ moiety reveals a σ/π-separation of 4.93 eV. The HOMO of both Ani-cAACs is the carbene σ-orbital, whereas the relevant π-orbital is the LUMO of Ani-cAAC-$B(CN)_3$ and the LUMO+2 of Ani-cAAC-$C_2F_5BF_2$ (**29**) (Figure 2.3.3.4). As evident from the plots in Figure 2.3.3.4, the $B(CN)_3$ group causes a significant lowering of the π-orbital compared to the $C_2F_5BF_2$ group. This different behavior is explained by an efficient delocalization of electron density into the $B(CN)_3$ group. A similar behavior was observed for related imidazolin-2-ylidenates with one or two $B(CN)_3$ groups at nitrogen, previously (Chapter 2.1.3).[179] The σ-orbital (HOMO) is significantly raised by the $C_2F_5BF_2$ group, because of the reduced Lewis acidity of this group compared to $B(CN)_3$, which is also reflected by the fluoride ion affinities (FIA) of 362 and 540 kJ·mol^{-1} of $C_2F_5BF_2$[223] and $B(CN)_3$.[113] Thus, Ani-cAAC-$B(CN)_3$ is predicted to be an excellent π-acceptor, while Ani-cAAC-$C_2F_5BF_2$ (**29**) should be a very potent σ-donor. Compared to neutral and anionic borane-functionalized NHCs IMe, $IMeB(CN)_3^-$ **5**, and $IB(CN)_3^{2-}$ **6**, Ani-cAAC-$B(CN)_3$ and Ani-cAAC-$C_2F_5BF_2$ (**29**) are significantly stronger σ-donors and π-acceptors.[179]

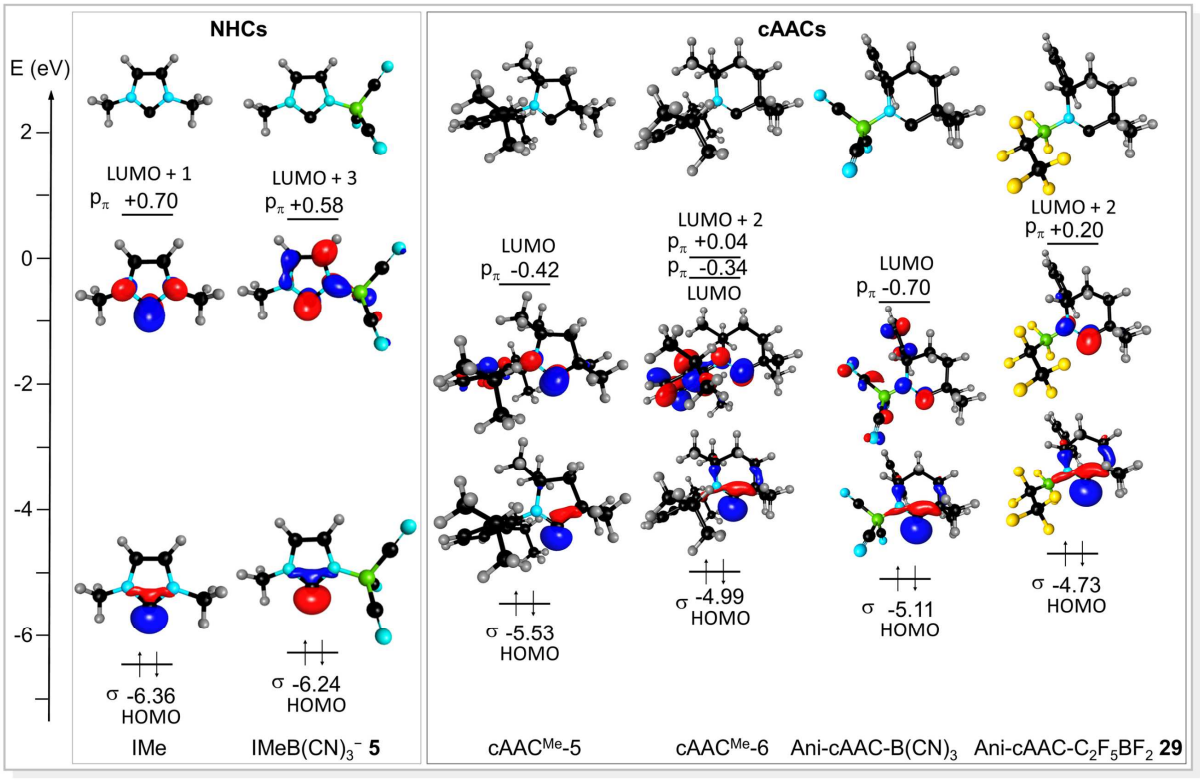

Figure 2.3.3.4 *σ- and π-orbitals of IMe, $IMeB(CN)_3^-$ **5**, cAAC^{Me}-5, cAAC^{Me}-6, Ani-cAAC-$B(CN)_3$, and Ani-cAAC-$C_2F_5BF_2$ **29**. Energies were calculated at the DFT/def2-TZVPP/B3LYP/D3(BJ)/COSMO [ε = infinite] level of theory and orbital plots are drawn at the 0.1 isosurface.*

2.3.4 Main Group Element Adducts and Transition Metal Complexes

The postulated intermediate formation of Ani-cAAC-B(CN)$_3$ was proven by deprotonation of **26** in the presence of selenium to result in selenium adduct **30**, which was isolated as tetraphenylphosphonium salt in 74% yield (Figure 2.3.4.1). The ^{77}Se signal of [PPh$_4$]**30** at 661.8 ppm in [D$_6$]DMSO (697.5 ppm for Li**30** in [D$_8$]THF) is indicative of an increased π-acceptor ability of Ani-cAAC-B(CN)$_3$ compared to neutral cAAC^{Me}-5 with δ(^{77}Se) of 492.4 ppm in [D$_8$]THF for the corresponding Se adduct cAAC^{Me}-5=Se.[224]. These results are in accordance with the calculated LUMO energies (Figure 2.3.3.4). The ^{77}Se NMR shift of 714.9 ppm in (CD$_3$)$_2$CO reported for cAAC^{Et}-6=Se[73] suggests a slightly stronger π-acceptor ability compared to Ani-cAAC-B(CN)$_3$. Considering the slightly higher LUMO energy of cAAC^{Me}-6, the increase in π-acceptor strength is rationalized by additional interactions with the π-acceptor orbital LUMO+2 leading to an overall stronger π-bonding. The ^1J(^{77}Se,^{13}C) coupling constant of **30** of 209.9 Hz was derived from the ^{13}C{^{1}H} NMR spectrum (Figure 2.3.4.2). This coupling constant is significantly smaller than values reported for selenium adducts of related neutral and anionic NHCs [228.0 Hz for the Se adduct of IMeB(CN)$^{3-}$ (**5**); 214.5 Hz for the Se adduct of IB(CN)$_3^{2-}$ (**6**) (Chapter 2.1.4);[179] 219 Hz for the Se adduct of SIMes[147] (SIMes = 1,3-dimesitylimidazolidin-2-ylidene)]. So, Ani-cAAC-B(CN)$_3$ should be a very potent σ-donor in agreement to the comparably high calculated HOMO energy (Figure 2.3.3.4).

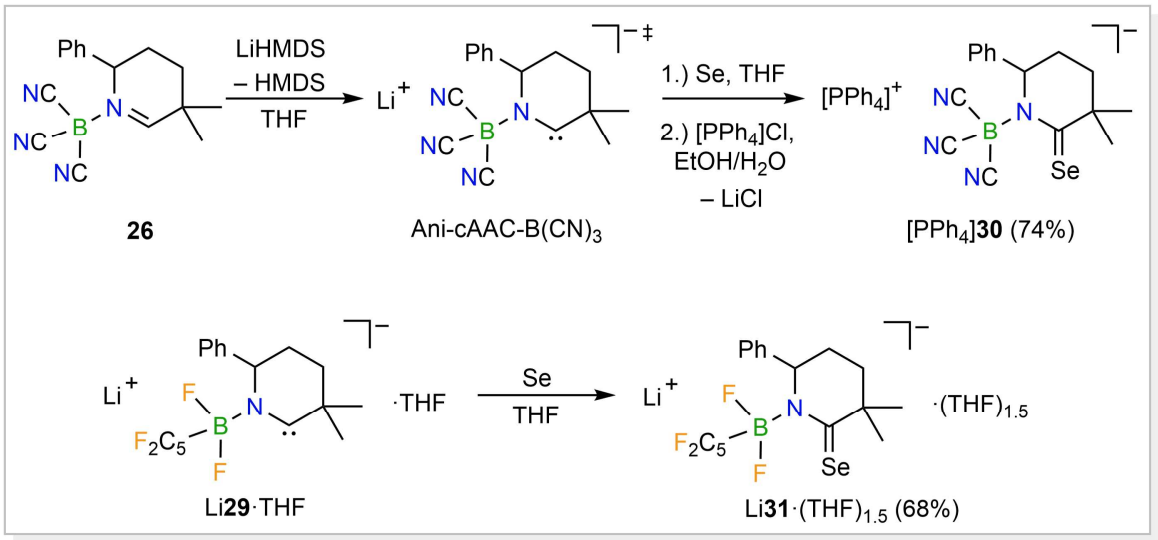

Figure 2.3.4.1 *Syntheses of [PPh$_4$]**30** and Li**31**·(THF)$_{1.5}$.*

The reaction of lithium salt of Ani-cAAC-C$_2$F$_5$BF$_2$, Li**29**·THF, with selenium gave the lithium salt of the corresponding selenium derivative Li**31**·(THF)$_{1.5}$ (Figure 2.3.4.1). In accordance with the relatively high energy of the π-acceptor orbital of **29** (Figure 2.3.3.4), δ(^{77}Se) of Li**31**·(THF)$_{1.5}$ is comparably low ~~(454.7 ppm in [D$_8$]THF) with respect to the Se derivatives of neutral cAAC^{Me}-5 and cAAC^{Et}-6, and anionic~~ Ani-cAAC-B(CN)$_3$. The small ^1J(^{77}Se,^{13}C) coupling constant of Li**31**·(THF)$_{1.5}$ of 206.0 Hz underlines the strong σ-donor ability of **29** compared to Ani-cAAC-B(CN)$_3$, which is attributed to the low Lewis acidity of the borane C$_2$F$_5$BF$_2$. The ^1J(^{13}C,^{1}H) coupling constants of the parent protonated adducts **26** and **27** of

178.7 and 179.7 Hz display the same trend in σ-donor strength for Ani-cAAC-B(CN)$_3$ and Ani-cAAC-$C_2F_5BF_2$ (**29**), as well.

The selenium derivatives [PPh$_4$]**30** and Li**31**·(THF)$_2$ were crystallized from acetone and pentane/THF solutions, respectively (Figure 2.3.4.2). The C2=Se1 distances of **30** (184.2(3) pm) and **31** (186.3(3) pm) are in the typical range for selenium carbene adducts, e.g. the selenourea derivative of IMeB(CN)$_3^-$ (**5**) *d*(C=Se) = 185.3(5) pm[179] and IB(CN)$_3^{2-}$ (**6**) *d*(C=Se) = 184.2(4) pm (Chapter 2.1.4).[218] The Li ion in Li**31**·(THF)$_2$ is tetrahedrally coordinated by the O atoms of two THF ligands, the boron bonded fluorine substituent F1, and Se1.

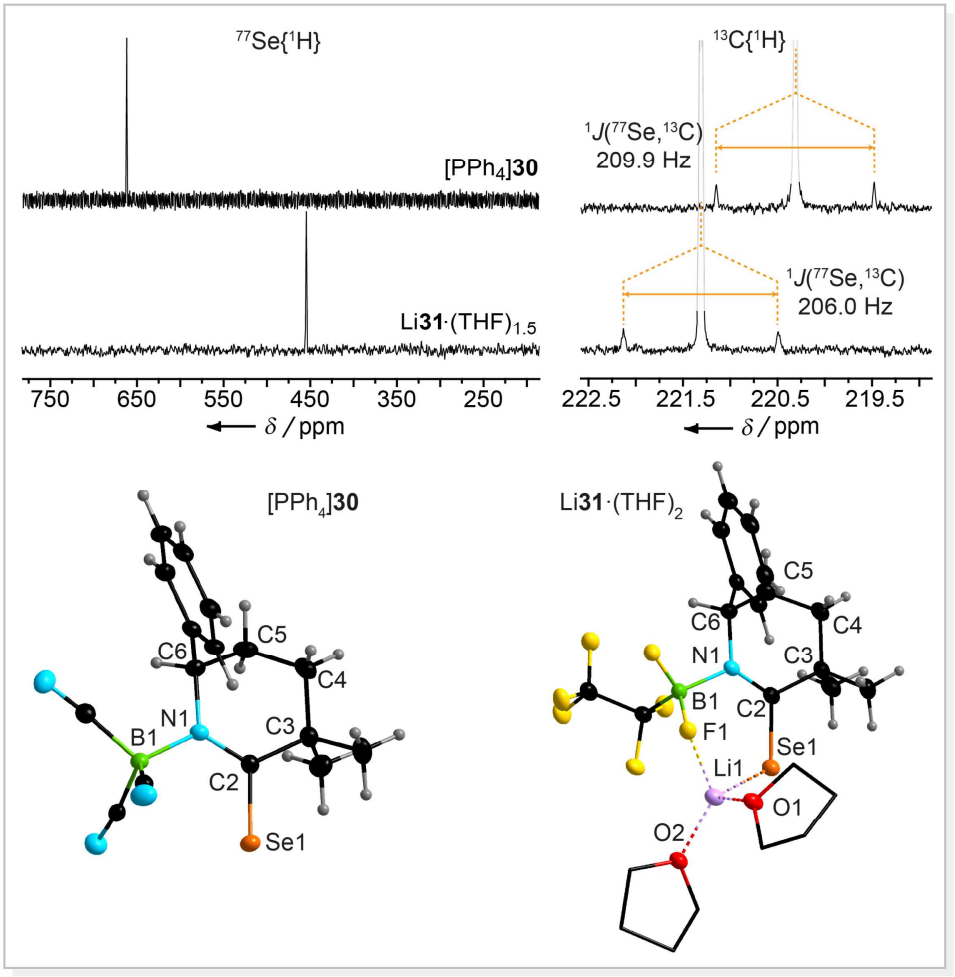

Figure 2.3.4.2 *NMR spectra (top), and crystal structures (bottom) of [PPh$_4$]**30** and Li**31**·(THF)$_{1.5}$ (ellipsoids are drawn at the 50% ([PPh$_4$]**30**) or 30% (Li**31**·(THF)$_2$) probability level except for the H atoms that are depicted with arbitrary radii, [PPh$_4$]$^+$ cation of [PPh$_4$]**30** is omitted for clarity, H atoms of the THF solvate molecules of Li**31**·(THF)$_2$ are not shown and their C atoms are depicted as wireframe model). Selected bond lengths [pm] and angles [°] (mean value where applicable): [PPh$_4$]**30**: N1–C2 133.6(4), C2–C3 155.0(5), C3–C4 152.9(5), C4–C5 151.5(5), C5–C6 152.4(5), C6–N1 148.1(4), B1–N 156.2(5), B1–CN 160.7(5), C≡N 115.0(5), C2–Se1 184.2(3), N1–C2–C3 121.6(3); Li**31**·(THF)$_2$: N1–C2 132.3(3), C2–C3 154.4(3), C3–C4 152.9(4), C4–C5 152.0(4), C5–C6 151.6(4), C6–N1 149.8(3), B1–N 158.1(3), B1–F1 141.0(3), B1–F2 138.4(3), B1–C^{F2} 165.4(5), C^{F2}–F 137.6(3), C^{F2}–C^{F3} 152.7(4), C^{F3}–F 133.4(4), C2–Se1 186.3(3), Li1···Se1 250.5(4), Li1···O1 190.0(5), Li1···O2 192.4(6), Li1···F1 185.5(5), N1–C2–C3 122.3(2).*

Chloro(triphenylphosphine)gold(I) was reacted with Li**29**·THF to result in the linear complex [Ani-cAAC−Au−PPh_3] (**32**) under salt elimination, which was isolated as benzene solvate in 92% yield (Figure 2.3.4.3). Crystals of **32** were obtained by slow diffusion of hexane into a benzene solution of the neutral complex. The C2−Au1 distance of 207.7(5) pm in **32** is similar do *d*(C−Au) of related linear carbene-gold(I) complexes, for instance 199.0(5) pm in $cAAC^{Ad}$-6−AuCl.[218] The PPh_3 ligand is slightly bent into the direction of the sterically less demanding methyl groups of the Ani-cAAC ligand with an C2−Au1−P1 angle of 175.9(2)°. The sterically more demanding $C_2F_5BF_2$ group effectively shields the gold atom, as evident from the steric map of the ligand (Figure 2.3.4.3). The buried volume (%V_{bur})[155,182] of **29** was determined from the X-ray crystal structural data to be 39.9%. So, it is larger than %V_{bur} reported for $cAAC^{Me}$-5 (38.0%)[225] and identical to %V_{bur} reported for $IB(CN)_3^{2-}$ **6** (Chapter 2.1.4).[218] Noteworthy, a significantly larger %V_{bur} of 43.3% was evaluated for **29** from the structural parameters of the selenium compound Li**31**·$(THF)_2$. This difference in %V_{bur} is attributed to the rotational freedom of the $C_2F_5BF_2$ unit, rendering Ani-cAAC **29** a ligand with a flexible steric environment. Assessment of the steric demand of Ani-cAAC-$B(CN)_3$ from the structure parameters of the selenium derivative **30** (44.4%) highlights the even greater steric demand of this carbene compared to Ani-cAAC-$C_2F_5BF_2$.

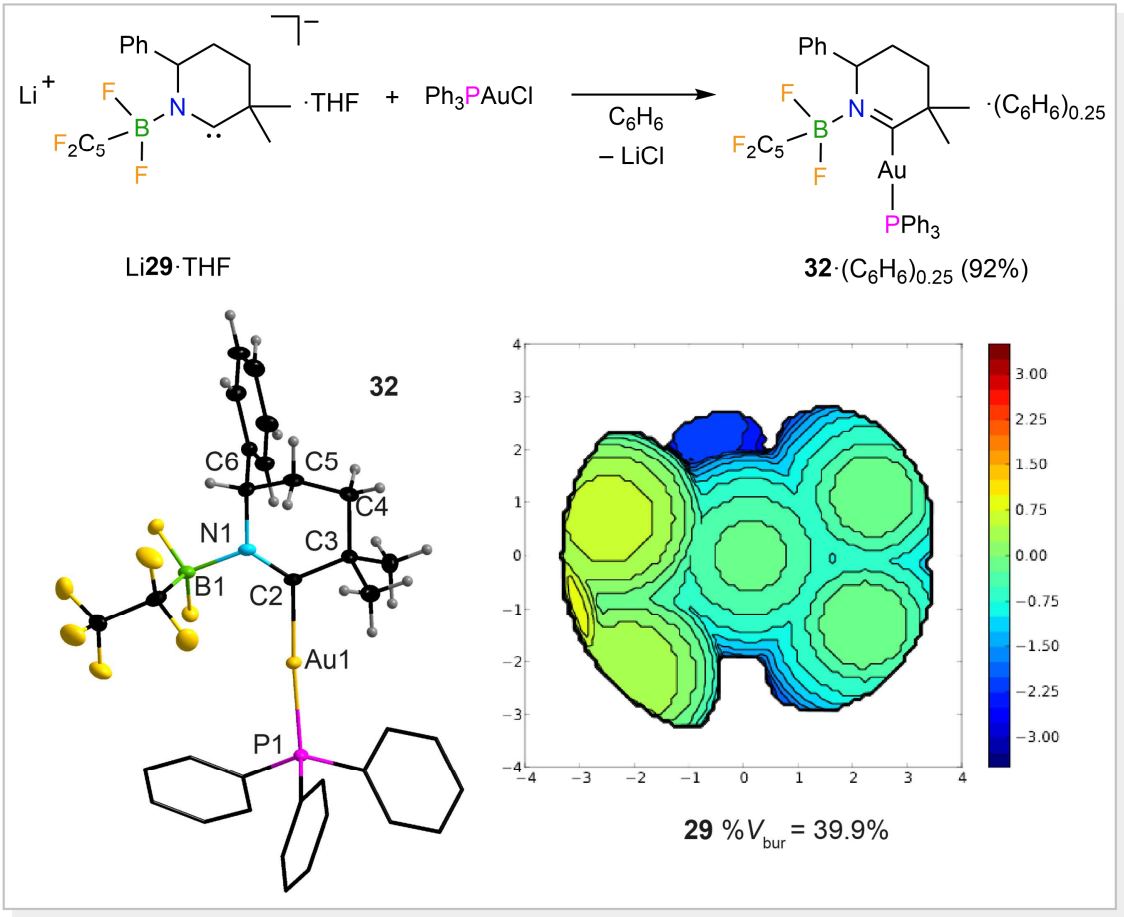

Figure 2.3.4.3 *Synthesis of* ***32***·$(C_6H_6)_{0.25}$ *(top), crystal structure of* ***32*** *and steric map of Ani-cAAC* ***29*** *(bottom; ellipsoids are drawn with 40% probability except for H atoms that are depicted with arbitrary radii, H atoms of the phenyl groups in* PPh_3 *are omitted for clarity and the C atoms are shown as stick model). Selected bond lengths [pm] and angles [°] (mean value where applicable): N1–C2 130.4(7), C2–C3 151.9(9), C3–C4 154.2(9), C4–C5 152.0(9), C5–C6 152.3(9), C6–N1 150.5(6), B1–N 159.1(8), B1–F1 139.5(7), B1–F2 138.7(8), B1–*C^{F2} *164.8(9),* C^{F2}*–F 138.1(7),* C^{F2}*–*C^{F3} *152.4(9),* C^{F3}*–F 133.7(8), C2–Au1 207.7(5), Au1–P1 228.4(1), N1–C2–C3 123.0(5), C2–Au1–P1 175.9(2).*

2.3.5 Conclusion

First anionic cAACs with $B(CN)_3$ and $C_2F_5BF_2$ substituents at the N atom of the central six-membered heterocycle have been synthesized. Ani-cAAC-$B(CN)_3$ could be generated *in situ* only since it undergoes intermolecular B−C bond activation. In contrast, Ani-cAAC-$C_2F_5BF_2$ **29** was isolated on a multi-gram scale (Figure 2.3.3.2). The precursors **26** and **27** of these carbenes are easily accessible in high yield *via* straightforward Lewis acid-base reactions. Noteworthy, multistep ring closure syntheses are unnecessary, which is in stark contrast to established syntheses of related neutral cAACs. The novel, broad modular synthetic approach may in principle be adopted for the preparation of enantiomerically pure hydropyridines providing access to novel chiral neutral and anionic cAACs. The anionic cAACs reported in this work show the strong influence of the borane substituent on the σ-donor and π-acceptor properties, which enables a tuning of the electronic properties, as demonstrated by quantum chemical calculations (Figure 2.3.3.4) and the corresponding selenium adducts **30** and **31** (Figure 2.3.4.1). Furthermore, the steric demand can be easily modified as evident from the buried volumes of Ani-cAAC-$B(CN)_3$ and Ani-cAAC-$C_2F_5BF_2$ (**29**). In summary, the potential variations, *i.e.* electronic properties, steric demand, charge, enabling customized properties in combination with the ease of accessibility, render borane-substituted Ani-cAACs a highly promising class of novel carbenes.

CHAPTER IV

EVALUATION OF STERIC PROPERTIES OF LEWIS ACIDS

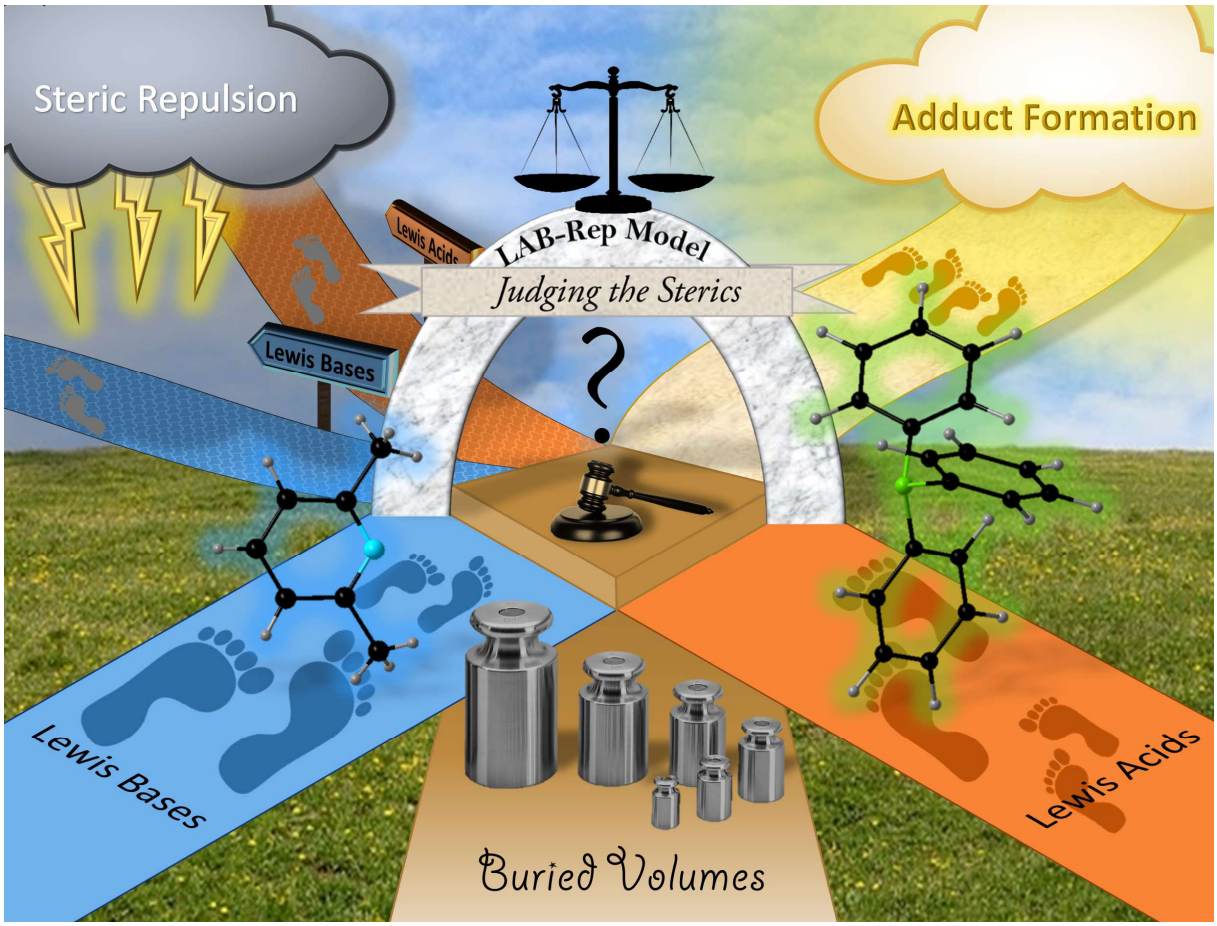

2.4 Evaluation of Steric Properties of Lewis Acids

2.4.1 Introduction

About a century ago, Gilbert N. Lewis reported Lewis acids and characterized these compounds as electron pair acceptors.[1,2] Since then, the synthesis of new Lewis acids and the investigation of their properties have become an intensely studied area of research.[226-231] It was shown that Lewis acids are efficient catalysts for various transformations,[232-235] and that sterically hindered Lewis acids are part of frustrated Lewis pairs (FLPs),[236-243] which are capable to activate small molecules such as H_2, CO, CO_2, and many more. The addition of a suitable Lewis acid to a transition metal complex often leads to catalytically active species, and thus Lewis acids are often used as co-catalysts for the activation of transition metal complexes.[244-250] Research on Lewis acids is often closely linked to the formation of weakly coordinating anions (WCAs),[251-255] as they are converted into WCAs upon reaction with a suitable metal complex precursor. For example, the reaction of metal fluoride complexes such as [(IDipp)CuF] with tris(pentafluoroethyl)difluorophosphorane $(C_2F_5)_3PF_2$ gave the dimeric cationic copper(I) complex $[\{(IDipp)Cu\}_2]^{2+}$ stabilized by the WCA $[(C_2F_5)_3PF_3]^-$.[165] In addition, the application of a transition metal complex in combination with a Lewis acid can enable tandem or bifunctional catalysis, in which two catalytic processes are combined; one of these processes is catalyzed by the transition metal complex and the other by the Lewis acid.[256]

A common feature of many Lewis acids is that they consist of a central atom that is surrounded by electronegative elements or substituents. Among the easiest and most widely used Lewis acids are group 13 and 15 molecules such as BF_3, $AlCl_3$, $GaCl_3$, PF_5, AsF_5, and SbF_5. Since trivalent boron(III) compounds have a vacant p_z orbital at boron, these molecules can be regarded as prime examples for Lewis acids.[257] Consequently, much effort has been made in the synthesis of boron-based Lewis acids.[13,112,117,258-271] Formal substitution of fluorine in BF_3 by strong electron withdrawing groups allows the tuning of both steric and electronic properties of a Lewis acid.[116,223,272] Different experimental and theoretical methods serve as measures for the Lewis acceptor properties and thus for Lewis acidity.[257] As an experimental scale of Lewis acidity the Gutmann-Beckett method is often used, which relies on ^{31}P NMR shifts of Et_3PO adducts of the Lewis acid under investigation.[273-276] According to Pearson's HSAB concept (hard and soft acids and bases)[277] the "hard" Lewis base Et_3PO should readily form adducts with "hard" Lewis acids such as BF_3. Thus, to extend the Gutmann-Beckett method towards "soft" Lewis acids, Lichtenberg *et al*. recently proposed the application of Me_3PS and Me_3PSe for adduct formation and a proper assessment of "soft" Lewis acids.[278,279] Another scale for Lewis acidity

The results of the chapter *Evaluation of Steric Properties of Lewis Acids* were published in:
"*An easy-to-perform evaluation of steric properties of Lewis acids"* L. Zapf, M. Riethmann, S. A. Föhrenbacher, M. Finze, U. Radius, *Chem. Sci.* **2023**, *14*, 2275–2288.
Experimental details can be found in the corresponding Supporting Information.

was suggested by Childs and co-workers, which relies on ^{1}H NMR chemical shifts of crotonaldehyde adducts (and other aldehydes) of Lewis acids.[280] An evaluation based on IR spectroscopy, that relies on the C≡N stretching frequency of acetonitrile CH_3CN[281-283] and its deuterated homologue CD_3CN,[284,285] which increases with increasing strength of the Lewis acid upon adduct formation, was established.[226] Baumgartner, Caputo and co-workers recently introduced a Lewis acidity scale based on the bathochromic shifts of the emission wavelengths of adducts of several Lewis acids and fluorescent dithienophosphole oxides,[286,287] and Ofial *et al*. developed a Lewis acidity scale for several triarylboranes based on the equilibrium constants of several N-, O-, P-, and S-donor Lewis acid/base adducts.[265,288] The most wide-spread measure to evaluate the strength of a Lewis acid nowadays is probably the fluoride ion affinity (FIA), which is defined as the negative reaction enthalpy of the addition of a fluoride ion to a Lewis acid in the gas phase.[289-291] Since a naked fluoride ion is difficult to approach by means of quantum chemical calculations, FIAs are typically calculated *via* isodesmic reactions, which use experimentally determined FIAs (e.g. of carbonyl fluoride OCF_2) or FIAs calculated on a high level of theory (e.g. of $Me_3Si–F$) as anchor points.[113,289-297] This concept has been expanded to ion affinities with respect to other anions such as chloride, hydride, and methide or alkoxide and also neutral Lewis bases such as water or ammonia and others, in part to also account for the differences between “hard” and “soft” Lewis acids.[113,116,223,289-297] Thus, a variety of Lewis acidity scales is available and easily applicable. A great advantage of calculated affinities is that, in contrast to Lewis acidities derived from experimental data, they can also be obtained for hypothetical or not yet isolated Lewis acids. Thus, quantum chemical calculations typically serve as a starting point for the synthesis of Lewis acids with tailored properties.

Beside electronic effects, steric effects play an important role in chemistry, in general. Steric interactions influence the shape and reactivity of molecules such as Lewis acids and Lewis bases. As steric effects have a decisive impact on properties and reactivity, several methods to assess steric properties have been developed.[298] In theory, the steric contributions to the activation free energy were typically analyzed and classified into potential and kinetic energy factors.[299-303] For experimentalists, the introduction of the cone angle to quantify the steric properties of phosphines by Tolman was a game-changer, as this method provided an easy-to perform evaluation of steric properties of ligands in organometallic chemistry.[304,305] Since then, many approaches for the quantification of steric effects of phosphines and other Lewis bases have been suggested.[154,155,306-312] However, to date there has been no comprehensive study dealing with steric effects of differently substituted Lewis acidic centers.

Working with Lewis acid/base adducts, the evaluation of stereo-electronic properties of Lewis acids, which specifically includes the steric properties of Lewis acids and their influence on the formation of Lewis acid/base adducts is a key research interest. In the following, an easy-to-apply model to estimate

the steric properties of Lewis acids without accounting for electronic factors or different electronic interaction models is presented. As there was no easy approach available to characterize steric properties of differently substituted Lewis acids, this problem was addressed and a model to access and quantify steric properties of Lewis acids was developed, which allows some prediction as to whether Lewis acid/base adduct formation can happen or not just by considering steric properties of the reactants (*i.e.*, waiving electronic factors). This model is based on the well-established concept of the percent buried volume (%V_{Bur}) developed by Cavallo and co-workers for ligands in coordination chemistry,[154,155,309-312] and was applied to different fluoride ion adducts of Lewis acids for cataloging steric properties of a large number (240) of different fluoride adducts of Lewis acids of group 13, 14, and 15 elements using low level DFT (def2-SV(P)/BP86) optimized geometries. Furthermore, a simple repulsion model, which predicts if Lewis acid/base adduct formation is, with respect to sterics, possible or not within seconds, just considering the steric demand of Lewis acids and bases. The capability of this LAB-Rep (**L**ewis **a**cid/**b**ase **rep**ulsion) model is demonstrated using several examples.

2.4.2 Evaluation of the Steric Demand of Lewis Acids *via* the Percent Buried Volume (%V_{Bur}) Model

It has been demonstrated in the past that the model of the percent buried volume (%V_{Bur}) that has been developed by Cavallo and co-workers is a versatile descriptor of steric properties of NHCs, phosphines, and related ligands in transition metal chemistry.[154,155,309-312] For transition metal complexes, the buried volume serves as a measure of the space occupied by a ligand in the first coordination sphere of a metal center. The calculation requires a definition of the metal center, to which the ligand is coordinated in a certain distance *d*. Then, a sphere of radius *R*, which is centered at the metal atom is created and the volume the ligand captures is assigned to the buried volume V_{Bur} of this sphere. The buried volume V_{Bur} indicates already the volume of the coordination sphere, which is occupied by the ligand, but typically the percentage of the volume buried by the ligand with respect to the volume of the total sphere (%V_{Bur}) leads to a meaningful result, which can be compared. However, the results obtained depend on the M–L distance *d* and the sphere radius *R*. So, both parameters should be chosen wisely and must be compared for any values given. This concept can be easily adopted to Lewis acid/base adducts, for example to fluoride ion adducts, of Lewis acids. If the fluorine atom of an anionic fluoride ion adduct [F–*LA*]$^-$ of the corresponding Lewis acid (*LA*) is used as anchor point of the system, %V_{Bur} can be estimated. This is shown in Figure 2.4.2.1 for two examples of Lewis acid/base adducts of the fluoride ion with BPh_3 and $(C_2F_5)_3PF_2$.

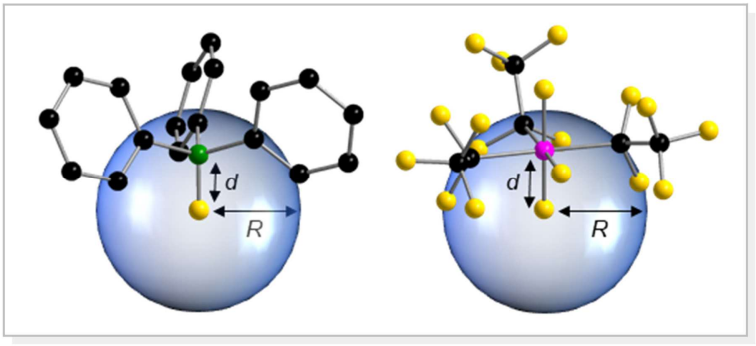

Figure 2.4.2.1 *Illustration of %V_{Bur}, exemplified by the Lewis acid/base adducts of the fluoride ion with BPh_3 (left) and $(C_2F_5)_3PF_2$ (right).*

It should be emphasized that any anchor point (chloride, methyl, hydride etc. adducts) can be chosen since electronic factors and hard and soft properties play no role in an exclusively steric model, as long as this anchor point is consistent. The steric properties of fluoride ion adducts [*LA*–F]$^-$ were chosen since these geometries are often available from calculations on fluoride ion affinities. In addition, fluoride adducts are often experimentally accessible *via* the reaction of a Lewis acid and a fluoride ion source. The model simply uses either calculated (geometry refined) or experimentally determined structures and the fluorine atom and the fluorine atom of the fluorine adducts [*LA*–F]$^-$ is placed at the

center of the sphere, which is then processed using the user-friendly SambVca 2.1 web application.[313] SambVca 2.1 was used to determine $\%V_{Bur}$ for several Lewis acids for a radius R = 3.50 Å. The latter radius is typically used for the determination of $\%V_{Bur}$ of transition metal ligands. Thus, the same radius R was chosen for the assessment of the steric demand of Lewis acids because all atoms that pose steric pressure to the center of consideration typically lie within this radius. For example, for the anion $[F{-}AlPh_3]^-$ the aluminum atom, the *ipso* carbon atom and the *ortho*-C−H units pointing at the fluoride are located within R = 3.50 Å (for an illustration of the lighter homologue $[F{-}BPh_3]^-$ see Figure 2.4.2.1, left side). Table 2.4.2.1 provides a list of $\%V_{Bur}$ of selected group 13 Lewis acids obtained from DFT (density functional theory) optimized geometries and Table 2.4.2.2 a list for selected group 14 and Table 2.4.2.3 a list of group 15 Lewis acids. A full list of all 240 Lewis acids considered together with cartesian coordinates of the oriented molecules suitable for the SambVca 2.1 web application, as well as different FIA values taken from the literature, is provided in the Supporting Information of the corresponding publication.[170]

Table 2.4.2.1 *$\%V_{Bur}$ of selected homoleptic group 13 Lewis acids (LAs) obtained from geometry optimized fluoride ion adducts $[LA{-}F]^-$ (R = 3.50 Å).*

LA	$\%V_{Bur}$	***LA***	$\%V_{Bur}$	***LA***	$\%V_{Bur}$
BH_3	27.3	**AlH_3**	24.8	**GaH_3**	24.7
BF_3	33.3	**AlF_3**	29.6	**GaF_3**	28.9
BCl_3	40.9	**$AlCl_3$**	34.5	**$GaCl_3$**	33.3
BBr_3	43.0	**$AlBr_3$**	35.6	**$GaBr_3$**	34.4
BI_3	45.5	**AlI_3**	37.2	**GaI_3**	36.0
$B(CN)_3$	38.9	**$Al(CN)_3$**	33.4	**$Ga(CN)_3$**	32.7
$B(C{\equiv}CH)_3$	39.3	**$Al(C{\equiv}CH)_3$**	33.5	**$Ga(C{\equiv}CH)_3$**	32.8
$B(CH_3)_3$	40.7	**$Al(CH_3)_3$**	34.1	**$Ga(CH_3)_3$**	33.4
$B(CF_3)_3$	50.8	**$Al(CF_3)_3$**	40.5	**$Ga(CF_3)_3$**	39.7
$B(C_2F_5)_3$	63.0	**$Al(C_2F_5)_3$**	47.5	**$Ga(C_2F_5)_3$**	46.9
BPh_3	53.1	**$AlPh_3$**	44.2	**$GaPh_3$**	42.7
BAr^F_3 [a]	53.7	**$AlAr^F_3$** [a]	45.5	**$GaAr^F_3$** [a]	45.1
$B(C_6F_5)_3$	58.9	**$Al(C_6F_5)_3$**	47.4	**$Ga(C_6F_5)_3$**	46.7
$B(C_6Cl_5)_3$	70.2	**$Al(C_6Cl_5)_3$**	59.0	**$Ga(C_6Cl_5)_3$**	58.1

[a] Ar^F = 3,5-$(CF_3)_2C_6H_3$

Table 2.4.2.2 *$\%V_{Bur}$ of selected group 14 homoleptic Lewis acids (LAs) obtained from geometry optimized fluoride ion adducts $[LA–F]^-$ (R = 3.50 Å).*

LA	Anion	$\%V_{Bur}$	***LA***	Anion	$\%V_{Bur}$	***LA***	Anion	$\%V_{Bur}$
SiF_4	$[SiF_5]^-$	37.9	**GeF_4**	$[GeF_5]^-$	37.2	**SnF_4**	$[SnF_5]^-$	36.3
$SiCl_4$	$[Cl_4SiF]^-_{eq}$	44.6	**$GeCl_4$**	$[Cl_4GeF]^-_{eq}$	42.6	**$SnCl_4$**	$[Cl_4SnF]^-_{eq}$	39.7
	$[Cl_4SiF]^-_{ax}$	46.0		$[Cl_4GeF]^-_{ax}$	44.2		$[Cl_4SnF]^-_{ax}$	41.8
$SiBr_4$	$[Br_4SiF]^-_{eq}$	46.7	**$GeBr_4$**	$[Br_4GeF]^-_{eq}$	44.4	**$SnBr_4$**	$[Br_4SnF]^-_{eq}$	41.1
	$[Br_4SiF]^-_{ax}$	48.3		$[Br_4GeF]^-_{ax}$	46.3		$[Br_4SnF]^-_{ax}$	43.5
SiI_4	$[I_4SiF]^-_{eq}$	49.4	**GeI_4**	$[I_4GeF]^-_{eq}$	46.9	**SnI_4**	$[I_4SnF]^-_{eq}$	43.1
	$[I_4SiF]^-_{ax}$	51.3		$[I_4GeF]^-_{ax}$	49.1		$[I_4SnF]^-_{ax}$	45.9
$Si(CN)_4$	$[(NC)_4SiF]^-_{eq}$	43.2	**$Ge(CN)_4$**	$[(NC)_4GeF]^-_{eq}$	41.7	**$Sn(CN)_4$**	$[(NC)_4SnF]^-_{eq}$	39.3
	$[(NC)_4SiF]^-_{ax}$	44.2		$[(NC)_4GeF]^-_{ax}$	42.7		$[(NC)_4SnF]^-_{ax}$	40.8
$Si(CF_3)_4$	$[(CF_3)_4SiF]^-_{eq}$	54.6	**$Ge(CF_3)_4$**	$[(CF_3)_4GeF]^-_{eq}$	51.8	**$Sn(CF_3)_4$**	$[(CF_3)_4SnF]^-_{eq}$	47.1
	$[(CF_3)_4SiF]^-_{ax}$	57.4		$[(CF_3)_4GeF]^-_{ax}$	54.6		$[(CF_3)_4SnF]^-_{ax}$	50.0
$Si(C_6F_5)_4$	$[(C_6F_5)_4SiF]^-_{eq}$	63.9	**$Ge(C_6F_5)_4$**	$[(C_6F_5)_4GeF]^-_{eq}$	61.8	**$Sn(C_6F_5)_4$**	$[(C_6F_5)_4SnF]^-_{eq}$	58.7
	$[(C_6F_5)_4SiF]^-_{ax}$	65.4		$[(C_6F_5)_4GeF]^-_{ax}$	61.9		$[(C_6F_5)_4SnF]^-_{ax}$	56.6

Table 2.4.2.3 *$\%V_{Bur}$ of selected group 15 homoleptic Lewis acids (LAs) obtained from geometry optimized fluoride ion adducts $[LA–F]^-$ (R = 3.50 Å).*

LA	anion	$\%V_{Bur}$	***LA***	anion	$\%V_{Bur}$	***LA***	anion	$\%V_{Bur}$
PF_3	$[PF_4]^-$	29.6	**AsF_3**	$[AsF_4]^-$	19.2			
PCl_3	$[Cl_3PF]^-$	42.0	**$AsCl_3$**	$[Cl_3AsF]^-$	34.1			
PBr_3	$[Br_3PF]^-$	45.0	**$AsBr_3$**	$[Br_3AsF]^-$	34.4			
PI_3	$[I_3PF]^-$	45.9	**AsI_3**	$[I_3AsF]^-$	34.5			
$P(CF_3)_3$	$[(CF_3)_3PF]^-$	46.4	**$As(CF_3)_3$**	$[(CF_3)_3AsF]^-$	35.3			
$P(C_2F_5)_3$	$[(C_2F_5)_3PF]^-$	51.6	**$As(C_2F_5)_3$**	$[(C_2F_5)_3AsF]^-$	43.3			
PF_5	$[PF_6]^-$	38.4	**AsF_5**	$[AsF_6]^-$	35.6	**SbF_5**	$[SbF_6]^-$	37.4
PCl_5	$[Cl_5PF]^-$	49.6	**$AsCl_5$**	$[Cl_5AsF]^-$	45.1	**$SbCl_5$**	$[Cl_5SbF]^-$	45.0
$P(CN)_5$	$[(NC)_5PF]^-$	48.0	**$As(CN)_5$**	$[(NC)_5AsF]^-$	44.4	**$Sb(CN)_5$**	$[(NC)_5SbF]^-$	43.4
$P(CF_3)_5$	$[(CF_3)_5PF]^-$	63.9	**$As(CF_3)_5$**	$[(CF_3)_5AsF]^-$	59.1	**$Sb(CF_3)_5$**	$[(CF_3)_5SbF]^-$	55.4
$P(C_6F_5)_5$	$[(C_6F_5)_5PF]^-$	77.8	**$As(C_6F_5)_5$**	$[(C_6F_5)_5AsF]^-$	73.5	**$Sb(C_6F_5)_5$**	$[(C_6F_5)SbF]^-$	69.5

In addition, topographic steric maps[313] of the Lewis acids BF_3, $B(CN)_3$, BCl_3, BPh_3, $B(C_6F_5)_3$, and $B(C_6Cl_5)_3$ in their fluoride adducts $[BF_4]^-$, $[(NC)_3BF]^-$, $[Cl_3BF]^-$, $[Ph_3BF]^-$, $[(C_6F_5)_3BF]^-$, and $[(C_6Cl_5)_3BF]^-$ (R = 3.50 Å) are provided in Figure 2.4.2.2, and the full set of topographic steric maps of all Lewis acids studied is provided in the Supporting Information of the corresponding publication.[170]

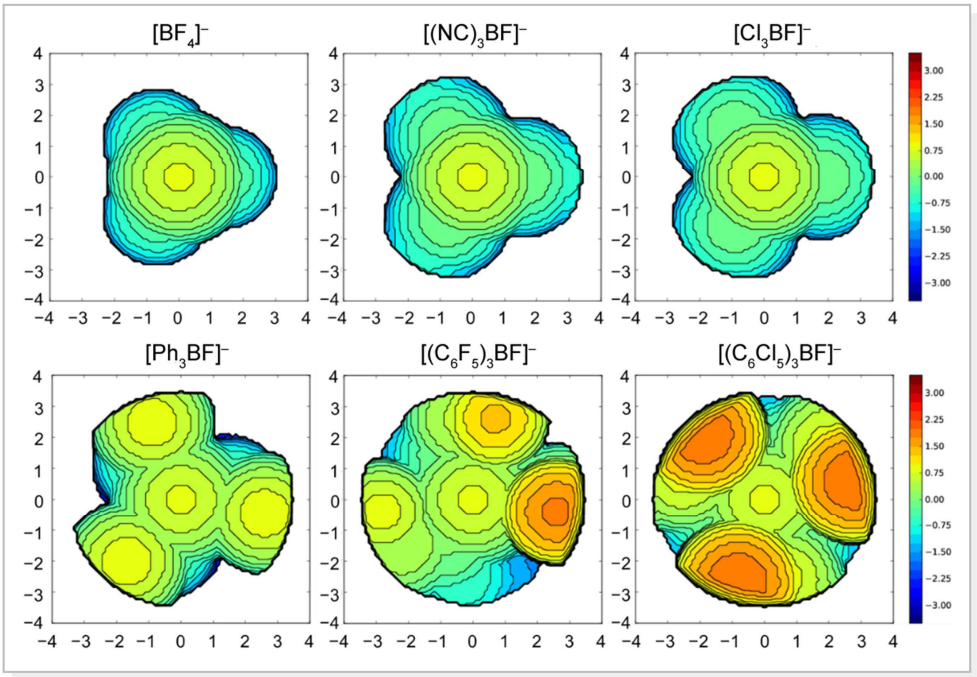

Figure 2.4.2.2 *Topographic steric maps of the Lewis acids BF_3, $B(CN)_3$, BCl_3, BPh_3, $B(C_6F_5)_3$, and $B(C_6Cl_5)_3$ in their fluoride adducts $[BF_4]^-$, $[(NC)_3BF]^-$, $[Cl_3BF]^-$, $[Ph_3BF]^-$, $[(C_6F_5)_3BF]^-$, and $[(C_6Cl_5)_3BF]^-$ (d(B–F) = 1.40 Å, R = 3.50 Å). The isocontour scheme is given in Å, red and blue zones indicate the more- and less-hindered zones with respect of the origin.*

As intuitively expected, the smallest $\%V_{Bur}$ of the boranes studied was obtained for BH_3 (27.3%). Substitution of hydrogen by halogen led to an increase of $\%V_{Bur}$: BH_3 (27.3%) < BF_3 (33.3%) < BCl_3 (40.9%) < BBr_3 (43.0%) < BI_3 (45.5%). The steric demand of boron Lewis acids with linear substituents such as $B(CN)_3$ (38.9%) and $B(C{\equiv}CH)_3$ (39.3%) is similar to the one of BCl_3 (40.9%). The substituents CH_3, CF_3, and C_2F_5 are bulkier $B(CH_3)_3$ (40.7%) < $B(CF_3)_3$ (50.8%) < $B(C_2F_5)_3$ (63.0%); the latter imposes more steric bulk than C_6H_5, C_6F_5, and 3,5-$(CF_3)_2C_6H_3$: BPh_3 (53.1%) < BAr^F_3 (Ar^F = 3,5-$(CF_3)_2C_6H_3$; 53.7%) < $B(C_6F_5)_3$ (58.9%). The extraordinary steric protection of the pentafluoroethyl substituent $–C_2F_5$ has been demonstrated experimentally, earlier.[18,165,168,314-323] Substitution of hydrogen in *meta*-position of BPh_3 with CF_3 groups has only little influence on the bulkiness of the Lewis acid (cf. 53.1% for BPh_3 vs. 53.7% for BAr^F_3). In $B(C_6Cl_5)_3$ the high steric demand of the C_6Cl_5 group results in an increase of $\%V_{Bur}$ to 70.2%. *ortho*-Substituted boranes exceed these values and the bulkiest boron Lewis acid considered in this study is B{2,4,6-$(CF_3)_3C_6H_2$}$_3$ (85.9%). However, B{2,4,6-$(CF_3)_3C_6H_2$}$_3$ and the related borane B{2,6-$(CF_3)_2C_6H_3$}$_3$ remain unknown. Examples for synthetically accessible sterically highly demanding Lewis acids are B{$OC(CF_3)_3$}$_3$ (FIA = 423 kJ·mol^{-1})[324,325] and $B(1,2\text{-}C_2B_{10}H_{11})_3$ (FIA = 605 kJ·mol^{-1})[326] with

a buried volume of %V_{Bur} = 71.9%. For aluminum, the Lewis acids Al{OC(CF$_3$)$_3$}$_3$ (FIA = 543 kJ·mol^{-1}; 56.8%)[327] and Al{N(C$_6$F$_5$)$_2$}$_3$ (FIA = 555 kJ·mol^{-1}; 68.1%),[328] and the recently reported Al(OTeF$_5$)$_3$ (FIA = 591 kJ·mol^{-1}; 51.5%)[329] provide excellent combinations of steric bulk and high Lewis acidity.

A chart of %V_{Bur} vs. Lewis-acidic atoms of all Lewis acids considered shows that there is a wide range of %V_{Bur} covered by the different Lewis acids and that any steric demand between %V_{Bur} = 30% and %V_{Bur} = 75% can be realized, easily (details provided in the Supporting Information of the corresponding publication[170]). Thus, easy tuning of %V_{Bur} is possible by proper choice of the central atom and the substituents. Lewis acids of aluminum and gallium typically exhibit smaller %V_{Bur} than related boron-based Lewis acids, which reflects the larger E–X distances of E = Al, Ga compared to that of E = B. The values of %V_{Bur} range from 29.6% (AlF$_3$) to 37.2% (AlI$_3$) for aluminum halides and from 28.9% (GaF$_3$) to 36.0% (GaI$_3$) for gallium halides. All %V_{Bur} values decrease in the order B >> Al > Ga.

Even more valuable than solely considering steric aspects are diagrams that correlate %V_{Bur} and fluoride ion affinity (FIA) as a scale for the Lewis acidity of a compound. In the 1970s, Tolman demonstrated that the IR frequency of the A1 stretch in Ni(CO)$_3$L, where L was a monodentate phosphorus donor ligand of interest, was a useful probe to quantify the electron-donating ability of the ligand L,[305,330] nowadays known as the Tolman electronic parameters TEPs. Charts of the Tolman electronic parameter with the Tolman cone angle as the quantification of the steric demand for many phosphines usually serve the organometallic community as a basis for phosphine ligand choice. Recently, the method was applied to the determination of the electronic and steric properties of various NHC donor ligands.[148,331,332] Diagrams which correlate the steric properties *via* %V_{Bur} and the Lewis acidity *via* fluoride ion affinity (FIA) can serve in a similar way for proper choice of Lewis acids. Such correlation diagrams combine steric and electronic features of the Lewis acid and a plot of %V_{Bur} vs. FIA of all Lewis acids considered herein is provided in the Supporting Information of the corresponding publication.[170] This chart shows that a wide range of combinations of %V_{Bur} (30–75%) and FIA (200–600 kJ·mol^{-1}) is available by choosing the central atom and its substituents. A comparison of the stereo-electronic properties of boron, aluminum, and gallium halides is shown in Figure 2.4.2.3. This chart reveals the dispersion in the stereo-electronic features of boron-based Lewis acids, which span a range of 12.2% in %V_{Bur} and 100 kJ·mol^{-1} in FIA,[296,297] compared to those of aluminum- (7.6% and 28 kJ·mol^{-1}) and gallium-based (7.1% and 20 kJ·mol^{-1}) Lewis acids. The wider range of %V_{Bur} and FIAs accessible with boron-based Lewis acids, in general, is mainly due to shorter E–X distances between boron and its substituents compared to Al and Ga. These relatively short B–X distances compared to Al–X and Ga–X distances are accompanied by a pronounced impact not only on the steric situation but also on the electronic features of the central boron atom compared to aluminum or gallium.[333-346]

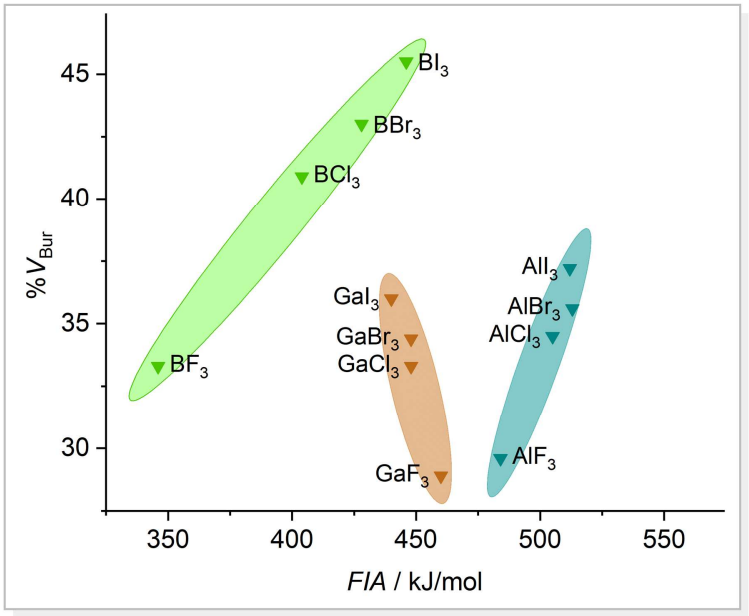

Figure 2.4.2.3 *Comparison of the stereo-electronic properties of group 13 halides (FIAs were taken from the literature[296,297]).*

For the evaluation of group 14 Lewis acids EX_4 (Figure 2.4.2.5) two isomers formed with the Lewis base (*LB*) were considered, e.g., the fluoride ion, either in equatorial or in axial position (Figure 2.4.2.4). A selection of $\%V_{Bur}$ values of group 14 and group 15 Lewis acids obtained from geometry optimized fluoride ion adducts $[LA–F]^-$ is provided in Table 2.4.2.2 and Table 2.4.2.3.

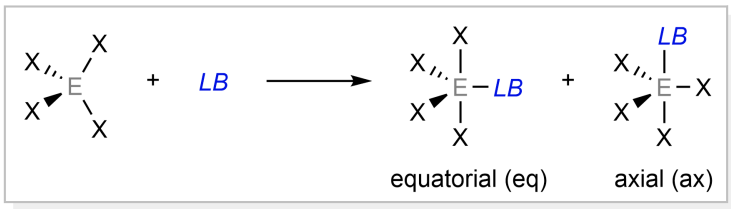

Figure 2.4.2.4 *Stereoisomers of Lewis acid/base adducts of a Lewis base LB with a group 14 Lewis acid EX_4.*

First of all, even the small Lewis acids EF_4 (E = Si, $\%V_{Bur}$ = 37.9%; Ge, 37.2%; Sn, 36.3%) are sterically more demanding than their group 13 and group 15 counterparts EF_3 (E = Al, $\%V_{Bur}$ = 29.6%; Ga, 28.9%; P, 29.6%; As, 19.2%), which is mostly a consequence of the additional fourth substituent. Thus, the increase in steric demand is even more pronounced for group 15 Lewis acids EF_5 (E = P, $\%V_{Bur}$ = 38.4%; As, 35.6%; Sb, 37.4%; Table 2.4.2.3). In the case of group 14 Lewis acids, the Lewis base bonded in axial position usually experiences a larger EX_4 group than the Lewis base coordinated in the equatorial position; c.f. $SiCl_4$ (eq: $\%V_{Bur}$ = 44.6%; ax: $\%V_{Bur}$ = 46.0%) or $Si(CF_3)_4$ (eq: $\%V_{Bur}$ = 54.6%; ax: $\%V_{Bur}$ = 57.4%), which is in line with the general expectation that the equatorial positions of trigonal bipyramids are less sterically demanding.

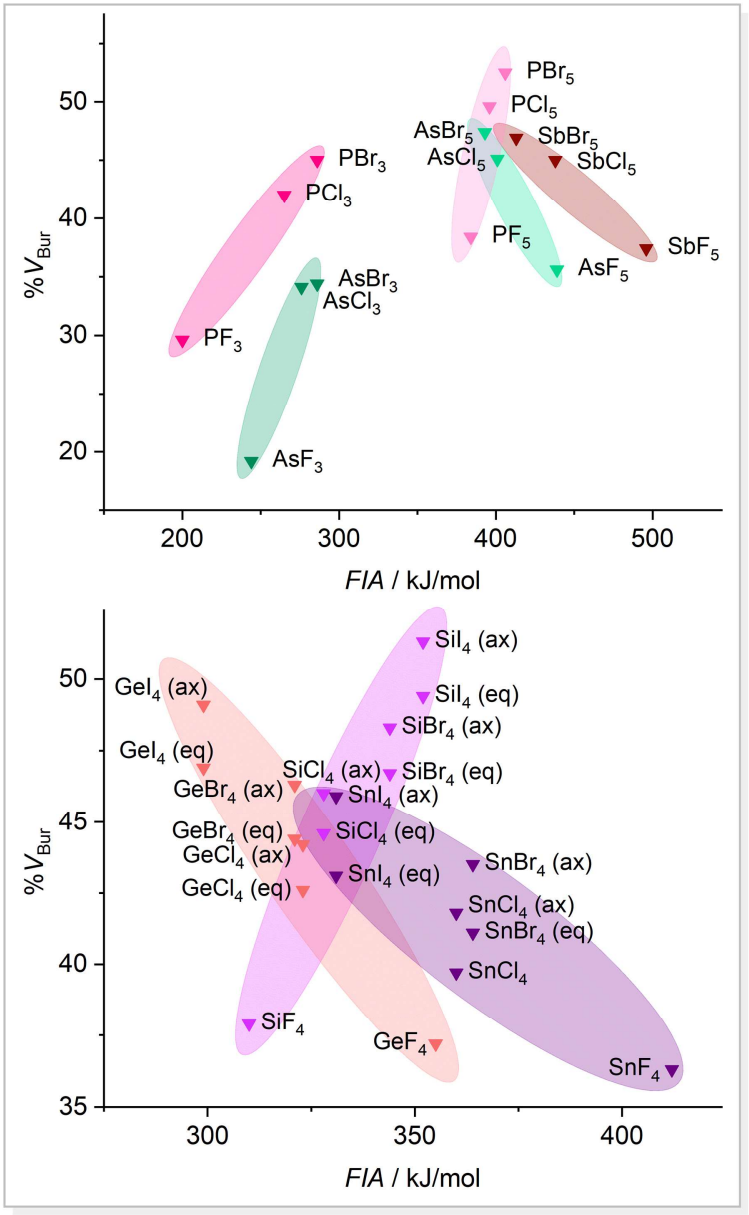

Figure 2.4.2.5 *Comparison of the stereo-electronic properties of group 14 (top) and group 15 (bottom) halides (FIAs were taken from the literature[296,297]).*

For group 13–15 element halides FIA increases for the lighter elements such as B, Al, Si, and P with the heavier and larger halogen, *i.e.* $EF_n > ECl_n < EBr_n < EI_n$ (E = B, Al, Si, P; n = 3 {B, Al, P}, 4 {Si}, 5 {P}), whereas for the heavier elements Ge, Sn, As, and Sb the opposite trend occurs, *i.e.* FIA increases on going to the lighter and sterically less demanding halogen, $EF_n > ECl_n > EBr_n > EI_n$ (E = Ge, Sn, As, and Sb; n = 4 {Ge, Sn}, 5 {Sb}). The halides of Ga and As are borderline cases, as the dispersion of the FIA values of Ga(III) halides is small (FIA{GaF_3} = 460 kJ·mol^{-1} vs. FIA{GaI_3} = 440 kJ·mol^{-1}; a larger FIA value for the fluoride) and for As the FIAs are in opposite direction for the As(III) halides (FIA{AsF_3} = 244 kJ·mol^{-1} vs. FIA{$AsBr_3$} = 286 kJ·mol^{-1}; a smaller FIA value for the fluoride) and the As(V) halides (FIA{AsF_5} = 439 kJ·mol^{-1} vs. FIA{$AsBr_5$} = 393 kJ·mol^{-1}; a larger FIA value for the fluoride).

Since the Lewis acidities of B, Al, and Si halides EX_3 and EX_4 increase with the less electronegative, larger halogen substituents, “cigars” with a positive slope result in the diagrams shown in Figure 2.4.2.3 and Figure 2.4.2.5. In contrast, “cigars” with a negative slope are observed for Ge and Sn halides EX_4 with the higher, less electronegative halogen substituents because the Lewis acidity decreases on going to the heavier halogens. The FIA calculated for the gallium halides GaX_3 are almost invariant to changes in the halogen substituent and thus differ only in their steric demand.

In addition, the percent buried volume of PF_5 and the related pentafluoroethyl(fluoro)phosphoranes $(C_2F_5)_nPF_{5-n}$ was examined. Due to the higher coordination number of the phosphorus(V) derivatives, the $\%V_{Bur}$ of PF_5 (38.4%) is higher than those of AlF_3 (29.6%), SiF_4 (37.9%), and PF_3 (29.6%). The evaluation of $\%V_{Bur}$ of unsymmetrical Lewis acids such as the phosphoranes $(C_2F_5)_nPF_{5-n}$ is easily resolved using the model described herein. The evaluation of $\%V_{Bur}$ can be performed for the different isomers that are either experimentally observed or considered in a theoretical study. The assessment of the different isomers of the pentafluoroethyl(fluoro)phosphate anions in Figure 2.4.2.6 demonstrates the strong influence of isomers on the steric demand *via* the $\%V_{Bur}$, in general. Typically, the lowest value for $\%V_{Bur}$ is the most reasonable.

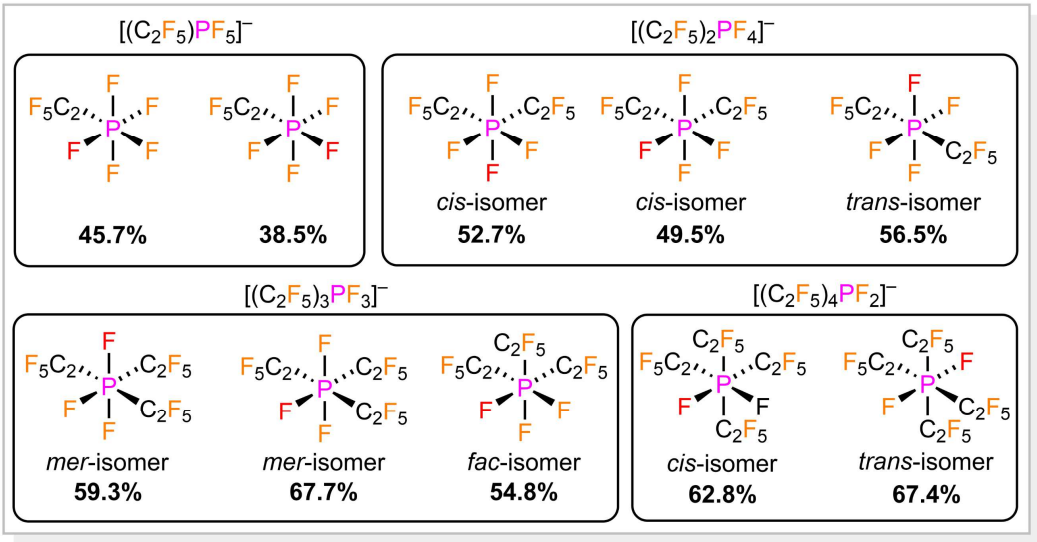

Figure 2.4.2.6 *Pentafluoroethyl(fluoro)phosphoranes $(C_2F_5)_nPF_{5-n}$ and their $\%V_{Bur}$ values.*

2.4.3 LAB-Rep – An Empirical Model for the Evaluation of Lewis Acid/Base Adduct Formation

With the percent buried volumes $\%V_{Bur}$ of various Lewis acids in hand, an empirical model (LAB-Rep model; **L**ewis **a**cid/**b**ase **rep**ulsion model) was developed to predict whether an arbitrary pair of Lewis acid and Lewis base may form an adduct with respect to their steric properties. This model just requires the principal shape of the Lewis acid and Lewis base and their buried volumes $\%V_{Bur\_LA}$ and $\%V_{Bur\_LB}$, respectively, to provide a prediction if Lewis acid/base complexes can form for steric reasons. It should be emphasized that this estimation is executed at no cost (computational time, etc.) and an Excel sheet (see also Figure 2.4.3.4) for this purpose that requires minimum input data is provided in the Supporting Information of the corresponding publication.[170] The shape of the components can be derived from experimental data, from quantum chemical calculations, from models prepared with Chem3D,[347] or similar programs. The $\%V_{Bur}$ are accessible as described in the preceding section. In the model to determine $\%V_{Bur}$ of a Lewis acid (*LA*) or a Lewis base (*LB*), the compounds are bonded to a coordinating center *Z* at a certain distance *d* and projected into a sphere *S* with a radius *R* (Figure 2.4.2.1). For Lewis acids, *Z* may be fluorine (*vide supra*), for Lewis bases, *Z* may be a transition metal, e.g. nickel, gold, etc., located at the center of the sphere (Figure 2.4.3.1). For the evaluation of whether an acid/base adduct can form, or not, both entities, the Lewis acid and the Lewis base, were projected into a single sphere *S* with radius *R* as demonstrated in Figure 2.4.3.1.

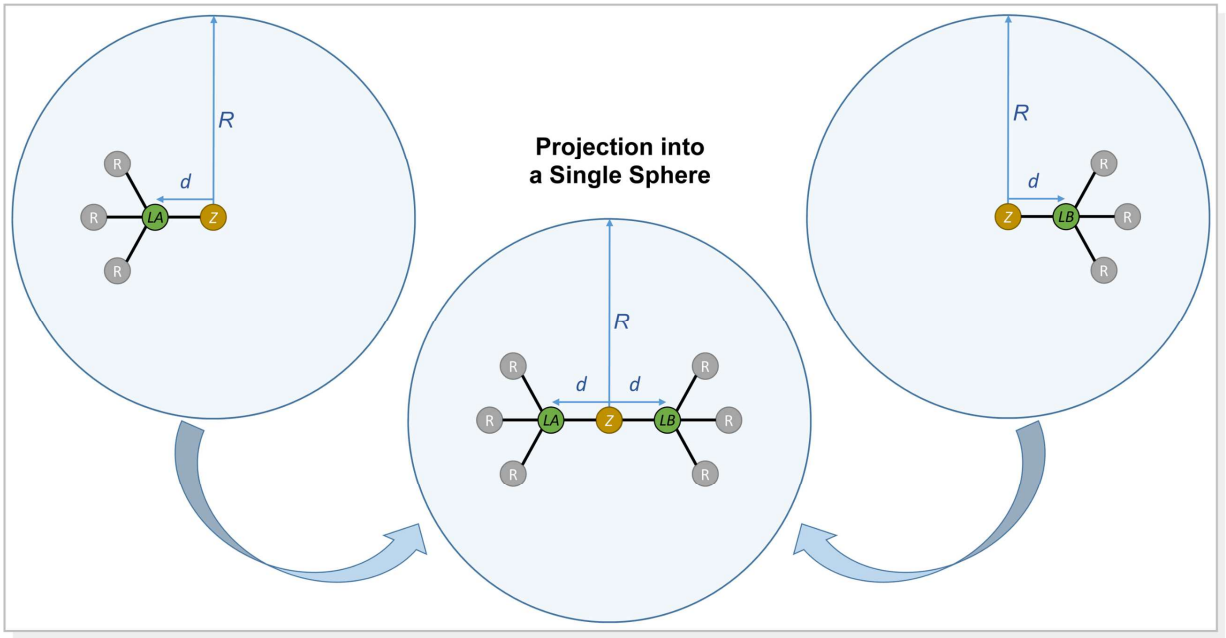

Figure 2.4.3.1 *Illustration of $\%V_{Bur}$ exemplified for a Lewis acid (left) and a Lewis base (right) and projection of the compounds into a single sphere (middle).*

However, since the real distance *D* of a potential acid/base adduct, *i.e.*, the distance between the donor atom of the Lewis base and the acceptor atom of the Lewis acid, is typically shorter than 2*d* as shown in Figure 2.4.3.1 (*D* < 2*d*) a correction volume V_{corr} must be applied. Adding up its percentage share $\%V_{corr}$ of the sphere *S* with the buried volumes of the Lewis acid $\%V_{Bur\_LA}$ and the Lewis base $\%V_{Bur\_LB}$ provides a prediction whether a stable acid/base adduct can be formed, or not, by the number of $\%V_{Bur\_all}$ (Equation 1, Figure 2.4.3.2).

Equation 1

$$\%\boldsymbol{V}_{\boldsymbol{Bur\_all}} = \%\boldsymbol{V}_{\boldsymbol{Bur\_LA}} + \%\boldsymbol{V}_{\boldsymbol{Bur\_LB}} + \%\boldsymbol{V}_{\boldsymbol{corr}}$$

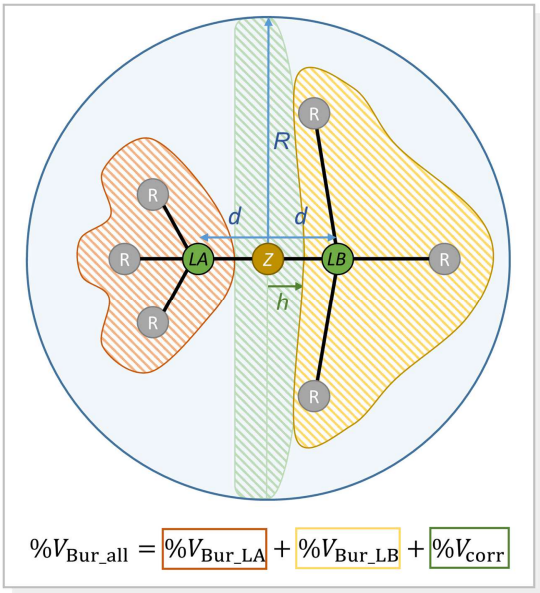

Figure 2.4.3.2 *Illustration of Equation 1 with $\%V_{Bur\_LA}$, $\%V_{Bur\_LB}$, and $\%V_{corr}$.*

When $\%V_{Bur\_all}$ significantly exceeds 100% (>110%), the steric repulsion is too large to allow formation of a stable adduct. In case that $\%V_{Bur\_all}$ is significantly smaller than 100% (<90%), the steric repulsion is small enough to enable adduct formation. Buried volumes in between 90 and 110% are indicative of weakly interacting Lewis acids and bases, for example with unusually long bonds between the donor and the acceptor atoms, which often lead to equilibria of the free acid and the free base and the respective Lewis acid/base adduct (*vide infra*). For a proper evaluation, the different shapes of different Lewis acids and Lewis bases have to be taken into account. Thus, three different prototype shapes for the respective Lewis acid and Lewis base were considered, leading to five designs for the correction volume V_{corr} (Figure 2.4.3.3, for a mathematical description see the Supporting Information of the corresponding publication.[170]). Prototype **I** comprises cone-shaped molecules, BMe_3 as an example for a Lewis acid and PMe_3 as an example for a Lewis base. When two prototype **I** molecules are combined into a Lewis acid/base pair, V_{corr} is approximated using the volume of a segment V_{seg} of sphere *S* (design **1**). Prototype **II** conflates fan-like and more bulky molecules such as NHCs or PF_5. For the combination of two prototype **II** molecules V_{corr} is approximated using the volume of a biconvex lens V_{bcl} (design **2**). Design **3** is suitable for the combination of a prototype **I** molecule and a prototype

II molecule, e.g. BMe_3 and an NHC, with V_{corr} being a convex lens V_{cl} (design **3**). Prototype **III** molecules are sterically overcrowded and thus have a $\%V_{Bur}$ of more than 50%. Examination of a combination of a prototype **I** and a prototype **III** molecule leads to an approximation of V_{corr} as a half-segment V_{hseg} (design **4**). For the pair of a prototype **II** and a prototype **III** molecule, the volume of a half-biconvex lens V_{hbcl} (design **5**) should be applied as correction volume (Figure 2.4.3.3).

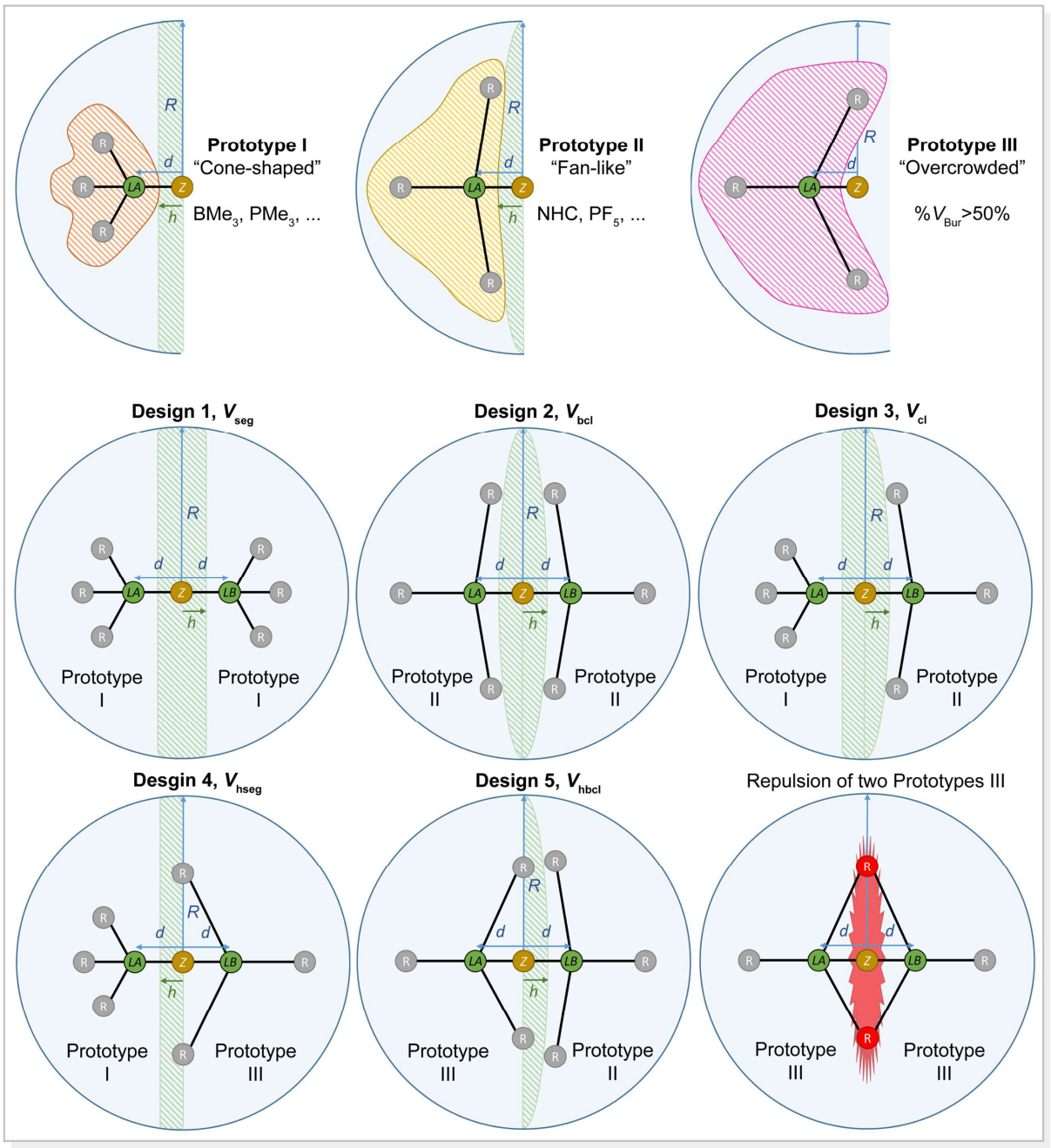

Figure 2.4.3.3 *Illustration of the three prototypes and the resulting five designs for the correction volume* V_{corr}.

To take into account that prototype **III** molecules extend into the hemisphere of the potential adduct partner when their $\%V_{bur}$ exceeds 50%, an empirical correction was introduced for the correction volumes V_{corr} of design **4** V_{hseg} and design **5** V_{hbcl} (for details including the mathematical description of the five designs see the Supporting Information of the corresponding publication.[170]). The distance *h* for the different types of correction volumes was estimated to be *d*/2 (Figure 2.4.3.3). This estimation gives very accurate results, as outlined below. In principle, the combination of a prototype **III** Lewis base with a prototype **III** Lewis acid is possible. However, a combination of two molecules with $\%V_{Bur}$ of more than 50% usually results in a repulsive, and thus nonbonding interaction.

It is worth mentioning that the choice of the prototype for the Lewis acid and base requires some intuition and the only necessary inputs for the LAB-Rep model are the buried volumes and the *d* values of the Lewis acids and bases, which can be derived from tabulated values (Table S1 of the Supporting Information of the corresponding publication[170]). To examine the reliability of the novel LAB-Rep model and to demonstrate its feasibility, some examples for the application of this model are presented in the following, which also include selected borderline cases where a prediction whether an acid/base adduct is formed or not is less obvious. The application of the LAB-Rep model is easy and can be performed by using the Excel spreadsheet as provided in the Supporting Information of the corresponding publication[170] (see also Figure 2.4.3.4). This spreadsheet provides a prediction according to the LAB-Rep model for arbitrary Lewis acid/base pairs without the preselection of the prototype of Lewis acid and Lewis base, respectively, but calculates $\%V_{Bur\_all}$ for all five different designs, which makes an assessment of the possible formation of a stable Lewis acid/base adduct even more convenient. All data needed for input are the values for $\%V_{Bur}$ and the distance *d* used for the determination of $\%V_{Bur}$ for the Lewis acid and the Lewis base Figure 2.4.3.4).

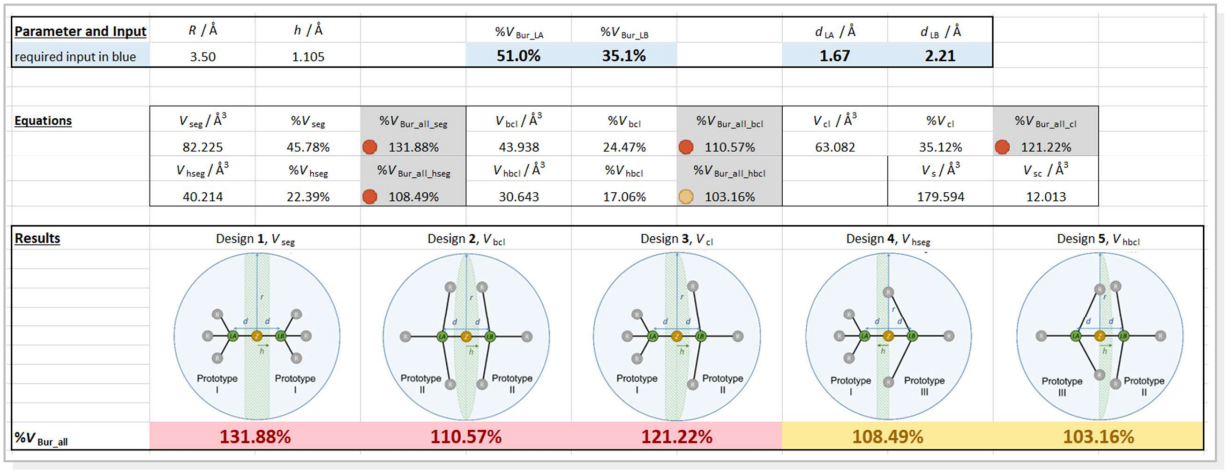

Figure 2.4.3.4 *Example for the input and output for the application of the LAB-Rep model by using the Excel spreadsheet.*

I) A historic example introduced by H. C. Brown: BF_3/2,6-lutidine vs. BMe_3/2,6-lutidine

H. C. Brown *et al*. reported already in 1942 a Lewis acid/base combination, which in part did not show a classical, anticipated Lewis acid/base behavior.[348,349] Different pyridines were investigated for their reactivity towards BF_3 and BMe_3. For 2,6-lutidine, adduct formation was only observed with BF_3 but not with BMe_3 (Figure 2.4.3.5). Molecular models were used already at that time to attribute the failed adduct formation to steric repulsion of the *o*-methyl groups of lutidine with BMe_3.[348,349]

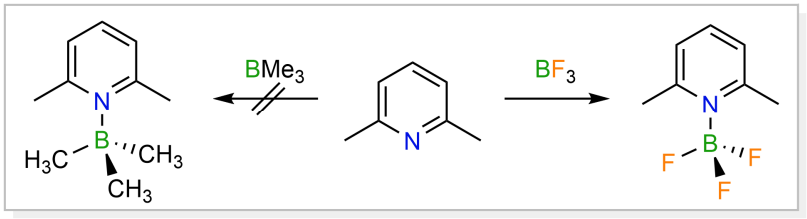

Figure 2.4.3.5 *Reaction of 2,6-lutidine with BMe_3 and BF_3.*

Applying the LAB-Rep model, the convex lens design **3** is the obvious choice for the correction volume V_{corr} since BF_3 and BMe_3 are cone-shaped Lewis acids while 2,6-lutidine can be considered as fan-like with the methyl groups in *ortho* position to the Lewis basic nitrogen. The correction volume of design **3** $\%V_{cl}$ was calculated using values for *d* of 1.42 Å for BF_3, 1.47 Å for BMe_3, and 2.11 Å for 2,6-lutidine to give a $\%V_{cl}$ of 28.5% for BF_3/2,6-lutidine and 28.6% for BMe_3/2,6-lutidine, respectively. The *d* values have been derived from the calculated structures of the fluoroborate anions $[BF_4]^-$ and $[BMe_3F]^-$ and from the 2,6-lutidine nickel tricarbonyl complex $[Ni(CO)_3$(2,6-lutidine)] (for details see the Supporting Information of the corresponding publication[170]). With the $\%V_{Bur}$ of BF_3 (33.3%, *d* = 1.42 Å), BMe_3 (40.7%, *d* = 1.47 Å), and 2,6-lutidine (28.6%, *d* = 2.11 Å), the corresponding total buried volumes $\%V_{Bur\_all}$ were calculated according to Equation 1 (Figure 2.4.3.2). In case of BF_3/2,6-lutidine, the $\%V_{Bur\_all}$ of 89.7% is significantly smaller than 100%, and therefore the formation of an acid/base-adduct is predicted in accordance with the experiment. For BMe_3/2,6-lutidine $\%V_{Bur\_all}$ was estimated to be 97.9%, which is within the limit of the model (90–110%).

In order to check whether the different *d* values have a significant influence on the results of the LAB-Rep model, the calculations for $\%V_{Bur}$ and $\%V_{cl}$ were performed with an equilibrium B–N distance of 1.72 Å, which was derived for BF_3/2,6-lutidine by quantum chemical calculations (details in the Supporting Information of the corresponding publication[170]). This resulted in a $\%V_{Bur\_all}$ of 91.8% for BF_3/2,6-lutidine and 97.7% for BMe_3/2,6-lutidine. Thus, the different *d* values applied do not alter the assessment of the possibility of the formation of a Lewis acid/base adduct. This in turn demonstrates the stability of the LAB-Rep model and its practical value.

II) FLP chemistry: $B(C_6F_5)_3/PPh_3$ and BPh_3/PPh_3

Tris(pentafluorophenyl)borane $B(C_6F_5)_3$ is a strong and sterically demanding Lewis acid often used in FLP chemistry.[232-238,240-243,249] The reaction of PPh_3 with $B(C_6F_5)_3$ results in the formation of the weakly bound adduct $(C_6F_5)_3B–PPh_3$[260] that features a long B–P bond of 2.180(6) Å according to an X-ray crystallographic analysis.[350] Later on, Stephan and co-workers reported on the rearrangement of $(C_6F_5)_3B–PPh_3$ at elevated temperatures to yield the *para* tetrafluorophenyl-bridged zwitterion $Ph_3P–C_6F_4–BF(C_6F_5)_2$,[351] which is in line with the long and thus weak B–P bond. Obviously, the Lewis acid/pair $B(C_6F_5)_3$ and PPh_3 is at the border of forming a stable adduct and thus, this example was chosen as a model for the evaluation of the LAB-Rep model. Since PPh_3 is cone-shaped and the $\%V_{Bur}$ of $B(C_6F_5)_3$ exceeds 50%, design **4** (half segment) was chosen for the correction volume leading to a $\%V_{hseg}$ of 23.3% for $B(C_6F_5)_3/PPh_3$. In conjunction with the $\%V_{Bur}$ of $B(C_6F_5)_3$ (58.9%, d = 1.46 Å) and PPh_3 (31.1%, d = 2.25 Å), $\%V_{Bur\_all}$ was calculated to be 108.8% for $B(C_6F_5)_3/PPh_3$. This value is at the upper end of the range (110%), where equilibria are expected and weakly bound adducts can form, nicely highlighting the versatility of the LAB-Rep model.

Similarly, Stephan and co-worker expanded the combination of Lewis bases capable of FLP chemistry with tris(pentafluorophenyl)borane to the sterically encumbered NHC IDipp. This system shows effective FLP reactivity including H–H bond cleavage to yield imidazolium borates and amine N–H bond cleavage to afford aminoborate salts, although the molecular structure of the adduct $(C_6F_5)_3B–IDipp$ was reported.[352] By calculation of this system with the LAB-Rep model, using the typical input for $B(C_6F_5)_3$ ($\%V_{Bur}$ = 58.9%, d = 1.46 Å) and IDipp ($\%V_{Bur}$ = 36.8%, d = 1.96 Å), $\%V_{Bur\_all}$ was found to be 108.0% for $(C_6F_5)_3B/IDipp$, which is again at the upper end of the range (110%), where equilibria are expected and weakly bound adducts may form.

The Lewis acid/base combination BPh_3 and PPh_3 is a closely related example that was investigated by Wittig *et al*. already in the 1950s. These authors reported that with triphenylborane and triphenylphosphine, 1,2-dehydrobenzene forms an *o*-phenylene-bridged zwitterionic phosphonium-borate instead of a simple Lewis acid/base adduct between BPh_3 and PPh_3.[353] Later on, Horner and Haufe reported that an adduct $Ph_3B–PPh_3$ was formed from the reaction of $[\{Ph_3P\}_2Hg]^{2+}$ and sodium tetraphenylborate.[354] Adduct formation of $Ph_3B–PPh_3$ from Ph_3B and PPh_3 was reported at the same time in the patent literature, but no spectroscopic data is available for this adduct.[355] Triphenylborane is sterically less demanding than tris(pentafluorophenyl)borane, which leads to a smaller $\%V_{Bur\_all}$ of 105.9% for design **4** using $\%V_{Bur}$ of BPh_3 (53.1%, d = 1.46 Å) and PPh_3 (31.1%, d = 2.25 Å). Thus, adduct formation should be possible according to the LAB-Rep model, but the adduct formed should experience steric pressure due to steric repulsion of the Lewis acid BPh_3 and the Lewis base PPh_3. To probe this prediction, BPh_3 and PPh_3 were reacted to yield the Lewis acid/base adduct $Ph_3B–PPh_3$ **33** in almost quantitative yield of 96% (Figure 2.4.3.6).

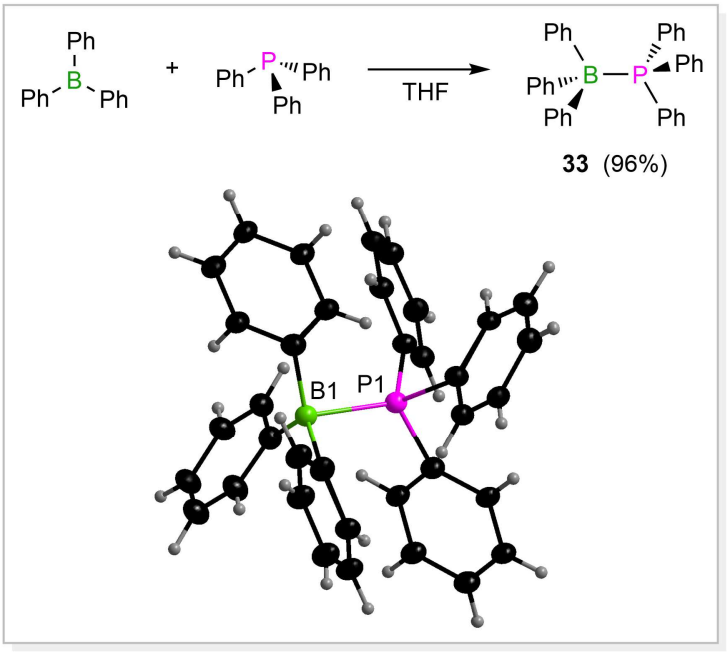

Figure 2.4.3.6 *Synthesis and crystal structure of* ***33*** *(ellipsoids are shown with 25% probability except for H atoms that are depicted with arbitrary radii, disorder is omitted for clarity).*

The reaction was carried out in THF, and product formation and isolation were enhanced by immediate precipitation of the product. Adduct formation was evidenced from solid state NMR spectroscopy, as resonances were detected in the region of four-coordinate boron at $\delta(^{11}B)$ = −1.7 ppm in the $^{11}B\{^{1}H\}$ NMR RSHE/MAS NMR solid state spectrum and at $\delta(^{31}P)$ = 4.6 ppm in the $^{31}P\{^{1}H\}$ CP/MAS solid state NMR spectrum. Crystals of **33** suitable for X-ray diffraction were obtained by recrystallizing the compound in THF. The adduct $Ph_3B–PPh_3$ **33** (Figure 2.4.3.6) crystallizes in the hexagonal space group $P6_3cm$. Adduct **33** is heavily disordered, and thus the crystallographic result serves as mere evidence for the connectivity in the solid state, but a discussion of the metric data would be arbitrary. In solution, only BPh_3 ($\delta(^{11}B)$ = 65.8 ppm in the $^{11}B\{^{1}H\}$-NMR spectrum) and PPh_3 ($\delta(^{31}P)$ = −5.0 ppm in the $^{31}P\{^{1}H\}$-NMR spectrum) can be observed *via* NMR spectroscopy at room temperature, but not the adduct $Ph_3B–PPh_3$. Adduct formation in solution takes place at temperatures below approximately −20 °C, according to low-temperature NMR spectroscopy. Thus, $Ph_3B–PPh_3$ **33** can be formed and exists in the solid state, the melting point of the solid is 213 °C, but easily decomposes upon dissolution into the Lewis acidic and Lewis basic components.

III) NHC and phosphine adducts of phosphoranes

Recently adduct formation of *N*-heterocyclic carbenes with tris(pentafluoroethyl)difluorophosphorane and the FLP reactivity of some combinations of $(C_2F_5)_3PF_2$ and selected NHCs was reported.[18] For NHCs with small alkyl substituents at nitrogen (*i.e.* Me, *n*Pr, and *i*Pr) adducts of the general formula $(C_2F_5)_3PF_2$·NHC were isolated.[18] Here, the phosphorus moiety reveals solely a *meridional* arrangement of the C_2F_5 groups and the NHC unit is in *trans* position to one of the C_2F_5 substituents. The reaction of sterically more demanding NHCs such as IDipp and I*t*Bu yielded abnormal NHC adducts with the phosphorane being bonded to one of the backbone C atoms. Furthermore, it was demonstrated that $(C_2F_5)_3PF_2$ forms a mixture of isomeric adducts (*mer* and *fac*) with PMe_3 but does not react with PPh_3 or PCy_3. Moreover, mixtures of the Lewis acid $(C_2F_5)_3PF_2$ and the sterically encumbered NHCs I*t*Bu, IDipp, and SIDipp revealed FLP reactivity and ring cleavage of THF or deprotonation of CH_3CN, acetone, and ethyl acetate was observed (Figure 2.4.3.7).

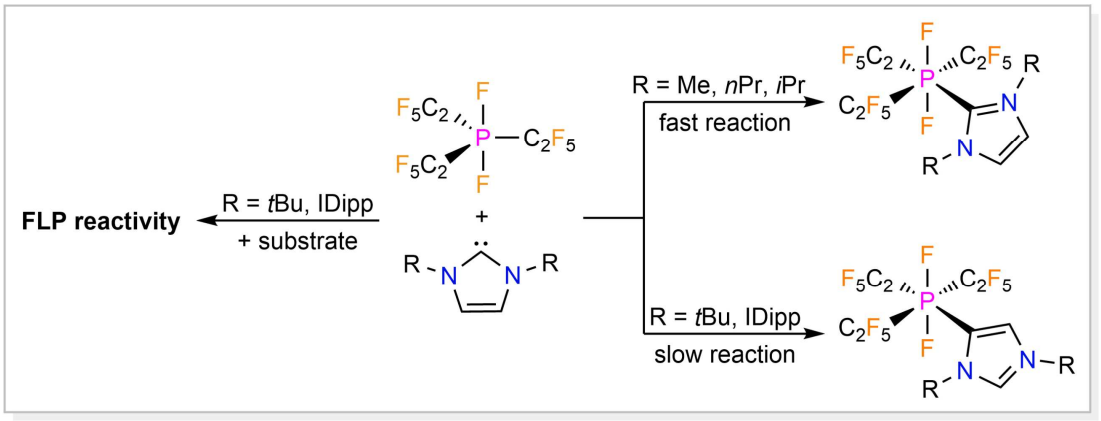

Figure 2.4.3.7 *Reactivity of NHCs with $(C_2F_5)_3PF_2$.*

The reactivity of $(C_2F_5)_3PF_2$ with different sterically demanding bases makes its reactions an ideal case study for the LAB-Rep model. In addition, the closely related but sterically less encumbered Lewis acid PF_5 is ideally suited as it forms stable adducts with all bases studied. In Table 2.4.3.1 the applied correction volumes $\%V_{corr}$, $\%V_{Bur}$, and the calculated $\%V_{Bur\_all}$ are listed for different combinations of $(C_2F_5)_3PF_2$ and PF_5 with selected NHCs and phosphines. For PF_5, adduct formation is predicted for most bases as $\%V_{Bur\_all}$ is at the lower end (>90%) of the range indicative for equilibria or weakly bound adducts. The calculated $\%V_{Bur\_all}$ for the different Lewis acid/base adducts with $(C_2F_5)_3PF_2$ as Lewis acid nicely mirrors the experimental findings. Sterically encumbered Lewis bases do not result in stable adducts while sterically less demanding bases lead to $\%V_{Bur\_all}$ which do not exclude adduct formation, which is again in agreement to experimental data. Furthermore, both experimentally observed isomers of adducts between $(C_2F_5)_3PF_2$ and PMe_3 (*mer* and *fac*) give similar $\%V_{Bur\_all}$.

Table 2.4.3.1 *Assessment of $\%V_{Bur\_all}$ in NHC and phosphine adducts of phosphoranes via the LAB-Rep model.*

LA	***LB***	*isomer*	V_{corr}	*d*(LA) / Å	*d*(LB) / Å	$\%V_{corr}$	$\%V_{LA}$	$\%V_{LB}$	$\%V_{Bur\_all}$
PF_5	**IMe**	-	bcl	1.65	2.01	20.1	38.4	27.4	**85.9**
PF_5	**I*i*Pr**	-	bcl	1.65	1.99	21.0	38.4	28.8	**89.7**
PF_5	**I*t*Bu**	-	bcl	1.65	2.06	20.3	38.4	37.9	**96.6**
PF_5	**aI*t*Bu**	-	bcl	1.65	2.01	20.1	38.4	28.8	**87.3**
PF_5	**IDipp**	-	bcl	1.65	1.96	19.8	38.4	36.5	**94.7**
PF_5	**aIDipp**	-	bcl	1.65	1.98	19.9	38.4	31.8	**90.1**
$PF_2(C_2F_5)_3$	**IMe**	*mer-trans*	hbcl	1.69	2.01	16.0	67.7	27.4	**102.3**
$PF_2(C_2F_5)_3$	**I*i*Pr**	*mer-trans*	hbcl	1.69	1.99	15.8	67.7	28.8	**103.5**
$PF_2(C_2F_5)_3$	**I*t*Bu**	*mer-trans*	hbcl	1.69	2.06	16.4	67.7	37.9	**113.1**
$PF_2(C_2F_5)_3$	**aI*t*Bu**	*mer-trans*	hbcl	1.69	2.01	16.0	67.7	28.8	**103.7**
$PF_2(C_2F_5)_3$	**IDipp**	*mer-trans*	hbcl	1.69	1.96	15.6	67.7	36.5	**111.0**
$PF_2(C_2F_5)_3$	**aIDipp**	*mer-trans*	hbcl	1.69	1.98	15.8	67.7	31.8	**106.4**
PF_5	**PMe_3**	-	cl	1.65	2.21	30.8	38.4	24.1	**93.3**
$PF_2(C_2F_5)_3$	**PMe_3**	*mer-cis*	hseg	1.67	2.21	18.2	59.3	24.1	**101.6**
		fac		1.67		20.5	54.8		**99.4**
PF_5	**PPh_3**	-	cl	1.65	2.25	31.1	38.4	31.1	**100.6**
$PF_2(C_2F_5)_3$	**PPh_3**	*mer-cis*	hseg	1.67	2.25	18.7	59.3	31.1	**109.1**
		fac		1.67		20.9	54.8		**106.8**

IV) NHC adducts of diborane(IV) ester

Over the last few years, combinations of Lewis-basic NHCs and Lewis-acidic diborane(IV) esters which either lead to classical Lewis acid/base complexes or to NHC ring-expanded products were reported.[207,209,356-360] Depending on the nature of the diborane(IV) compound and the NHC used, Lewis acid/base adducts or NHC ring expansion products stemming from B−B and C−N bond activation have been observed. Several of the corresponding NHC adducts and NHC ring-expanded products were isolated and characterized, and in general B−B bond and C−N bond activation was observed at low temperature for B_2eg_2, at room temperature for B_2neop_2 and at higher temperature for B_2cat_2 (eg = ethylene glycolato, neop = neopentyl glycolato, cat = catecholato). Thus, the reactivity strongly depends on steric effects of the NHCs and the diborane(IV) compounds, as well as on the corresponding Lewis-basicity and Lewis-acidity. However, the steric components in these systems were well described by using the LAB-Rep model. For example, B_2pin_2 (pin = pinacolato; $\%V_{Bur}$ = 45.1%, *d* = 1.44 Å) as the most common and very well established diborane(IV) compound in organic and inorganic syntheses was reacted with the NHC I*i*Pr ($\%V_{Bur}$ = 28.8%, *d* = 1.99 Å) and the formation of the mono-NHC adduct B_2pin_2·I*i*Pr ($\%V_{Bur\_all}$ = 101.3%; design **3**; V_{cl}) was observed (Figure 2.4.3.8).[358] This stable adduct was isolated and characterized including by single-crystal X-ray diffraction. However, during the work on the defluoroborylation of fluoroaromatics using $[Ni(NHC)_2]$ complexes as catalysts, it was recognized that formation of this adduct leads to degradation of the nickel catalyst. This side reaction can be suppressed if an NHC is used which cannot react with the boron source, and application of the LAB-Rep model pointed to IMes ($\%V_{Bur}$ = 35.9%, *d* = 1.97 Å) as a likely NHC ligand that should not react with B_2pin_2 ($\%V_{Bur}$ = 45.1%, *d* = 1.44 Å) to yield an adduct B_2pin_2·IMes ($\%V_{Bur\_all}$ = 108.2%; design **3**; V_{cl}). The use of $[Ni(IMes)_2]$ then paved the way for successful defluoroborylation catalysis.[361-363] In contrast, for the ethyl glycol ether B_2eg_2 ($\%V_{Bur}$ = 40.5 %, *d* = 1.43 Å) adduct formation to yield B_2eg_2·IMes ($\%V_{Bur\_all}$ = 103.5%; design **3**; V_{cl}) was observed and the adduct was structurally characterized.[358]

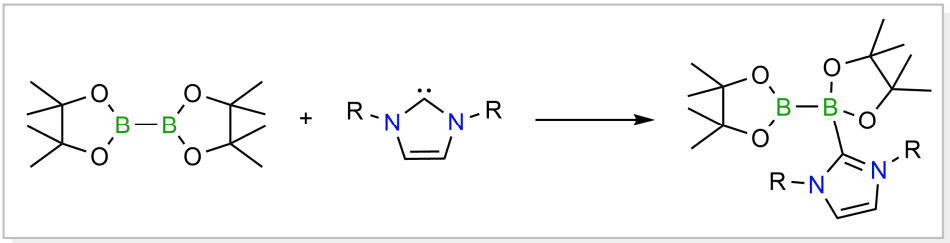

Figure 2.4.3.8 *Reaction of B_2pin_2 with an NHC to yield the mono-NHC adduct B_2pin_2·NHC.*

2.4.4 Conclusion

Steric and electronic effects are decisive parameters in chemistry, which determine the shape and the reactivity of molecules. For Lewis acids and Lewis bases, different models have been developed in the last few decades to scale their acid/base strengths in a rather easy way; the most prominent are probably fluoride ion affinity (FIA) for Lewis acids and the Tolman parameter for Lewis bases. Both can be derived from experiments, but in practice, they are most often evaluated by simple, low-cost (DFT) calculations. Steric effects of Lewis bases are nowadays quantified by judging the percent buried volume (%V_{Bur}), which can be easily performed thanks to the SambVca 2.1 web application. It has been demonstrated over the last decade that %V_{Bur} is a versatile and reliable descriptor of steric properties of different ligands such as NHCs and phosphines. As there was no easy approach dealing with steric effects of differently substituted Lewis acidic centers before this work, herein the first general approach to easily access and quantify steric properties of Lewis acids was introduced. In addition, based on this approach an easy-to-use model for the prediction of whether a specific Lewis acid/base adduct may form considering steric effects was developed. This model implies the application of the concept of the percent buried volume (%V_{Bur}) to fluoride ion adducts of Lewis acids. In principle, this model can be extended to other adducts, but fluoride adducts were chosen as those are frequently calculated to judge fluoride ion affinities, and thus data such as cartesian coordinates are easily available. Furthermore, many fluoride adducts have been characterized crystallographically, providing additional access to the coordinates required.

This model was applied to a large number (240) of different fluoride adducts of Lewis acids of group 13, 14, and 15 elements using low level DFT (def2-SV(P)/BP86) optimized geometries and their percent buried volume as well as their topographic steric maps are report herein. This evaluation does not require the fluorine atom of the anionic fluoride adduct $[LA–F]^-$ located in a fixed distance to the Lewis acidic center of the LA *d*(LA–F), as the values obtained for *d*(LA–F) of a certain Lewis-acidic center (e.g., of boron) vary only little for the different systems and these small differences translate into minor differences of %V_{Bur}, only. Note also that these distances $[LA–F]^-$ can be set to any value wanted within the user-friendly SambVca 2.1 web application if this is required. A chart of %V_{Bur} vs. Lewis-acidic main group element of all Lewis acids considered in this study revealed that there is a wide range of %V_{Bur} covered by known Lewis acids and that any steric demand between %V_{Bur} = 30% and %V_{Bur} = 75% can be realized easily by the choice of the proper element, coordination number and substituent. Very valuable are charts, which correlate %V_{Bur} and FIA as a scale for the Lewis acidity of the compound, which combine steric and electronic features of the Lewis acid under consideration and provide valuable information about stereo-electronic properties of the Lewis acid. As there is no general correlation between Lewis acidity and steric demand, both factors have to be addressed. Thus, the present model presents a highly valuable tool for synthetic and materials chemists.

With these data in hand, the novel LAB-Rep (**L**ewis **a**cid/**b**ase **rep**ulsion) model was introduced, which judges steric repulsion in Lewis acid/base pairs and helps to predict if an arbitrary pair of Lewis acid and Lewis base can form an adduct with respect to their steric properties. The reliability of this model is demonstrated by four selected case studies, which show the versatility of the model. Using listed buried volumes of Lewis acids $\%V_{Bur\_LA}$ and of Lewis bases $\%V_{Bur\_LB}$ it has to be emphasized that no crystal structure or quantum chemical calculation is required to evaluate steric repulsion in Lewis acid/base pairs. A user-friendly Excel spreadsheet was programmed, which can be used for this purpose.

3. SUMMARY

Within the scope of this thesis, novel borane- and phosphorane-functionalized anionic carbenes have been synthesized and their characteristics as ligands in main group element- and transition metal chemistry as well as further reactivities have been studied. Furthermore, a method for the evaluation of the steric demand of Lewis acids was developed, and a model for the prediction of whether a specific Lewis acid/base adduct can be formed considering steric effects was designed.

Chapter 2.1 deals with the synthesis of novel tricyanoborane-functionalized anionic *N*-heterocyclic carbenes and the investigation of their properties and reactivity. Anionic NHCs Li**5** and Li_2**6** were isolated in high yields on a multi-gram scale via deprotonation reactions of the neutral imidazole borane adduct **1** and the anionic imidazolate Li**3**, respectively. The carbene precursors **1** and **3** as well as the anionic NHCs **5** and **6** are characterized by their high stabilities, which are due to a stabilization by the strong Lewis acid $B(CN)_3$ bonded to the N atoms of the heterocycle. Furthermore, the cyanoboraneimidazole compounds described herein are promising ligands for coordination chemistry, as demonstrated by the synthesized salts and complexes (Figure 3.1)

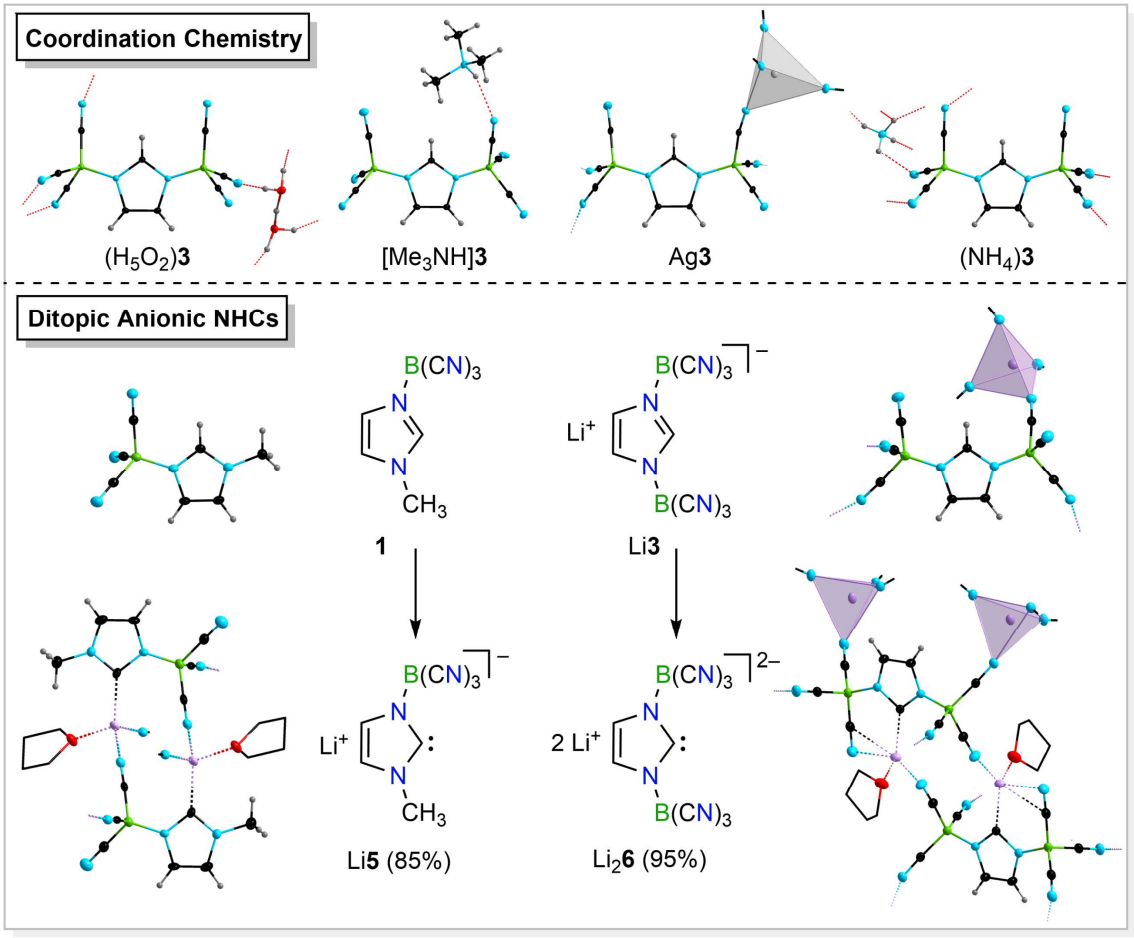

Figure 3.1 *Coordination polymers of imidazolate **3** (top) and synthesis of borane-functionalized ditopic anionic NHCs (bottom).*

While anion **5** is a novel unsymmetrically substituted ditopic ligand with coordination being possible at the carbene center and the Lewis basic nitrogen atoms of the cyano groups alike, dianionic NHC **6** even exceeds the strength of its σ-donor and π-acceptor abilities. Therefore, the electronic properties of the NHCs can be efficiently tuned by the number of $B(CN)_3$ groups, as underlined by quantum chemical calculations, multi-nuclear NMR spectroscopic characterization of the NHC selenium compounds IMe=Se, Li**10**, and Li_2**11**, and evaluation of the Tolman electronic parameter (TEP) of the nickel tricarbonyl complexes [(IMe)Ni$(CO)_3$], Li**16**, and Li_2**17**. Additionally, the steric features of the carbene, for example the buried volume $\%V_{Bur}$, can be controlled by the choice of the substituents attached to the nitrogen atoms of the imidazole ring (Figure 3.2). Thus, the combination of outstanding properties, e.g. the high thermal stabilities, the tunable steric and electronic properties, the large buried volumes, the possibility to introduce negative charge, the ability to act as a ditopic ligand and the ease of accessibility render anionic and dianionic NHCs **5** and **6** unique novel NHCs.

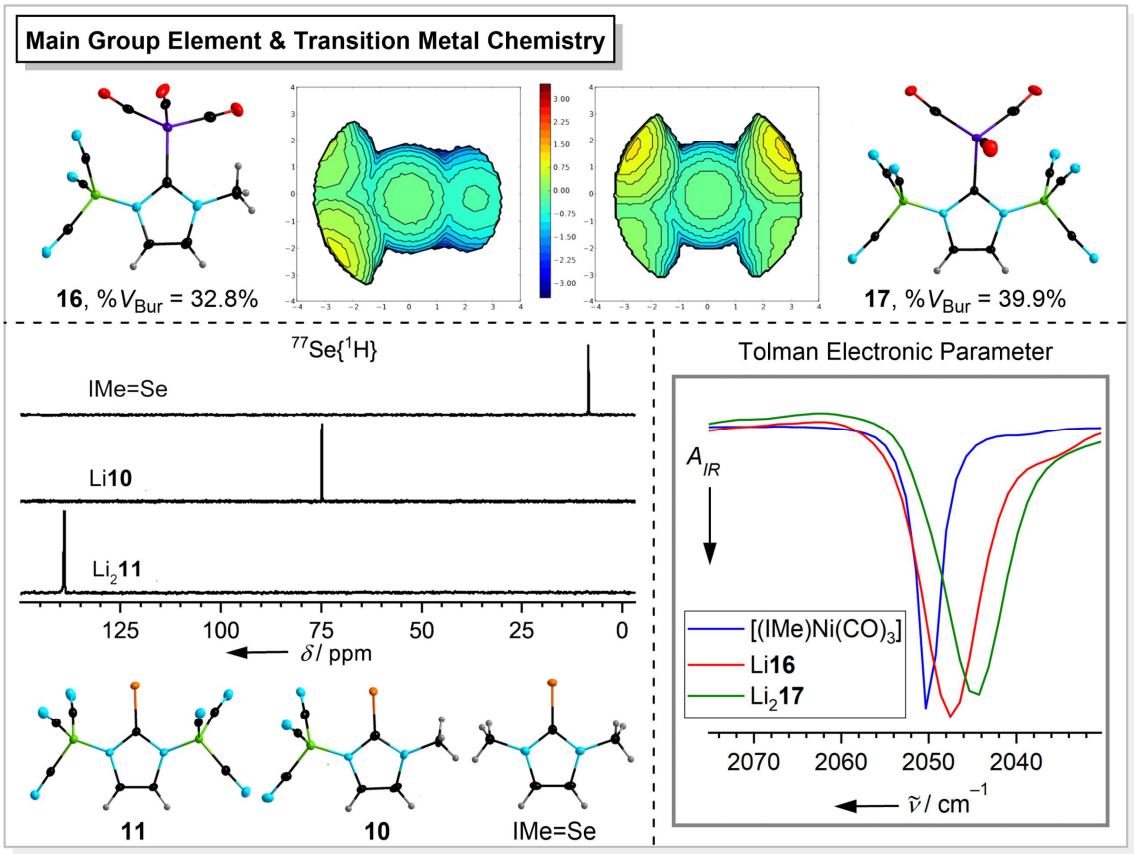

Figure 3.2 *Nickel tricarbonyl complexes **16** and **17** with steric maps and buried volumes of the anionic NHCs **5** and **6** (top), evaluation of the Tolman electronic parameter (bottom right), and NMR spectroscopic characterization of the selenium compounds **11**, **10**, and IMe=Se (bottom left).*

The second part of this thesis (Chapter 2.2) is about the synthesis of anionic phosphorane-functionalized NHCs. In contrast to the tricyanoborane-substituted carbenes, these novel ligands, which were obtained in high yield on gram scale, characterize themself by their highly fluorinated and therefore weakly coordinating phosphorane moieties. The anionic and dianionic carbenes K**20** and K_2**21** are readily accessible via deprotonation of the corresponding neutral or anionic precursors **18** and K**19** (Figure 3.3).

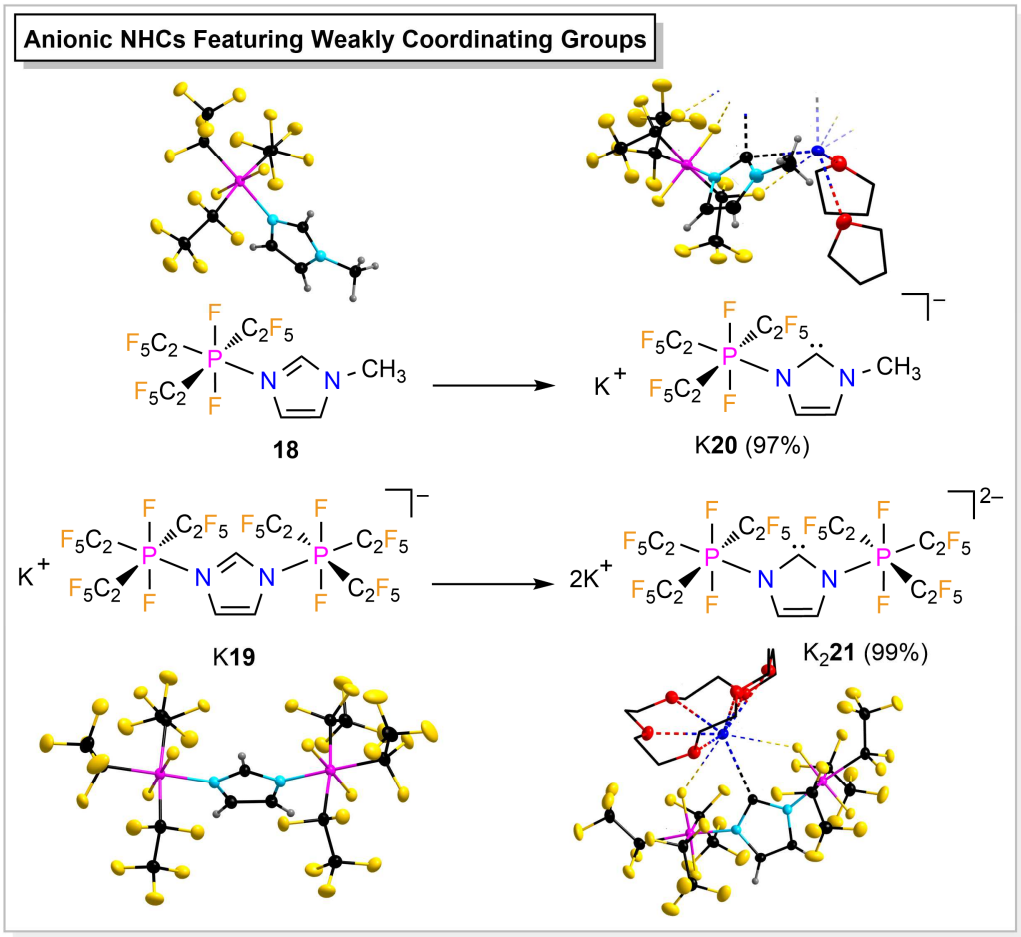

Figure 3.3 *Syntheses of phosphorane-functionalized anionic NHCs K**20** and K_2**21**.*

These carbenes are promising novel ligands for main group element and transition metal compounds, as demonstrated in first reactions with phosphinegold(I) complexes and elemental selenium. In comparison with neutral NHCs such as IMe, anionic carbenes **20** and **21** stand out for their enhanced σ-donor- und π-acceptor strength. Furthermore, these NHCs feature immense buried volumes (%V_{Bur}), which provide effective shielding of a metal center. The crystal structure of compound **23** underlines the flexibility of the steric demand of the phosphorane moieties, which is due to the rotational freedom of the C_2F_5 groups (Figure 3.4). The different properties such as the large buried volumes, the strong σ-donor- und π-acceptor properties, the single or double negative charge, the possibility to act as ligands with a flexible steric environment, the weakly coordinating groups, and the ease of accessibility distinguish the phosphorane-functionalized anionic NHCs as promising novel ligands.

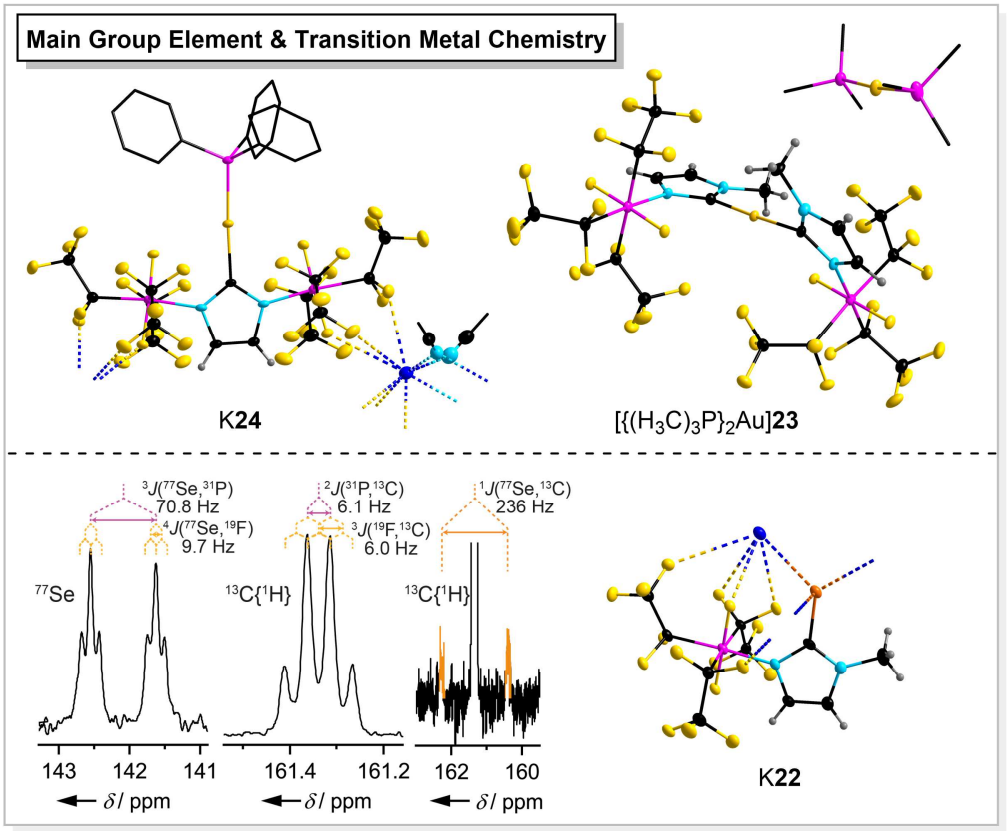

Figure 3.4 *Gold(I) complexes K**24** and [{(H$_3$C)$_3$P}$_2$Au]**23** of anionic carbenes **20** and **21** (top) and NMR spectroscopic characterization of selenium adduct K**22** (bottom).*

The synthesis of first examples of anionic cyclic (alkyl)(amino)carbenes (Ani-cAAC) is described in chapter 2.3. Ani-cAAC-B(CN)$_3$ was generated and used *in situ* only, since it undergoes rapid intermolecular B–C bond activation. In contrast, pentafluoroethyldifluoroborane-functionalized Ani-cAAC **29** was isolated on a multi-gram scale (Figure 3.5). The precursors **26** and **27** of these anionic carbenes are easily accessible in high yield via Lewis acid/base reactions of the corresponding boranes with hydropyridines. Therefore, tedious multistep ring-closing syntheses are circumvented, which is in stark contrast to established syntheses of neutral cAACs. This novel broad modular synthetic approach could in principle be adopted for the preparation of enantiomerically pure hydropyridines providing access to novel chiral neutral and anionic carbenes. The electronic properties of the anionic cAACs reported in this work show the strong influence of the corresponding borane substituent, as demonstrated by quantum chemical calculations, which not only enables a tuning of the steric properties of Ani-cAACs, but also of the σ-donor- und π-acceptor strength.

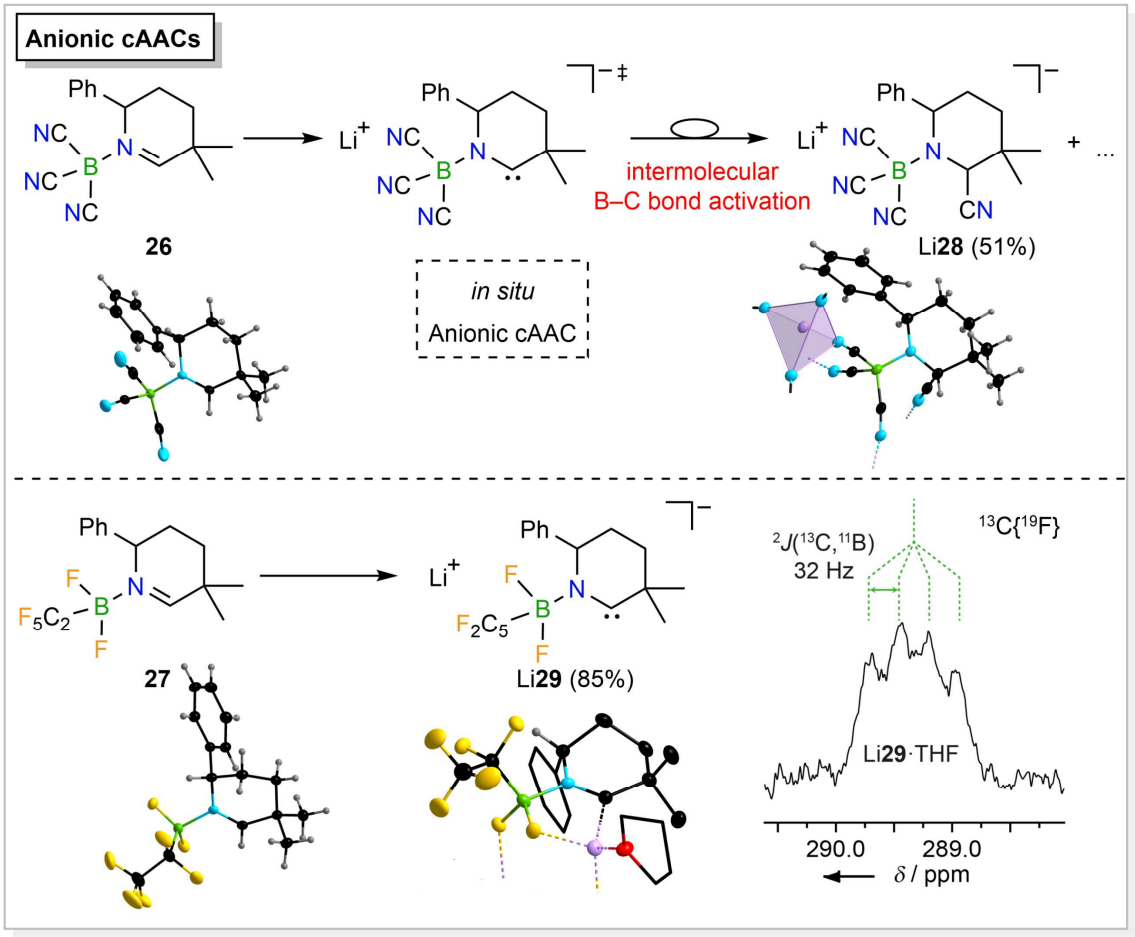

Figure 3.5 *Syntheses of borane-functionalized anionic cAACs.*

The potential of Ani-cAACs to serve as ligands for main group elements and in transition metal complexes was demonstrated by reactions with elemental selenium and chloro(triphenylphosphine)gold(I). The latter shows, that Ani-cAAC can replace anionic substituents like chloride at transition metals under salt elimination, which represents a novel way to introduce cyclic (alkyl)(amino)carbenes (Figure 3.6).

The final section of this thesis (Chapter 2.4) deals with the evaluation of the steric properties of Lewis acids. This issue was addressed since the steric demand of Lewis bases like phosphines and NHCs can be quantified by judging the buried volume (%V_{Bur}), but there was no easy to perform approach dealing with steric effects of differently substituted Lewis acidic centers. Therefore, a model was developed, which applies the concept of the percent-buried volume to fluoride adducts of Lewis acids. In principle, other adducts could also be used, but geometries of fluoride adducts are frequently calculated to judge fluoride ion affinities, and thus data such as cartesian coordinates are easily available. Furthermore, many fluoride adducts have been characterized crystallographically, providing additional access to the coordinates required.

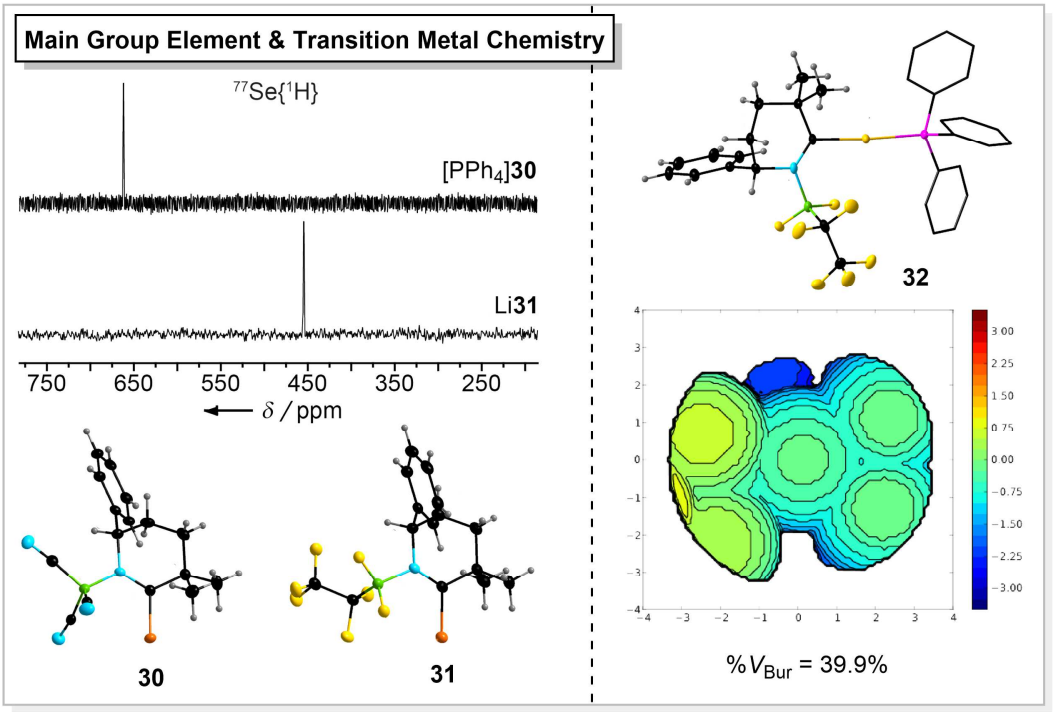

Figure 3.6 *NMR spectroscopic characterization of selenium adducts* ***30*** *and* ***31*** *(left) and Ani-cAAC gold(I) complex* ***32*** *with steric map and buried volume (right).*

This model was applied to a large number (240) of different fluoride adducts of Lewis acids of group 13, 14, and 15 elements. The evaluation does not require the fluorine atom of the anionic fluoride adduct [LA−F]$^-$ located in a fixed distance to the Lewis acidic center of the LA *d*(LA−F), as the values obtained for *d*(LA−F) translate only into minor differences of %V_{Bur}. A chart of %V_{Bur} vs. Lewis-acidic main group element of all Lewis acids considered in this study revealed that there is a wide range of %V_{Bur} covered by known Lewis acids and that any steric demand between %V_{Bur} = 30% and %V_{Bur} = 75% can be realized easily by the choice of the proper element, coordination number, and substituents. Very valuable are also charts, which correlate %V_{Bur} and FIA (Figure 3.7), which combine steric and electronic features. Thus, the present model presents a highly valuable tool for synthetic and materials chemists. With the data of the steric demand of various Lewis acids in hand, the novel LAB-Rep (**L**ewis **a**cid/**b**ase **rep**ulsion) model was introduced. It judges steric repulsion in Lewis acid/base pairs and helps to predict if an arbitrary pair of Lewis acid and Lewis base can form an adduct with respect to their steric properties (Figure 3.7). The reliability of this model is demonstrated by four selected case studies, which show the versatility of the model. Using listed buried volumes of Lewis acids %V_{Bur_LA} and of Lewis bases %V_{Bur_LB} it has to be emphasized that no crystal structure or quantum chemical calculation is required to evaluate steric repulsion in Lewis acid/base pairs.

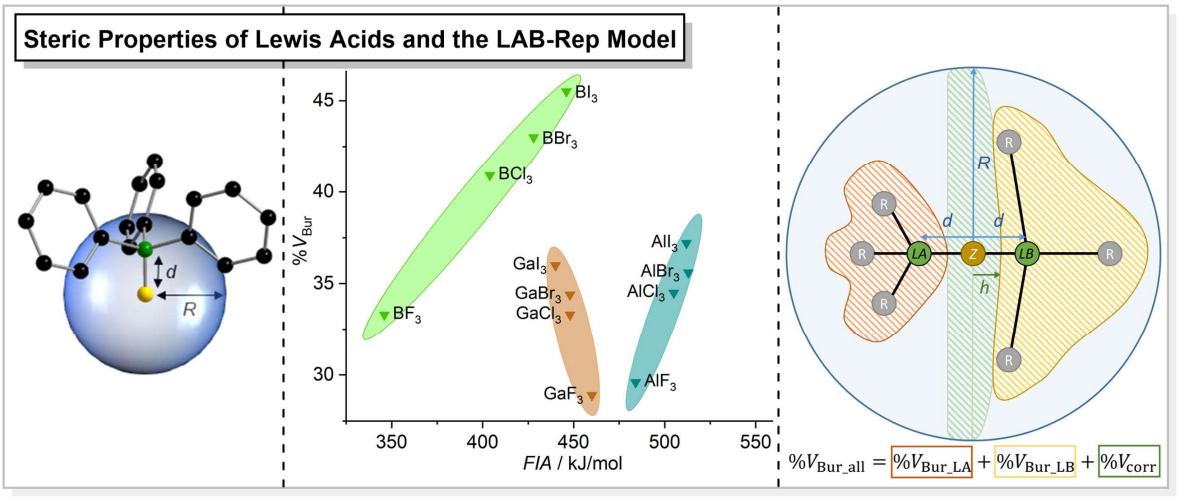

Figure 3.7 *Evaluation of the steric demand of Lewis acids applying the concept of the buried volume to their fluoride adducts (left), plot of $\%V_{Bur}$ against FIA (middle), and illustration of the LAB-Rep model, which predicts steric repulsion in Lewis acid/base adducts (right).*

4. ZUSAMMENFASSUNG

Im Rahmen dieser Arbeit wurden neuartige Boran- und Phosphoran-funktionalisierte anionische Carbene synthetisiert und deren Eigenschaften als Liganden in der Hauptgruppen- und Übergangsmetallchemie sowie weitere Reaktivitäten untersucht. Zusätzlich wurde eine Methode zur Evaluierung des sterischen Anspruchs von Lewis Säuren entwickelt und ein Modell entworfen, welches eine Vorhersage über die Bindungssituation in Lewis Säure/Base Paaren hinsichtlich sterischer Repulsion trifft.

In Kapitel 2.1 ist die Synthese neuartiger Tricyanoboran-funktionalisierter anionischer *N*-heterocyclischer Carbene beschrieben sowie Untersuchungen zu deren Eigenschaften und Folgechemie. Ausgehend von dem neutralen Imidazol-Boran-Addukt **1**, bzw. dem anionischen Imidazolat Li**3** wurden die anionischen NHCs Li**5** und Li_2**6** durch Deprotonierung in sehr guter Ausbeute im Multigrammmaßstab erhalten. Sowohl die Carben-Vorstufen **1** und **3** als auch die anionischen NHCs **5** und **6** zeichnen sich durch ihre hohe Stabilität aus, welche auf den stabilisierenden Effekt der starken Lewis Säure $B(CN)_3$ zurückzuführen ist. Außerdem stellen die beschriebenen Cyanoboranimidazolverbindungen vielversprechende Liganden für die Koordinationschemie dar, wie anhand der synthetisierten Salze und Komplexe gezeigt wurde (Abbildung 4.1).

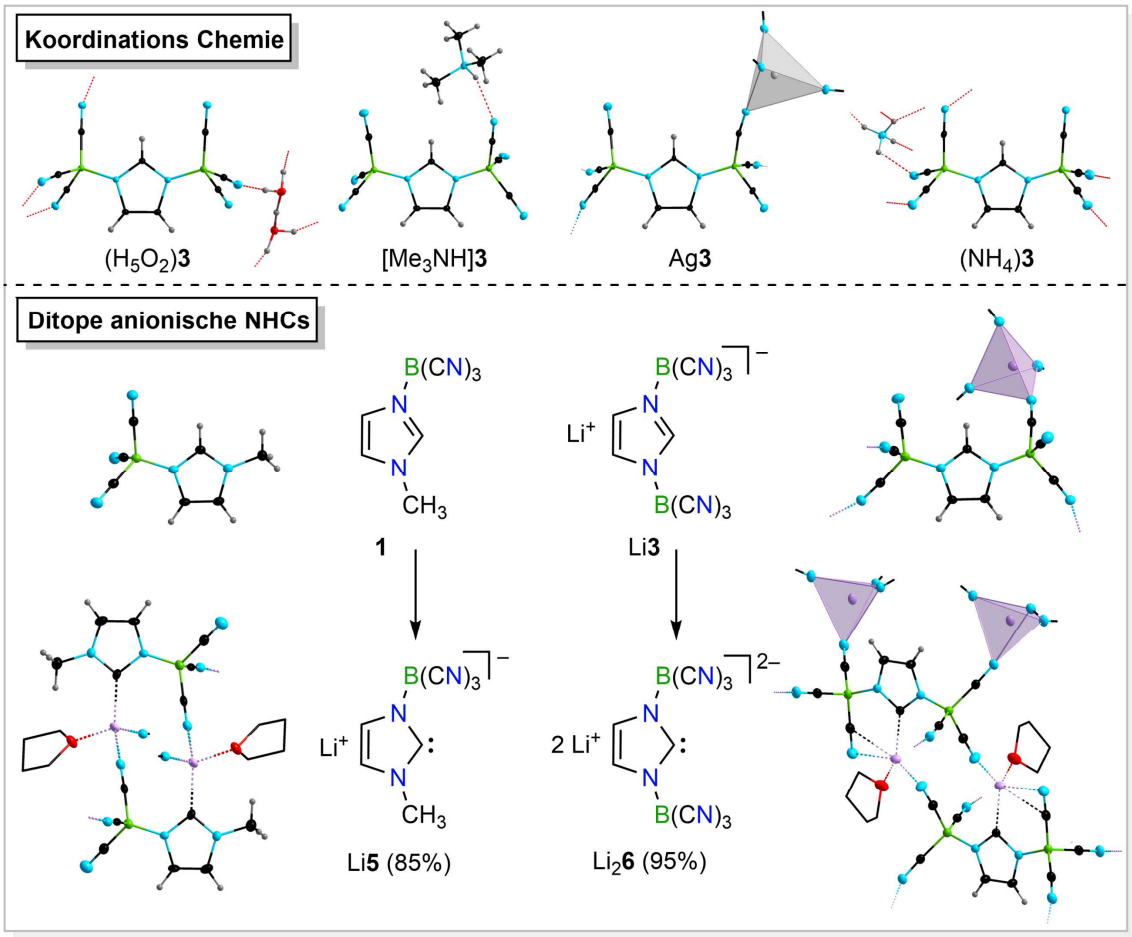

Abbildung 4.1 *Koordinationsverbindungen des Imidazolats* ***3*** *(oben) und Synthese Boran-substituierter ditoper anioinischer NHCs (unten).*

Während es sich bei Anion **5** um einen neuartigen unsymmetrisch substituierten ditopen Liganden handelt, welcher sowohl über das Carbenzentrum als auch über die Lewis basischen Stickstoffatome der Cyanogruppen koordinieren kann, übersteigt das dianionische NHC **6** sogar noch dessen σ-Donor- und π-Akzeptorstärke. Wie durch quantenchemische Rechnungen, multinukleare NMR-spektroskopische Charakterisierung der NHC-Selen-Verbindungen IMe=Se, Li**10** und Li_2**11** und Evaluation des Tolman-Electronic-Parameters der Nickeltricarbonylkomplexe [(IMe)Ni$(CO)_3$], Li**16** und Li_2**17** gezeigt wurde, können die elektronischen Eigenschaften des NHCs gezielt durch die Zahl der $B(CN)_3$-Substituenten eingestellt werden. Ebenso lassen sich die sterischen Eigenschaften des NHCs, zum Beispiel das verdeckte Volumen $\%V_{Bur}$, über die Wahl der, an die Stickstoffe des Imidazols gebundenen, Gruppen steuern (Abbildung 4.2). Somit macht die Kombination herausragender Eigenschaften, wie die hohen Stabilitäten, die einstellbaren elektronischen und sterischen Eigenschaften, das große verdeckte Volumen, die Möglichkeit negative Ladung einzuführen, die Fähigkeit als ditoper Ligand zu fungieren und die einfache Zugänglichkeit, die anionischen, bzw. dianionischen NHCs **5** und **6** zu einzigartigen neuartigen Liganden.

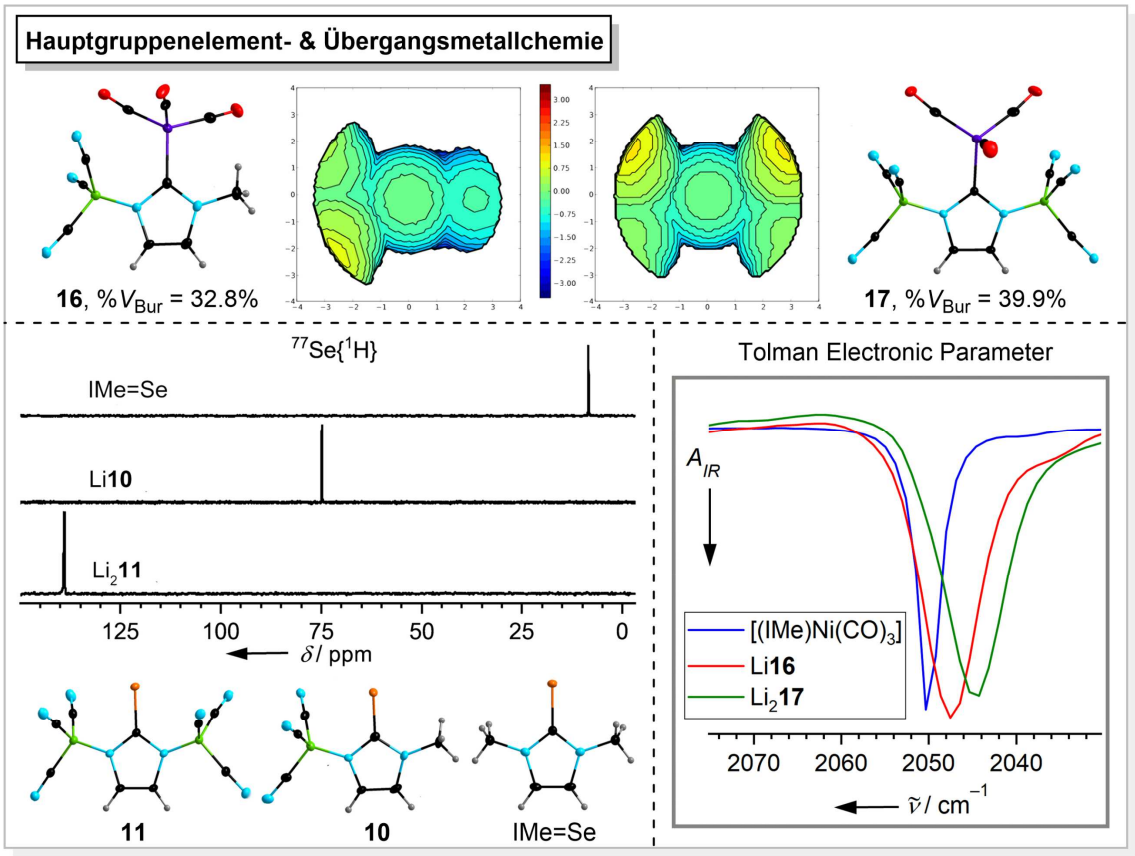

Abbildung 4.2 *Nickeltricarbonyl-Komplexe* ***16*** *und* ***17*** *mit sterischen Karten und verdeckten Volumina der anionischen NHCs* ***5*** *und* ***6*** *(oben), Bestimmung des Tolman Electronic Parameters (und rechts) und NMR-spektroskopische Charakterisierung der Selenverbindungen* ***11***, ***10*** *und IMe=Se (unten links).*

Der Zweite Teil der Arbeit (Kapitel 2.2) beschäftigt sich mit der Synthese anionischer Phosphoran-funktionalisierter NHCs. Diese neuartigen Liganden, welche ebenfalls in hoher Ausbeute im Grammaßstab isoliert werden konnten, zeichnen sich im Gegensatz zu den zuvor beschriebenen Boran-substituierten NHCs, durch die hochfluorierten und somit schwach koordinierenden Phosphoraneinheiten aus. Die anionischen Carbene K**20** und K_2**21** sind durch Deprotonierungs-reaktionen der neutralen bzw. anionischen Vorstufen **18** und K**19** sehr gut zugänglich (Abbildung 4.3).

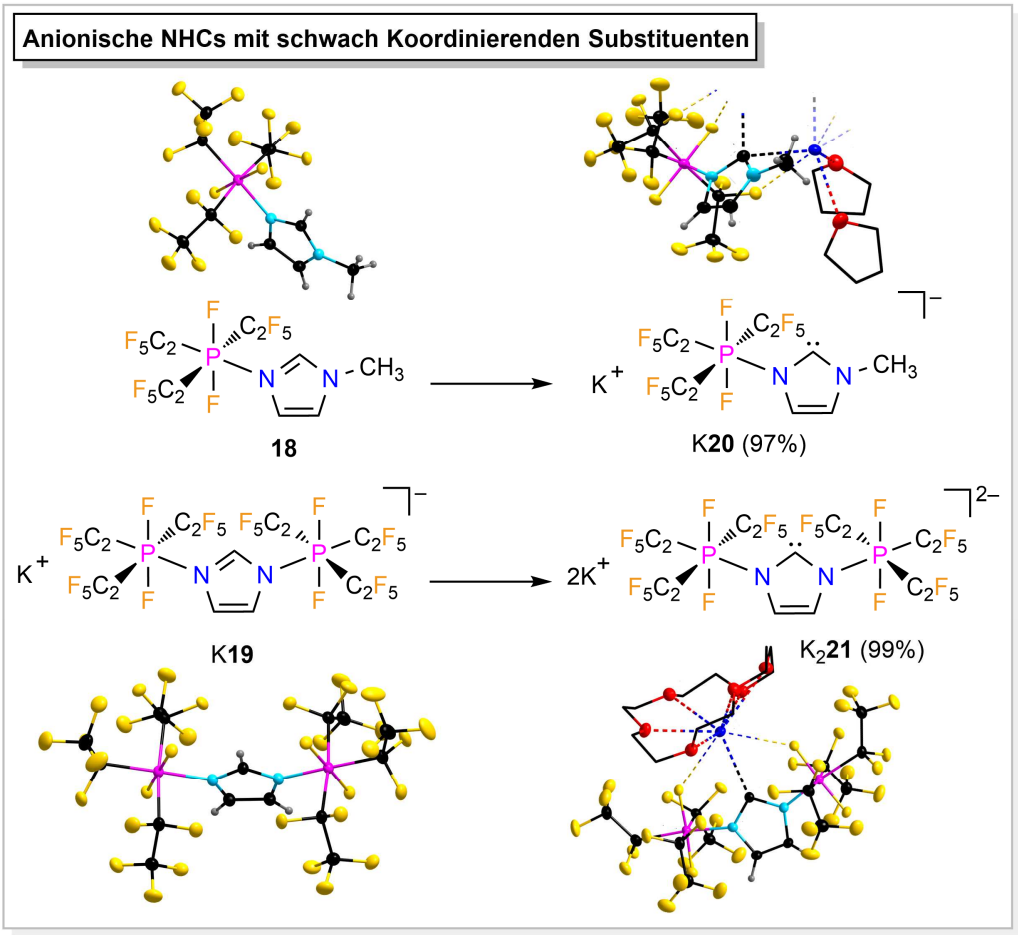

Abbildung 4.3 *Synthese der Phosphoran-funktionalisierten anionischen NHCs K**20** und K_2**21**.*

Diese NHCs sind vielversprechende Liganden für Hauptgruppenelement und Übergangsmetall-verbindungen, wie in ersten Reaktionen mit Phosphangold(I)-Komplexen und elementarem Selen gezeigt werden konnte. Verglichen mit neutralen NHCs wie IMe, zeichnen sich **20** und **21** durch stärkere σ-Donor- und π-Akzeptorfähigkeiten aus. Zusätzlich weisen die Carbene immense verdeckte Volumina (%V_{Bur}) auf, die eine effektive Abschirmung des Metallzentrums ermöglichen. Die Kristallstruktur der Verbindung **23** unterstreicht die Flexibilität des sterischen Anspruchs der Phosphoransubtituenten, die durch die Rotation der C_2F_5-Gruppen erreicht wird (Abbildung 4.4). Aufgrund verschiedener Eigenschaften, wie dem großen verdeckten Volumen, den starken σ-Donor- und π-Akzeptorfähigkeiten, der einfachen bzw. zweifachen negativen Ladung, der Möglichkeit als

sterisch flexibler Ligand eingesetzt zu werden, den schwach koordinierenden Gruppen und der einfachen Zugänglichkeit, können die vorgestellten Phosphoran-funktionalisierten anionischen NHCs als vielversprechende neuartige Liganden angesehen werden.

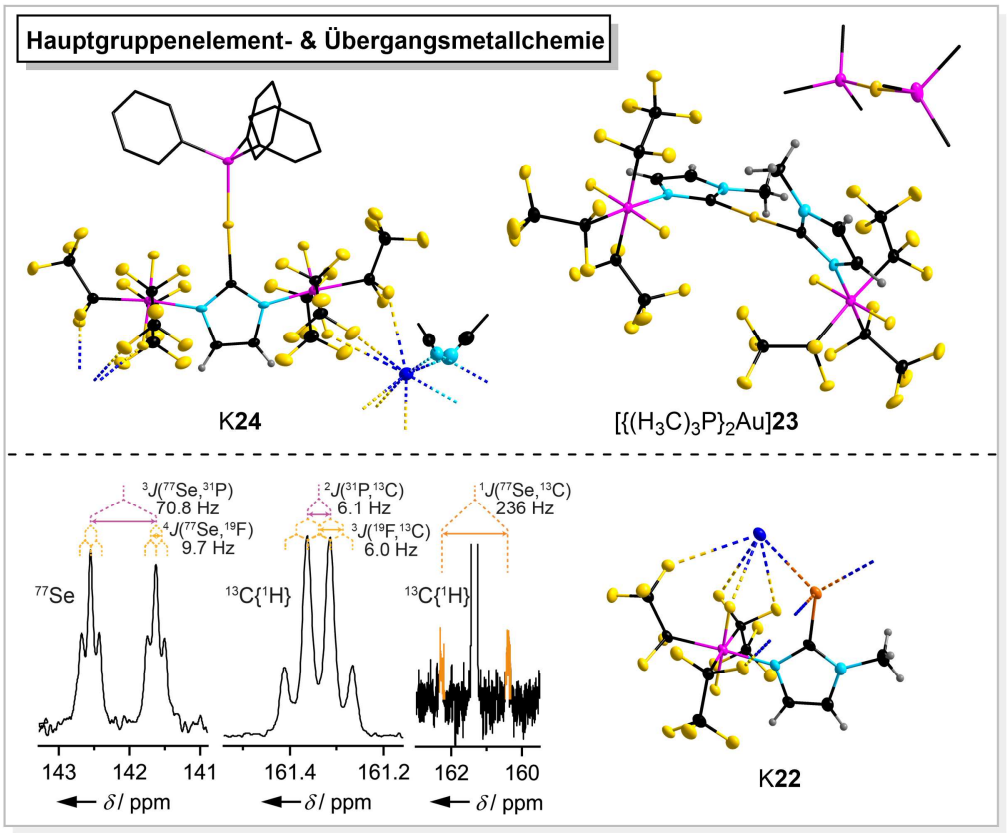

Abbildung 4.4 *Gold(I)-Komplexe K**24** und [{(H₃C)₃P}₂Au]**23** der anionischen Carbene **20** und **21** (oben) und NMR-spektroskopische Charakterisierung der Selenverbindung K**22** (unten).*

In Kapitel 2.3 ist die Synthese erster Vertreter anionischer cyclischer (Alkyl)(amino)carbene (Ani-cAACs) beschrieben. Während das Tricyanoboran-funktionalisierte Ani-cAAC-B(CN)$_3$ ausschließlich *in situ* erzeugt und umgesetzt werden konnte, da die Verbindung einen schnellen B–C-Bindungsaktivierungs-prozess durchläuft, wurde das Pentafluorethyldifluoroboran-substituierte anionische Carben Li**29** im Multigrammmaßstab isoliert (Abbildung 4.5). Die Vorstufen **26** und **27** dieser anionischen Carbene sind durch einfache Lewis Säure-Base-Reaktionen der Borane mit Hydropyridinen zugänglich, sodass eine aufwendige, mehrstufige Ringschlusssynthese, wie sie für neutrale cAACs verwendet wird, elegant umgangen wird. Dieser neue modulare Syntheseweg könnte somit in Zukunft auch für die Isolierung chiraler enantiomerenreiner neutraler oder anioinischer cAACs dienen. Wie anhand von quantenchemischen Rechnungen gezeigt werden konnte, zeigen die elektronischen Eigenschaften der Carbene eine starke Abhängigkeit vom jeweiligen verwendeten Boran. Somit kann nicht nur der sterische Anspruch des anionischen cAACs durch die Wahl des Stickstoff-Substituenten gezielt gesteuert werden, sondern auch dessen σ-Donor- und π-Akzeptorfähigkeit eingestellt werden.

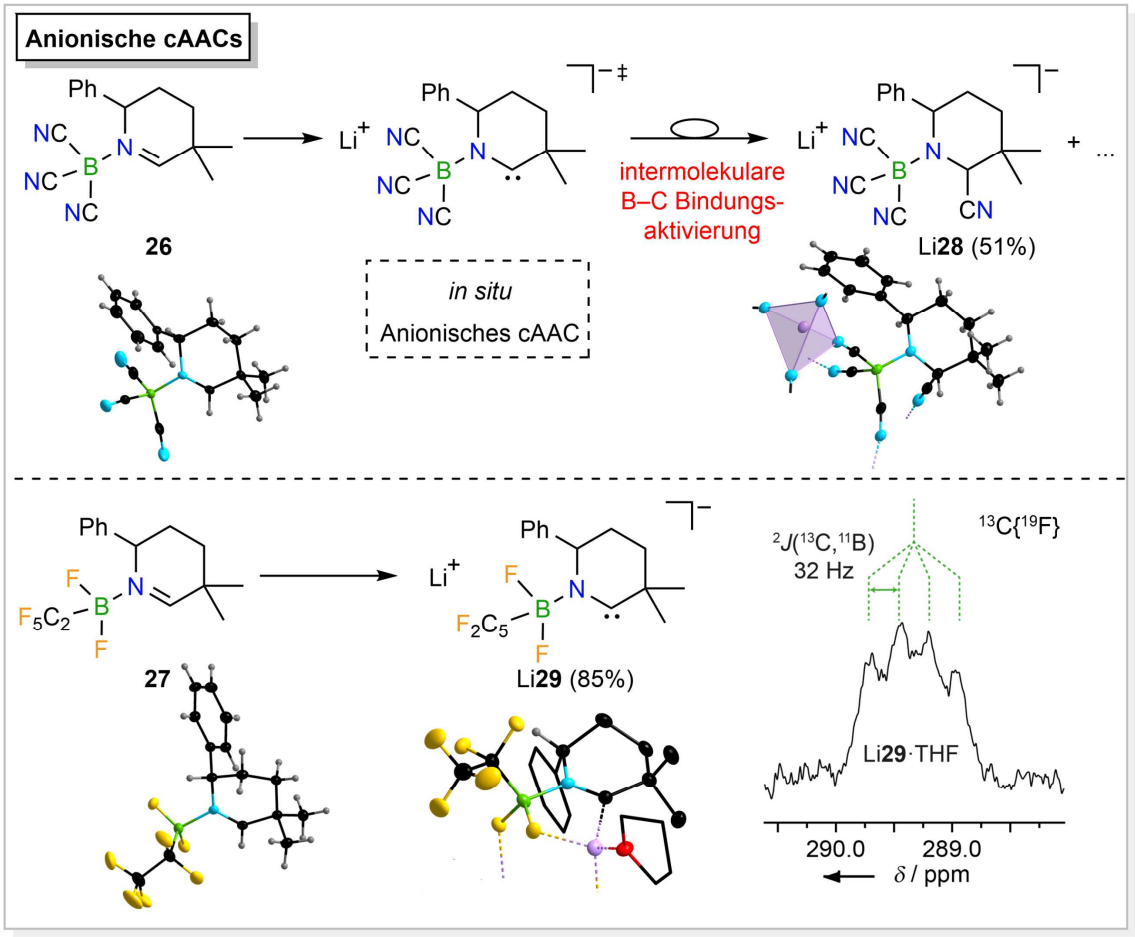

Abbildung 4.5 *Synthese Boran-funktionalisierter anionischer cAACs.*

Die Folgechemie der anionischen cAACs wurde exemplarisch anhand ihrer Selenaddukte und der Reaktion mit Triphenylphosphangold(I)chlorid untersucht. Letztere zeigt, dass eine Substitution anionischer Liganden wie Chlorid am Übergangsmetall unter Salzeliminierung möglich ist, was eine neue Methode zur Einführung cyclischer (Alkyl)(amino)carbene darstellt (Abbildung 4.6).

Der letzte Teil dieser Arbeit (Kapitel 2.4) beschäftigt sich mit der Quantifizierung des sterischen Anspruchs von Lewis-Säuren. Da der sterische Anspruch von Lewis-Basen, wie Phosphanen oder NHCs, sehr gut durch das verdeckte Volumen (%V_{Bur}) abgeschätzt werden kann, es jedoch bisher kein einfach anwendbares Modell zur Beschreibung des räumlichen Anspruchs unterschiedlich substituierter Lewis-acider Verbindungen gab, wurde ein solches entwickelt. Dieses wendet das Konzept des verdeckten Volumens auf Fluorid-Addukte an. Grundsätzlich könnten auch andere Addukte verwendet werden, allerdings werden die Geometrien der Fluorverbindungen ohnehin häufig berechnet, zum Beispiel zur Bestimmung der Fluoridionenaffinität (FIA). Außerdem sind viele Fluorid-Addukte auch synthetisch sehr gut zugänglich, sodass kristallografische Daten ebenfalls einen Zugang zu den Koordinaten der Molekülgeometrien bieten.

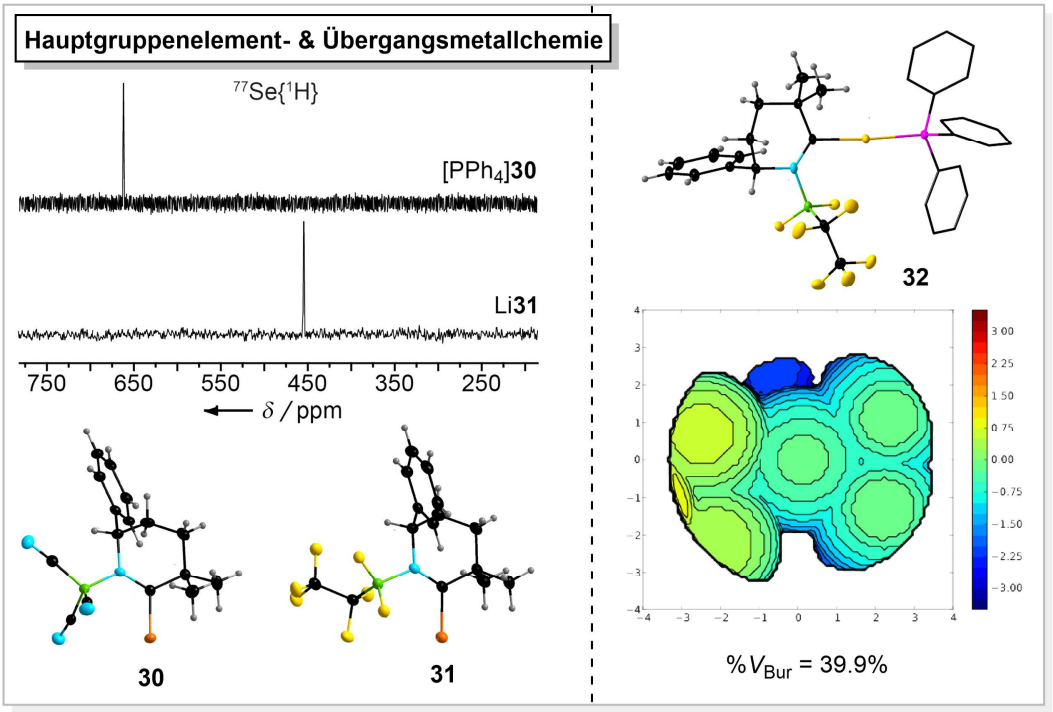

Abbildung 4.6 *NMR-spektroskopische Charakterisierung der Selenverbindungen* ***30*** *und* ***31*** *(links) und Ani-cAAC-Gold(I)-Komplex* ***32*** *mit sterischer Karte und verdecktem Volumen (rechts).*

Das Modell wurde auf eine große Anzahl (240) verschiedener Fluorid-Addukte von Lewis-Säuren mit Elementen der Gruppen 13, 14 und 15 angewendet. Hierbei muss das Fluoratom der Verbindungen $[LA–F]^-$ keinen einheitlich festgelegten Abstand *d*(LA–F) zum Lewis-aciden Zentrum haben, da die unterschiedlichen Werte *d*(LA–F) verschiedener Addukte nur eine geringe Auswirkung auf das verdeckte Volumen %V_{Bur} haben. Die Gegenüberstellung von %V_{Bur} und dem Lewis-aciden Hauptgruppenelement aller untersuchten Lewis-Säuren zeigt, dass eine große Spanne von %V_{Bur} durch bekannte Lewis-Säuren abgedeckt wird und der Bereich von %V_{Bur} = 30% bis %V_{Bur}= 75% problemlos durch die Wahl des geeigneten Elements, der Koordinationszahl und der Substituenten realisiert werden kann. Besonders hilfreich sind Auftragungen von %V_{Bur} gegen die Fluoridionenaffinität (Abbildung 4.7), in welchen der sterische Anspruch mit den elektronischen Eigenschaften in Beziehung gebracht wird. Somit bietet das vorgestellte Modell ein wertvolles Werkzeug für die Synthesechemie. Ausgehend von den %V_{Bur} der Lewis-Säuren wurde das LAB-Rep-Modell (**L**ewis **a**cid/**b**ase **rep**ulsion) erstellt. Dieses beurteilt die sterische Repulsion in Lewis-Säure/Base-Paaren und trifft eine Vorhersage, ob für eine beliebige Kombination von Lewis-Säure und Lewis-Base ein Addukt gebildet werden kann, hinsichtlich der sterischen Eigenschaften (Abbildung 4.7). Die Verlässlichkeit des LAB-Rep-Modells wurde in vier ausgewählten Fallstudien, welche dessen vielseitige Anwendbarkeit zeigen, belegt. Da tabellierte Werte für die verdeckten Volumina der Lewis-Säuren %V_{Bur_LA} und Lewis-Basen %V_{Bur_LB} verwendet werden können, sind keine Daten aus Kristallstrukturen oder quantenchemischen Rechnungen notwendig.

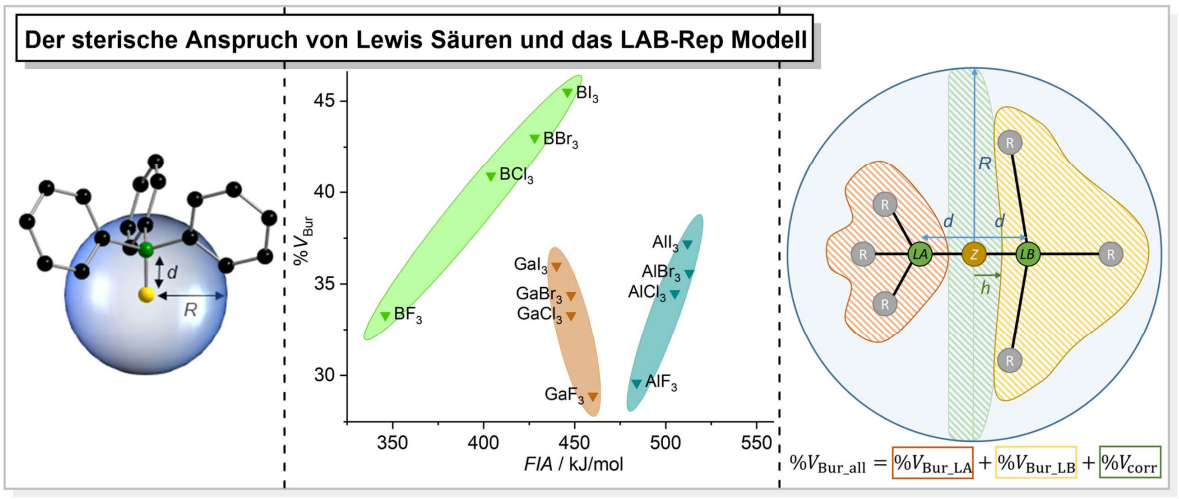

Abbildung 4.7 *Evaluation des sterischen Anspruchs von Lewis-Säuren anhand des verdeckten Volumens der Fluoridverbindungen (links), Gegenüberstellung von sterischem Anspruch und Fluoridionenaffinität (mittig) und grafische Darstellung des LAB-Rep Modells zur Untersuchung der Bindungssituation in Lewis-Säure/Base-Paaren (rechts).*

5. REFERENCES

[1] G. N. Lewis, *Valence and the Structure of Atoms and Molecules*, Chemical Catalog Company, New York, **1923**.
[2] G. N. Lewis, *J. Frankl. Inst.* **1938**, *226*, 293–313.
[3] B. Swanson, D. F. Shriver, J. A. Ibers, *Inorg. Chem.* **1969**, *8*, 2182–2189.
[4] C. Y. Wong, D. K. Kennepohl, R. G. Cavell, *Chem. Rev.* **1996**, *96*, 1917–1952.
[5] P. T. Hennig, Dissertation, Julius-Maximilians-Universität, Würzburg **2019**.
[6] J. Bader, N. Ignat'ev, B. Hoge, *Inorg. Chem.* **2014**, *53*, 7547–7553.
[7] H. C. Brown, *Tetrahedron* **1961**, *12*, 117–138.
[8] H. C. Brown, *Boranes in Organic Chemistry*, *11*, Advances in Organometallic Chemistry, Academic Press, **1973**.
[9] V. Cornel, C. J. Lovely, *Boron Trifluoride Etherate*, Encyclopedia of Reagents for Organic Synthesis, **2007**.
[10] H. C. Brown, G. M. Chen, M. P. Jennings, P. V. Ramachandran, *Angew. Chem.* **1999**, *111*, 2088–2090.
[11] P. Knochel, J. Skotnitzki, *Synfacts* **2020**, *16*, 295.
[12] W. A. G. Graham, F. G. A. Stone, *J. Inorg. Nucl. Chem.* **1956**, *3*, 164–177.
[13] A. Chizmeshya, C. Ritter, T. Groy, J. Tice, J. Kouvetakis, *Chem. Mater.* **2007**, *19*, 5890–5901.
[14] S. G. Shore, K. W. Boddeker, *Inorg. Chem.* **1964**, *3*, 914–915.
[15] A. D. Phillips, P. P. Power, *Acta Crystallogr. Sect. C: Cryst. Struct. Commun.* **2005**, *61*, 291–293.
[16] M. E. Brokke, G. E. Lukes, D. R. Arneklev, Patent US 3558301, **1971**.
[17] A. J. Arduengo, R. Krafczyk, W. J. Marshall, R. Schmutzler, *J. Am. Chem. Soc.* **1997**, *119*, 3381–3382.
[18] S. A. Föhrenbacher, V. Zeh, M. J. Krahfuss, N. V. Ignat'ev, M. Finze, U. Radius, *Eur. J. Inorg. Chem.* **2021**, 1941–1960.
[19] E. Waldmann, A. Chwala, Patent AT159423, **1940**.
[20] K. V. Giri, P. R. Krishnaswamy, *Nature* **1957**, *180*, 1427.
[21] N. Rani, A. Sharma, G. Kumar Gupta, R. Singh, *Mini Rev. Med. Chem.* **2013**, *13*, 1626–1655.
[22] A. Bhatnagar, P. Sharma, N. Kumar, *Int. J. Pharmtech Res.* **2011**, *3*, 268–282.
[23] B. Seed, U.S. Patent No. 5726293, **1998**.
[24] E. B. Anderson, T. E. Long, *Polymer* **2010**, *51*, 2447–2454.
[25] M. N. Hopkinson, C. Richter, M. Schedler, F. Glorius, *Nature* **2014**, *510*, 485–496.
[26] C. J. Bradaric, A. Downard, C. Kennedy, A. J. Robertson, Y. J. G. C. Zhou, *Green Chem.* **2003**, *5*, 143–152.
[27] P. Wasserscheid, W. Keim, *Angew. Chem. Int. Ed.* **2000**, *39*, 3772–3789.
[28] D. Kuang, P. Wang, S. Ito, S. M. Zakeeruddin, M. Grätzel, *J. Am. Chem. Soc.* **2006**, *128*, 7732–7733.
[29] U. Kernchen, B. Etzold, W. Korth, A. Jess, *Chem. Eng. Technol.* **2007**, *30*, 985–994.
[30] A. Wacker, H. Pritzkow, W. Siebert, *Eur. J. Inorg. Chem.* **1998**, 843–849.
[31] A. Xiao, W. M. Lamanna, J. R. Dahn, M. Nie, K. A. Smith, V. J. Chevrier, Patent WO2016126534A1, **2016**.
[32] T. Shirasaka, Y. Takesawa, T. Nishikubo, Y. Nanbu, Patent JP2012197400A, **2012**.
[33] N. Kuhn, H. Kotowski, D. Bläser, R. Boese, *Z. Naturforsch.* **1997**, *52*, 351–354.
[34] R. E. LaPointe, G. R. Roof, K. A. Abboud, J. Klosin, *J. Am. Chem. Soc.* **2000**, *122*, 9560–9561.
[35] D. Vagedes, G. Erker, R. Fröhlich, *J. Organomet. Chem.* **2002**, *641*, 148–155.
[36] T. J. Barbarich, P. F. Driscoll, S. Izquierdo, L. N. Zakharov, C. D. Incarvito, A. L. Rheingold, *Inorg. Chem.* **2004**, *43*, 7764–7773.
[37] T. J. Barbarich, P. F. Driscoll, *Electrochem. Solid-State Lett.* **2003**, *6*, A113–A116.
[38] S. Feng, G. L. Jialanella, P. Nickias, T. Ristoski, Patent US 20070079931A1, **2007**.
[39] Y. Kim, L. L. Liu, D. W. Stephan, *Chem. Eur. J.* **2019**, *25*, 7110–7113.
[40] K. A. Chernyshev, L. I. Larina, E. A. Chirkina, L. B. Krivdin, *Magn. Reson. Chem.* **2012**, *50*, 120–127.

[41] L. Larina, V. Rozinov, E. Rudyakova, V. Savosik, G. Levkovskaya, M. Y. Dmitrichenko, I. Bidusenko, *Russ. J. Gen. Chem.* **2010**, *80*, 374–375.
[42] E. G. Il'in, A. D. Garnovskii, Y. A. Buslaev, *Dokl. Akad. Nauk* **1995**, *344*, 347–351.
[43] C. Tian, W. Nie, Q. Chen, G. Sun, J. Hu, M. Borzov, *Russ. Chem. Bull.* **2014**, *63*, 2668–2674.
[44] J.-B. Dumas, E. M. Peligot, *Ann. Chim. Phys.* **1835**, *58*, 5–74.
[45] A. Igau, H. Grutzmacher, A. Baceiredo, G. Bertrand, *J. Am. Chem. Soc.* **1988**, *110*, 6463–6466.
[46] A. J. Arduengo, R. L. Harlow, M. Kline, *J. Am. Chem. Soc.* **1991**, *113*, 361–363.
[47] A. J. Arduengo Iii, R. Krafczyk, *Chem. Unser Zeit* **1998**, *32*, 6–14.
[48] F. Nahra, D. J. Nelson, S. P. Nolan, *Trends Chem.* **2020**, *2*, 1096–1113.
[49] S. C. Sau, P. K. Hota, S. K. Mandal, M. Soleilhavoup, G. Bertrand, *Chem. Soc. Rev.* **2020**, *49*, 1233–1252.
[50] V. V. Nesterov, D. Reiter, P. Bag, P. Frisch, R. Holzner, A. Porzelt, S. Inoue, *Chem. Rev.* **2018**, *118*, 9678–9842.
[51] E. Peris, *Chem. Rev.* **2018**, *118*, 9988–10031.
[52] S. Würtemberger-Pietsch, U. Radius, T. B. Marder, *Dalton Trans.* **2016**, *45*, 5880–5895.
[53] M. H. Wang, K. A. Scheidt, *Angew. Chem.* **2016**, *128*, 15134–15145.
[54] Y. Wang, G. H. Robinson, *Inorg. Chem.* **2014**, *53*, 11815–11832.
[55] C. D. Martin, M. Soleilhavoup, G. Bertrand, *Chem. Sci.* **2013**, *4*, 3020–3030.
[56] M. Asay, C. Jones, M. Driess, *Chem. Rev.* **2011**, *111*, 354–396.
[57] L. Mercs, M. Albrecht, *Chem. Soc. Rev.* **2010**, *39*, 1903–1912.
[58] F. E. Hahn, M. C. Jahnke, *Angew. Chem. Int. Ed.* **2008**, *47*, 3122–3172.
[59] D. Bourissou, O. Guerret, F. P. Gabbaï, G. Bertrand, *Chem. Rev.* **2000**, *100*, 39–91.
[60] W. A. Herrmann, C. Köcher, *Angew. Chem.* **1997**, *109*, 2256–2282.
[61] W. Kirmse, *Angew. Chem.* **2010**, *122*, 8980–8983.
[62] L. Benhamou, E. Chardon, G. Lacvigne, S. Bellemin-Laponnaz, V. César, *Chem. Rev.* **2011**, *111*, 2705–2733.
[63] M. Melaimi, M. Soleilhavoup, G. Bertrand, *Angew. Chem. Int. Ed.* **2010**, *49*, 8810–8849.
[64] A. J. Arduengo, H. V. R. Dias, R. L. Harlow, M. Kline, *J. Am. Chem. Soc.* **1992**, *114*, 5530–5534.
[65] A. J. Arduengo, H. Bock, H. Chen, M. Denk, D. A. Dixon, J. C. Green, W. A. Herrmann, N. L. Jones, M. Wagner, R. West, *J. Am. Chem. Soc.* **1994**, *116*, 6641–6649.
[66] A. J. Arduengo Iii, R. Krafczyk, R. Schmutzler, H. A. Craig, J. R. Goerlich, W. J. Marshall, M. Unverzagt, *Tetrahedron* **1999**, *55*, 14523–14534.
[67] A. J. Arduengo, III, J. R. Goerlich, W. J. Marshall, *J. Am. Chem. Soc.* **1995**, *117*, 11027–11028.
[68] R. Dorta, E. D. Stevens, N. M. Scott, C. Costabile, L. Cavallo, C. D. Hoff, S. P. Nolan, *J. Am. Chem. Soc.* **2005**, *127*, 2485–2495.
[69] D. Enders, K. Breuer, G. Raabe, J. Runsink, J. H. Teles, J.-P. Melder, K. Ebel, S. Brode, *Angew. Chem. Int. Ed.* **1995**, *34*, 1021–1023.
[70] T. Wurm, F. Mulks, C. R. N. Böhling, D. Riedel, P. Zargaran, M. Rudolph, F. Rominger, A. S. K. Hashmi, *Organometallics* **2016**, *35*, 1070–1078.
[71] G. Kundu, K. Balayan, S. Tothadi, S. S. Sen, *Inorg. Chem.* **2022**, *61*, 12991–12997.
[72] U. Siemeling, C. Färber, M. Leibold, C. Bruhn, P. Mücke, R. F. Winter, B. Sarkar, M. von Hopffgarten, G. Frenking, *Eur. J. Inorg. Chem.* **2009**, *2009*, 4607–4612.
[73] C. M. Weinstein, G. P. Junor, D. R. Tolentino, R. Jazzar, M. Melaimi, G. Bertrand, *J. Am. Chem. Soc.* **2018**, *140*, 9255–9260.
[74] J. P. Moerdyk, D. Schilter, C. W. Bielawski, *Acc. Chem. Res.* **2016**, *49*, 1458–1468.
[75] A. J. Arduengo Iii, J. R. Goerlich, W. J. Marshall, *Liebigs Ann.* **1997**, *1997*, 365–374.
[76] D. M. Andrada, N. Holzmann, T. Hamadi, G. Frenking, *Beilstein J. Org. Chem.* **2015**, *11*, 2727–2736.
[77] A. A. Tukov, A. T. Normand, M. S. Nechaev, *Dalton Trans.* **2009**, 7015–7028.
[78] R. Jazzar, J.-B. Bourg, R. D. Dewhurst, B. Donnadieu, G. Bertrand, *J. Org. Chem.* **2007**, *72*, 3492–3499.
[79] V. Lavallo, Y. Canac, C. Präsang, B. Donnadieu, G. Bertrand, *Angew. Chem. Int. Ed.* **2005**, *44*, 5705–5709.

[80] J. Chu, D. Munz, R. Jazzar, M. Melaimi, G. Bertrand, *J. Am. Chem. Soc.* **2016**, *138*, 7884–7887.
[81] E. Tomás-Mendivil, M. M. Hansmann, C. M. Weinstein, R. Jazzar, M. Melaimi, G. Bertrand, *J. Am. Chem. Soc.* **2017**, *139*, 7753–7756.
[82] U. S. D. Paul, M. J. Krahfuß, U. Radius, *Chem. unserer Zeit* **2019**, *53*, 212–223.
[83] E. Aldeco-Perez, A. J. Rosenthal, B. Donnadieu, P. Parameswaran, G. Frenking, G. Bertrand, *Science* **2009**, *326*, 556–559.
[84] A. Nasr, A. Winkler, M. Tamm, *Coord. Chem. Rev.* **2016**, *316*, 68–124.
[85] U. Kernbach, M. Ramm, P. Luger, W. P. Fehlhammer, *Angew. Chem. Int. Ed.* **1996**, *35*, 310–312.
[86] C. Santini, M. Marinelli, M. Pellei, *Eur. J. Inorg. Chem.* **2016**, *2016*, 2312–2331.
[87] R. Fränkel, C. Birg, U. Kernbach, T. Habereder, H. Nöth, W. P. Fehlhammer, *Angew. Chem. Int. Ed.* **2001**, *40*, 1907–1910.
[88] I. Nieto, F. Cervantes-Lee, J. M. Smith, *Chem. Commun.* **2005**, 3811–3813.
[89] J. J. Scepaniak, C. S. Vogel, M. M. Khusniyarov, F. W. Heinemann, K. Meyer, J. M. Smith, *Science* **2011**, *331*, 1049–1052.
[90] J. A. Valdez-Moreira, A. E. Thorarinsdottir, J. A. DeGayner, S. A. Lutz, C.-H. Chen, Y. Losovyj, M. Pink, T. D. Harris, J. M. Smith, *J. Am. Chem. Soc.* **2019**, *141*, 17092–17097.
[91] S. Kronig, E. Theuergarten, C. G. Daniliuc, P. G. Jones, M. Tamm, *Angew. Chem. Int. Ed.* **2012**, *51*, 3240–3244.
[92] J. Frosch, M. Koneczny, T. Bannenberg, M. Tamm, *Chem. Eur. J.* **2021**, *27*, 4349–4363.
[93] L. P. Ho, L. Anders, M. Tamm, *Chem. Asian J.* **2020**, *15*, 845–851.
[94] L. P. Ho, L. Körner, T. Bannenberg, M. Tamm, *Dalton Trans.* **2020**, *49*, 13207–13217.
[95] L. P. Ho, M. Tamm, *Chem. Eur. J.* **2022**, *28*, e202200530.
[96] E. L. Kolychev, S. Kronig, K. Brandhorst, M. Freytag, P. G. Jones, M. Tamm, *J. Am. Chem. Soc.* **2013**, *135*, 12448-12459.
[97] K. Nomura, G. Nagai, A. Nasr, K. Tsutsumi, Y. Kawamoto, K. Koide, M. Tamm, *Organometallics* **2019**, *38*, 3233–3244.
[98] M. Koneczny, L. Phong Ho, A. Nasr, M. Freytag, P. G. Jones, M. Tamm, *Adv. Synth. Catal.* **2020**, *362*, 3857–3863.
[99] A. El-Hellani, V. J. Lavallo, *Angew. Chem. Int. Ed.* **2014**, *126*, 4578–4582.
[100] M. J. Asay, S. P. Fisher, S. E. Lee, F. S. Tham, D. Borchardt, V. Lavallo, *Chem. Commun.* **2015**, *51*, 5359–5362.
[101] S. P. Fisher, A. El-Hellani, F. S. Tham, V. Lavallo, *Dalton Trans.* **2016**, *45*, 9762–9765.
[102] J. Estrada, V. Lavallo, *Angew. Chem. Int. Ed.* **2017**, *56*, 9906–9909.
[103] S. P. Fisher, S. G. McArthur, V. Tej, S. E. Lee, A. L. Chan, I. Banda, A. Gregory, K. Berkley, C. Tsay, A. L. Rheingold, G. Guisado-Barrios, V. Lavallo, *J. Am. Chem. Soc.* **2020**, *142*, 251–256.
[104] V. Tej Raviprolu, S. E. McArthur, I. Banda, A. Gregory, S. G. McArthur, S. P. Fisher, V. Lavallo, *Chem. Commun.* **2022**, *58*, 10580–10582.
[105] D. Vagedes, G. Kehr, D. König, K. Wedeking, R. Fröhlich, G. Erker, C. Mück-Lichtenfeld, S. Grimme, *Eur. J. Inorg. Chem.* **2002**, 2015–2021.
[106] Y. Wang, Y. Xie, M. Y. Abraham, P. Wei, H. F. Schaefer, P. v. R. Schleyer, G. H. Robinson, *J. Am. Chem. Soc.* **2010**, *132*, 14370–14372.
[107] L. P. Ho, M. Koneczny, T. Bannenberg, M. Tamm, *Inorg. Chem.* **2021**, *60*, 9019–9028.
[108] P. K. Majhi, G. Schnakenburg, Z. Kelemen, L. Nyulaszi, D. P. Gates, R. Streubel, *Angew. Chem. Int. Ed.* **2013**, *52*, 10080–10083.
[109] A. A. Danopoulos, P. Braunstein, *Chem. Commun.* **2014**, *50*, 3055–3057.
[110] F. Medici, G. Gontard, E. Derat, G. Lemière, L. Fensterbank, *Organometallics* **2018**, *37*, 517–520.
[111] N. V. Ignat'ev, M. Finze, *Eur. J. Inorg. Chem.* **2019**, 3539–3560.
[112] D. Williams, B. Pleune, J. Kouvetakis, M. D. Williams, R. A. Andersen, *J. Am. Chem. Soc.* **2000**, *122*, 7735–7741.
[113] H. Böhrer, N. Trapp, D. Himmel, M. Schleep, I. Krossing, *Dalton Trans.* **2015**, *44*, 7489–7499.
[114] L. A. Bischoff, M. Drisch, C. Kerpen, P. T. Hennig, J. Landmann, J. A. P. Sprenger, R. Bertermann, M. Grüne, Q. Yuan, J. Warneke, X.-B. Wang, N. V. Ignat'ev, M. Finze, *Chem. Eur. J.* **2019**, *25*, 3560–3574.

[115] J. Landmann, F. Keppner, D. B. Hofmann, J. A. P. Sprenger, M. Häring, S. H. Zottnick, K. Müller-Buschbaum, N. V. Ignat'ev, M. Finze, *Angew. Chem. Int. Ed.* **2017**, *56*, 2795–2799.
[116] C. Kerpen, J. A. P. Sprenger, L. Herkert, M. Schaefer, L. A. Bischoff, P. Zeides, M. Gruene, R. Bertermann, F. A. Brede, K. Mueller-Buschbaum, N. V. Ignat'ev, M. Finze, *Angew. Chem., Int. Ed.* **2017**, *56*, 2800–2804.
[117] E. Bernhardt, G. Henkel, H. Willner, *Z. Anorg. Allg. Chem.* **2000**, *626*, 560–568.
[118] J. A. P. Sprenger, J. Landmann, M. Drisch, N. Ignat'ev, M. Finze, *Inorg. Chem.* **2015**, *54*, 3403–3412.
[119] M. Drisch, L. A. Bischoff, J. A. P. Sprenger, P. T. Hennig, R. Wirthensohn, S. Z. Konieczka, M. Hailmann, N. V. Ignat'ev, M. Finze, *Chem. Eur. J.* **2020**, *26*, 11625–11633.
[120] J. Landmann, F. Keppner, D. B. Hofmann, J. A. P. Sprenger, M. Häring, S. H. Zottnick, K. Müller-Buschbaum, N. V. Ignat'ev, M. Finze, *Angew. Chem.* **2017**, *129*, 2839–2843.
[121] T. Ribbeck, C. Kerpen, C. Schmidle, F. Keppner, J. A. P. Sprenger, M. Arrowsmith, H. Braunschweig, N. V. Ignat'ev, M. Finze, *Inorg. Chem.* **2019**, *58*, 16689–16702.
[122] N. Schopper, J. A. P. Sprenger, L. Zapf, G. J. Reiss, N. V. Ignat'ev, M. Finze, *New J. Chem.* **2021**, *45*, 14973–14987.
[123] J. Landmann, J. A. P. Sprenger, M. Hailmann, V. Bernhardt-Pitchougina, H. Willner, N. Ignat'ev, E. Bernhardt, M. Finze, *Angew. Chem., Int. Ed.* **2015**, *54*, 11259–11264.
[124] J. Riefer, L. Zapf, R. Wirthensohn, P. T. Hennig, T. Ribbeck, J. A. P. Sprenger, N. Ignat'ev, M. Finze, *Eur. J. Org. Chem.* **2023**, *26*, e202300031.
[125] S.-E. Tsai, J.-C. Lee, N. Uramaru, H. Takayama, G.-J. Huang, F. F. Wong, *Heteroat. Chem* **2017**, *28*, e21372.
[126] M. Momenteau, B. Loock, D. Lavalette, C. Tétreau, J. Mispelter, *J. Chem. Soc., Chem. Commun.* **1983**, 962–964.
[127] A. R. Czardybon, G. R. Goward, *Solid State Ion.* **2006**, *177*, 1405–1411.
[128] N. S. Rannulu, R. Amunugama, Z. Yang, M. T. Rodgers, *J. Phys. Chem. A* **2004**, *108*, 6385–6396.
[129] F. Blanco, I. Alkorta, J. Elguero, *J. Phys. Chem. A* **2008**, *112*, 7682–7688.
[130] Y. Sun, H. Sun, *J. Mol. Model.* **2013**, *19*, 1641–1650.
[131] Y. Hu, N. Dunlap, S. Wan, S. Lu, S. Huang, I. Sellinger, M. Ortiz, Y. Jin, S.-h. Lee, W. Zhang, *J. Am. Chem. Soc.* **2019**, *141*, 7518–7525.
[132] J. Zhang, T. Wu, C. Zhou, S. Chen, P. Feng, X. Bu, *Angew. Chem. Int. Ed.* **2009**, *48*, 2542–2545.
[133] T. D. Bennett, J.-C. Tan, S. A. Moggach, R. Galvelis, C. Mellot-Draznieks, B. A. Reisner, A. Thirumurugan, D. R. Allan, A. K. Cheetham, *Chem. Eur. J.* **2010**, *16*, 10684–10690.
[134] C. Lambert, P. v. R. Schleyer, M. G. Newton, P. Otto, P. Schreiner, *Z. Naturforschung B* **1992**, *47*, 869–876.
[135] T. Küppers, E. Bernhardt, C. W. Lehmann, H. Willner, *Z. Anorg. Allg. Chem.* **2007**, *633*, 1666–1672.
[136] A. J. Arduengo, M. Tamm, J. C. Calabrese, F. Davidson, W. J. Marshall, *Chem. Lett.* **1999**, 1021–1022.
[137] A. Koch, H. Görls, S. Krieck, M. Westerhausen, *Dalton Trans.* **2017**, *46*, 9058–9067.
[138] A. L. Spek, *Acta Crystallogr. C* **2015**, *71*, 9–18.
[139] A. L. Spek, *Acta Crystallogr. D* **2009**, *65*, 148–155.
[140] V. B. Saptal, B. M. Bhanage, *ChemSusChem* **2016**, *9*, 1980–1985.
[141] A. Fürstner, M. Alcarazo, R. Goddard, C. W. Lehmann, *Angew. Chem. Int. Ed.* **2008**, *47*, 3210–3214.
[142] D. Bibelayi, A. S. Lundemba, F. H. Allen, P. T. A. Galek, J. Pradon, A. M. Reilly, C. R. Groom, Z. G. Yav, *Acta Crystallogr. Sect. B* **2016**, *72*, 317–325.
[143] L. Infantes, S. Motherwell, *CrystEngComm* **2002**, *4*, 454–461.
[144] S. V. C. Vummaleti, D. J. Nelson, A. Poater, A. Gómez-Suárez, D. B. Cordes, A. M. Z. Slawin, S. P. Nolan, L. Cavallo, *Chem. Sci.* **2015**, *6*, 1895–1904.
[145] G. P. Junor, J. Lorkowski, C. M. Weinstein, R. Jazzar, C. Pietraszuk, G. Bertrand, *Angew. Chem.* **2020**, *132*, 22212–22217.
[146] A. Liske, K. Verlinden, H. Buhl, K. Schaper, C. Ganter, *Organometallics* **2013**, *32*, 5269–5272.

[147] K. Verlinden, H. Buhl, W. Frank, C. Ganter, *Eur. J. Inorg. Chem.* **2015**, *2015*, 2416–2425.
[148] H. V. Huynh, *Chem. Rev.* **2018**, *118*, 9457–9492.
[149] D. J. Williams, M. R. Fawcett-Brown, R. R. Raye, D. VanDerveer, Y. T. Pang, R. L. Jones, K. L. Bergbauer, *Heteroat. Chem* **1993**, *4*, 409–414.
[150] D. W. Tomlin, D. P. Campbell, P. A. Fleitz, W. W. Adams, *Acta Crystallog. Sect. C* **1997**, *53*, 1153–1154.
[151] K. Srinivas, P. Suresh, C. N. Babu, A. Sathyanarayana, G. Prabusankar, *RSC Adv.* **2015**, *5*, 15579–15590.
[152] C. A. Tolman, *Chem. Rev.* **1977**, *77*, 313–348.
[153] K. Öfele, W. A. Herrmann, D. Mihalios, M. Elison, E. Herdtweck, W. Scherer, J. Mink, *J. Organomet. Chem.* **1993**, *459*, 177–184.
[154] A. Gómez-Suárez, D. J. Nelson, S. P. Nolan, *Chem. Commun.* **2017**, *53*, 2650–2660.
[155] H. Clavier, S. P. Nolan, *Chem. Commun.* **2010**, *46*, 841–861.
[156] U. S. D. Paul, U. Radius, *Organometallics* **2017**, *36*, 1398–1407.
[157] J. Frosch, M. Koneczny, T. Bannenberg, M. Tamm, *Chem. Eur. J.* **2021**, *27*, 4349–4363.
[158] L. P. Ho, L. Anders, M. Tamm, *Chem. Asian J.* **2020**, *15*, 845–851.
[159] L. P. Ho, L. Körner, T. Bannenberg, M. Tamm, *Dalton Trans.* **2020**, *49*, 13207–13217.
[160] E. L. Kolychev, S. Kronig, K. Brandhorst, M. Freytag, P. G. Jones, M. Tamm, *J. Am. Chem. Soc.* **2013**, *135*, 12448–12459.
[161] S. Kronig, E. Theuergarten, C. G. Daniliuc, P. G. Jones, M. Tamm, *Angew. Chem.* **2012**, *124*, 3294–3298.
[162] N. Phillips, R. Tirfoin, S. Aldridge, *Dalton Transactions* **2014**, *43*, 15279–15282.
[163] N. Ignat'ev, P. Sartori, *J. Fluor. Chem.* **2000**, *103*, 57–61.
[164] N. V. Ignat'ev, H. Willner, P. Sartori, *J. Fluorine Chem.* **2009**, *130*, 1183–1191.
[165] S. A. Föhrenbacher, M. J. Krahfuss, L. Zapf, A. Friedrich, N. V. Ignat'ev, M. Finze, U. Radius, *Chem. Eur. J.* **2021**, *27*, 3504–3516.
[166] H. Kimata, T. Mochida, *Cryst. Growth Des.* **2018**, *18*, 7562–7569.
[167] M. Schmidt, U. Heider, A. Kuehner, R. Oesten, M. Jungnitz, N. Ignat'ev, P. Sartori, *J. Power Sources* **2001**, *97–98*, 557–560.
[168] J. Bader, B. Neumann, H.-G. Stammler, N. Ignat'ev, B. Hoge, *Chem. Eur. J.* **2018**, *24*, 6975–6982.
[169] N. V. Ignat'ev, J. Bader, K. Koppe, B. Hoge, H. Willner, *J. Fluorine Chem.* **2015**, *171*, 36–45.
[170] L. Zapf, M. Riethmann, S. A. Föhrenbacher, M. Finze, U. Radius, *Chem. Sci.* **2023**, *14*, 2275–2288.
[171] A. P. Marchenko, H. N. Koidan, A. N. Huryeva, E. V. Zarudnitskii, A. A. Yurchenko, A. N. Kostyuk, *J. Org. Chem.* **2010**, *75*, 7141–7145.
[172] P. Ai, A. A. Danopoulos, P. Braunstein, K. Y. Monakhov, *Chem. Commun.* **2014**, *50*, 103–105.
[173] Y. Hoshimoto, T. Kinoshita, M. Ohashi, S. Ogoshi, *Angew. Chem. Int. Ed.* **2015**, *54*, 11666-11671.
[174] Y. Hoshimoto, T. Asada, S. Hazra, T. Kinoshita, P. Sombut, R. Kumar, M. Ohashi, S. Ogoshi, *Angew. Chem. Int. Ed.* **2016**, *55*, 16075-16079.
[175] A. J. Arduengo, H. Bock, H. Chen, M. Denk, D. A. Dixon, J. C. Green, W. A. Herrmann, N. L. Jones, M. Wagner, R. West, *J. Am. Chem. Soc.* **1994**, *116*, 6641–6649.
[176] A. J. Arduengo, H. V. R. Dias, R. L. Harlow, M. Kline, *J. Am. Chem. Soc.* **1992**, *114*, 5530–5534.
[177] T. Wang, M. Xu, A. R. Jupp, Z.-W. Qu, S. Grimme, D. W. Stephan, *Chem. Asian J.* **2021**, *16*, 3640–3644.
[178] A. Koch, H. Görls, S. Krieck, M. Westerhausen, *Dalton Trans.* **2017**, *46*, 9058–9067.
[179] L. Zapf, S. Peters, R. Bertermann, U. Radius, M. Finze, *Chem. Eur. J.* **2022**, *28*, e202200275.
[180] K. Verlinden, H. Buhl, W. Frank, C. Ganter, *Eur. J. Inorg. Chem.* **2015**, 2416–2425.
[181] G. P. Junor, J. Lorkowski, C. M. Weinstein, R. Jazzar, C. Pietraszuk, G. Bertrand, *Angew. Chem. Int. Ed.* **2020**, *59*, 22028–22033.
[182] A. Góméz-Suárez, D. J. Nelson, S. P. Nolan, *Chem. Commun.* **2017**, *53*, 2650–2660.
[183] R. Dorta, E. D. Stevens, N. M. Scott, C. Costabile, L. Cavallo, C. D. Hoff, S. P. Nolan, *J. Am. Chem. Soc.* **2005**, *127*, 2485–2495.
[184] L. Zapf, U. Radius, M. Finze, *Angew. Chem.* **2021**, *133*, 18118–18125.

[185] B. Rao, H. Tang, X. Zeng, L. Liu, M. Melaimi, G. Bertrand, *Angew. Chem. Int. Ed.* **2015**, *54*, 14915–14919.
[186] J. Lorkowski, M. Krahfuß, M. Kubicki, U. Radius, C. Pietraszuk, *Chem. Eur. J.* **2019**, *25*, 11365–11374.
[187] D. R. Anderson, V. Lavallo, D. J. O'Leary, G. Bertrand, R. H. Grubbs, *Angew. Chem. Int. Ed.* **2007**, *46*, 7262–7265.
[188] V. Lavallo, G. D. Frey, B. Donnadieu, M. Soleilhavoup, G. Bertrand, *Angew. Chem. Int. Ed.* **2008**, *47*, 5224–5228.
[189] X. Hu, M. Soleilhavoup, M. Melaimi, J. Chu, G. Bertrand, *Angew. Chem. Int. Ed.* **2015**, *54*, 6008–6011.
[190] L. Jin, E. A. Romero, M. Melaimi, G. Bertrand, *J. Am. Chem. Soc.* **2015**, *137*, 15696–15698.
[191] L. Jin, D. R. Tolentino, M. Melaimi, G. Bertrand, *Sci. Adv.* **2015**, *1*, e1500304.
[192] V. M. Marx, A. H. Sullivan, M. Melaimi, S. C. Virgil, B. K. Keitz, D. S. Weinberger, G. Bertrand, R. H. Grubbs, *Angew. Chem. Int. Ed.* **2015**, *54*, 1919–1923.
[193] Y. Wei, B. Rao, X. Cong, X. Zeng, *J. Am. Chem. Soc.* **2015**, *137*, 9250–9253.
[194] D. Butilkov, A. Frenklah, I. Rozenberg, S. Kozuch, N. G. Lemcoff, *ACS Catal.* **2017**, *7*, 7634–7637.
[195] R. Gawin, A. Kozakiewicz, P. A. Guńka, P. Dąbrowski, K. Skowerski, *Angew. Chem. Int. Ed.* **2017**, *56*, 981–986.
[196] E. A. Romero, R. Jazzar, G. Bertrand, *Chem. Sci.* **2017**, *8*, 165–168.
[197] M. P. Wiesenfeldt, Z. Nairoukh, W. Li, F. Glorius, *Science* **2017**, *357*, 908–912.
[198] B. L. Tran, J. L. Fulton, J. C. Linehan, J. A. Lercher, R. M. Bullock, *ACS Catal.* **2018**, *8*, 8441–8449.
[199] R. Jazzar, M. Soleilhavoup, G. Bertrand, *Chem. Rev.* **2020**, *120*, 4141–4168.
[200] Y. Gao, N. Kim, S. D. Mendoza, S. Yazdani, A. Faria Vieira, M. Liu, A. Kendrick, D. B. Grotjahn, G. Bertrand, R. Jazzar, K. M. Engle, *ACS Catal.* **2022**, *12*, 7243–7247.
[201] V. Lavallo, Y. Canac, B. Donnadieu, W. W. Schoeller, G. Bertrand, *Angew. Chem. Int. Ed.* **2006**, *45*, 3488–3491.
[202] D. Frey Guido, V. Lavallo, B. Donnadieu, W. Schoeller Wolfgang, G. Bertrand, *Science* **2007**, *316*, 439–441.
[203] G. D. Frey, J. D. Masuda, B. Donnadieu, G. Bertrand, *Angew. Chem. Int. Ed.* **2010**, *49*, 9444–9447.
[204] D. Martin, M. Soleilhavoup, G. Bertrand, *Chem. Sci.* **2011**, *2*, 389–399.
[205] C. Mohapatra, P. P. Samuel, B. Li, B. Niepötter, C. J. Schürmann, R. Herbst-Irmer, D. Stalke, B. Maity, D. Koley, H. W. Roesky, *Inorg. Chem.* **2016**, *55*, 1953–1955.
[206] Z. R. Turner, *Chem. Eur. J.* **2016**, *22*, 11461–11468.
[207] S. Würtemberger-Pietsch, H. Schneider, T. B. Marder, U. Radius, *Chem. Eur. J.* **2016**, *22*, 13032–13036.
[208] A. V. Zhukhovitskiy, M. G. Mavros, K. T. Queeney, T. Wu, T. Van Voorhis, J. A. Johnson, *J. Am. Chem. Soc.* **2016**, *138*, 8639–8652.
[209] A. F. Eichhorn, L. Kuehn, T. B. Marder, U. Radius, *Chem. Commun.* **2017**, *53*, 11694–11696.
[210] U. S. D. Paul, U. Radius, *Chem. Eur. J.* **2017**, *23*, 3993–4009.
[211] R. Kinjo, B. Donnadieu, M. A. Celik, G. Frenking, G. Bertrand, *Science* **2011**, *333*, 610–613.
[212] Y. Li, K. C. Mondal, H. W. Roesky, H. Zhu, P. Stollberg, R. Herbst-Irmer, D. Stalke, D. M. Andrada, *J. Am. Chem. Soc.* **2013**, *135*, 12422–12428.
[213] J. Böhnke, H. Braunschweig, W. C. Ewing, C. Hörl, T. Kramer, I. Krummenacher, J. Mies, A. Vargas, *Angew. Chem. Int. Ed.* **2014**, *53*, 9082–9085.
[214] K. Chandra Mondal, S. Roy, B. Dittrich, B. Maity, S. Dutta, D. Koley, S. K. Vasa, R. Linser, S. Dechert, H. W. Roesky, *Chem. Sci.* **2015**, *6*, 5230–5234.
[215] M. Arrowsmith, H. Braunschweig, M. A. Celik, T. Dellermann, R. D. Dewhurst, W. C. Ewing, K. Hammond, T. Kramer, I. Krummenacher, J. Mies, K. Radacki, J. K. Schuster, *Nat. Chem.* **2016**, *8*, 890–894.
[216] Y. Li, Y.-C. Chan, Y. Li, I. Purushothaman, S. De, P. Parameswaran, C.-W. So, *Inorg. Chem.* **2016**, *55*, 9091–9098.
[217] C. D. Martin, M. Soleilhavoup, G. Bertrand, *Chem. Sci.* **2013**, *4*, 3020–3030.
[218] L. Zapf, U. Radius, M. Finze, *Angew. Chem. Int. Ed.* **2021**, *60*, 17974–17980.

[219] H. Zondler, W. Pfleiderer, *Liebigs Ann. Chem.* **1972**, *759*, 84–106.
[220] W. Maison, M. Kosten, A. Charpy, J. Kintscher-Langenhagen, I. Schlemminger, A. Lützen, O. Westerhoff, J. Martens, *Eur. J. Org. Chem* **1999**, *1999*, 2433–2441.
[221] W. Maison, A. Lützen, M. Kosten, I. Schlemminger, O. Westerhoff, J. Martens, *J. Chem. Soc., Perkin Trans. 1* **1999**, 3515–3525.
[222] C. Müller, D. M. Andrada, I.-A. Bischoff, M. Zimmer, V. Huch, N. Steinbrück, A. Schäfer, *Organometallics* **2019**, *38*, 1052–1061.
[223] M. Finze, E. Bernhardt, M. Zaehres, H. Willner, *Inorg. Chem.* **2004**, *43*, 490–505.
[224] M. Tretiakov, Y. G. Shermolovich, A. P. Singh, P. P. Samuel, H. W. Roesky, B. Niepötter, A. Visscher, D. Stalke, *Dalton Trans.* **2013**, *42*, 12940–12946.
[225] U. S. D. Paul, C. Sieck, M. Haehnel, K. Hammond, T. B. Marder, U. Radius, *Chem. Eur. J.* **2016**, *22*, 11005–11014.
[226] L. Greb, *Chem. Eur. J.* **2018**, *24*, 17881–17896.
[227] J. M. Bayne, D. W. Stephan, *Chem. Soc. Rev.* **2016**, *45*, 765–774.
[228] H. F. T. Klare, L. Albers, L. Süsse, S. Keess, T. Müller, M. Oestreich, *Chem. Rev.* **2021**, *121*, 5889–5985.
[229] H. F. T. Klare, M. Oestreich, *Dalton Trans.* **2010**, *39*, 9176–9184.
[230] J. C. L. Walker, H. F. T. Klare, M. Oestreich, *Nat. Rev. Chem.* **2020**, *4*, 54–62.
[231] W. E. Piers, *Adv. Organomet. Chem.* **2005**, *52*, 1–76.
[232] A. Corma, H. García, *Chem. Rev.* **2003**, *103*, 4307–4366.
[233] J. R. Lawson, R. L. Melen, *Inorg. Chem.* **2017**, *56*, 8627–8643.
[234] J. L. Carden, A. Dasgupta, R. L. Melen, *Chem. Soc. Rev.* **2020**, *49*, 1706–1725.
[235] H. Fang, M. Oestreich, *Chem. Sci.* **2020**, *11*, 12604–12615.
[236] G. C. Welch, R. R. S. Juan, J. D. Masuda, D. W. Stephan, *Science* **2006**, *314*, 1124–1126.
[237] D. W. Stephan, *Org. Biomol. Chem.* **2008**, *6*, 1535–1539.
[238] D. W. Stephan, G. Erker, *Angew. Chem. Int. Ed.* **2010**, *49*, 46–76.
[239] G. Erker, *Pure Appl. Chem.* **2012**, *84*, 2203–2217.
[240] D. W. Stephan, *J. Am. Chem. Soc.* **2015**, *137*, 10018–10032.
[241] D. W. Stephan, *Acc. Chem. Res.* **2015**, *48*, 306–316.
[242] D. W. Stephan, *Science* **2016**, *354*, aaf7229.
[243] J. Paradies, *Coord. Chem. Rev.* **2019**, *380*, 170–183.
[244] A. Andresen, H.-G. Cordes, J. Herwig, W. Kaminsky, A. Merck, R. Mottweiler, J. Pein, H. Sinn, H.-J. Vollmer, *Angew. Chem. Int. Ed.* **1976**, *15*, 630–632.
[245] H. Sinn, W. Kaminsky, H.-J. Vollmer, R. Woldt, *Angew. Chem. Int. Ed.* **1980**, *19*, 390–392.
[246] W. E. Piers, T. Chivers, *Chem. Soc. Rev.* **1997**, *26*, 345–354.
[247] M. Bochmann, *J. Chem. Soc., Dalton Trans.* **1996**, 255–270.
[248] M. Bochmann, *Top. Catal.* **1999**, *7*, 9–22.
[249] G. Erker, *Dalton Trans.* **2005**, 1883–1890.
[250] E. Y.-X. Chen, T. J. Marks, *Chem. Rev.* **2000**, *100*, 1391–1434.
[251] W. Beck, K. Suenkel, *Chem. Rev.* **1988**, *88*, 1405–1421.
[252] S. H. Strauss, *Chem. Rev.* **1993**, *93*, 927–942.
[253] I. Krossing, I. Raabe, *Angew. Chem. Int. Ed.* **2004**, *43*, 2066–2090.
[254] T. A. Engesser, M. R. Lichtenthaler, M. Schleep, I. Krossing, *Chem. Soc. Rev.* **2016**, *45*, 789–899.
[255] I. M. Riddlestone, A. Kraft, J. Schaefer, I. Krossing, *Angew. Chem. Int. Ed.* **2018**, *57*, 13982–14024.
[256] D. E. Fogg, E. N. dos Santos, *Coord. Chem. Rev.* **2004**, *248*, 2365–2379.
[257] I. B. Sivaev, V. I. Bregadze, *Coord. Chem. Rev.* **2014**, *270–271*, 75–88.
[258] E. Krause, R. Nitsche, *Ber. Dtsch. Chem. Ges* **1922**, *55*, 1261–1265.
[259] A. Massey, F. Stone, A. Park, **1963**, *127*, 212.
[260] A. G. Massey, A. J. Park, *J. Organomet. Chem.* **1964**, *2*, 245–250.
[261] D. Naumann, H. Butler, R. Gnann, *Z. Anorg. Allg. Chem.* **1992**, *618*, 74–76.
[262] J. A. Nicasio, S. Steinberg, B. Inés, M. Alcarazo, *Chem. Eur. J.* **2013**, *19*, 11016–11020.
[263] D. Chakraborty, A. Rodriguez, E. Y. X. Chen, *Macromolecules* **2003**, *36*, 5470–5481.
[264] D. M. C. Ould, J. L. Carden, R. Page, R. L. Melen, *Inorg. Chem.* **2020**, *59*, 14891–14898.

[265] M. M. Morgan, A. J. V. Marwitz, W. E. Piers, M. Parvez, *Organometallics* **2013**, *32*, 317–322.
[266] H. J. Frohn, V. Bardin, *Z. Anorg. Allg. Chem.* **2001**, *627*, 15–16.
[267] M. Finze, E. Bernhardt, A. Terheiden, M. Berkei, H. Willner, D. Christen, H. Oberhammer, F. Aubke, *J. Am. Chem. Soc.* **2002**, *124*, 15385–15398.
[268] A. Terheiden, E. Bernhardt, H. Willner, F. Aubke, *Angew. Chem. Int. Ed.* **2002**, *41*, 799–801.
[269] M. Finze, E. Bernhardt, H. Willner, *Angew. Chem. Int. Ed.* **2007**, *46*, 9180–9196.
[270] M. Finze, E. Bernhardt, H. Willner, C. W. Lehmann, *J. Am. Chem. Soc.* **2005**, *127*, 10712–10722.
[271] M. Gerken, G. Pawelke, E. Bernhardt, H. Willner, *Chem. Eur. J.* **2010**, *16*, 7527–7536.
[272] J. Landmann, J. A. P. Sprenger, P. T. Hennig, R. Bertermann, M. Grüne, F. Würthner, N. V. Ignat'ev, M. Finze, *Chem. Eur. J.* **2018**, *24*, 608–623.
[273] U. Mayer, V. Gutmann, W. Gerger, *Monatsh. Chem.* **1975**, *106*, 1235–1257.
[274] V. Gutmann, *Electrochim. Acta* **1976**, *21*, 661–670.
[275] M. A. Beckett, G. C. Strickland, J. R. Holland, K. Sukumar Varma, *Polymer* **1996**, *37*, 4629–4631.
[276] P. Erdmann, L. Greb, *Angew. Chem. Int. Ed.* **2022**, *61*, e202114550.
[277] R. G. Pearson, *J. Am. Chem. Soc.* **1963**, *85*, 3533–3539.
[278] A. Hanft, K. Radacki, C. Lichtenberg, *Chem. Eur. J.* **2021**, *27*, 6230–6239.
[279] J. Ramler, C. Lichtenberg, *Chem. Eur. J.* **2020**, *26*, 10250–10258.
[280] R. F. Childs, D. L. Mulholland, A. Nixon, *Can. J. Chem.* **1982**, *60*, 809–812.
[281] I. R. Beattie, T. Gilson, *J. Chem. Soc.* **1964**, 2292–2295.
[282] K. F. Purcell, R. S. Drago, *J. Am. Chem. Soc.* **1966**, *88*, 919–924.
[283] B. Swanson, D. F. Shriver, *Inorg. Chem.* **1970**, *9*, 1406–1416.
[284] D. F. Shriver, B. Swanson, *Inorg. Chem.* **1971**, *10*, 1354–1365.
[285] H. Knoezinger, H. Krietenbrink, *J. Chem. Soc.* **1975**, *71*, 2421–2430.
[286] J. R. Gaffen, J. N. Bentley, L. C. Torres, C. Chu, T. Baumgartner, C. B. Caputo, *Chem* **2019**, *5*, 1567–1583.
[287] J. N. Bentley, S. A. Elgadi, J. R. Gaffen, P. Demay-Drouhard, T. Baumgartner, C. B. Caputo, *Organometallics* **2020**, *39*, 3645–3655.
[288] R. J. Mayer, N. Hampel, A. R. Ofial, *Chem. Eur. J.* **2021**, *27*, 4070–4080.
[289] J. W. Larson, T. B. McMahon, *J. Am. Chem. Soc.* **1985**, *107*, 766–773.
[290] M. O'Keeffe, *J. Am. Chem. Soc.* **1986**, *108*, 4341–4343.
[291] K. O. Christe, D. A. Dixon, D. McLemore, W. W. Wilson, J. A. Sheehy, J. A. Boatz, *J. Fluorine Chem.* **2000**, *101*, 151–153.
[292] I. Krossing, I. Raabe, *Chem. Eur. J.* **2004**, *10*, 5017–5030.
[293] A. Y. Timoshkin, G. Frenking, *Organometallics* **2008**, *27*, 371–380.
[294] D. J. Grant, D. A. Dixon, D. Camaioni, R. G. Potter, K. O. Christe, *Inorg. Chem.* **2009**, *48*, 8811–8821.
[295] E. Blokker, C. G. T. Groen, J. M. van der Schuur, A. G. Talma, F. M. Bickelhaupt, *Results in Chem.* **2019**, *1*, 100007.
[296] P. Erdmann, J. Leitner, J. Schwarz, L. Greb, *Chemphyschem* **2020**, *21*, 987–994.
[297] P. Erdmann, L. Greb, *Chemphyschem* **2021**, *22*, 935–943.
[298] B. Pinter, T. Fievez, F. M. Bickelhaupt, P. Geerlings, F. De Proft, *Phys. Chem. Chem. Phys.* **2012**, *14*, 9846–9854.
[299] I. Fernández, F. M. Bickelhaupt, *Chem. Soc. Rev.* **2014**, *43*, 4953–4967.
[300] L. P. Wolters, F. M. Bickelhaupt, *WIREs Comput. Mol. Sci.* **2015**, *5*, 324–343.
[301] F. M. Bickelhaupt, K. N. Houk, *Angew. Chem. Int. Ed.* **2017**, *56*, 10070–10086.
[302] T. A. Hamlin, F. M. Bickelhaupt, I. Fernández, *Acc. Chem. Res.* **2021**, *54*, 1972−1981.
[303] P. Vermeeren, T. A. Hamlin, F. M. Bickelhaupt, *Chem. Commun.* **2021**, *57*, 5880–5896.
[304] C. A. Tolman, *Chem. Rev.* **1977**, *77*, 313–348.
[305] C. A. Tolman, *J. Am. Chem. Soc.* **1970**, *92*, 2956–2965.
[306] N. Fey, A. G. Orpen, J. N. Harvey, *Coord. Chem. Rev.* **2009**, *253*, 704–722.
[307] N. Fey, *Dalton Trans.* **2010**, *39*, 296–310.
[308] D. J. Durand, N. Fey, *Chem. Rev.* **2019**, *119*, 6561–6594.

[309] A. C. Hillier, W. J. Sommer, B. S. Yong, J. L. Petersen, L. Cavallo, S. P. Nolan, *Organometallics* **2003**, *22*, 4322–4326.
[310] A. Poater, F. Ragone, S. Giudice, C. Costabile, R. Dorta, S. P. Nolan, L. Cavallo, *Organometallics* **2008**, *27*, 2679–2681.
[311] S. Díez-González, S. P. Nolan, *Coord. Chem. Rev.* **2007**, *251*, 874–883.
[312] L. Falivene, Z. Cao, A. Petta, L. Serra, A. Poater, R. Oliva, V. Scarano, L. Cavallo, *Nat. Chem.* **2019**, *11*, 872–879.
[313] L. Falivene, R. Credendino, A. Poater, A. Petta, L. Serra, R. Oliva, V. Scarano, L. Cavallo, *Organometallics* **2016**, *35*, 2286-2293.
[314] S. Pelzer, B. Neumann, H.-G. Stammler, N. Ignat'ev, B. Hoge, *Angew. Chem. Int. Ed.* **2016**, *55*, 6088–6092.
[315] S. Pelzer, B. Neumann, H.-G. Stammler, N. Ignat'ev, B. Hoge, *Chem. Eur. J.* **2016**, *22*, 16460–16466.
[316] N. Schwarze, B. Kurscheid, S. Steinhauer, B. Neumann, H.-G. Stammler, N. Ignat'ev, B. Hoge, *Chem. Eur. J.* **2016**, *22*, 17460–17467.
[317] S. Solyntjes, J. Bader, B. Neumann, H.-G. Stammler, N. Ignat'ev, B. Hoge, *Chem. Eur. J.* **2017**, *23*, 1557–1567.
[318] S. Pelzer, B. Neumann, H.-G. Stammler, N. Ignat'ev, R. Eujen, B. Hoge, *Synthesis* **2017**, *49*, 2389–2393.
[319] J. Bader, B. Neumann, H.-G. Stammler, N. Ignat'ev, B. Hoge, *J. Fluorine Chem.* **2018**, *207*, 12–17.
[320] J. Bader, N. Ignat'ev, B. Hoge, *Eur. J. Inorg. Chem.* **2018**, *2018*, 861–866.
[321] M. Niemann, B. Neumann, H.-G. Stammler, B. Hoge, *Angew. Chem. Int. Ed.* **2019**, *58*, 8938–8942.
[322] M. Niemann, B. Neumann, H.-G. Stammler, B. Hoge, *Eur. J. Inorg. Chem.* **2019**, *2019*, 3462–3475.
[323] N. Tiessen, B. Neumann, H.-G. Stammler, B. Hoge, *Chem. Eur. J.* **2020**, *26*, 13611–13614.
[324] D. E. Young, L. R. Anderson, W. B. Fox, *Chem. Commun.* **1971**, 736.
[325] D. E. Young, L. R. Anderson, W. B. Fox, *Inorg. Chem.* **1971**, *10*, 2810–2812.
[326] M. O. Akram, J. R. Tidwell, J. L. Dutton, C. D. Martin, *Angew. Chem. Int. Ed.* **2022**, *61*, e202212073.
[327] L. O. Müller, D. Himmel, J. Stauffer, G. Steinfeld, J. Slattery, G. Santiso-Quiñones, V. Brecht, I. Krossing, *Angew. Chem. Int. Ed.* **2008**, *47*, 7659–7663.
[328] J. F. Kögel, D. A. Sorokin, A. Khvorost, M. Scott, K. Harms, D. Himmel, I. Krossing, J. Sundermeyer, *Chem. Sci.* **2018**, *9*, 245–253.
[329] K. F. Hoffmann, A. Wiesner, S. Steinhauer, S. Riedel, *Chem. Eur. J.* **2022**, *28*, e202201958.
[330] W. Strohmeier, F.-J. Müller, *Chem. Ber.* **1967**, *100*, 2812–2821.
[331] D. G. Gusev, E. Peris, *Dalton Trans.* **2013**, *42*, 7359–7364.
[332] D. G. Gusev, *Organometallics* **2009**, *28*, 763–770.
[333] V. Branchadell, A. Sbai, A. Oliva, *J. Phys. Chem.* **1995**, *99*, 6472–6476.
[334] A. Y. Timoshkin, A. V. Suvorov, H. F. Bettinger, H. F. Schaefer, *J. Am. Chem. Soc.* **1999**, *121*, 5687–5699.
[335] G. Frenking, S. Fau, C. M. Marchand, H. Grützmacher, *J. Am. Chem. Soc.* **1997**, *119*, 6648–6655.
[336] H. Fleischer, *Eur. J. Inorg. Chem.* **2001**, *2001*, 393–404.
[337] A. Ogawa, H. Fujimoto, *Inorg. Chem.* **2002**, *41*, 4888–4894.
[338] A. Y. Timoshkin, T. N. Sevast'yanova, E. I. Davydova, A. V. Suvorov, H. F. Schaefer, *Russ. J. Gen. Chem.* **2003**, *73*, 765–775.
[339] F. Bessac, G. Frenking, *Inorg. Chem.* **2003**, *42*, 7990−7994.
[340] I. Krossing, I. Raabe, *J. Am. Chem. Soc.* **2004**, *126*, 7571−7577.
[341] R. Vianello, Z. B. Maksić, *Inorg. Chem.* **2005**, *44*, 1095−1102.
[342] E. I. Davydova, A. Y. Timoshkin, T. N. Sevastianova, A. V. Suvorov, G. Frenking, *J. Mol. Stru.* **2006**, *767*, 103–111.
[343] J. A. Plumley, J. D. Evanseck, *J. Phys. Chem. A* **2009**, *113*, 5985–5992.
[344] A. R. Jupp, T. C. Johnstone, D. W. Stephan, *Inorg. Chem.* **2018**, *57*, 14764−14771.
[345] A. Ben Saida, A. Chardon, A. Osi, N. Tumanov, J. Wouters, A. I. Adjieufack, B. Champagne, G. Berionni, *Angew. Chem. Int. Ed.* **2019**, *58*, 16889–16893.

[346] D. Rodrigues Silva, L. de Azevedo Santos, M. P. Freitas, C. F. Guerra, T. A. Hamlin, *Chem. Asian J.* **2020**, *15*, 4043–4054.
[347] https://perkinelmerinformatics.com/products/research/chemdraw, **2022**, 22.11.2022.
[348] H. C. Brown, H. I. Schlesinger, S. Z. Cardon, *J. Am. Chem. Soc.* **1942**, *64*, 325–329.
[349] H. C. Brown, B. Kanner, *J. Am. Chem. Soc.* **1966**, *88*, 986–992.
[350] H. Jacobsen, H. Berke, S. Döring, G. Kehr, G. Erker, R. Fröhlich, O. Meyer, *Organometallics* **1999**, *18*, 1724–1735.
[351] G. C. Welch, T. Holtrichter-Roessmann, D. W. Stephan, *Inorg. Chem.* **2008**, *47*, 1904–1906.
[352] P. A. Chase, D. W. Stephan, *Angew. Chem. Int. Ed.* **2008**, *47*, 7433–7437.
[353] G. Wittig, E. Benz, *Chem. Ber.* **1959**, *92*, 1999–2013.
[354] L. Horner, J. Haufe, *Chem. Ber.* **1968**, *101*, 2921–2924.
[355] C. J. Stern, E. G. Budnick, Patent US 3372200A, **1968**.
[356] S. Pietsch, E. C. Neeve, D. C. Apperley, R. Bertermann, F. Mo, D. Qiu, M. S. Cheung, L. Dang, J. Wang, U. Radius, Z. Lin, C. Kleeberg , T. B. Marder *Chem. Eur. J.* **2015**, *21*, 7082–7098.
[357] S. Pietsch, U. Paul, I. A. Cade, M. J. Ingleson, U. Radius, T. B. Marder, *Chem. Eur. J.* **2015**, *21*, 9018–9021.
[358] M. Eck, S. Würtemberger-Pietsch, A. Eichhorn, J. H. J. Berthel, R. Bertermann, U. S. D. Paul, H. Schneider, A. Friedrich, C. Kleeberg, U. Radius, T. B. Marder, *Dalton Trans.* **2017**, *46*, 3661–3680.
[359] A. F. Eichhorn, S. Fuchs, M. Flock, T. B. Marder, U. Radius, *Angew. Chem. Int. Ed.* **2017**, *56*, 10209–10213.
[360] L. Kuehn, L. Zapf, L. Werner, M. Stang, S. Würtemberger-Pietsch, I. Krummenacher, H. Braunschweig, E. Lacôte, T. B. Marder, U. Radius, *Chem. Sci.* **2022**, *13*, 8321–8333.
[361] J. Zhou, M. W. Kuntze-Fechner, R. Bertermann, U. S. D. Paul, J. H. J. Berthel, A. Friedrich, Z. Du, T. B. Marder, U. Radius, *J. Am. Chem. Soc.* **2016**, *138*, 5250–5253.
[362] Y.-M. Tian, X.-N. Guo, M. W. Kuntze-Fechner, I. Krummenacher, H. Braunschweig, U. Radius, A. Steffen, T. B. Marder, *J. Am. Chem. Soc.* **2018**, *140*, 17612–17623.
[363] M. W. Kuntze-Fechner, H. Verplancke, L. Tendera, M. Diefenbach, I. Krummenacher, H. Braunschweig, T. B. Marder, M. C. Holthausen, U. Radius, *Chem. Sci.* **2020**, *11*, 11009–11023.

6. APPENDIX

6.1 List of Publications

6.1.1 Publications with Peer Review Process

1. "*Anionic N-heterocyclic Carbenes Featuring Weakly Coordinating Perfluoroalkylphosphorane Moieties"*
   L. Zapf, U. Radius, M. Finze
   Manuscript submitted **2023**.

2. "*Pyridine Adducts of Tricyano- and Dicyanoboranes"*
   J. Riefer, L. Zapf, R. Wirthensohn, P. T. Hennig, T. Ribbeck, J. A. P. Sprenger, N. V. Ignat'ev, M. Finze
   Eur. J. Org. Chem. **2023**, *26*, e2023000031.

3. "*An easy-to-perform evaluation of steric properties of Lewis acids"*
   L. Zapf, M. Riethmann, S. A. Föhrenbacher, M. Finze, U. Radius
   Chem. Sci. **2023**, *14*, 2275–2288.

4. *"Boranes Paving the Way to Anionic Cyclic (Alkyl)(amino)carbenes (Ani-cAACs)"*
   L. Zapf, S. Peters, U. Radius, M. Finze
   Angew. Chem. Int. Ed. **2023**, *62*, e202300056.

5. *"Insights to Structure-Property Relationships in Ionic Liquids using Cyclic Perfluoroalkyl-sulfonylimides"*
   Y. K. J. Bejaoui, F. Philippi, G. Stammler, K. Radacki, L. Zapf, N. Schopper, K. Goloviznina, K. A. M. Maibom, R. Graf, J. A. P. Sprenger, R. Bertermann, H. Braunschweig, T. Welton, N. V. Ignat'ev, M. Finze
   Chem. Sci. **2023**, *14*, 2200–2214.

6. "*Cyano(fluoro)borate ionic liquids: Low-viscosity ionic media for electrochemical applications"*
   J. Riefer, L. Zapf, J. A. P. Sprenger, R. Wirthensohn, S. Endres, A.-C. Pöppler, M. Gutmann, L. Meinel, N. V. Ignat'ev, M. Finze
   Phys. Chem. Chem. Phys. **2023**, *25*, 5037−5048.

7. *"NHC induced radical formation via hemolytic cleavage of B–B bonds and its role in organic reactions"*
   L. Kuehn, L. Zapf, L. Werner, M. Stang, S. Wuertemberger-Pietsch, I. Krummenacher, H. Braunschweig, E. Lacote, T. B. Marder, U. Radius
   Chem. Sci. **2022**, *13*, 8321–8333.

8. *"Tricyanoborane-Functionalized Anionic N-Heterocyclic Carbenes: Adjustment of Charge and Stereo-Electronic Properties"*
   L. Zapf, S. Peters, R. Bertermann, U. Radius, M. Finze
   Chem. Eur. J. **2022**, *28*, e202200275.

9. "*Ethyl-, vinyl- and ethynylcyanoborates: room temperature borate ionic liquids with saturated and unsaturated hydrocarbon chains*"
   N. Schopper, L. Zapf, J. A. P. Sprenger, N. V. Ignat'ev, M. Finze
   Chem. Commun. **2022**, *58*, 1223–1226.

10. *"Alkoxycyanoborates: metal salts and low-viscosity ionic liquids"*
    N. Schopper, J. A. P. Sprenger, L. Zapf, N. V. Ignat'ev, M. Finze
    New J. Chem. **2021**, *45*, 14973–14987.

11. *"The crystal structure of poly[(μ_3-imidazolato-κ^3N:N:N')(tetrahydrofuran-κ^1O)lithium(I)], $C_7H_{11}LiN_2O$"*
    L. Zapf, M. Finze
    Z. Kristallogr. NCS **2021**, *236*, 1007−1009.

12. *"Stable and Storable $N(CF_3)_2$ Transfer Reagents"*
    L. N. Schneider, E.-M. Tanzer Krauel, C. Deutsch, K. Urbahns, T. Bischof, K. A. M. Maibom, J. Landmann, F. Keppner, C. Kerpen, M. Heilmann, L. Zapf, T. Knuplez, R. Bertermann, N. V. Ignat'ev, M. Finze
    Chem. Eur. J. **2021**, *27*, 10973−10978.

13. "*1,3-Bis(tricyanoborane)imidazolin-2-ylidenate Anion – A Ditopic Dianionic N-Heterocyclic Carbene Ligand"*
    L. Zapf, U. Radius, M. Finze
    Angew. Chem. Int. Ed. **2021**, *60*, 17974−17980.

14. *"BNB-doped phenalenyls – aromaticity switch upon one-electron reduction"*
    M. Crumbach, O. Ayhan, L. Fritze, J. A. P. Sprenger, L. Zapf, M. Finze, H. Helten
    Chem. Commun. **2021**, *57*, 2408−2411.

15. *"Tris(pentafluoroethyl)difluorophosphorane: A Versatile Fluoride Acceptor for Transition Metal Chemistry"*
    S. A. Föhrenbacher, M. J. Krahfuss, L. Zapf, A. Friedrich, N. V. Ignat'ev, M. Finze, U. Radius
    Chem. Eur. J. **2021**, *27*, 3504−3516.

6.1.2 Conference Talks

1. *"Novel anionic N-heterocyclic carbenes featuring weakly coordinating borane and phosphorane moieties"*
   L. Zapf, U. Radius, M. Finze
   26th Winter Fluorine Conference **2023**, Clearwater Beach (USA).

2. *"Lewis-Säuren als Schlüssel zu neuartigen anionischen N-heterocyclischen Carbenen"*
   L. Zapf, U. Radius, M. Finze
   19. Deutscher Fluortag **2022**, Schmitten (Germany).

3. *"Tricyanoboraneimidazolin-2-ylidenate Anions Ditopic – N-Heterocyclic Carbene Ligands"*
   L. Zapf, U. Radius, M. Finze
   Borchemikertreffen **2022**, Lichtenfels (Germany).

5. **"**Tricyanoboraneimidazolin-2-ylidenate Anions Ditopic – *N*-Heterocyclic Carbene Ligands"
   L. Zapf, U. Radius, M. Finze
   9th European Conference on Boron Chemistry **2022**, Barcelona (Spain).

6. *"Chiral Pentafluoroethylhydridocyano borates and boranes"*
   L. Zapf, P. T. Hennig, M. Finze
   Borchemikertreffen **2019**, Lichtenfels (Germany).

6.1.3 Conference Posters

1. *"Novel anionic N-heterocyclic carbenes"*
   L. Zapf, J. Kania, M. Weber, U. Radius, M. Finze
   ChemSyStM **2022**, Würzburg (Germany).

6.2 Printing Permissions

The publications listed below are partly reproduced in this dissertation with permission from John Wiley and Sons, The Royal Society of Chemistry, and R. Oldenbourg Verlag, De Gruyter.

"*1,3-Bis(tricyanoborane)imidazolin-2-ylidenate Anion – A Ditopic Dianionic N-Heterocyclic Carbene Ligand"*
L. Zapf, U. Radius, M. Finze
Angew. Chem. Int. Ed. **2021**, *60*, 17974−17980.

"The crystal structure of poly[(μ_3-imidazolato-κ^3N:N:N')(tetrahydrofuran-κ^1O)lithium(I)], $C_7H_{11}LiN_2O$"
L. Zapf, M. Finze
Z. Kristallogr. NCS **2021**, *236*, 1007−1009.

"Tricyanoborane-Functionalized Anionic N-Heterocyclic Carbenes: Adjustment of Charge and Stereo-Electronic Properties"
L. Zapf, S. Peters, R. Bertermann, U. Radius, M. Finze
Chem. Eur. J. **2022**, *28*, e202200275.

"*Anionic N-heterocyclic Carbenes Featuring Weakly Coordinating Perfluoroalkylphosphorane Moieties"*
L. Zapf, U. Radius, M. Finze
Manuscript submitted **2023**.

"Boranes Paving the Way to Anionic Cyclic (Alkyl)(amino)carbenes (Ani-cAACs)"
L. Zapf, S. Peters, U. Radius, M. Finze
Angew. Chem. Int. Ed. **2023**, *62*, e202300056.

"*An easy-to-perform evaluation of steric properties of Lewis acids"*
L. Zapf, M. Riethmann, S. A. Föhrenbacher, M. Finze, U. Radius
Chem. Sci. **2023**, *14*, 2275–2288.

6.3 Declaration of Authorship

Julius-Maximilians-
UNIVERSITÄT
WÜRZBURG

Fakultät für
CHEMIE UND
PHARMAZIE

Erklärung zur Autorenschaft

"1,3-Bis(tricyanoborane)imidazolin-2-ylidenate Anion – A Ditopic Dianionic N-Heterocyclic Carbene Ligand"

Ludwig Zapf, Udo Radius, Maik Finze*
Angew. Chem. Int. Ed. **2021**, *60*, 17974–17980.

Detaillierte Darstellung der Anteile an der Veröffentlichung (in %)
Angabe Autoren/innen (ggf. Haupt- / Ko- / korrespondierende/r Autor/in) mit Vorname Nachname (Initialen)

Ludwig Zapf (LZ), Udo Radius (UR), Maik Finze (MF)				
Autor	**LZ**	**UR**	**MF**	**∑ in Prozent**
Konzept	5%	0%	2%	7%
Synthese	50%	0%	0%	50%
Analytik	20%	0%	0%	20%
Verfassen der Veröffentlichung	13%	1.5%	1.5%	16%
Korrektur der Veröffentlichung	2%	1.5%	2%	5.5%
Koordination der Veröffentlichung	0%	0%	1.5%	1.5%
Summe	90%	3%	7%	100%

Erklärung zur Autorenschaft

"The crystal structure of poly[(μ_3-imidazolato-κ^3N:N:N')(tetrahydrofuran-κ^1O)lithium(I)], $C_7H_{11}LiN_2O$"

Ludwig Zapf, Maik Finze*
Z. Kristallogr. NCS **2021**, *236*, 1007−1009.

Detaillierte Darstellung der Anteile an der Veröffentlichung (in %)
Angabe Autoren/innen (ggf. Haupt- / Ko- / korrespondierende/r Autor/in) mit Vorname Nachname (Initialen)

Ludwig Zapf (LZ), Maik Finze (MF)

Autor	LZ	MF	∑ in Prozent
Konzept	5%	0%	5%
Synthese	48%	0%	48%
Analytik	30%	0%	30%
Verfassen der Veröffentlichung	10%	1.5%	11.5%
Korrektur der Veröffentlichung	2%	1.5%	3.5%
Koordination der Veröffentlichung	0%	2%	2%
Summe	95%	5%	100%

Julius-Maximilians-
UNIVERSITÄT
WÜRZBURG

Fakultät für
CHEMIE UND
PHARMAZIE

Erklärung zur Autorenschaft

"Tricyanoborane-Functionalized Anionic N-Heterocyclic Carbenes: Adjustment of Charge and Stereo-Electronic Properties"

Ludwig Zapf, Sven Peters, Rüdiger Bertermann, Udo Radius,* Maik Finze*
Chem. Eur. J. **2022**, *28,* e202200275.

Detaillierte Darstellung der Anteile an der Veröffentlichung (in %)
Angabe Autoren/innen (ggf. Haupt- / Ko- / korrespondierende/r Autor/in) mit Vorname Nachname (Initialen)

Ludwig Zapf (LZ), Sven Peters (SP), Rüdiger Bertermann (RB), Udo Radius (UR), Maik Finze (MF)

Autor	LZ	SP	RB	UR	MF	∑ in Prozent
Konzept	3%	0%	0%	0%	1%	4%
Synthese	44%	4%	0%	0%	0%	48%
Analytik	19%	1%	2%	0%	0%	22%
Quantenchemische Rechnungen	0%	0%	0%	2%	0%	2%
Verfassen der Veröffentlichung	15%	0%	0%	1%	1.5%	17.5%
Korrektur der Veröffentlichung	2%	0%	0%	1.5%	1.5%	5%
Koordination der Veröffentlichung	0%	0%	0%	0%	1.5%	1.5%
Summe	83%	5%	2%	4.5%	5.5%	100%

Erklärung zur Autorenschaft

"Anionic N-Heterocyclic Carbenes Featuring Weakly Coordinating Perfluoroalkylphosphorane Moieties"

Ludwig Zapf, Udo Radius,* Maik Finze*
2023, *submitted.*

Detaillierte Darstellung der Anteile an der Veröffentlichung (in %)
Angabe Autoren/innen (ggf. Haupt- / Ko- / korrespondierende/r Autor/in) mit Vorname Nachname (Initialen)

Ludwig Zapf (LZ), Udo Radius (UR), Maik Finze (MF)

Autor	LZ	UR	MF	∑ in Prozent
Konzept	7%	0%	0%	7%
Synthese	50%	0%	0%	50%
Analytik	25%	0%	0%	25%
Quantenchemische Rechnungen	0%	1%	0%	1%
Verfassen der Veröffentlichung	11%	0%	1%	12%
Korrektur der Veröffentlichung	2%	1%	1%	5%
Koordination der Veröffentlichung	0%	0%	1%	1%
Summe	95%	2%	3%	100%

Julius-Maximilians-
UNIVERSITÄT
WÜRZBURG

Fakultät für
CHEMIE UND
PHARMAZIE

Erklärung zur Autorenschaft

"Boranes Paving the Way to Anionic Cyclic (Alkyl)(amino)carbenes (Ani-cAACs)"

Ludwig Zapf, Sven Peters, Udo Radius,* Maik Finze*
Angew. Chem. Int. Ed. **2023**, *62*, e202300056.

Detaillierte Darstellung der Anteile an der Veröffentlichung (in %)
Angabe Autoren/innen (ggf. Haupt- / Ko- / korrespondierende/r Autor/in) mit Vorname Nachname (Initialen)

Ludwig Zapf (LZ), Sven Peters (SP), Udo Radius (UR), Maik Finze (MF)

Autor	LZ	SP	UR	MF	∑ in Prozent
Konzept	4%	0%	0%	1%	5%
Synthese	44%	4%	0%	0%	48%
Analytik	22.5%	0%	0%	0%	22.5%
Quantenchemische Rechnungen	0%	0%	2%	0%	2%
Verfassen der Veröffentlichung	15%	0%	1%	1%	17%
Korrektur der Veröffentlichung	2%	0%	1%	1%	4%
Koordination der Veröffentlichung	0%	0%	0%	1.5%	1.5%
Summe	87.5%	4%	4%	4.5%	100%

Erklärung zur Autorenschaft

"An easy-to-perform evaluation of steric properties of Lewis acids"

Ludwig Zapf, Melanie Riethmann, Steffen. A. Föhrenbacher, Maik Finze,* Udo Radius*
Chem. Sci. **2023**, *14*, 2275−2288.

Detaillierte Darstellung der Anteile an der Veröffentlichung (in %)
Angabe Autoren/innen (ggf. Haupt- / Ko- / korrespondierende/r Autor/in) mit Vorname Nachname (Initialen)

Ludwig Zapf (LZ), Melanie Riethmann (MR), Steffen. A. Föhrenbacher (SF), Maik Finze (MF), Udo Radius (UR)

Autor	LZ	MR	SF	MF	UR	∑ in Prozent
Konzept	3%	0%	2%	2%	3%	10%
Synthese	3%	0%	0%	0%	0%	3%
Analytik	3%	0%	0%	0%	0%	3%
Quantenchemische Rechnungen	0%	4%	0%	0%	6%	10%
Interpretation der Ergebnisse	14%	0%	0%	2%	4%	20%
LAB-Rep Modell	20%	0%	0%	0%	0%	20%
Verfassen der Veröffentlichung	15%	0%	2%	4%	4%	25%
Korrektur der Veröffentlichung	2%	0%	0%	2%	3%	7%
Koordination der Veröffentlichung	0%	0%	0%	0%	2%	2%
Summe	60%	4%	4%	10%	22%	100%

7. ACKNOWLEDGEMENTS

An erster Stelle bedanke mich bei meinem Doktorvater *Prof. Dr. Maik Finze*. Vielen Dank, Maik, für die Möglichkeit, nicht nur meine Bachelor- und Masterarbeit, sondern nun auch meine Doktorarbeit in deinem Arbeitskreis anfertigen zu dürfen. Danke, dass ich im Anschluss an meine Bachelorarbeit die Möglichkeit bekommen habe, als wissenschaftliche Hilfskraft fester Teil des Arbeitskreises zu werden und neue Arbeitstechniken zu erlernen. Danke für die stetige Diskussionsbereitschaft, die enorme wissenschaftliche Freiheit, eigenständig Themen erarbeiten zu können und das entgegengebrachte Vertrauen in meine Fähigkeiten. Vielen Dank für die Zusammenarbeit und Unterstützung beim Erstellen unserer gemeinsamen Publikationen. Danke für die Möglichkeit meine Forschungsergebnisse auf verschiedenen nationalen und internationalen Konferenzen präsentieren zu dürfen. Es hat mir sehr großen Spaß gemacht verschiedenste Themenbereiche unter diesen idealen Bedingungen zu erforschen.

Ein großer Dank geht ebenso an *Prof. Dr. Udo Radius*. Vielen Dank, Udo, ohne dich wären unsere Publikationen und damit auch diese Arbeit in dieser Form nicht möglich gewesen. Vielen Dank für die Diskussionsbereitschaft, deine Offenheit für meine Ideen, die schnelle und unkomplizierte Zusammenarbeit bei den Publikationen und das Durchführen der verschiedensten quanten-chemischen Rechnungen.

Dr. Philipp Hennig gilt ein besonderer Dank dafür, dass er mich während meiner Bachelorarbeit und meiner Zeit als wissenschaftliche Hilfskraft für die Chemie rund um Borane und Borate begeistert hat. Vielen Dank, Phil, für das Beibringen verschiedenster Arbeitstechniken, Tipps und Tricks. Du hast meine Begeisterung für Chemie mitgeprägt. Danke für die großartige Zeit, die wir zusammen im Labor 306 und 02.017 verbracht haben und in der wir gute Freunde geworden sind.

Jarno Riefer danke ich ebenfalls besonders für die gute Zusammenarbeit als Abzugs- und Schreibtischnachbar. Danke, Jarno, für deine stetige Hilfsbereitschaft, die wissenschaftlichen Diskussionen zu synthetischen Problemen sowie für viele unterhaltsame Gespräche in den Mittagspausen und die entstandene Freundschaft.

Nils Schopper danke ich für den hervorragenden wissenschaftlichen Austausch, die vielen Ideen und unser geteiltes Wissen zur Boran- und Boratchemie. Vielen Dank, Nils, auch für das Korrekturlesen der Arbeit, für die unzählbaren lustigen Sprüche und Situationen, das gemeinsame Feiern von Erfolgen und Überwinden von Motivationstiefs. Ich bin sehr dankbar, meine Promotionszeit mit dir als Freund und Laborpartner erlebt zu haben. Ein besonderes Highlight war definitiv unsere Zeit in Barcelona bei der EuroBoron.

Dr. Raphael Wirthensohn möchte ich besonders für die Unterstützung und Diskussionsbereitschaft zu Beginn meiner Doktorarbeit danken. Vielen Dank für deine fröhliche Art und deine Lebensweisheiten, danke für die Versorgung mit kulinarischen Highlights in den Mittagspausen und auch dir für die entstandene Freundschaft.

Ebenso gilt mein besonderer Dank *Dr. Lars Fritze*. Du bist eine super Bereicherung für unseren Arbeitskreis und es hat mir viel Spaß gemacht mit dir in einem Labor zu arbeiten, auch wenn es ab und zu zu ein paar unerwarteten Reaktionsausgängen kam. Vielen Dank für die schnell geschlossene Freundschaft und die gemeinsamen spaßigen Mittags- und Kaffeepausen.

Kristina Maibom danke ich ebenfalls für die gemeinen Mittagspausen und natürlich besonders für die hervorragende Organisation der vielen AK-Events, die erheblich zur guten Stimmung im Arbeitskreis beitragen. Vielen Dank, Kristina, für den ständigen Austausch im Laufe unsrer Promotionszeit und ebenfalls für die entstandene Freundschaft.

Sven Peters danke ich für die Arbeit während seiner Bachelorarbeit sowie seiner Zeit als wissenschaftliche Hilfskraft. Lieber Sven, auch du hast zum Gelingen dieser Arbeit besonders beigetragen, vielen Dank für deine tatkräftige Unterstützung im Labor. An dieser Stelle möchte ich auch meinen weiteren Forschungspraktikanten *Raphael Wichary* und *Matthäus Marek* für die hervorragende Arbeit im Labor danken.

Des Weiteren gilt mein Dank *Dr. Jan Sprenger* für die die Durchführung der DSC- und STA-Messungen. Vielen Dank, Jan, für deine Offenheit auch bei verschiedensten Fragen zu Arbeitstechniken, Verwaltungsangelegenheiten oder Bestellungen. *Leon Schneider* danke ich besonders für Hilfestellungen bei technischen Fragen und Problemen. Vielen Dank, Leon, besonders für deinen Einsatz beim Aufbau der alten/neuen Glovebox, die mich nach dem Umzug in den ersten Stock schnell wieder arbeitsfähig gemacht hat. *Tanja Knuplez* danke ich für die hervorragende Organisation der Abfallentsorgung, *Younes Bejaoui* danke ich für seine Arbeit als IT-Beauftragter. *Roland Graf* gilt ein Dank für die erstklassige Verwaltung und Durchführung des Bestellservices und die stetige Versorgung mit den gewünschten Chemikalien. *Jannik Kania* danke ich für die Organisation vieler Events, wie zum Beispiel der Weihnachtsfeier. *Sabine Lorenzen* möchte ich danken für ihre große Hilfsbereitschaft und die Versorgung mit getrockneten Lösemitteln. *Melanie Riethmann* und *Steffen Föhrenbacher* danke ich herzlich für die Arbeit an unserer gemeinsamen Publikation. Auch bei allen weiteren aktiven und ehemaligen Mitgliedern des Arbeitskreises möchte ich mich sehr für die gute Arbeitsatmosphäre und den Einsatz bei verschiedensten Aufgaben bedanken. Darüber hinaus bedanke ich mich bei allen weiteren Kollegen des Instituts und besonders den Mitarbeitern das AK-Radius für die stets gute Stimmung.

Dr. Rüdiger Bertermann, *Marie-Luise Schäfer* und *Laura Wolz* aus der NMR-Abteilung danke ich für das Aufnehmen vieler NMR-Spektren sowie Spezialmessungen. Ein weiterer Dank gilt *Christoph Mahler* für die Aufnahme der Massespektren. *Dr. Krzysztof Radacki* und *Dr. Alexandra Friedrich* möchte ich danken, dass sie mir alles rund um die Durchführung von Einkristallstrukturanalysen beigebracht haben. *Sabine Timmroth* und *Liselotte Michels* danke ich für die Anfertigung der Elementaranalysen. *Bernhard Werner* möchte ich für die Herstellung sowie Reparatur von Glasgeräten danken. *Stephan Köper*, *Alfred Schertzer* und *Gertrud Wunderling* danke ich für ihre stetige Hilfsbereitschaft und ihren großen Arbeitseinsatz im Institut.

Auch der Verwaltung möchte ich einen großen Dank aussprechen. Vielen Dank an *Uschi Rüppel*, *Conny Walter* und *Loretta Tietze* für die Hilfe und Unterstützung bei vertraglichen und organisatorischen Angelegenheiten.

Bei der *Studienstiftung des deutschen Volkes* möchte ich mich herzlich für die Unterstützung im Rahmen eines Promotionsstipendiums bedanken.

Ein Dankeschön geht auch an alle meine *Freunde aus Nürnberg und Würzburg*. Vielen Dank für die teils langjährigen Freundschaften, die mich ebenso durch das Studium und die Promotionszeit getragen haben.

Der wichtigste Dank geht an meine Familie: Liebe *Mama*, lieber *Papa*, auch ohne euch wäre dies Arbeit nicht möglich gewesen. Vielen vielen Dank für all die Jahre der Unterstützung in allen Lebenslagen. Ihr habt mich motiviert, meine Ziele zu erreichen, habt euch mit mir über Erfolge gefreut und mir geholfen über Schwierigkeiten hinweg zu kommen. Ihr standet mir immer mit Rat und Tat zur Seite und habt mir die Welt gezeigt. Danke, dass ihr mich immer ermutigt habt, meine Interessen zu verfolgen und ich mich immer auf eure Unterstützung verlassen konnte. Ebenso danke ich im Besonderen meinem Bruder. *Xaver*, auch du hast mich mein ganzes Leben geprägt und damit zu dem gemacht der ich jetzt bin, niemand kennt mich so lange wie du. Danke für die ganzen gemeinsamen Jahre, in denen wir immer viel zusammen gelacht haben und uns gegenseitig angespornt, unterstützt und geholfen haben. Liebe *Esther*, auch dir möchte ich von ganzem Herzen danken. Es ist ein unglaubliches Privileg, dich seit mehr als 8 Jahren kennen zu dürfen und dich als meine Frau an meiner Seite zu haben. Du hast mich nicht nur während der Zeit meiner Promotion immer unterstützt, motiviert und angefeuert, sondern warst seit meinem Abitur und während des ganzen Studiums für mich da. Danke für die ganze gemeinsame Zeit, für die vielen Dinge, die ich von dir und über dich lernen durfte und alles, was noch vor uns liegt. Auch du hast ganz besonders zum Gelingen dieser Arbeit beigetragen.

Ich will den *Herrn* loben und nie vergessen, wie viel Gutes er mir getan hat. – Psalm 103,2